HELLENIC REPUBLIC
National and Kapodistrian University of Athens
EST. 1837

School of Health Sciences

Department of Pharmacy

Section of Pharmaceutical Technology

Pharmacokinetic Studies Focusing on the Field of Absorption and Distribution of Drugs from the Lung and Gastrointestinal Tract

PhD thesis

Konstantina Soulele

Athens 2018

Doctoral Committee

V. Karalis, Assistant Professor NKUA (supervisor)

S. Markantonis-Kyroudis, Professor NKUA (tripartite committee member)

G. Valsami, Associate Professor NKUA (tripartite committee member)

D. Rekkas, Associate Professor NKUA

A. Dokoumetzidis, Assistant Professor NKUA

G. Colombo, Associate Professor, University of Ferrara, Italy

S. Giovagnoli, Associate Professor, University of Perugia, Italy

Former Tripartite Committees

26.10.2017 (622/20.11.2017)*

V. Karalis (supervisor)
S. Markantonis-Kyroudis
G. Valsami

25.4.2017 (1249/3-5-17/27.4.2017)

V. Karalis (supervisor)
P. Macheras
G. Valsami

16.2.2017 (940/21.2.2017)

V. Karalis (supervisor)
P. Macheras
A. Dokoumetzidis

11.4.2014 (773/16.6.2014)

P. Macheras (supervisor)
A. Dokoumetzidis
V. Karalis

11.12.2012 (391/17.12.2012)

P. Macheras (supervisor)
A. Dokoumetzidis
C. Tamvakopoulos

* Replacement of the committee member *Emeritus Prof. P. Macheras* from the *Prof. S.Markantonis-Kyroudis* on the basis of the decision of the Assembly (26.10.2017/622) of the Department of Pharmacy, according to par. 3, article 39, L.4485/2017.

* The approval of this PhD dissertation by the Department of Pharmacy University of the National and Kapodistrian University of Athens does not imply acceptance of the author's opinions.

* (L. 5343/1932, article 202)

Acknowledgements

This thesis represents not only my work within the university, but also a considerable attempt to contribute in more than a decade of research on population pharmacokinetics. During the course of the present work I had the chance to have two splendid supervisors. *Emeritus Professor Panos Macheras* has been the mentor of my early steps in research, and for this, I owe him sincere gratitude. He gave me the opportunity to be his PhD student, start the present thesis and fulfil my dream. Professor Macheras was always by my side with his help, advice and guidance.

As thanks are best when they are concrete, I have to express my deepest gratitude to my current supervisor *Assist. Professor Vangelis Karalis* for his enormous support, guidance and encouragement during my research. My supervisor, whose affection for science, selfless time and care were sometimes all that kept me going. I will never forget his innumerable efforts during our collaboration.

Many people have helped and taught me immensely at the laboratory of Biopharmaceutics and Pharmacokinetics. Among them I would like to distinguish *Assoc. Professor Georgia Valsami* for her prominent scientific contribution and friendship. I must express that she is a great woman and dedicated professor. She was always willing to offer invaluable advice and emotional support. I would also like to thank, *Professor Sophia Markantonis-Kyroudis,* for her significant contribution and for honoring me by being part of the tripartite committee. I am truly thankful to *Assoc. Professor Dimitris Rekkas* for supporting me through his positive perspective all these years. I must address many thanks to *Assist. Professor Aristeidis Dokoumetzidis* for his friendly attitude and collaboration during the early stages of my thesis. Most importantly I wish express my gratitude to *Assoc. Professor Stefano Giovagnoli* and *Assoc. Professor Gaia Colombo* for their willingness to participate in my PhD dissertation committee and for honoring me with their presence and friendship.

At this point, I must mention the significant contribution of the pharmaceutical companies *ELPEN S.A and RAFARM S.A.* that generously provided the experimental data for the present research. Without their contribution, it would be impossible to complete my thesis. In this vein, special thanks are addressed to Dr, George Ismailos for the productive collaboration. I would also like to thank the pharmaceutical company *UNI-PHARMA S.A*

and *Ms. Julia Tseti* for funding the research grant *'Excellence in Applied Pharmaceutical Technology',* that I was awarded by the Hellenic Pharmaceutical Society (HPS).

Most significantly, I must express my honest gratitude to *Mr. Yiannis Psarrakis* from *PHARMA-DATA S.A.*, that having an open-minded mentality gave me all the flexibility, support and understanding needed, to complete the present thesis.

Closing, I wish to address the most heartfelt thanks to my family, parents and brother, as they were the people who gave the most through their love and encouragement. I also have to thank all my friends who stood beside me during these years of academic pursuits. Despite the restricted time that I could dedicate them, they were always there whenever I needed their support.

I wish to finish with expressing my deepest gratitude to my husband, *Gregory,* as there resides the most basic source of my life energy. He was always there for me, providing selflessly love, help, time and patience.

Dedication

To my parents Charalampos and Anna

To my beloved husband Gregory

List of Contents

ABSTRACT

An in-depth understanding the factors affecting the pharmacokinetic behavior of drugs can help us improve their clinical performance and the overall drug therapy. Population pharmacokinetic modeling can exert a significant role in this exploration, as it can be a valuable tool for the description and prediction of this behavior. The objective of the current thesis is to apply these population modeling strategies in order to investigate the pharmacokinetics of inhaled and oral drugs showing special absorption and disposition characteristics. In this context, the first part of this work, concerns the analysis of four different inhaled drugs (fluticasone, salmeterol, budesonide, formoterol), using compartmental and classical pharmacokinetic methodologies, in an attempt to explore certain aspects of pulmonary absorption and factors related to the performance of inhaled drug therapy. In the second part of the thesis, pharmacokinetic investigation further focuses on the exploration of the complex distribution processes of a drug (total ezetimibe, free ezetimibe, and its metabolite) undergoing first-pass metabolism and enterohepatic re-circulation. In total, seven individual analyses are presented in this thesis, in an effort to further expand our understanding on the application of modeling and simulation to drugs exhibiting interesting pharmacokinetic characteristics.

ABBREVIATION LIST

Term	Description
ADME	Absorption, Disposition, Metabolism, Excretion
AIC	Akaike information criterion
ANOVA	Analysis of variance
AUC	Area under the C-t curve (pg/mL/h or ng/mL/h).
AUCinf	Area under the C-t curve from time zero extrapolated to infinity (pg/mL/h or ng/mL/h).
AUCt	Area under the concentration-time curve from time zero to the last sampling point or the last measurable concentration, whichever occurs earlier (pg/mL/h or ng/mL/h).
BBB	Blood brain barrier
BE	Bioequivalence
BIC	Bayesian information criterion
BLQ	Below the limit of quantification
BMI	Body Mass Index (kg/m^2)
BSV	Between Subject Variability (in %)
BUD	Budesonide
BW	Body weight (kg)
C	Concentration
CI	Confidence interval
CL	Clearance of the drug (L/h)
Clast	Last quantifiable concentration (pg/mL/h or ng/mL/h).
Cmax	The first recorded maximum plasma concentration value (pg/mL or ng/mL)
COPD	Chronic Obstructive Pulmonary Disease
CV	Coefficient of variation (in %)
C-t	Concentration-time
DPI	Dry-powder inhaler
ECG	Electrocardiographic
EHC	Enterohepatic recirculation

EMA	European Medicines Agency
EZE	Ezetimibe
EZEG	Ezetimibe glucuronide
F	Fraction of bioavailable dose
Fb	Fraction of dose undergoing EHC
Fp	Dose apportionment parameter for first-pass metabolism
FDA	Food and Drug Administration
FEV1	Forced expiratory volume in 1 second
FLP	Fluticasone propionate
FOR	Formoterol
h	Hours
GB	Gallbladder
GI	Gastrointestinal
GMR	Geometric Mean Ratio
IOV	Inter-occasion variability
IPRED	Individual predicted concentrations
IQR	Inter-quartile range
IV	Intravenous
IWRES	Individual weighted residuals
ka	First-order absorption rate constant from the GI (h^{-1})
kaf	Fast first-order absorption rate constant from the lungs (h^{-1})
kam	First-order absorption rate constant for the metabolite (h^{-1})
kap	First-order absorption rate constant for the parent drug (h^{-1})
kas	Slow first-order absorption rate constant from the lungs (h^{-1})
kb	First-order rate constant for transfer to the GB compartment (h^{-1})
kel	First-order elimination rate constant (h^{-1})
kelm	First-order elimination constant for the metabolite (h^{-1})
kelp	First-order elimination constant for the parent drug (h^{-1})
kfec	Fecal elimination rate constant (h^{-1})
kfp	First-pass rate constant (h^{-1})

kg	Bile release rate constant (h^{-1})
kg*	Baseline bile release rate constant for (h^{-1})
k_L	First-order absorption rate constant from the lungs (h^{-1})
km	First-order transformation constant of the parent to metabolite (h^{-1})
kmb	First-order transfer constant of the metabolite from the central to the GB compartment
kr	Transit compartment first-order transfer rate constant (h^{-1})
LC-MS/MS	Liquid Chromatography / Mass Spectrometry
LL	Log-likelihood
LLOQ	Lower limit of quantitation
Min	Minutes
NCA	Non-compartmental analysis
NPDE	Normalized prediction distribution errors
ODE	Ordinary differential equations
OFV	Objective function value
PK	Pharmacokinetic
pMDI	Pressurized metered-dose inhaler
POPPK	Population pharmacokinetic
PRED	Predicted concentrations
PPRED	Population predicted concentrations
Q	Inter-compartmental clearance (L/h)
Qm	Inter-compartmental clearance of the metabolite (L/h)
Qp	Inter-compartmental clearance of the parent drug (L/h)
R	Reference product
R_{fast}	Relative fraction of dose absorbed rapidly from the lungs
R_{GI}	Relative fraction of drug dose swallowed and deposited at the gastrointestinal tract.
R_L	Relative fraction of drug dose absorbed from the lungs
R_{slow}	Relative fraction of dose absorbed slowly from the lungs
RSE	Relative standard error (in %)

RUV	Residual unexplained variability
SAEM	Stochastic Approximation Expectation Maximization
SAL	Salmeterol
SD	Standard Deviation
t	Time (min or h)
T	Test product
T_{GE}	Duration of gallbladder emptying (h)
Tmax	The time (h) at which Cmax occurs
$t_{1/2}$	Elimination half-life (h)
UDP	Uridine 5'-diphospho-glucuronosyltransferase
VPC	Visual Predictive Check
V_B	Blood Volume (L)
Vd	Apparent volume of drug distribution (L)
Vc	Apparent volume of drug distribution of the central compartment (or V_1, L)
Vcm	Volume of distribution of the central compartment for the metabolite (L)
Vcp	Volume of distribution of the central compartment for the parent drug (L)
Vp	Apparent volume of drug distribution of the peripheral compartment (or V_2, L)
Vpm	Volume of distribution of the peripheral compartment for the metabolite (L)
Vpp	Volume of distribution of the peripheral compartment for the parent drug (L)
V_T	Tissue Volume (L)
z	Ratio of dose fractions absorbed either fast (R_{fast}) or slowly (R_{slow}) through the lungs (i.e. R_{fast}/R_{slow})
λz	Apparent terminal rate constant (h^{-1})

A. Introduction

A.1. Pharmacokinetics

Pharmacokinetics (PK) may be defined as the branch of pharmacology that investigates the fate of drug substances in the body (Benet and Zia-Amirhosseini, 1995). The term was first introduced by F. H. Dost in 1953 in his text, '*Der BliitspiegeI-Kinetic der Konzentrationsablaiife in der Frieslauffliissigkeit'*. Since then, pharmacokinetics has been defined in a number of ways. Literally, the word means the application of kinetics to 'pharmakon', the Greek word for drugs and poisons (Wagner, 1981). The purpose, therefore, of pharmacokinetics is to study the time course of a drug in the body and characterize its kinetic pathways, namely its absorption, distribution, metabolism and excretion. These pharmacokinetic processes, often referred to collectively as ADME (Figure A.1), determine when the drug appears in the blood stream and for how long it remains there (Ritter et al., 2008; Sakai, 2008).

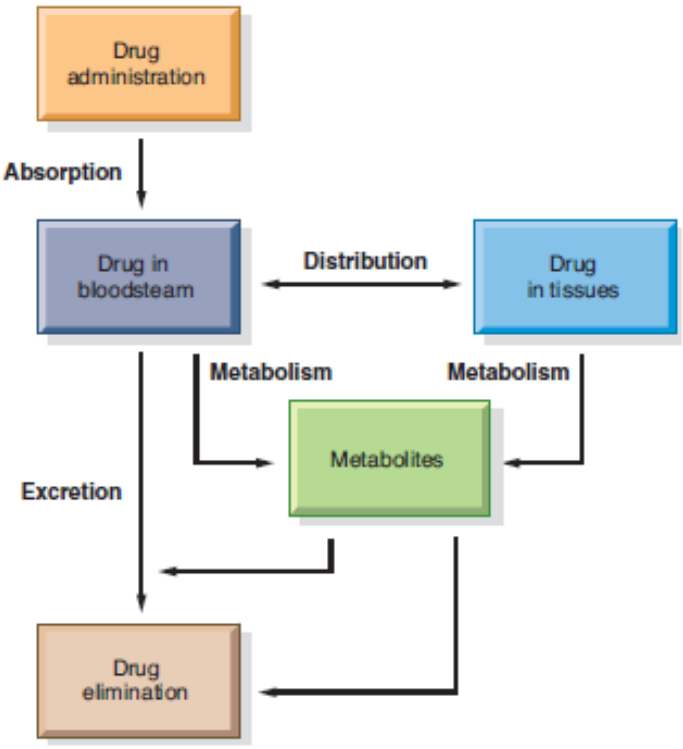

Figure A.1. A representation of the four fundamental pathways of drug movement and modification in the body, the ADME processes. *Adapted from reference (Sakai, 2008).*

Absorption and distribution processes indicate the passage of drug molecules from the administration site to the blood and from blood to tissues, respectively. Drug elimination may occur through biotransformation of the drug and its excretion from the body through the urines, feces or other routes (Urso et al., 2002). The course of drug action is, in most cases, directly correlated with the concentration of the drug in the blood stream and, thus, is highly dependent upon the ADME processes (Sakai, 2008). Therefore, knowledge of these PK processes and the ways that they can vary between individuals is an important part of understanding and predicting the therapeutic outcome of a selected drug therapy (Ritter et al., 2008).

A fundamental hypothesis of pharmacokinetics is that a relationship exists between a pharmacologic or toxic effect of a drug and its concentrations levels within the body (Benet and Zia-Amirhosseini, 1995). Ideally, the concentration of drugs should be measured at their site of action; that is, at the receptor. However, owing to inaccessibility, measurement of drugs or their metabolites is usually confined to determination of their concentrations in plasma or blood (Tozer, 1981). In spite of this limitation, such information can provide considerable information, since in most cases, the concentration of a drug at its site of action is related to the concentration of the drug in the systemic circulation (Bruton et al., 2008). After all, it is the blood which conveys drugs from the site of administration to the various organs, including those in which drugs act and those in which drugs undergo elimination by excretion and biotransformation. Analysis of other body fluids such as urine and feces, or saliva may also provide a means of obtaining several kinds of pharmacokinetic information (Tozer, 1981).

Data, collected from these type of biological sources are analyzed using a mathematical representation of a part or the whole of an organism. Broadly then, the purpose of pharmacokinetics is to reduce these data to a number of meaningful parameter values, and to use these reduced data in order to evaluate and predict the results of a therapeutic regimen (Wagner, 1981). In general the pharmacokinetic behavior of drugs can be grossly characterized with the following parameters: *bioavailability (F),* which denotes the available fraction of drug into the general circulation; *the apparent volume of distribution (Vd),* relating to the disposition of the drug within the body; and the *clearance (CL)* and *elimination half-life* ($t_{1/2}$) which are used as measures of the body's ability to eliminate

drug (Bruton et al., 2008). A brief description of these and other related PK parameters is given in the relevant paragraphs below.

A.1.1 Absorption

Before a drug can begin to exert any systemic effect on the body, it has to be absorbed into the bloodstream (Barber and Robertson, 2012). When medications are given orally, intramuscularly, subcutaneously, or by other extravascular routes, such as the pulmonary or rectal routes, the drug must pass through several physiological barriers before entering the vascular system (Bauer, 2008). For example, when a solid dosage form is given orally, the drug formulation must release drug molecules via dissolution, and the molecules must pass through the various layers of the gastrointestinal tract to enter the capillaries, which will further distribute it to the sites of action (Bauer, 2008; Bruton et al., 2008). This may result in a lower availability of the drug due to incomplete absorption (Sakai, 2008).

The fraction of the administered dose that is delivered to the systemic circulation is known as the bioavailable fraction of the drug (Bruton et al., 2008). Bioavailability (*F*) is defined as the relationship between the drug dose and the amount that is ultimately delivered to the bloodstream (Sakai, 2008). It cannot be measured directly, but it is calculated by comparing the concentration (C) versus time (t) curves following administration of the preparation via its intended route (e.g. orally) and of the same dose given intravenously (IV), which serves as a reference for complete absorption (Ritter et al., 2008). The area under the plasma C-t curve (AUC) represents the total amount of the drug reaching the circulatory system (see Figure A.2), therefore, the ratio of these two parameters defines the absolute bioavailability of the tested formulation (Sakai, 2008).

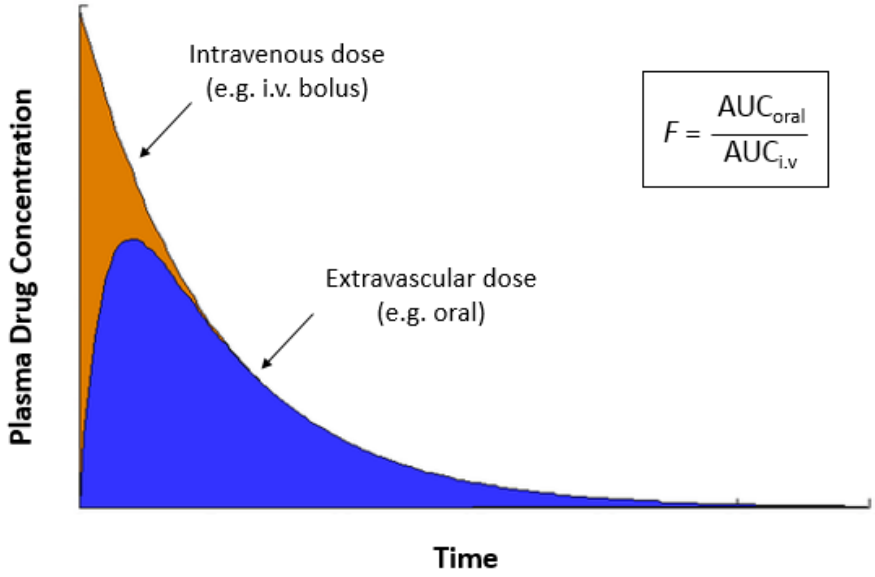

Figure A.2. Plasma C-t plots from an IV and extravascular administration for the calculation of absolute bioavailability. The two shaded areas refer to the AUC after oral and IV administration.

Since the most convenient route of drug administration is usually the oral, absorption processes in the gastro-intestinal tract are among the best studied (Ritter et al., 2008). When a tablet or capsule is swallowed, it must dissolve before it can be absorbed. Once dissolution has occurred, the drug molecules must pass through the selectively permeable membranes of the cells lining the gastrointestinal tract to reach the bloodstream. Depending on their chemical and physical properties, drugs will be absorbed either by passive diffusion or by carrier-mediated transport across these membranes, with the vast majority of drugs gaining access to the bloodstream by diffusion (Ritter et al., 2008; Sakai, 2008).

Following these processes, drug plasma concentrations rise while the drug is being absorbed into the bloodstream, reach a maximum concentration (Cmax) and eventually decrease according to the half-life of the drug. The phase of the curve over which absorption mainly takes place is known as the absorption phase, and the time that the maximum concentration occurs is called Tmax (Figure A.3) (Bauer, 2008).

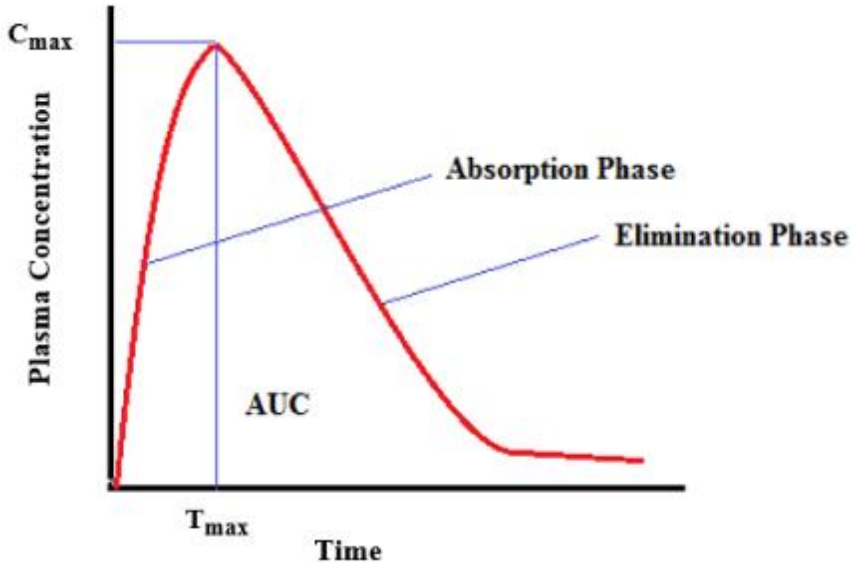

Figure A.3. Plasma C-t profile after oral administration, showing the absorption and elimination phases. The area under the plasma C-t curve (AUC), the maximum concentration (Cmax) and the time that the maximum concentration occurs (Tmax) (edited figure, source: https://www.intechopen.com).

Apart from Cmax and Tmax, an additional parameter for the characterization of the absorption phase, is the absorption rate constant, which defines the rate at which a drug enters the body following administration, and is represented by the symbol 'ka'. This rate influences both the peak plasma concentration and the time it takes to reach this peak. First-order absorption, where the rate is directly proportional to the amount remaining, is common for most drugs and the same is true for the absorption of drugs from many other extravascular sites, including the respiratory tract, the subcutaneous tissue and muscles. Nevertheless, there are also other models used to describe the absorption process such as zero-order (as is the case with extended-release tablets), Weibull (constantly changing absorption process), and bolus absorption (Tozer, 1981).

The rate and extent of absorption depends mainly on the route of administration, the pharmaceutical formulation and the physicochemical properties of the drug, as well as certain physiological factors that can impact the site of absorption. The latter relate to human physiological parameters, such as blood flow to the absorbing site, total surface area for absorption, time of arrival and the residence time of the drug at the absorption site, presence of a disease and concomitant medication or food intake among others (Sakai, 2008). On the other hand, physicochemical factors relate to the solubility of the

drug in body fluids, the degree of ionization, the chemical stability, and its lipid to water partition coefficient (Barber and Robertson, 2012).

Incomplete absorption of the drug into the systemic circulation and a reduced drug availability may produce ineffectiveness of the administered treatment (Urso et al., 2002). Several reasons of incomplete absorption exist. For drugs given in solid form, the solubility and rate of dissolution may be the limiting factor in their absorption (Bruton et al., 2008), whereas, their potential inability to cross epithelial membranes may further account for incomplete absorption. Also, decomposition of a drug within the GI tract may occur, or inactivation due to presence of enzymes in the gut lumen metabolizing the agent before reaching systemic circulation (Bauer, 2008; Tozer, 1981). One of the most common causes of reduced bioavailability is the 'first-pass' effect where, a fraction of the dose undergoes a pre-systemic metabolism within the GI tract or the liver, before gaining access to the rest of the body (Figure A.4) (Barber and Robertson, 2012).

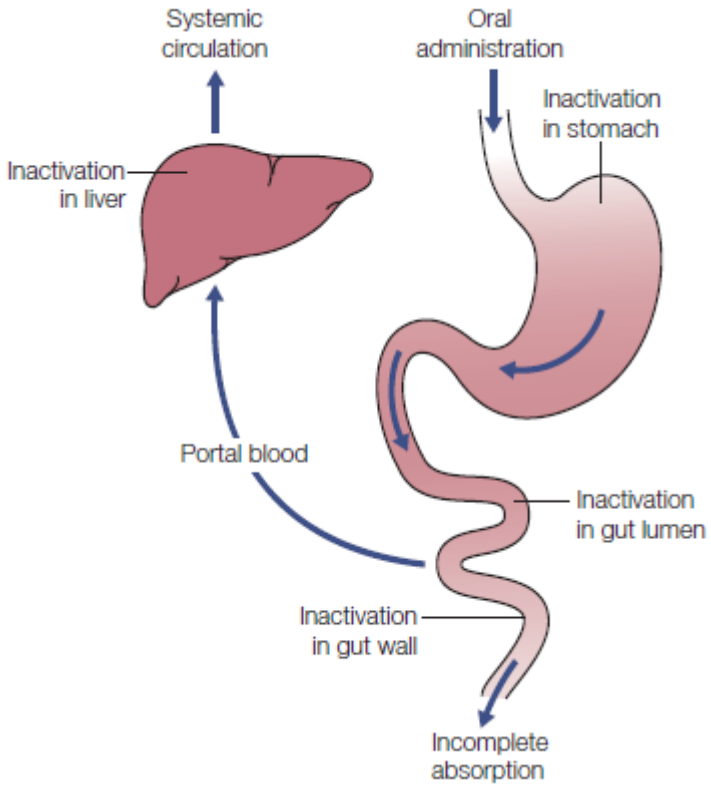

Figure A.4. Schematic representation for the reasons of reduced bioavailability following oral administration. Adapted from reference (Ritter et al., 2008).

Pronounced first-pass metabolism by either the gastro-intestinal mucosa or liver necessitates high oral doses by comparison with the intravenous route. Also pronounced

inter-individual variability in drug disposition is usually observed in drugs undergoing extensive pre-systemic metabolism. This results in highly variable responses to therapy, and is one of the major difficulties in their clinical use (Sakai, 2008). Therefore, the route of administration and pre-systemic metabolism markedly influence the pattern of drug profile in the body.

Similarly to the absorption following oral administration, pulmonary absorption of inhaled drugs is also a very complicated process. In particular, certain physiological parameters, such as lung deposition, variations in absorption rate between the different areas of the lung, the presence of mucociliary clearance, as well as certain formulation characteristics (e.g., particle size, dissolution rate) or patient-related factors (e.g., health status, lung function) can significantly influence the absorption PKs of these drugs (Weber and Hochhaus, 2013). For this reason, the description of absorption and special pharmacokinetic characteristics of drugs following inhaled administration is the subject of Chapter A2.

A.1.2 Distribution

Once a drug is absorbed into the bloodstream it can be carried throughout the body and be distributed to the sites of action. This process is called distribution, and is a reversible process, since some molecules may be interacting with receptors on cell membranes or inside the cells, other molecules may move back into the bloodstream (Sakai, 2008). There are four main elements regarding drug distribution (Barber and Robertson, 2012):

1. ***Distribution into body fluids***: These are mainly plasma, interstitial fluid and intracellular fluid. Molecular targets for drugs are found in these areas.
2. ***Body tissues/organs distribution***: Specific tissues can take up some drugs - such as the adipose tissue, the muscular system and the thyroid gland.
3. ***Plasma protein binding***: Plasma proteins such as albumin can bind to drug molecules. Drugs bound to plasma proteins are pharmacologically inert; only free drugs are active. Protein binding varies widely among drugs; some drugs do not bind (e.g. caffeine), some are highly bound (e.g. warfarin), whereas some can even displace others from their binding sites on plasma proteins.

4. ***Passage through barriers***: The two main examples are the placenta and the blood brain barrier (BBB). Drugs must be highly lipophilic to pass across these barriers. In another case, they may not be able to reach their site of action.

Cardiac output, regional blood flow, capillary permeability, and tissue volume determine the rate of delivery and potential amount of drug distributed into tissues. Initially, liver, kidney, brain, and other well-perfused organs receive most of the drug, whereas delivery to muscle, skin, and fat is much slower. Tissue distribution is determined by the partitioning of drug between blood and the particular tissue (Bruton et al., 2008).

The concentration of a drug in the blood, plasma, or plasma water depends on how a drug distributes and on the amount of drug in the body. From simple mass balance considerations, the amount in the body (A) can be accounted for from the concentration in the blood, or other blood fraction, if the space into which the drug appears to distribute is known. This apparent dilution space is called the volume of distribution (Tozer, 1981). The volume of distribution (Vd) is basically an equilibrium concept and has no direct physiological meaning; it is not a 'real' volume and is usually referred to as the apparent volume of distribution. It is defined as that volume of plasma in which the total amount of drug in the body would be required to be dissolved in order to reflect the drug concentration attained in plasma (Dhillon and Gill, 2006).

For an average 70-Kg human, typically the plasma volume is 3 L, the blood volume is 5.5 L, the extracellular fluid outside the plasma is 12 L, and the total body water is approximately 42 L. However, many classical drugs exhibit volumes of distribution far in excess of these known fluid volumes. For example, the volume of distribution for digoxin in a healthy volunteer is about 700 L, which is approximately 10 times greater than the total body volume of a 70-Kg human. This serves to emphasize that the volume of distribution does not represent a real volume. Rather, it is an *apparent* volume that should be considered as the size of the pool of body fluids that would be required if the drug was equally distributed throughout all portions of the body. In fact, the relatively hydrophobic digoxin has a high apparent volume of distribution because it distributes predominantly into muscle and adipose tissue, leaving only a very small amount of drug in the plasma in which the concentration of drug is measured (Benet and Zia-Amirhosseini, 1995).

The physiologic determinates of volume of distribution are the actual volume of blood (V_B) and size (measured as a volume) of the various tissues and organs of the body (V_T) (Bauer, 2008). Changes, therefore, in volume of distribution occur with body composition, age, in renal failure and cardiac decompensation (heart failure), and between the different sexes (Tozer, 1981). These factors all affect the apparent volume of distribution of a drug and ultimately play a role in determining the appropriate dose of a drug (Sakai, 2008).

A.1.3 Elimination

When a drug is taken into and distributed throughout the body, it must be subsequently removed which is referred to as *elimination*. The term drug elimination encompasses both the metabolism of the drug, and excretion mainly through the kidneys and the bile.

A.1.3.1 Metabolism

Drugs can be eliminated from the body either unchanged, or may undergo chemical changes that allow them to be more easily excreted. The process of undergoing chemical changes is called biotransformation, or metabolism (Sakai, 2008). *Metabolism* of drugs and other xenobiotics into more hydrophilic compounds is essential for their elimination from the body, as well as for the termination of their pharmacological activity. In general, biotransformation reactions generate more polar, inactive metabolites that are readily excreted from the body. However, in some cases, metabolites with pharmacological activity or toxic properties can be generated (Bruton et al., 2008). Therefore, a drug metabolite may decrease, increased or lead to no change in pharmacological activity compared to the parent drug, or even have a completely different activity (Barber and Robertson, 2012).

Drug metabolizing enzymes are expressed in most tissues in the body; the highest levels are found in the gastrointestinal (GI) tract (e.g., liver, small intestine, and colon). The high concentration of these enzymes in GI epithelium mediates the initial metabolic processing of most oral drugs and is the initial site for first-pass metabolism of drugs. Absorbed drugs then enter the portal circulation and transit to the liver, which is the major "metabolic clearing house" for both endogenous chemicals (e.g., cholesterol, steroid hormones, fatty acids, and proteins) and xenobiotics. While some active compounds may escape first-pass metabolism in the GI tract and liver, subsequent passes through the liver result in further metabolism of the parent drug until it is completely eliminated. Other organs that contain

potent metabolizing enzymes include the nasal mucosa and lung, which may play an important role in the first-pass metabolism of airborne pollutants and drugs that are administered through the inhalation route (Bruton et al., 2008).

Liver is the major metabolic site which converts drugs to more water-soluble compounds that can be then removed from the body through the excretion processes. There are two main metabolic pathways that drugs can follow in the liver. In the first type of reactions, drugs are made more polar through oxidation-reduction reactions or hydrolysis. The second type of metabolism involves conjugation reactions. In this type, the drug undergoing change is joined with another substance, such as a glucuronic acid, sulfuric acid, acetic acid, or an amino acid (Sakai, 2008).

Glucuronidation is the most common conjugation reaction. UDP-glucuronosyltransferase enzymes catalyze the transfer of glucuronic acid from the cofactor UDP-GA to a substrate to form b-D-glucopyranosiduronic acids (glucuronides), metabolites that are sensitive to cleavage by b-glucuronidase. The generation of glucuronides can be formed through alcoholic and phenolic hydroxyl groups, carboxyl, sulfuryl, and carbonyl moieties, as well as through primary, secondary, and tertiary amine linkages (Bruton et al., 2008). The result of conjugation is more water-soluble compounds that are easier for the kidneys to excrete. Glucuronidation also markedly increases the molecular weight of the compound, which favors biliary excretion (Bruton et al., 2008; Sakai, 2008). In this respect, many drugs that are glucuronidated and excreted in the bile may repeatedly reenter the systemic circulation by “enterohepatic recirculation”, a complex re-distribution process that is described in more detail in a following section (Chapter A2).

Drug metabolism can influence dose and frequency of dosing. Drugs which are metabolized quickly have a short duration of action and need to be administered more often, whereas drugs which are metabolized slowly can have a longer duration of action and may only need to be given on a once-daily basis (Barber and Robertson, 2012). Metabolism of drugs may also vary widely between population groups. Deficiency of some drug metabolizing enzymes is genetic and will result in poor tolerance of certain drugs. Age is another important variable that has a bearing on metabolism. Organ function gradually declines with age and the elderly may poorly tolerate drugs that require metabolism. The very young patients usually require special consideration of drug dosing

because of immaturity of their organ systems. Drug interactions may also occur between drugs that are metabolized by the same enzyme systems in the liver (Sakai, 2008).

A.1.3.2 Excretion

Once drugs have had their desired effect they need to be excreted by the body (Barber and Robertson, 2012). *Excretion* is defined as the irreversible removal of drug from the body (Bauer, 2008). Removal of drug may occur as a result of processes that occur in the liver, kidney, and other organs (Benet and Zia-Amirhosseini, 1995). Excretory organs, the lung excluded, eliminate polar compounds more efficiently than substances with high lipid solubility. Lipid-soluble drugs are, thus, not readily eliminated until they are metabolized to more polar compounds (Bruton et al., 2008; Ritter et al., 2008). Principles of excretion include renal elimination, secretion into bile for fecal elimination and enterohepatic recirculation (Barber and Robertson, 2012). Other routes of elimination could include that in saliva or sweat, partition into the gut, and metabolism at sites other than the liver (e.g., nitroglycerin, which is metabolized in all tissues of the body) (Benet and Zia-Amirhosseini, 1995).

Excretion into the urine is one of the most important mechanisms of drug removal. The kidneys act as a filter for the blood and create urine as a vehicle for removal of waste. Blood enters the kidney through renal arteries and then is filtered by the glomerulus. The glomerular filtrate becomes concentrated and substances are removed as it passes through the renal tubule and eventually becomes urine (Sakai, 2008). *Excretion into bile* is another method of eliminating drug molecules and metabolites. These are secreted from the liver into bile and into the gut for fecal elimination. As in renal excretion, not all of the drug and its metabolites are eliminated entirely at once, but may be repeatedly return to systemic circulation before complete elimination (Barber and Robertson, 2012). *Excretion of drugs in breast milk* is also important not because of the amounts eliminated, but because the excreted drugs will have unwanted pharmacological effects in the nursing infant. *Excretion from the lung* may also be important primarily for the elimination of anesthetic gases (Bruton et al., 2008).

The complete elimination of a drug from the body is, therefore, mainly dependent on normal liver and kidney function. When a patient has reduced kidney or liver function or another problem that lengthens the half-life of a drug, dosage adjustment is required. Age must be also considered in a discussion of drug excretion. The very young and very old

will have lower rates of excretion; the old because of deterioration in organ function and the very young, because the kidneys have not reached full maturity. Drug interactions, such as when multiple drugs compete for metabolic processes, can also reduce drug removal (Sakai, 2008).

Because the concentration of a drug in plasma or blood is measured rather than the amount of drug in the body and because the rate of elimination depends on the concentration of drug entering the organ in which elimination occurs, a PK parameter relating the rate of elimination to the measured concentration is useful. This PK parameter is *clearance* (*CL*). The meaning of clearance becomes evident when drug elimination is placed in physiologic perspective (Tozer, 1981). Clearance is the volume of biological fluid such as blood or plasma from which drug is completely removed (by metabolism and/or excretion) per unit time (Bruton et al., 2008). Thus, the dimension of clearance is volume per unit time, such as L/h or mL/min (Benet and Zia-Amirhosseini, 1995).

The factors affecting clearance are most readily classified on the basis of the organ in which elimination occurs. Inter-individual variability in hepatic clearance can be large, primarily due to genetic differences. Environmental effects, such as induction (food and drugs), competitive inhibition of metabolism, and hepatic disease can also produce large differences. Renal clearance is affected by any condition altering glomerular filtration, secretion, or reabsorption of a drug in the nephron (Tozer, 1981).

Another common PK parameter used to denote how quickly drug serum concentrations decline in a patient is the *elimination rate constant* (*kel*). Assuming first-order kinetics, the elimination rate for a drug can be computed by taking the product of the elimination rate constant by the amount of drug in the body (Bauer, 2008). Similarly, the elimination rate constant depends on how the drug is cleared by the organ(s) of elimination and how extensively it is distributed to the tissues. The dimension for the elimination rate constant is reciprocal time (h^{-1}, min^{-1}, etc.) (Tozer, 1981).

Finally, how long a drug remains in the body, is often measured by the *elimination half-life* ($t_{1/2}$). This parameter is very useful for estimating how long it will take for drug levels to be reduced to the one half (50%) of its initial concentration (Dhillon and Gill, 2006). The half-life provides a means to calculate the time for a drug to be removed from the body or to estimate the appropriate dosing interval of a drug regimen (i.e., five half-lives

result in 99% of a drug from the body) (Bruton et al., 2008). It can be also used as a good indication of the time required to reach steady state after a dosage regimen is initiated or changed a new steady state. The dimension of half-life is time (hours, minutes, days, etc.) (Bauer, 2008).

Assuming again first-order kinetics, the half-life and elimination rate constant are related to each other by the following equation, so it is easy to compute the one once the other is known: $t_{1/2} = 0.693/kel$. The half-life and elimination rate constant for a drug can change either because of a change in clearance or a change in the volume of distribution. Because the values for clearance and volume of distribution depend solely on physiological parameters and can vary independently of each other, they are known as *independent parameters* (Bauer, 2008).

A.2. Special cases in Pharmacokinetics

An appropriate characterization of all the above pharmacokinetic processes is a difficult task. This becomes even more complicated with drugs or routes of administration showing special kinetic features. Two such special cases are: a) the pharmacokinetic characterization of the highly complex enterohepatic re-circulation process b) the pulmonary absorption of inhaled drugs.

A.2.1. Enterohepatic re-circulation

In pharmacokinetics, enterohepatic recirculation (EHC) may be regarded as a re-distribution phenomenon (Dobrinska, 1989). This recirculation process occurs when a significant amount of a drug or its conjugated metabolites are excreted into bile and then return back to the intestine, where they can serve as a secondary source for drug absorption (Gao et al., 2014; Roberts et al., 2002). EHC has been shown to notably affect drug pharmacokinetics by prolonging drug elimination, increasing bioavailability and producing complicated concentration-time profiles (Roberts et al., 2002). For drugs that are excreted extensively into the bile, insight into the magnitude of EHC process is of crucial importance, as it can significantly affect PK parameters such as the elimination half-life, AUC and other estimates of systemic exposure (Jiao et al., 2007).

Enterohepatic circulation is a complex re-distribution process involving several organs and ducts such as the liver, portal vein, hepatic artery, hepatic vein, the biliary system, the gallbladder and the gastrointestinal tract (Figure A.5).

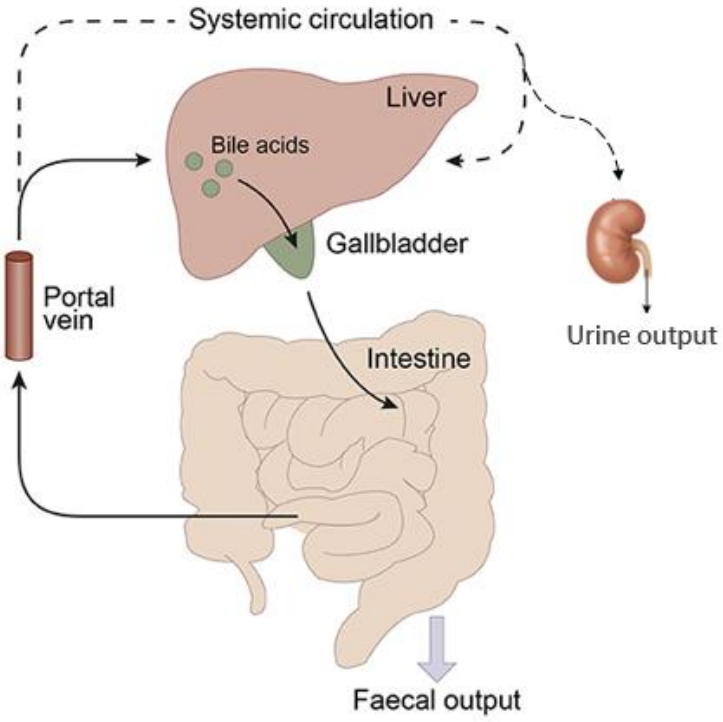

Figure A.5. Schematic representation of the enterohepatic re-cycling process of drugs. Adapted from ref (Mertens et al., 2017).

It initially occurs after the process of absorption of a solute from the gastrointestinal tract into the portal blood. Once in the portal circulation, drugs are absorbed from the sinusoids by a transport process, or they may diffuse across the hepatocyte plasma membranes. Compounds undergoing enterohepatic recirculation are usually transported as parent solutes through different carrier-mediated systems or by diffusion as uncharged solutes, which are later biotransformed in the liver to suitable polar solutes (Dobrinska, 1989). Liver plays a pivotal role in the biotransformation and elimination of the endogenous and exogenous compounds. However, drug-metabolizing enzymes can be also found in the intestinal wall leading to a pre-systemic biotransformation of the drug. Both phase I (oxidation and hydrolysis) and phase II (conjugation) metabolism exists in the liver and gut wall, and the resulting metabolites may also become involved in enterohepatic recirculation (Roberts et al., 2002).

Drug and metabolites may be secreted and concentrated in the gallbladder which, upon contraction, releases its contents into the lumen of the intestinal lumen. Generally, bile is

stored in the gall bladder and released into the small intestine via the sphincter of Oddi on the sight, smell or ingestion of food. As a consequence, gallbladder emptying is sporadic, leading to complex pharmacokinetics when enterohepatic recycling is substantial. Patrick and co-workers (Patrick et al., 2002) in recognizing that the multiple peaks in the plasma concentration-versus-time profiles of ezetimibe, conjugated ezetimibe and total ezetimibe were suggestive of enterohepatic recycling, commented that the multiple secondary peaks corresponded to the approximate time of meals. This timing was consistent with food intake stimulating the emptying of the gallbladder (Roberts et al., 2002). However, even in the absence of food, a partial discharge of gallbladder bile into the duodenum during the inter-digestive period could also been considered (Luiking et al., 1998). Northfield and Hofmann (Northfield and Hofmann, 1975) have previously reported that there is a secretion of bile acids into the duodenum during the fasting state. During the late phase of the inter-digestive period, intra-gallbladder pressure increments favor flow of a small amount of bile into the bile duct and, through the sphincter of Oddi, into the duodenum (Behar, 2013).

Excretion of drugs in bile depends mainly on their molecular weight and structure. A molecular weight threshold of >400 g/mole is associated with appreciable biliary excretion in humans (Malik et al., 2016; Roberts et al., 2002). Conjugation of drugs is also known to increase both the molecular weight and polarity, thus making these compounds even more pre-disposable to biliary excretion (Malik et al., 2016). For example, glucuronidation adds a weight of about 200 to the compound. Similarly, hydroxylation and glutathione conjugation make the metabolite fit for the biliary excretion. However, some compounds are also excreted unchanged in the bile (Dobrinska, 1989; Malik et al., 2016 .

Finally, metabolism of the conjugates by the intestinal microflora and reabsorption of the drug from the GI tract, integrates the enterohepatic cycle (Dobrinska, 1989; Malik et al., 2016). For either the parent drug or its metabolite, EHC can be finally terminated by elimination into the feces or, if the compound has entered the systemic circulation, by the urine. Therefore, a complete study of enterohepatic circulation would require determination of the rate of biliary excretion and re-excretion, intestinal absorption, and fecal and urinary elimination of the parent compound and all metabolites (Roberts et al., 2002).

Several therapeutic agents are known to undergo enterohepatic circulation. Examples of these drugs include the immunosuppressant agent mycophenolic acid, warfarin, morphine, erythromycin, doxycycline, ceftriaxone, and the cholesterol absorption inhibitor ezetimibe among others. Beside drugs, the EHC process occurs for endogenous compounds. Bile acids are the major endogenous compounds to undergo the EHC process. Other endogenous compounds that can also go through the EHC process include: hormones, like estrogen, thyroxine (T4) and triiodothyronine (T3), and vitamins like vitamin D and folic acid (Roberts et al., 2002).

- *Factors Affecting the EHC Process*

Enterohepatic recycling has been shown to be affected by several factors. These factors could be generally categorized into physiological, such as gastric emptying, lumen pH, composition of the gut microflora, liver and kidney function and potential disease effects; physiochemical, like the chemical structure, molecular weight, the polarity and solubility of the drug, the genetic variability and age- or gender-related effects, co-medication, and lastly, environmental factors including food intake and lifestyle (Roberts et al., 2002).

- *Pharmacokinetic characterization of EHC*

As reported above the PKs of drugs undergoing enterohepatic cycling is often associated with erratic C-t profiles showing multiple secondary peaks (Roberts et al., 2002). Pharmacokinetic investigation and determination of the primary PK parameters of drugs witnessing multiple peaks due to EHC through classical PK methodologies is extremely difficult. In such cases, pharmacokinetic modeling can act as a prognostic tool and quantitatively represent different PK processes, providing a better understanding on the consequences of EHC process. Many empirical and more physiologically based models have been published so far to address EHC of drugs with each one having its own merits and demerits. ADME of drugs undergoing EHC is complex, therefore, the modeling of such drugs becomes a highly complicated task. The situation is further complicated by many endogenous and exogenous factors influencing the EHC of the drugs. Factors like co-administration of the drugs, use of the bile sequestrating agents, genetic variations, species and gender differences, make the process even more intricate and knotty (Malik et al., 2016).

A.2.2 Pulmonary absorption

Pulmonary absorption of drugs is another PK process characterized by complex underlying mechanisms. The pharmacokinetic behavior of inhaled drugs is much more complicated compared to more conventional ways of administration (Cazzola et al., 2002; Reynolds et al., 2005; Singh et al., 2003; Weber and Hochhaus, 2013). In addition, the very low systemic drug levels reached following inhalation of therapeutic doses require analytical methods with high sensitivity and specificity (Callejas et al., 1998; Krishnaswami et al., 2000). This low systemic absorption is however desirable, since inhalation therapy mainly focuses on the topical treatment of lung inflammations, and the potential of any systemic adverse events (mainly cardiovascular and non-pulmonary effects) should be minimized.

Prediction of absorption parameters, free drug concentration in the lungs and systemic exposure levels following inhalation drug delivery is key to the successful development of novel inhaled medicines (Ehrhardt, 2017). The aim of inhalation therapy is to deliver drug to the lungs, where it exerts a local therapeutic effect. Almost all of the drug that is deposited in the lung will be absorbed systemically, however, a large proportion of the administered dose will be deposited in the oropharynx. After being swallowed, some of this drug can be further absorbed into the systemic circulation from the gut, contributing to the total systemic levels of the drug (Pritchard, 2001). In fact, it has been demonstrated by numerous lung deposition studies, that most of the inhaled drug does not undergo pulmonary absorption, but is deposited (either after swallowing or from the mucociliary clearance) in the GI tract and can enter the general circulation. Even with optimal inhalation conditions, most of the drug (60–90%) is impacting the oropharynx and the upper airways and is subsequently swallowed, with a much smaller fraction (10–20%) reaching the lungs (Figure A.6) (Cazzola et al., 2002; Lipworth, 1996; Pritchard, 2001).

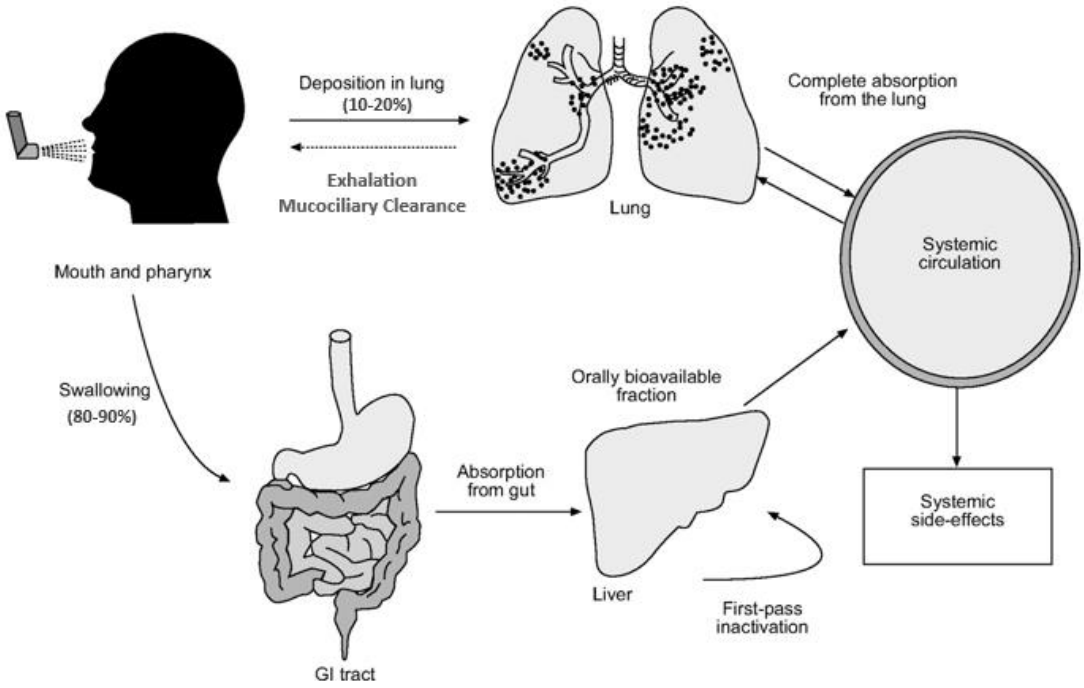

Figure A.6. Schematic representation of the fate of an inhaled corticosteroid. Adapted from (Derendorf, 1997).

Apart from the use and type of inhalation device, an important determinant for the relative drug deposition to the lungs or the GI tract is the drug particle size, with the reduction of particle size within an optimal size range (0.5–6 μm) leading to increased pulmonary deposition (Labiris and Dolovich, 2003; Mobley and Hochhaus, 2001; Tena and Clarà, 2012). Optimum drug delivery to the conducting airways occurs with particles ranging from 2.5 to 6 μm, whereas particles below 2.5 μm are deposited mainly in the alveoli (Figure A.7) (Pritchard, 2001).

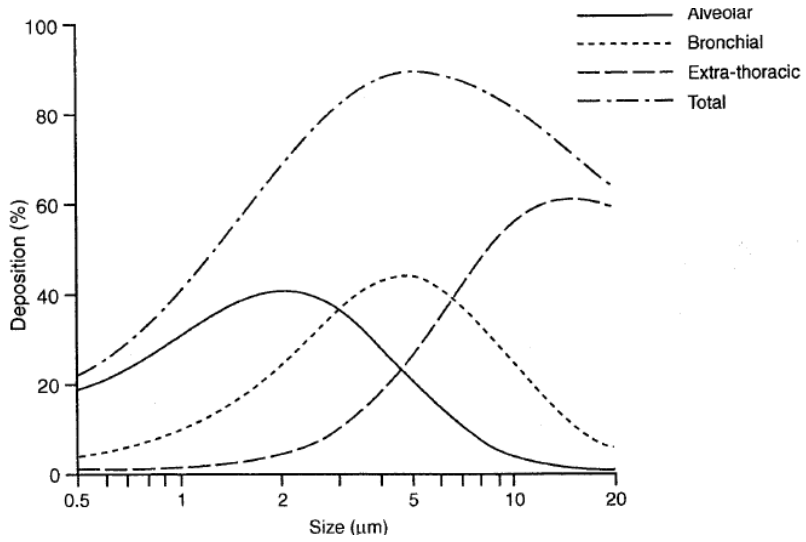

Figure A.7. Extent and site of lung deposition of inhaled particles relative to their size. Adapted from ref. (Pritchard, 2001).

The environment that inhaled particles encounter following lung deposition determines their pharmacokinetic performance and hence, deserves a closer look (Ehrhardt, 2017). The lung is not a homogenous organ and for this reason drug deposited in the airways may not exert the same kinetics as drug deposited in the alveoli (Pritchard, 2001). Complex absorption kinetics for inhaled drugs, like multiple parallel pulmonary absorption processes, has been described in the literature (Bartels et al., 2013; Borghardt et al., 2016; Weber and Hochhaus 2015). In these publications a differentiation between a central and a peripheral lung region presenting different absorption rates has been discussed. In general, drug absorption from the alveolar space (peripheral lung regions) is often assumed to be fast due to high local perfusion, large absorption surface area, and a thin diffusion barrier. Conversely, in the conducting airways (central lung regions), absorption of inhaled drugs is found to be slower compared to the peripheral regions, due to less perfusion and thicker airway walls (Borghardt et al., 2015) .

Another point that requires special attention in pulmonary pharmacokinetics is the fact that for several lipophilic substances, pulmonary dissolution may significantly affect absorption kinetics, by acting in essence as the rate limiting step of the entire process and delaying pulmonary absorption (Horhota et al., 2015; Weber and Hochhaus, 2015). In PK analysis, such effects require special attention, as they can lead to a possible mismatching of the estimated absorption and elimination parameters, a situation referred to as '*flip-flop'* kinetics (Krishnaswami et al., 2005; Liang and Derendorf, 1998).

Apart from the dissolution limitations, delayed absorption of drugs through the lungs may also occur in some cases due to *first-pass metabolism*. Specifically, a reversible fatty acid conjugation process within the airways has been observed for some drugs, which may create a slow-release reservoir within the lung and thus increase pulmonary retention and further prolong the absorption phase of inhaled drugs (Brattsand and Larsson, 2003; Edsbacker and Brattsand, 2002) .

Taking into consideration all the above, it can be appreciated that pulmonary pharmacokinetics require special treatment and an in-depth knowledge of the underlying physiological mechanisms. The description of pharmacokinetics of inhaled drugs is much more complicated than that of other routes of administration, as it requires the development of relatively simple mathematical schemes that can adequately represent the complex absorption and disposition processes following inhalation.

Another important point is that highly variable C-t profiles are observed following inhaled administration. Likely contributors to this variation are the high variability associated with patients' inhalation techniques and the inadequate understanding of device-administration interactions, differences in absorption, distribution and elimination processes of the inhaled drug and possible differences in demographic characteristics, such as the gender, age, and body weight among others. The case becomes even more perplexing, though, in the presence of coexisting respiratory diseases and the varying degrees of symptom severity encountered in those patients (Smaldone, 2005).

A.3. Pharmacotherapeutic aspects in Pulmonary Diseases

It can be generally considered that the airway state of patients with respiratory diseases may significantly affect the pulmonary deposition and absorption of inhaled drugs (Lipworth and Clark, 1997; Vaisman et al., 1987). The lung bioavailability of an inhaled drug is dependent on respiratory disease severity with the associated airway caliber and mouth or throat deposition in those patients being highly variable (Lipworth and Clark, 1997; Svartengren et al., 1994).

A.3.1 Asthma and Chronic Obstructive Pulmonary Disease

Asthma is a highly prevalent, chronic inflammatory disease of the airways. It is characterized by airway inflammation, hyper-responsiveness and a reversible airflow obstruction (Usmani, 2015). These manifest as the triad of wheeze, cough and breathlessness (Gerritsenet et al., 1989; Murdoch and Lloyd, 2010). These symptoms are due to a combination of constriction of bronchial smooth muscle, oedema of the mucosa lining the small bronchi, and plugging of the bronchial lumen with viscous mucus and inflammatory cells (Figure A.8) (Ritter et al., 2008).

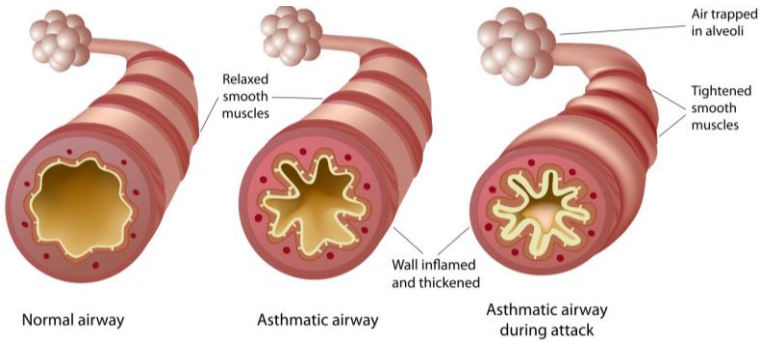

Figure A.8. Airway state in different asthma stages.
Adapted from: https://www.educationforhealth.org/asthma-pathology-of-asthma/

Asthma is a consequence of complex gene–environment interactions, with heterogeneity in clinical presentation and the type and intensity of airway inflammation (Papi et al., 2017). It is broadly categorized into non-allergic and allergic, but there is considerable overlap. In allergic asthma, which is usually of early onset, extrinsic allergens produce a type I allergic reaction in atopic subjects. Type I reactions are triggered via reaginic antibodies (IgE) on the surface of mast cells and other immune effector cells, especially activated Th2 lymphocytes, which release cytokines that recruit eosinophils and promote further IgE synthesis and sensitivity. Patients with non-allergic (late-onset) asthma do not appear to be sensitive to any single well-defined antigen, although infection (usually viral) often precipitates an attack. Inflammatory mediators implicated in asthma include histamine, several leukotrienes (LTC_4/D_4 and E_4) 5-hydroxytryptamine (serotonin), prostaglandin D_2, platelet-activating factor, neuropeptides and tachykinins. Increased parasympathetic tone due to local and centrally mediated stimuli also promotes bronchoconstriction (Ritter et al., 2008).

Signs of asthma are few and non-specific. With diverse underlying mechanisms, some asthma phenotypes might be distinguishable at the time of initial clinical presentation, but others might not be easily distinguishable from each other. No gold standard exists for diagnosis of asthma. Diagnosis is probability-based, and considers symptoms and variable expiratory airflow limitation. Asthma is heterogeneous, and for some patients, one or both of these features might not be found. Asthma treatment goals in children and adults are to minimize both the symptom burden (day-to-day symptoms, disturbed sleep, and activity limitation) and the risk of adverse asthma outcomes (exacerbations, persistent airflow limitation, and medication side-effects). Together, these two domains constitute asthma control (Papi et al., 2017).

Chronic obstructive pulmonary disease (COPD) is another debilitating chronic lung disorder with a wide prevalence and considerable morbidity worldwide (Csikesz and Gartman, 2014). In addition to the increased morbidity, COPD decreases patients' quality of life due to shortness of breath and chronic cough, which can progress over years to chronic hypoxemic and/or respiratory failure. Cigarette smoking is the major known risk factor; however, it remains unknown why only 15–20% of those that smoke develop COPD. In addition, the factors that contribute to this variability in susceptibility remain undetermined (Ariel et al., 2018; Van de Moortele et al., 2017).

COPD is characterized by progressive airflow limitation that is not fully reversible (Hassett et al., 2014). The pathological abnormalities of COPD are associated with lung inflammation, imbalances of proteinase and antiproteinase, and oxidative stress, which are induced by noxious particles and gases in susceptible individuals. The physiological changes of COPD are mucus hyper-secretion, ciliary dysfunction, airflow limitation, pulmonary hyperinflation, gas exchange abnormalities, pulmonary hypertension and systemic effects. The airflow limitation principally results from an increase in the resistance of the small conducting airways and a decrease in pulmonary elastic recoil due to emphysematous lung destruction (Kim and Lee, 2005).

Implementation of an effective management strategy is required to reduce symptoms, preserve lung function, quality of life, and exercise capacity. Management of COPD focuses primarily on reducing exposure to risk factors, alleviating respiratory symptoms, preventing exacerbations, and treating COPD-related co-morbidities (Ariel et al., 2018; Falk et al., 2008).

A.3.2. Treatment Options

The primary objectives of the pharmacological management of asthma and COPD are to obtain full symptom control, prevent exacerbations and achieve the best possible pulmonary function, with minimal side effects (Ritter et al., 2008). Treatment guidelines encourage a ‘step-up’ approach in pharmacological treatment to achieve disease control and a ‘step-down’ strategy when the disease is under control. In this strategy, inhaled drug therapy remains the foundation in managing those patients. Inhalation has long been established as an effective way to deliver drug to the lungs to manage respiratory diseases. Compared to oral tablets, inhaled medicines are delivered directly to the airways and allow for a smaller dose to be administered leading to a quicker onset of action and minimizing of adverse effects. A range of devices is used to deliver an inhaled drug. These include pressurized metered-dose inhalers (pMDIs), spacers, nebulizers and dry-powder inhalers (DPIs) (Ehrhardt, 2017; Usmani, 2015).

- **Pressurized metered-dose inhalers**

The development of the first commercial pMDIs was carried out by Riker Laboratories in 1955 and marketed in 1956 as the first portable, multi-dose delivery system for bronchodilators. Since that time, the pMDI has become the most widely prescribed

inhalation device for drug delivery to the respiratory tract to treat obstructive airway diseases such as asthma and chronic obstructive pulmonary disease (Lavorini, 2013). The pMDI is a multi-dose device that consists of an aluminum canister, lodged in a plastic support, containing a pressurized suspension or solution of micronized drug particles dispersed in propellants (Figure A.9). A surfactant (usually sorbitan trioleate or lecithin) is also added to the formulation to reduce the particle agglomeration and is responsible for the characteristic taste of specific inhaler brands. The key component of the pMDI is a metering valve, which delivers an accurately known volume of propellant, containing the micronized drug at each valve actuation. Pressing the bottom of the canister into the actuator seating causes decompression of the formulation within the metering valve, resulting in an explosive generation of a heterodisperse aerosol of droplets that consist of tiny drug particles contained within a shell of propellant. The latter evaporates with time and distance, which reduces the size of the particles that use a propellant under pressure to generate a metered dose of an aerosol through an atomization nozzle (Figure xxx) (Lavorini, 2013).

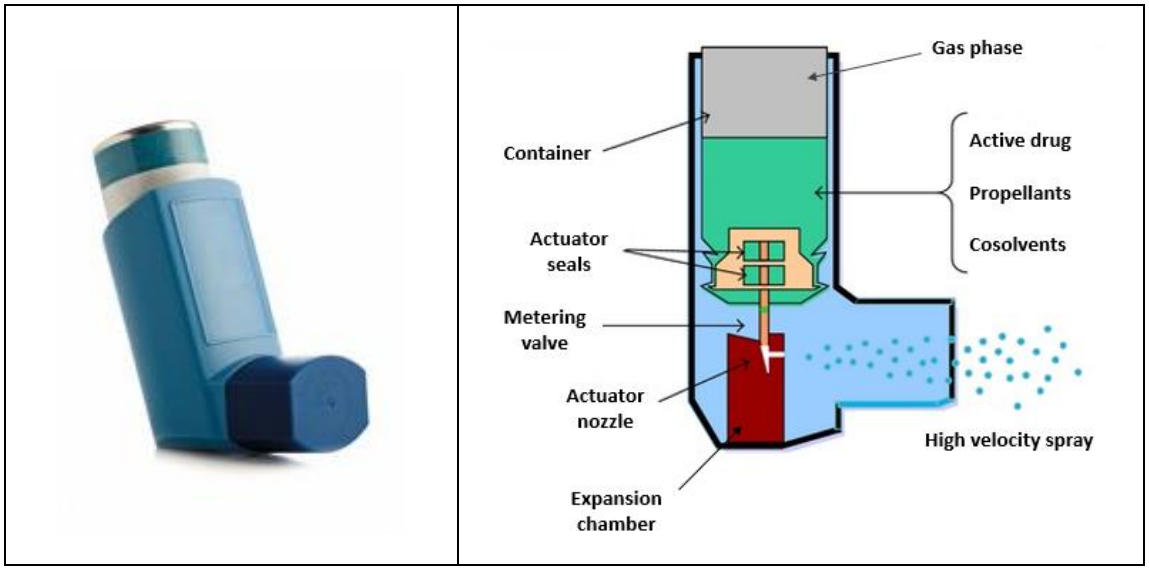

Figure A.9. A pressurized metered-dose inhaler and its components.
Adapted from ref. (Lavorini, 2013).

The recommended inhalation technique from a pMDI is to comfortably breathe out, place the inhaler in the mouth between the lips, then actuate at the start of a deep breath and undertake a slow inhalation lasting for five seconds, followed by a breath-hold pause of ten seconds. A deep and slow inhalation avoids drug depositing in the throat, as on actuation of the pMDI canister the drug spray is forced out at a high velocity. Patient co-

ordination between inhalation and actuation can be a problem with pMDIs especially in elderly patients with difficulties in manual dexterity and handling (Usmani, 2015).

In addition to handling difficulties, other drawbacks of pMDIs are related to aerosol formulation and generation. Pressurized MDIs may contain surfactants, such as oleic acid, that could pose a risk of inducing bronchospasm in patients suffering from advanced airway hyperactivity. Also, the large size and high velocity of many droplets leaving the pMDI nozzle produce extensive oropharyngeal deposition (up to 90% of the dose), although this can be reduced by using a spacer or add-on device (FDA, 1999).

Spacer devices are an extension attachment to the pMDI device and simply provide a 'space' and distance between the patient's mouth and the inhaler device to slow down the high velocity of the emitted aerosol cloud (Figure A.10).

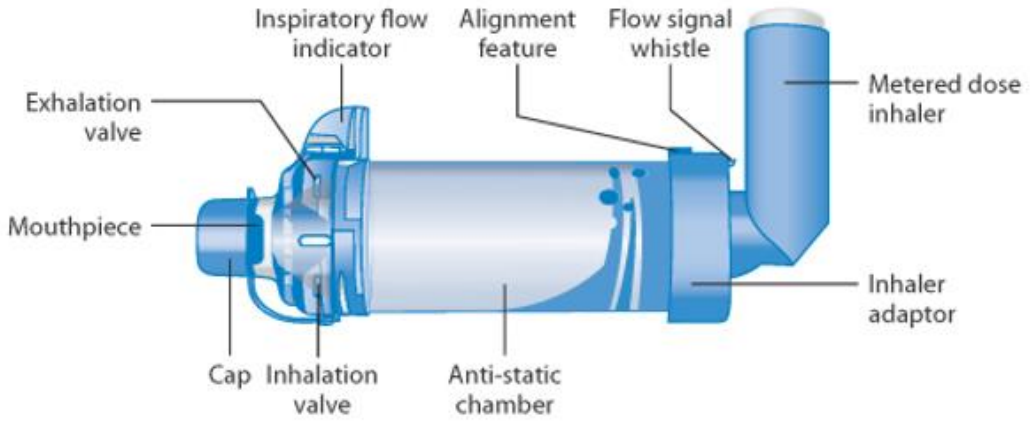

Figure A.10. Diagram of a holding chamber or spacer for use with a pressurized metered-dose inhaler. Adapted from: https://basicmedicalkey.com/paediatric-and-geriatric-formulations/

This leads to reduced throat deposition and allows time for greater evaporation of the propellant, leading to relatively smaller drug particles that have greater potential to deposit within the lungs. One consideration is that electrostatic charge on the walls of plastic spacers can decrease the amount of drug that will be deposited in the lungs. However, in case of an emergency scenario, spacer attachments with pMDIs are as effective as nebulizers in the management of patients with asthma exacerbations (Usmani, 2015).

➢ Nebulizers

Ultrasonic and jet nebulizers are those commonly used in clinical practice (Figure A.11). Ultrasonic nebulizers work by using high frequency vibrations directed at the drug liquid in order to generate aerosol clouds for inhalation. Generally, compared with conventional pMDI and DPI inhalers, nebulizer devices lack portability, are large and have longer treatment times.

Figure A.11. Different types of nebulizers: ultrasonic nebulizer (left), jet nebulizer (right).

The recommended inhalation technique from nebulizers requires comfortable tidal breathing and there is little need for patient co-ordination. Attention should be given to the nebulizer/facemask combination and its correct insertion to avoid drug depositing on the face and eyes, especially in children. However, between the many devices there are great differences in the aerosol output, and the inhalation manoeuvres being used by the patient will affect drug delivery to the lungs; for example, crying or shallow and rapid inhalations can decrease the amount of drug delivered to the lungs. New nebulizer devices are being developed that allow an improvement in the amount of drug reaching the lungs (Usmani, 2015).

➢ Dry powder inhalation devices

Last but not least, *dry powder inhalers* are considered as one of the most attractive drug delivery system for the treatment of asthma and COPD (Frijlink and De Boer, 2004; Olsson et al., 2011). The over-riding consideration for long-term basic care in Europe is often a dry powder inhaler. Several studies have shown that DPIs are at least as effective as pMDIs with a spacer in most patients (Ehrhardt, 2017). Many companies are now

prioritizing the development of dry powder inhalers above pressurized formulations for asthma drugs. It has been shown that a well-designed DPI and an appropriate powder formulation can optimize the effectiveness of inhaled drug therapy (FDA, 1999).

A.3.2 Dry powder inhalers

Dry powder inhalation devices are convenient and efficient drug delivery systems. In London in 1864, Newton first patented an inhaling apparatus for the delivery of dry powder medications (Sanders, 2007). DPIs are used to treat respiratory diseases such as asthma and COPD and other pulmonary diseases such as cystic fibrosis and pulmonary infectious diseases, as well as systemic disorders such as diabetes, cancer, neurological diseases (including pain). The efficacy of DPIs is highly dependent on the patient's inspiratory effort (Usmani, 2015). A DPI must be able to deliver medications effectively for most patients, and an ideal inhaler would provide a dose that does not significantly vary with inspiratory flow rate (FDA, 1999).

DPIs are propellant-free and usually contain powdered drug particles that are formulated as either pure drug or mixed with an inactive excipient (Usmani, 2015). Powder blends contain micronized particles of the drug with an excipient, usually lactose, which may be micronized, but which more often comprises larger ''carrier'' particles. The use of excipients can help to improve dose uniformity, partly because a larger mass of powder is generally easier to meter accurately. Under specific manufacturing conditions, the micronized particles can be combined to form stabilized agglomerates with controlled uniformity and hardness. Agglomerates of drug particles, or of drug and lactose, must be deagglomerated by shear forces during inhalation, producing fine particles which are carried by the airflow into the lungs (Figure A.12). Particles below 5μm in size can be distributed deep into the smaller airways and this penetration correlates with good clinical response (FDA, 1999).

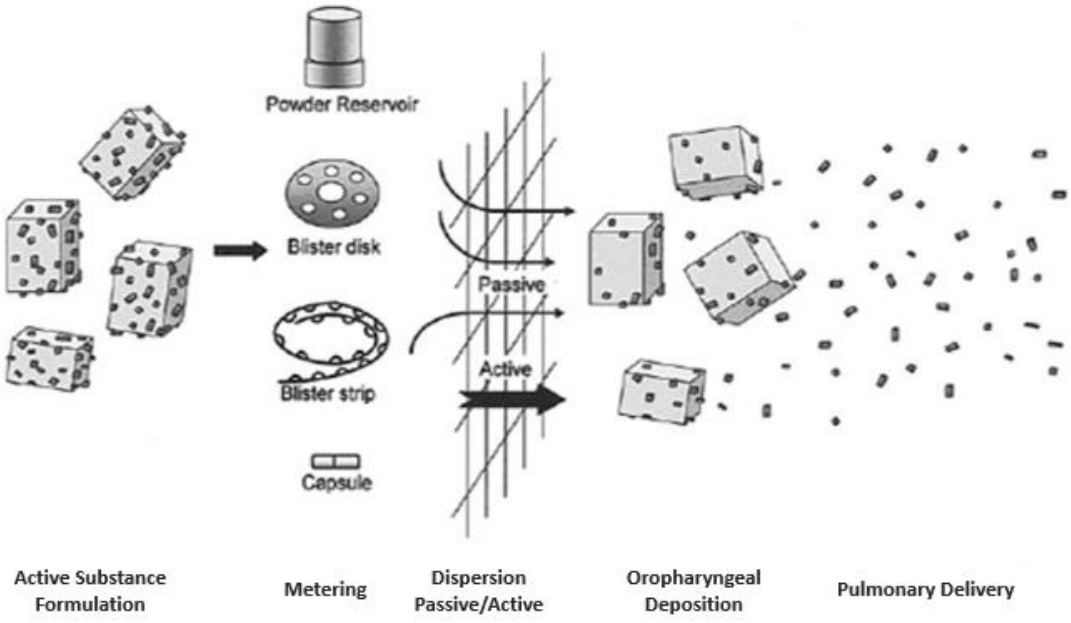

Figure A.12. Principle of dry powder inhaler design. Adapted from ref (Thorat et al., 2015).

DPIs come in a variety of devices. Figure A.13 shows some examples of dry powder inhalation devices currently available in the market. The design of a DPI must be coordinated with the formulation of the drug. Inhaler design, particularly the geometry of the mouthpiece, is critical for patients to produce an airflow sufficient to lift the drug from the dose chamber or capsule, break up the agglomerates in a turbulent airstream, and deliver a dose to the lungs as therapeutically effective fine particles (FDA, 1999).

Figure A.13. Dry powder inhalers available in market.

DPIs can be classified by the number of doses the device can carry, the patient contribution to aerosolize the powder, or by the mechanism of powder dispersion (Ibrahim et al., 2015).

By the number of doses the device can carry, DPIs can be classified into three different categories, i.e. single-unit dose, multi-unit dose, and multi-dose reservoirs (Figure A.14) (Ibrahim et al., 2015). In "single-dose" devices, individual doses are provided, usually in gelatin capsules, and have to be loaded into the inhaler before use. Single-dose DPIs can further be classified as *disposable* or *reusable* (FDA, 1999; Ibrahim et al., 2015). With a *disposable* single-dose DPI, the powder-containing capsule is placed in a holder inside the DPI, the capsule is opened within the device, and then the powder is inhaled. The spent capsule must be discarded after use and a new capsule inserted for the next dose. Although these single-dose devices have performed well in clinical use for many years, the main criticism of them is the cumbersome nature of loading the capsule, which might not be easily accomplished by a patient who is undergoing an asthma attack and requires immediate delivery of the drug. In addition, elderly patients may not have the manual dexterity to accomplish all the necessary maneuvers to take the capsule from the package, load it, and pierce the capsule in the device. {26} Given the inherent limitations of unit-dose devices, since the past decade or so there has been considerable focus on developing multi-dose DPIs (Atkins, 2005).

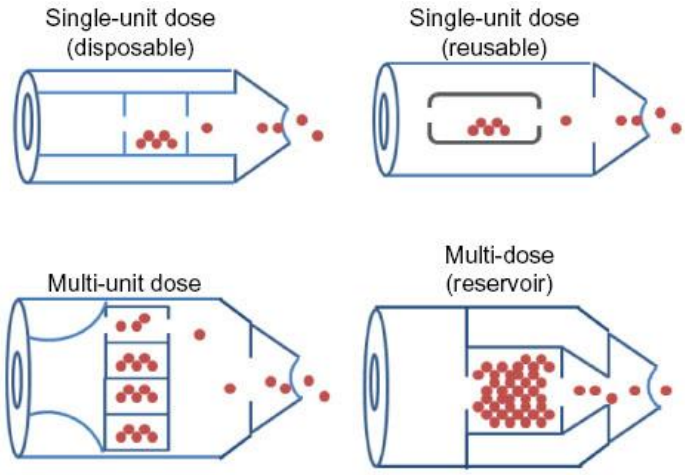

Figure A.14. Different types of dry powder inhalers classified by the number of doses. Adapted from ref (Ibrahim et al., 2015).

"Multiple unit dose" inhalers contain a number of individually packaged doses, either as multiple gelatin capsules or in blisters (Figure A.15) (FDA, 1999). In such type of devices, drug is stored in a bulk powder reservoir, from which individual doses are metered. Multi-

dose devices incorporating powder reservoirs are generally capable of delivering more than100 metered doses, providing a level of convenience equivalent to a pMDI (FDA, 1999). These devices use factory-metered and sealed doses packaged so that the device can hold multiple doses at the same time without having to be reloaded (Ibrahim et al., 2015). Multiple unit dose devices may offer other advantages in terms of more accurate metering of individual doses and better protection against ingress of moisture, but are generally more expensive to produce (FDA, 1999).

Figure A.15. Design of a multiple unit dose dry powder inhaler.

Based on the mechanism for powder aerosolization, DPIs can be also classified as *passively*- or *actively*-actuated devices. The original passive DPI was a breath-actuated device, relying solely on the patient's inspiration to provide sufficient air flow for entrainment and de-aggregation of the formulation. Device actuation was intrinsically tied to the patient's inhalation, thus avoiding coordination issues associated with pMDIs. The main issue with passive DPIs was the lack of uniformity between the inspiratory force among patients with different age and disease state, as well as variation in the inspiratory force of the same patient. These variations significantly affect dose uniformity, even when the same device is used. Active (power assisted) DPI devices are designed with an internal energy source to aerosolize the powder bed in the DPI, so that dose administration is no longer dependent on the patient inspiratory flow rate. This energy source can be a battery, compressed gas, or a spring mechanism. In active devices, the powder is dispersed by vibration, gas discharge, or an impeller. The motor is activated by a very low breathing rate, which is convenient for asthmatic patients. Although active DPIs appear easier to use

than passive DPIs, none of these advanced devices has been marketed yet (Ibrahim et al., 2015).

Factors to consider when choosing between individual DPIs to adequately deliver the drug to the patient include: the need to be held in the correct position; not blowing into the device/mouthpiece prior to inhalation; and some capsule devices requiring more than one inhalation. In general, the patient should comfortably breathe out, hold the inhaler in the correct position, place the inhaler in the mouth between the lips and then inhale deep and fast followed by a breath-hold pause of ten seconds (in most devices). Newer DPIs have recently been developed that do not rely so critically on the patient's inspiratory effort, needing gentler and slower inhalation flows than conventional DPI devices to achieve optimal drug delivery to the lungs (Usmani, 2015).

Treatment with inhalation devices allows the administration of relatively low doses of drugs, since these are delivered directly to the site of inflammation, achieving high local pulmonary concentrations. This in turn leads to a high therapeutic ratio and minimization of the systemic adverse effects (Lipworth, 1996). In view of the therapeutic effectiveness of inhaled drug therapy, research and development efforts have predominantly focused on the development of new but also generic inhalation devices, drugs and formulations thereof (Ehrhardt, 2017). However, a rigorous evaluation and comparison of the clinical performance of such products is requisite, and questions like what happens to the inhaled particle after landing, how it interacts with its environment and what the environment does to the drug particle have to be satisfactorily addressed.

A.4. Equivalence of orally inhaled medicinal products

When the patent expires for drug entities, generic drugs are manufactured that are less expensive than brand name products. This is because the drug company manufacturing the generic drug does not have to prove that the drug is safe and effective since those studies were done by the pharmaceutical company producing the brand name drug. An indispensable attribute of a generic drug dosage form is that it produces the same plasma C-t profile as its brand name counterpart (Bauer, 2008). As the relationship between the drug levels and the effects is very often independent on the formulation, formulations which produce superimposable drug levels can be considered interchangeable and this is the basis of the concept of bioequivalence (Urso et al., 2002).

Bioequivalence (BE) is actually the comparison of the bioavailability of two drug products. It is defined as the absence of a significant difference in the rate and extent to which the active ingredient or active moiety in pharmaceutical equivalents or pharmaceutical alternatives becomes available at the site of drug action when administered at the same molar dose under similar conditions in appropriately designed studies (FDA, 2003).

The basis of a BE study is the comparison of the drug product to be tested with an appropriate reference product (branded innovator drug product). In BE studies the systemic exposure profile of a test (T) drug is compared to that of a reference (R) drug product. Generally single-dose pharmacokinetic studies are recommended for both immediate- and modified-release drug products as they are more sensitive in assessing the active ingredient released from drug into circulation. For assessing BE of two formulations of a drug, two-sequence, two-period, crossover study is usually conducted after administration of a single dose under fasted conditions (Figure A.16). In crossover design, the subjects serve as their own controls and they crossover from one treatment to the other. Parallel studies are appropriate if the drug has extremely long half-life, repeated pharmacokinetic profile is difficult to obtain, or residual pharmacodynamic effects are relevant (Noreddin, 2012).

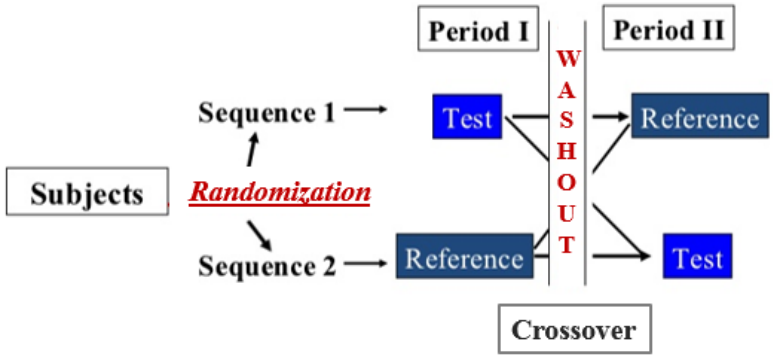

Figure A.16. Design of a two-sequence, two-period, crossover bioequivalence study. Adapted from: https://www.slideshare.net/bhaswatchakraborty/abe-ibe-pbe.

Bioequivalence for most orally administered medicinal products is demonstrated *in vivo* by comparing the rate and extent of absorption, that is comparing the bioavailability of the generic product with that of the innovator product. This is done by measuring the active ingredient and when appropriate, its active metabolites in blood, plasma, serum or other biological fluids over a certain period of time for the test and reference drug,

respectively. By doing so, BE assessment then relies on the comparison of pharmacokinetic measures, such as area under the concentration-time curve (AUC), the maximum concentration (Cmax), and time that the maximum concentration occurs (Tmax) (Noreddin, 2012).

The concepts of peak exposure (Cmax), its time (Tmax) and overall exposure (AUC) have proven extremely useful in the evaluation of comparative bioavailability of the different drug formulations (Bonate and Howard, 2005). With the exception of Tmax parameter, both AUCs and Cmax are analyzed using the recommended statistical test procedures to determine if the average values between the T and R products are comparable. To establish bioequivalence, the calculated 90% confidence interval for these two parameters should fall within the BE range, i.e. 80-125%. This is equivalent to the rejection of two one sided t-tests, with the null hypothesis of non-bioequivalence at 5% level of significance. The non-parametric 90% confidence interval (CI) for Tmax should also lie within a clinically acceptable range (EMA, 2010; FDA, 2003). The most widely used commercial software package for BE and non-compartmental analyses is Phoenix® WinNonlin®, which offers an integrated tool for data processing and is a software particularly useful in drug development setting (https://www.certara.com).

The regulatory framework regarding the comparisons between orally inhaled drugs is a field of ongoing evolution. Demonstration of therapeutic equivalence for inhaled drug products presents a unique challenge, since the traditional PK approach used for systemically acting drugs is not directly applicable to the BE of these medicinal products that deliver drugs directly to the site of action, that is the lung. In fact, it is suggested that the conduct of a BE study may not always be sufficient to establish therapeutic equivalence of these locally acting drugs (Lu et al., 2015).

In this vein, not all regulatory authorities share the same thinking on the approaches used to demonstrate equivalence and no universal guidance exists for the establishment of bioequivalence of locally acting inhaled drugs (Apiou-Sbirlea et al., 2013). The European Medicines Agency (EMA) currently suggests a stepwise evaluation of *in vitro* and *in vivo* pharmacokinetic and pharmacodynamics studies, while the US Food and Drug Administration (FDA) endorses an 'aggregate weight of evidence' approach for establishing the BE of inhalation drugs (Apiou-Sbirlea et al., 2013; Lu et al., 2015). In a recent article discussing the reports form the 'Orlando inhalation conference', it was noted

that pharmacokinetics studies may serve as the most appropriate methodology for assessing BE (Hochhaus et al., 2015). However, the issue whether PK studies represent the most sensitive marker of BE is still under extensive discussion (Hendeles et al., 2015).

Even though the performance of a bioequivalence study is not always considered sufficient to establish therapeutic equivalence between two locally acting orally inhaled drugs (Lu et al., 2015), and certain critical issues when conducting such studies exist (Thakkar et al., 2015), PK studies are still considered the most sensitive methodology in detecting differences between two inhalation drug products (Hochhaus et al., 2015). Particularly in cases where a drug substance exhibits negligible gastrointestinal bioavailability or oral absorption can be prevented through an activated charcoal scheme, plasma PK studies are considered the most sensitive methodology in this respect (Hochhaus et al., 2015). Besides, the additional application of PK modeling approaches based on data derived from PK studies may be also used as an alternative method for determining the pulmonary fate of two inhaled products and can serve as surrogate evidence in the demonstration of their bioequivalence (Al-Numani et al., 2015).

A.5. Pharmacokinetic analysis

Knowledge of a drug's PK behavior following either oral or inhaled administration is very important, since an increasing number of different medicinal products, novel or generics make their appearance on the market and require clinical assessment. Pharmacokinetic analysis aims at investigating the absorption, distribution, biotransformation, and elimination processes of a drug administered to a living organism. When analyzing pharmacokinetic data, one generally employs either model fitting using nonlinear regression analysis or non-compartmental analysis techniques. The method one actually employs depends on what is required from the analysis. If the primary requirement is to determine the degree of exposure following administration of a drug (such as AUC), and perhaps the drug's associated pharmacokinetic parameters, such as clearance, elimination half-life, Tmax, Cmax, etc., then non-compartmental analysis is generally the preferred methodology to use in that it requires fewer assumptions than model-based approaches (Gabrielsson and Weiner, 2012).

A.5.1 Non-compartmental Analysis – Bioequivalence

Non-compartmental analysis (NCA) methods have been used in pharmacokinetics for many years. Until today this approach has been used to describe most aspects of the pharmacokinetic behavior of drugs and still represents an essential component of the PK analysis package for regulatory submissions (Bonate and Howard, 2005). The non-compartmental analysis provides a framework to introduce and use statistical moment analysis to estimate pharmacokinetic parameters. Non-compartmental PK analysis methods provide a means for data reduction in a wide range of settings with a minimum number of assumptions. Despite the limited assumptions required, NCA allows the estimation of the most basic PK parameters characterizing the absorption, distribution and elimination processes of a drug following single- or repeated-dosage regimens (Bonate and Howard, 2005). The total drug exposure may be well summarized by Cmax, Tmax, AUC and $t_{1/2}$. A short description of these parameters is presented below:

Tmax and Cmax

The peak time (Tmax) and the peak concentration (Cmax) may be directly obtained from the experimental observations of each subjects. Following drug administration, Cmax and Tmax are dependent on the extent and rate of drug absorption and on the disposition profile of the drug, consequently these may characterize the absorption rate of different formulations in the same subject. The under the curve (AUC) is a parameter that may be used in different ways depending on the experimental context. This parameter may be used as an index of the drug exposure of the body, when referred to the plasma drug levels, or as an index of the drug exposure of particular tissues if referred to the drug levels in tissues. Under very general assumptions, the area under the plasma or blood drug concentrations is a parameter that is closely dependent on the drug amount that enter into the systemic circulation and on the ability that the system has to eliminate the drug (clearance). Therefore, it can be used to measure the drug amount absorbed or the efficiency of physiological processes that characterize drug elimination. In most cases, a sufficiently accurate estimate of the AUC can be obtained by applying the trapezoidal rule (numerical integration) as illustrated in (Urso et al., 2002). As depicted in Figure A.17, the rule involves treating the area under a plasma concentration–time curve as a series of trapezoidal slices and approximates the integration over an interval by breaking the area down into more easily computable areas. Due to the dependence on the length of x in the trapezoidal rule, the area estimation is highly dependent on the blood/plasma sampling

schedule. That is, the closer time points are, the closer the trapezoids reflect the actual shape of the concentration-time curve.

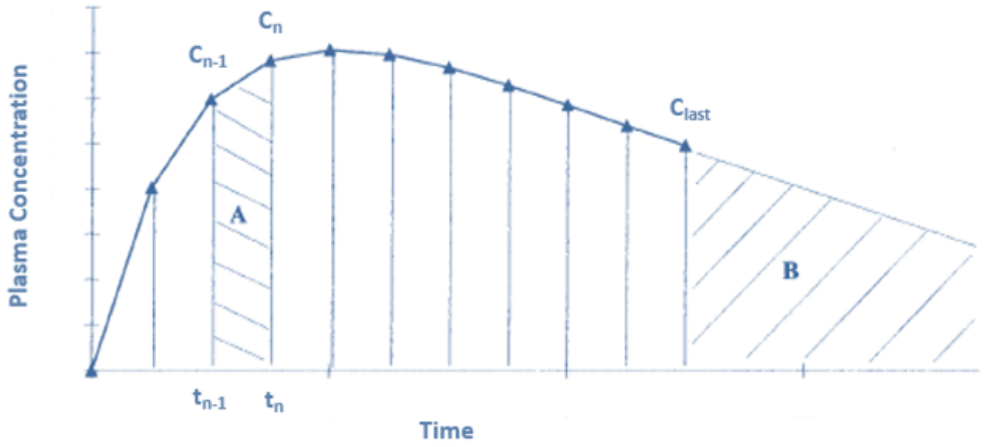

Figure A.17. The area under the curve (AUC) and the trapezoidal rule. The AUC is given by the sum of all trapezoids and of the terminal extrapolation B. The dimensions of the AUC are always given by the time x concentration. Adapted from ref (Urso et al., 2002).

Elimination Half-life ($t_{1/2}$)

The terminal half-life ($t_{1/2}$) is a parameter used to describe the decay of the drug concentration. It is the time required for the amount of drug (or concentration) in the body to decrease by half. For the determination of half-life in non-compartmental PK analysis, the terminal data from a concentration-time plot are used. Plotting the logarithms of the concentrations or using a semi-logarithmic scale, a straight line can be obtained in the terminal phase (Urso et al., 2002). Assuming first-order kinetics, the slope (λz) of the terminal phase offers a way for estimating elimination half-life through the relationship:

$$t_{1/2} = \frac{ln2}{\lambda z} \qquad \text{(Eq. 1)}$$

NCA methods permit model-independent analyses and provide an empirical description of the correlation between the dose administered and measured drug concentrations. The results generated by NCA can be further used to formulate a rationale for decision-making in various disciplines of drug development. One such discipline is the bioequivalence assessment of medicinal products (as presented in section A.4).

As described above, NCA can summarize the C-t profile of a drug into simple and useful pharmacokinetic parameters. Besides, NCA can also provide an initial descriptive analysis of the pharmacokinetic properties for use in subsequent, mechanistic model-based

strategies. Model-driven approaches are developed to obtain a better understanding of the biological or physicochemical events, responsible for or associated with the observed effects. Considering that drug development is an information-gathering process, the role of PK models remains crucial for the investigation of drug properties and the interaction mechanisms with the biological systems (Bonate and Howard, 2005).

A.5.2 Population Pharmacokinetic Analysis

Population pharmacokinetic (POPPK) analysis, in contrast to classical or traditional pharmacokinetic approaches, focuses on the central tendency of a pharmacokinetic parameter across an entire population, and its deviations from that central tendency in a subgroup of individual patients (Greenblatt et al., 2002). POPPK modeling is not a new concept; it was first introduced in 1972 by Sheiner *et al*. (Sheiner et al., 1972). Although this approach was initially developed to deal with sparse PK data collected during therapeutic drug monitoring, it was soon expanded to include models linking drug concentration to response (e.g., pharmacodynamics). Thereafter, PK modeling has grown to become an important tool in drug development and individualized therapy worldwide (FDA, 1999; Mould and Upton, 2012), with the first reports associated with population pharmacokinetic modeling in Greek litetarute appearing in 2003 (Inclan et al., 2005; Lukas et al., 2004; Macheras and Lukas, 2003).

A primary goal of most population pharmacokinetic modeling analyses is determining the population PK parameters and the sources of PK variability in a population. Other goals include relating and predicting the plasma concentrations to the administered drug doses through identification of predictive covariates in a target population (Mould and Upton, 2013). In contrast to traditional pharmacokinetic evaluation, the population PK approach encompasses some or all of the following features (FDA, 1999):

- The collection of relevant pharmacokinetic information in patients who are representative of the target population to be treated with the drug.
- The identification and measurement of variability during drug development and evaluation.
- The explanation of variability by identifying factors of demographic (weight, gender, age, etc.), pathophysiological, environmental, or concomitant drug-related origin that may influence the pharmacokinetic behavior of a drug.
- The quantitative estimation of the magnitude of the unexplained variability in the patient population.

In population pharmacokinetics the nonlinear mixed-effects modeling approach is most commonly implemented, in which data from all individuals in a population are evaluated simultaneously. “Nonlinear” refers to the fact that the dependent variable (e.g., concentration) is nonlinearly related to the model parameters and independent variable(s).

"Mixed-effects" refers to the parameterization: parameters that do not vary across individuals are referred to as "fixed effects," parameters that vary across individuals are called "random effects" (Mould and Upton, 2013). Analysis according to the nonlinear mixed-effects model provides estimates of population characteristics that define the population distribution of the pharmacokinetic parameter (FDA, 1999). A nonlinear mixed-effects modeling approach to the population analysis of pharmacokinetic data, therefore, consists of estimating directly the parameters of the population from the full set of individual concentration values. The individuality of each subject is maintained and accounted for, through the quantification of the variability observed across the population subjects (FDA, 1999).

Model Development

In the broadest sense, models are representations of a "system" designed to provide knowledge or understanding of its function. Generally, models are simplified representations of systems, and it is the simplification that can make them useful. The nature of the simplification is related to the intended use of the PK model. Models are therefore better judged by their "fitness for purpose" rather than for being "right" or "true" (Mould and Upton, 2012).

In this context, PK models provide a basis for describing and understanding the time-course of drug exposure and response in a biological system (Mould and Upton, 2012). Using models, new meaningful pharmacokinetic parameters may be defined which can be used to find relationships between the drug kinetic profile and the physiological process which drive the drug absorption, distribution and elimination (Urso et al., 2002). PK models usually consist of "compartments" - a region of the body in which the drug is well mixed and kinetically homogenous. Compartments have proven to be ubiquitous and fundamental building blocks of PK models, with differences between models often being defined by the way the compartments are connected. These compartments can sometimes be real physiologic spaces in the body (such as the blood or the liver), but usually are abstract concepts that do not necessarily represent any particular region of the body (Mould and Upton, 2012). Nevertheless, compartmental models allow to define easily the clearance of a drug which is dependent on the drug elimination process, or the volume of distribution which depends on the drug distribution in the tissues. Moreover, the compartmental models allow to describe more complex kinetic process of a drug (e.g.

enterohepatic recycling) and make predictions for relationships between the drug dose and its PK profile (Urso et al., 2002).

Population models are comprised of three main components, i.e. the structural model, the stochastic or statistic model, and the covariate model. Structural models are functions that describe the time course of a measured response, and can be represented as algebraic or differential equations. Stochastic models describe the variability or random effects in the observed data, and covariate models describe the influence of factors such as demographic characteristics or environmental factors on the time course of a drug (Mould and Upton, 2012). Six major aspects have to be considered when developing a population pharmacokinetic model: (i) the data interpretation, (ii) the structural model, (iii) the stochastic/statistical model, (iv) the covariate model, (v) model evaluation, and (vi) the modeling software employed for the analysis. All these components are briefly described below.

I) Data Interpretation

- *Exploratory Data Analysis*

Generating data for population analysis is one of the most critical and time-consuming portions of the evaluation. Data should be scrutinized to ensure accuracy. Exploratory data analysis isolates and reveals patterns and features in the population data set using graphical and statistical techniques (Mould and Upton, 2013). An important element of the exploratory approach is its flexibility, both in tailoring the analysis to the structure of the data and in responding to patterns that are uncovered by successive analysis steps. Most population PK analysis procedures are based on explicit assumptions about the data, and the validity of the analyses depends upon the validity of assumptions. For example, determining whether the data must be parent drug or an active metabolite is important. If a drug has an active metabolite, describing metabolite formation may be crucial in understanding clinical properties of a drug (Mould and Upton, 2013). Exploratory data analysis techniques provide powerful diagnostic tools for confirming assumptions or, when the assumptions are not met, for suggesting corrective actions (FDA, 1999).

- *Handling Missing Data and Outliers*

After assembling data for population analysis, the issue of any missing data should be addressed, since they represent a potential source of bias. Thus, every effort should be

made to reduce the amount of missing data. If there is a pattern to the missing data, appropriate statistical procedures should be used to address the problem. Some simple methods of imputation of missing data include the use of median, mean, mode for missing values, or maximum likelihood procedures for predicting each predictor from all other predictors. However, if the concentration data are missing randomly, the process that caused the missing data can be ignored and the observed data can be analyzed without regard to the missing data (FDA, 1999).

During data cleaning and initial model evaluations, data records may also be identified as erroneous (e.g., a sudden, transient decrease in concentration) and can be commented out if they can be justified as an outlier or error that impairs model development (Mould and Upton, 2013). The statistical definition of an outlier is, to some extent, arbitrary. A distinction should be made between outlying individuals (inter-subject variability) and outlier data points (intra-subject variability) (FDA, 1999).

- *Below the limit of quantification (BLQ) data*

All assays have a lower concentration limit below which concentrations cannot be reliably measured that should be reported with the data. BLQ data are generally censored but in some cases may be also considered as missing data. Several methods to handle BLQ data statistically as censored observations have been proposed (Jusko, 2012). In population-modeling methods, however, censoring may account for differences in the results when applied to the same data set (Mould and Upton, 2013).

II) Structural Model

Structural models describe the typical concentration time course of a drug within the population. The choice of the structural model has implications both on PK parameter estimation and covariate selection. Therefore, an extra care should be taken when evaluating structural models (Mould and Upton, 2013).

Model building is a complex multistep process where new hypothesis are proven and disproven through a continuous interaction between the experimenter and the computer (Urso et al., 2002). Structural models are usually represented in the form of ordinary differential equations, representing physiological or empirical compartments, where the change of a variable over time is described (Mould and Upton, 2012). The structural model is analogous to a disposition model (describing kinetics of distribution and elimination)

and an absorption model (describing the drug uptake into the systemic circulation following an extravascular administration). An insight into the appropriate compartment number can be gained by plotting the log concentration of a drug vs. time. Each distinct linear phase when log concentrations are declining will generally need its own compartment (Mould and Upton, 2013). Figure A.18(A,B) shows an example of a two-compartment model with the respective C-t plots in normal and log scale.

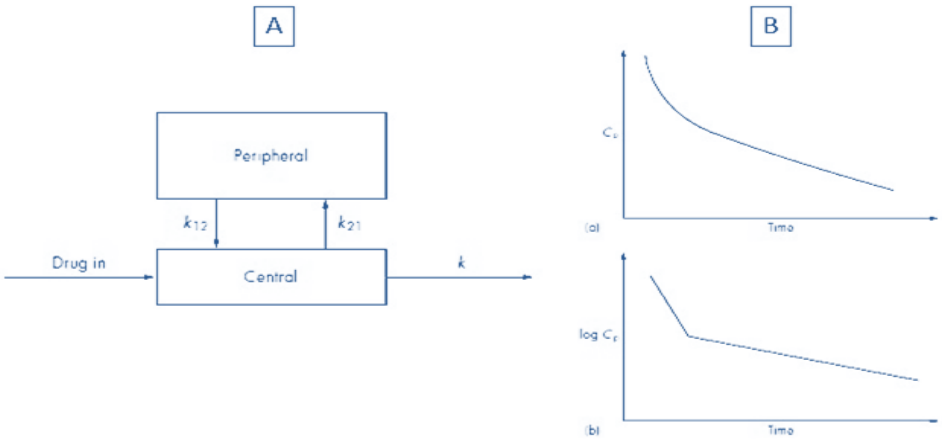

Figure A.18. Schematic representation of a two-compartment PK model (A) and the respective plasma concentration-time profiles (B): a) in normal and b) log scale. *Key*: k_{12} and k_{21}, first-order rate constants for the peripheral compartment; k, is the first-order elimination rate constant.

In this example the two-compartment model resolves the body into a central compartment and a peripheral compartment (Figure A.18(A)). Although these compartments have no physiological or anatomical meaning, it is assumed that the central compartment comprises tissues that are highly perfused such as heart, lungs, kidneys, liver, and brain. The peripheral compartment comprises less well-perfused tissues such as muscle, fat and skin. A two-compartment model assumes that, following drug administration into the central compartment, the drug distributes between that compartment and the peripheral compartment. The drug C-t profile in Figure A.18(B,a) shows a curve, but in the log scale biphasic elimination is evident (Figure A.18(B,b)) with each exponential phase describing a separate compartment (Dhillon and Gill, 2006). Therefore, the initial fast declining phase accounts for the first central compartment and the second slower elimination phase for the peripheral.

PK compartment models are usually parameterized as derived rate constants (e.g., k_{12}, k_{21}, k) or preferentially as volumes and clearance (e.g., Vc, CL, Vp, Q where Q is the inter-compartmental CL between the central and peripheral compartments). Rate constants have

units of 1/time; and inter-compartmental clearances (Q) have the units of flow (volume/time). The overall bioavailability, *'F'*, and the absorption rate constant, *'ka'*, i.e. the rate the drug enters the blood stream are key processes describing drug absorption. F represents the fraction of the extravascular dose that enters the blood and can range between 0 (no dose absorbed) and 1 (completely absorbed dose), while ka classically describes a first-order process representing extravascular absorption as a passive process driven by the concentration gradient between the absorption site and blood. For extravascular absorption, different kinetic processes such as zero-order and bolus kinetics or absorption through transit compartment models may be also applicable (Mould and Upton, 2013).

*III) **Stochastic model***

The stochastic model describes the variability around the structural model. Population models often partition variability into two or more levels. Commonly, the variability of a parameter across individuals called *between-subject variability (BSV)* or *inter-individual variability*. *Inter-occasion variability (IOV)* is also incorporated in certain cases in the stochastic model, accounting for the differences that a drug exhibits in the same patient between occasions (e.g. different treatment periods). The final level is the *residual unexplained variability*, which is the variability after accounting for all the other sources of variability (Mould and Upton, 2012). Developing an appropriate statistical model is important for covariate evaluations and simulations and for determining the amount of remaining variability in the data (Mould and Upton, 2013).

- *Between-subject variability*

Analyzing inter-individual variability and understanding its origins is of critical importance in population pharmacokinetic analysis. Inter-individual variability of anatomical and physiological characteristics may contribute to the observed variations in blood concentrations and potentially to the overall clinical outcome of a drug.

Pharmacokinetic data are often modeled assuming lognormal distributions because parameters must be positive and often right-skewed. When parameters are treated as arising from a log-normal distribution, the variance estimate (ω^2) is the variance in the log-domain, which does not have the same magnitude as the fixed parameter values.

Within an individual, pharmacokinetic parameters (e.g., CL and volume) are not correlated. However, across a patient population, correlations between parameters may be observed when a common covariate affects more than one parameter. Extensive correlation between variance terms of PK parameters (e.g., an r value $\geq \pm 0.8$) is similar to a high-condition number, in that it indicates that both variance terms cannot be independently estimated (Mould and Upton, 2013). In general, efficient estimation of both fixed parameters and variance terms requires correct specification of both the covariance structure as well as the residual variance structure. Specifying the correlations is generally less important than correctly specifying the variance terms themselves. However, failure to include covariance terms can negatively impact simulations because the correlation between parameters that is inherent in the data is not captured in the resulting simulations (Mould and Upton, 2013).

- *Inter-occasion Variability*

Individual pharmacokinetic parameters can change between study occasions. This source of the variability can be identified through the IOV model. IOV was first defined as a component of residual unexplained variability and subsequently cited as a component of BSV. Inter-occasion variability should be evaluated separately and included in the statistical model when appropriate. For example, variability between study or treatment periods (such as in crossover studies), or between studies can be handled using this approach. Failing to account for IOV can result in a high incidence of statistically significant spurious period effects. Ignoring IOV, on the other hand can lead to a falsely optimistic impression of the potential value of therapeutic drug monitoring (Mould and Upton, 2013).

- *Residual Variability*

Population models need to include a description of RUV which is defined by a quantity reflecting the difference between the observed data for an individual and the model's prediction (the residual) (Mould and Upton, 2012). RUV arises from multiple sources, including assay variability, errors in sample time collection, and model misspecification. Selection of the RUV model is usually dependent on the type of data being evaluated (Mould and Upton, 2013). Common functions used to describe RUV are listed in Table A.1.

Table A.1. Common forms of some basic residual error models. Table from ref (Mould and Upton, 2013).

Residual error function	**Formula**
Untransformed data	
Additive	$Y = f(\theta, \text{Time}) + \varepsilon$
Proportional	$Y = f(\theta, \text{Time}) \cdot (1 + \varepsilon)$
Exponential	$Y = f(\theta, \text{Time}) \cdot \exp(\varepsilon)$
Combined additive and proportional	$Y = f(\theta, \text{Time}) \cdot (1 + \varepsilon_1) + \varepsilon_2$
Combined additive and exponential	$Y = f(\theta, \text{Time}) \cdot \exp(\varepsilon_1) + \varepsilon_2$
Ln-transformed data	
Additive	$Y = \text{Log}\,(f(\theta, \text{Time})) + \sqrt{\left(\frac{\theta_y^2}{f\,(\theta, \text{Time})^2}\right)} \cdot \varepsilon_1$ where the variance of ε_1 is fixed to 1 and θ_y is the additive component of residual error
Exponential	$Y = \text{Log}\,(f(\theta, \text{Time})) + \sqrt{(\theta_x^2)} \cdot \varepsilon_1$ where the variance of ε_1 is fixed to 1 and θ_x is the proportional component of residual error
Combined additive and exponential	$Y = \text{Log}\,(f(\theta, \text{Time})) + \sqrt{\left(\theta_x^2 + \frac{\theta_y^2}{f\,(\theta, \text{Time})^2}\right)} \cdot \varepsilon_1$ where the variance of ε_1 is fixed to 1 and θ_x is the proportional component and θ_y is the additive component of residual error

Under all these models, the term describing RUV (ε) is assumed to be normally distributed, independent, with a mean of zero, and a variance σ^2. For dense pharmacokinetic data, the combined additive and proportional error models are often utilized because it broadly reflects assay variability. Exponential and proportional models are generally avoided because of the tendency to "overweight" low concentrations. This happens because RUV is proportional to the observation; low values have a correspondingly low error (Mould and Upton, 2013).

RUV may significantly depend on covariates (Mould and Upton, 2013). Covariate models may explain part of the residual variability predicted by subject characteristics (Mould

and Upton, 2013). When a significant covariate effect (e.g., age) is introduced into the model the overall BSV should be reduced (Mould and Upton, 2012).

IV) Covariate model

The identification of covariates that explain variability is an important objective of any population PK analysis. Population modeling develops quantitative relationships between covariates (such as age) and parameters, accounting for "explainable" BSV by incorporating the influence of covariates on the fixed parameters (Mould and Upton, 2012). A general approach is outlined below (Mould and Upton, 2013):

1. *Selection of potential covariates*: This is usually based on known properties of the drug, drug class, or physiology. Covariates may be continuous (e.g., weight, age, laboratory measurements) or nominal (e.g., gender, race, genotype). Continuous covariate effects can be introduced into the population model using a variety of functions (linear, power, exponential or allometric functions), they can be centered or normalized, whereas discrete data can be either dichotomous (e.g., taking one of two possible values such as sex) and polychotomous (e.g., taking one of several possible values such as race or metabolizer status). It is important for both types of data to ensure that the parameterization of the covariate models returns physiologically reasonable results.

2. *Preliminary evaluation of covariates*: Because run times can sometimes be extensive, it is often necessary to limit the number of covariates evaluated in the model. Covariate screening using regression-based techniques, generalized additive models, or correlation analysis evaluating the importance of selected covariates can reduce the number of evaluations.

3. *Building of the covariate model*: Different methodologies are applied. Usually a combination of forward addition and backward elimination is followed. In the first method, covariates are tested separately for their significance and those meeting the inclusion criteria are included, whereas in the backward elimination process all covariates are initially included in the model and are sequentially dropped based on their significance. Covariate selection is usually based on both statistical and goodness-of-fit criteria and the process continues until all covariates have been tested and the reduced or final model cannot be further simplified (Mould and Upton, 2013).

V) Model Evaluation

The assessment of how good a model fits to a given set of data is important in all model-based data analyses. There are many aspects to the evaluation of a population

pharmacokinetic model. The agreement between observations and model predictions is evaluated by numerical and graphical tools. Numerical metrics are generally used to discriminate between models during early stages of model development, allowing elimination of unsatisfactory models. In later stages when a few candidate models are being considered for the final model, simulation-based methods such as the visual predictive check (VPC) and other goodness-of-fit plots are more useful (Mould and Upton, 2013). In the following sections the evaluation techniques that are commonly used are described.

- *Numerical Criteria for Model Comparison*

Checking the robustness and physiological soundness of parameter estimates, the standard errors, and the values of BSV and RUV of the model is one of the most crucial steps in model assessment.

An important statistical criterion that is also systematically used in model selection procedures is the maximum likelihood estimation. For a given pair of observed and predicted data values, concentration is considered to have a possible range of values described by a normal distribution. The likelihood of the observed data (closely associated with probability) is a metric summarizing the deviation of the observed data from the center of this distribution. For ease of computation, the maximum likelihood estimation objective function is usually expressed as minus twice the log of the likelihood (-2LL), and is a single number that provides an overall summary of how closely the model predictions (given a set of parameter values) match the data. The lower value of -2LL for a particular model and data set is associated with a better fitting, but the absolute value of -2LL is not important. It is used within a model for comparing parameter values, and is compared between models for ranking them in order of goodness of fit for the same dataset (Mould and Upton, 2012; 2013).

The Akaike information criterion (AIC) and Bayesian information criterion (BIC or Schwarz criterion) constitute two other useful metrics for model comparison. The AIC is generally considered the one of the most important model selection criteria that should be used in practice. The AIC derives from the following equation (Eq. 2):

$$\mathrm{AIC} = -2\log L(\hat{\theta}) + 2k \qquad \text{(Eq. 2)}$$

where θ is the vector of model parameters, $L(\hat{\theta})$ is the likelihood of the candidate model given the data when evaluated at the maximum likelihood estimate of θ, and k is the

number of estimated parameters in the candidate model (Fabozzi et al., 2014). The AIC in isolation is meaningless. Rather, this value is calculated for every candidate model and the "best" model is the candidate model with the smallest AIC. The first component, $-2\log L(\hat{\theta})$, is the value of the likelihood function, $\log L(\hat{\theta})$, which is the probability of obtaining the data given the candidate model. Since the likelihood function's value is multiplied by -2, ignoring the second component, the model with the minimum AIC is the one with the highest value for the likelihood function. However, to this first component an adjustment is added based on the number of estimated parameters. The more parameters, the greater the amount added to the first component, increasing the value for the AIC and penalizing the model. Hence, there is a trade-off: the better fit, created by making a model more complex by requiring more parameters, must be considered in light of the penalty imposed by adding more parameters. This is why the second component of the AIC is thought of in terms of a penalty.

BIC is another model selection criterion based on information theory but set within a Bayesian context. The difference between the BIC and the AIC is the greater penalty imposed for the number of parameters by the former than the latter. The BIC is computed as follows (Fabozzi et al., 2014):

$$\text{BIC} = -2\log L(\hat{\theta}) + k\log n \qquad \text{(Eq. 3)}$$

where the terms above are the same as described in our description of the AIC. As in the case of -2LL and AIC, the best model is the one that provides the minimum BIC value. Differences in AIC and BIC between models of more than 10 are categorized as "very strong" evidence in favor of the model with the lower BIC; between 6 and 10 as "strong" evidence; between 2 and 6 as "positive" evidence; and less than 2 as "weak" evidence. In practice, a drop in AIC or BIC of 2 is often a threshold for considering one model over another (Fabozzi et al., 2014; Mould and Upton, 2013).

- *Goodness-of-Fit Plots*

The reliability of the analysis results can be further checked by careful examination of the diagnostic plots. The graphical assessment of a model fit is very important to detect model misspecification and to discriminate between competing models, especially in situations when numerical methods are not reliable or not applicable. A basic plot is a plot of observed and individual-predicted concentrations against time (Figure A.19). Individual-predicted concentrations should provide an acceptable fitting to the observed data.

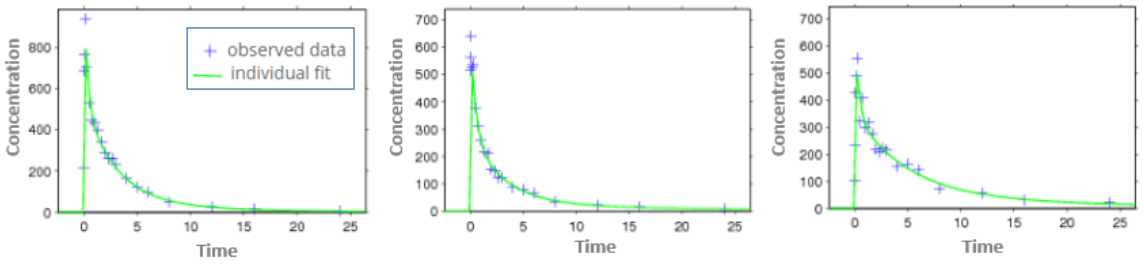

Figure A.19. Plots of observed and individual-predicted concentrations *versus* time.

The observed values can be also directly compared to the individual-predicted or population-predicted values from the model in observed versus individual or population predicted plots, which can depict the degree of correlation between these values and unveil a possible trend or bias in the estimated values. On the left, Figure A.20 displays the scatter plot of the observed concentration with respect to the predicted concentration using the estimated population parameters. On the right, the scatter plot of the observed concentration with respect to the predicted concentration using the individual parameters is depicted.

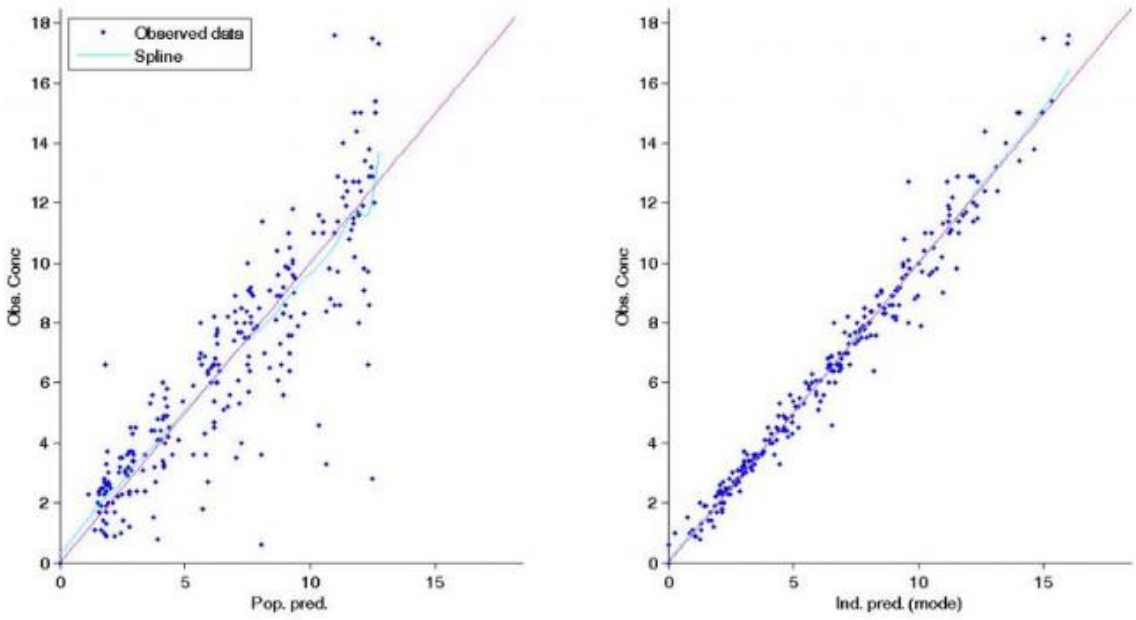

Figure A.20. Plots of observed *versus* model predicted concentrations: Population (left) and individual concentrations (right).

Another very important evaluation graphic is the plot of individual weighted residuals (IWRES) versus the predicted concentrations (PRED) or time (Figure A.21). Weighted residuals normalize the residuals so that the standard deviation (SD) is 1 allowing informative residual plots. IWRES is analogous to a Z-score for the deviation between the model prediction and the data.

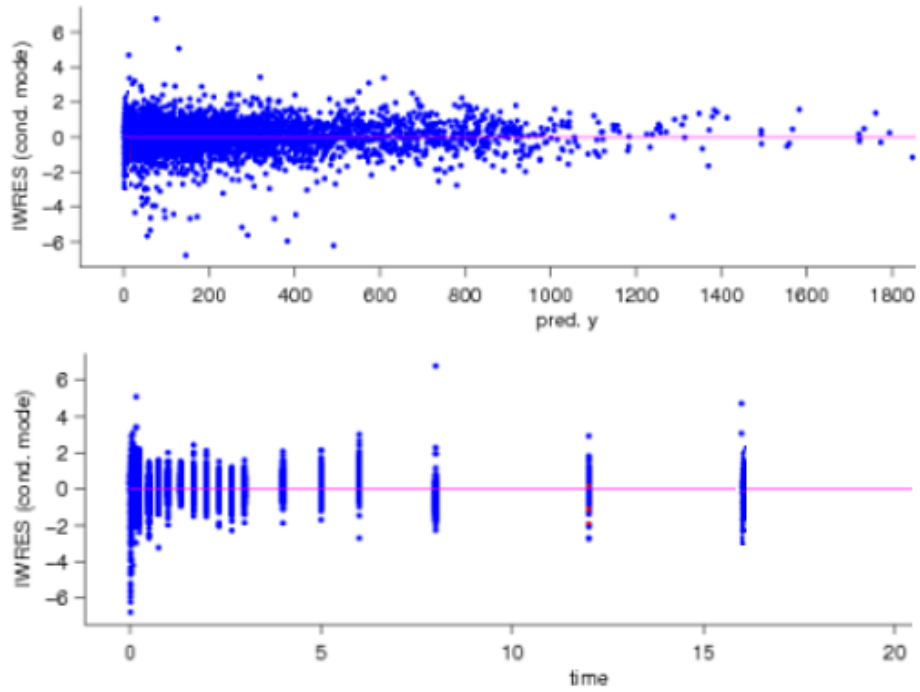

Figure A.21. Plots of individual weighted residuals (IWRES) versus the predicted concentrations (top) or time (bottom).

IWRES should be normally distributed, evenly centered around zero, without systematic bias, and most values within −2 to +2 Standard Errors (marking the ~5th and 95th percentiles of a normal distribution). Systematic deviations may imply deficiencies in the structural model. Similarly, plots of IWRES against predicted concentrations should be evenly centered around zero, without systematic bias, with most values within −2 to +2 Standard Errors. Systematic deviations may imply deficiencies in the RUV model (Mould and Upton, 2013).

The normalized prediction distribution errors (NPDE), i.e., the observation percentiles within the empirical distribution obtained from the model simulations, de-correlated and normalized using the inverse function of the normal cumulative density function can be also plotted against the predicted concentrations and time (Figure A.22). Again no trend should be observed and the data should be symmetrically distributed around zero.

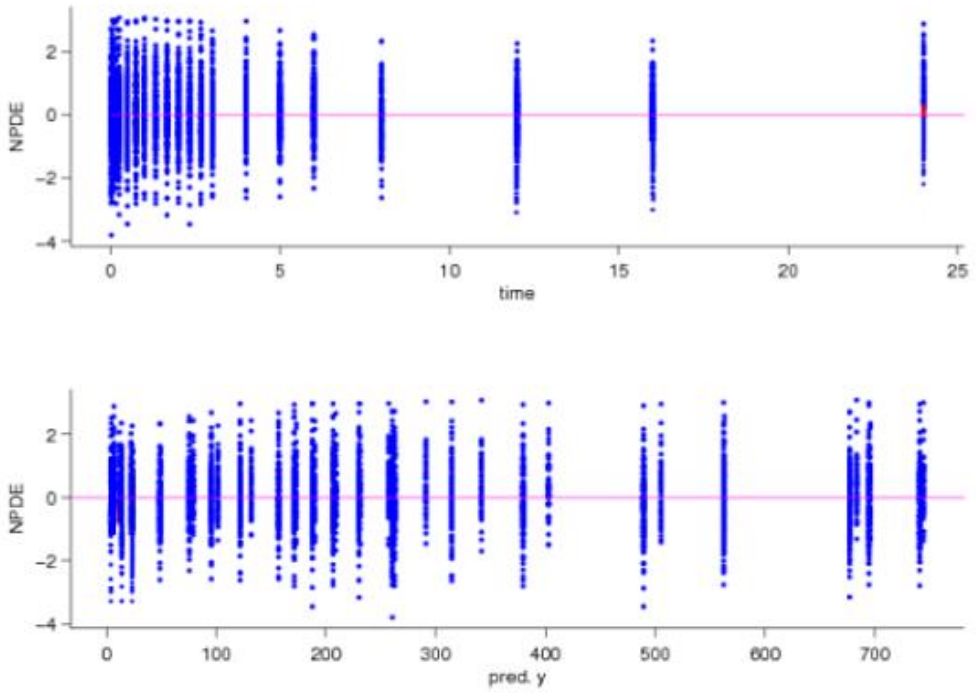

Figure A.22. Plots of normalized prediction distribution errors (NPDE) versus the predicted concentrations (top) or time (bottom).

Finally, visual predictive check (VPC) plots are generated and assessed. The principle of VPCs is to assess graphically whether simulations from a model of interest are able to reproduce both the central trend and variability in the observed data, when plotted versus an independent variable (typically time). A VPC is based on multiple simulations with the model of interest and the design structure of the observed data (i.e., dosing, timing, and number of samples). Percentiles of the simulated data are compared to the corresponding percentiles of the observed data (Bonate, 2005; Gabrielsson and Weiner, 2007; Post et al, 2008).

VPCs generally involve simulation of data from the original or new database and offer benefits over standard diagnostic plots. The final model is used to simulate new data sets using the selected database design, and prediction intervals are constructed from simulated concentration time profiles and compared with observed data. Usually, the median and 10^{th} and 90^{th} percentiles are presented. The inter-percentile range between the outer percentiles of all the simulated data, i.e. the prediction interval, is displayed with a level of 90% (Figure A.23).

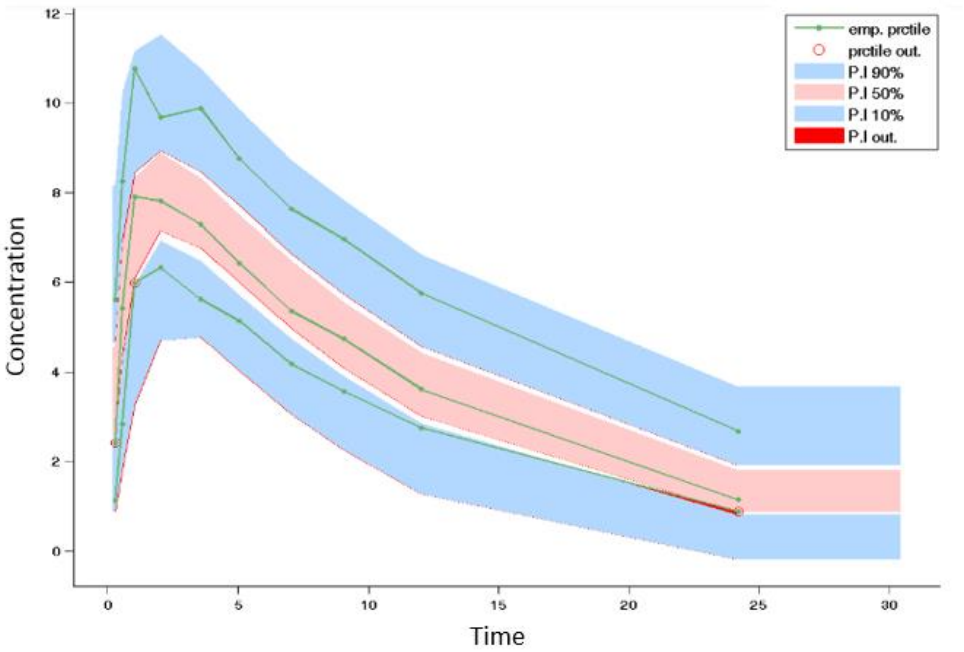

Figure A.23. Visual predictive check (VPC) plot.

VPC can ensure that simulated data are consistent with observed data. VPC plots stratified for relevant covariates (such as age or weight groups), doses, or routes of administration can be also constructed to demonstrate model performance in these subsets (Mould and Upton, 2013).

VI) Modeling Software

An important role in model building is played by the modeling software programs (Urso et al., 2002). Nonlinear mixed effects modeling software brings data and models together, implementing an estimation method for finding parameters for the structural, statistical, and covariate models that describe the data (Mould and Upton, 2013). Numerous population modeling software packages are available. Choosing a package requires careful consideration including number of users in your location familiar with the package, support for the package, and how well established the package is with regulatory reviewers. For practical reasons, most pharmacometricians are competent in only one or two packages (Mould and Upton, 2013).

One software program widely applied to population pharmacokinetic problems is the nonlinear mixed-effects model (NONMEM) (Greenblatt et al., 2002). NONMEM was the first software available for population PK modeling, but subsequently other packages have been developed and are in use today (Mould and Upton, 2012). Most packages share the

concept of parameter estimation based on minimizing an objective function value (OFV), often using maximum likelihood estimation (Mould and Upton, 2013). Yet, more robust alternatives have been proposed that avoid simplifying the equation for the likelihood, such as the Stochastic Approximation Expectation Maximization (SAEM) algorithm implemented in the MONOLIX software (Bertrand et al., 2011).

SAEM is a stochastic version of the well-known expectation maximization algorithm, where the individual random effects are the missing variables. In the expectation step, the individual parameters are simulated using a Monte Carlo Markov Chain approach and then used to compute a stochastic approximation of the conditional expectation of the complete loglikelihood which is the loglikelihood of the complete data, i.e., the observations and the imputed individual parameter estimates at the current iteration of the SAEM algorithm. Then, the complete loglikelihood is maximized to obtain the updated estimates of the population parameters (Bertrand et al., 2011; Comets et al., 2007; Lavielle and Mentré, 2007; Savic and Lavielle, 2009). Additionally to the visual inspection of convergence graphics, stopping rules are available which are based on the absence of decrease of the complete loglikelihood sequence during the stochastic step and small variability between subsequent population parameter estimates and estimates of the complete loglikelihood during the cooling step. Even though the NONMEM software still remains the most popular tool in population PK analysis because of its superior flexibility, of note, the SAEM algorithm has been also implemented in NONMEM, suggesting the utility and importance of this stochastic algorithm (Bertrand et al., 2011).

Both the US FDA and EMA have acknowledged the value of population PK modeling. Today, population modeling and exposure-response evaluations are systematically used to support registration decisions and labeling, since they enable the identification of the sources of variability that ultimately have an impact on both safety and efficacy of a drug. Most importantly, pharmacometric tools can be very helpful in the development of drugs showing special PK characteristics. They can aid in determining the *in vivo* fate of a drug and further facilitate the selection of the drug/formulation/device combination (Bhagwat et al., 2017). Finally, modeling and simulation can play a pivotal role in personalized medicine, aiming to provide more accurate predictions of individual responses to therapy based on the characteristics of each individual (Mould and Upton, 2012).

A.6. Scope

The aim of this thesis was to apply population pharmacokinetic modeling approaches in order to investigate the absorption and disposition kinetics of certain drugs, showing special pharmacokinetic characteristics. For the purpose of this work, five different substances with interesting pharmacokinetic properties, administered either orally or by the inhaled route, were investigated. In this context, seven independent population PK analyses were performed, presented in five separate studies.

The first study refers to an inhaled medicinal product containing the anti-inflammatory corticosteroid agent, fluticasone propionate (FLP) and the β_2-adrenergic agonist, salmeterol (SAL). The data for this analysis derived from a single-dose BE study in healthy volunteers receiving the FLP/SAL combination via two dry powder inhalation devices, under fasting conditions and the presence of an activated charcoal scheme. An extensive population PK analysis was applied to the FLP and SAL data separately, in order to develop a PK model that could adequately describe the PKs of the two drugs, quantify the variability of PK parameters and elucidate the impact of various demographic and environmental factors on their performance. Besides, the typical non-compartmental PK approaches were also applied for reasons of completeness and characterization of the basic exposure PK parameters of both FLP and SAL.

SAL pharmacokinetics were further investigated in a subsequent study. In this study, the PK analysis of salmeterol is extended to an asthma patient population, in order to explore the influence of airway state on its PK behavior. The data used for this analysis came from a BE study where the FLP/SAL combination was administered in asthma patients, without the presence of activated charcoal. The latter allowed the gastrointestinal absorption of SAL and enabled us to examine the total systemic exposure of the drug following inhalation. As previously, population, and non-compartmental PK analyses were applied to the C-t data, putting the main focus on constructing a PK model, which will able to describe the parallel lung and oral absorption of SAL following inhalation, determine the fraction of dose that is absorbed through the lungs, and unveil the role of potential covariates on SAL pharmacokinetics.

The last inhaled combination that was analyzed in the third study, referred to the corticosteroid budesonide (BUD) and another β_2-adrenergic agonist, formoterol (FOR), also incorporated in dry powder inhalation devices. Since both drugs exhibit a distinct

pharmacokinetic behavior following inhalation, the main goal of this study was to apply population PK modeling in order to investigate the complex absorption and disposition characteristics of these two drugs, as well as to determine the role of potential covariates on the variability of these processes. The data for the analysis derived from a BE study with the drug combination administered via two different dry powder inhalers in asthma patients, under fasting conditions and in the presence of an activated charcoal scheme. A non-compartmental analysis was implemented in this case for the initial characterization of the rate and extent of systemic exposure of inhaled BUD and FOR.

The last two studies of this thesis concern the widely used cholesterol absorption inhibitor, ezetimibe (EZE), administered orally via a solid dosage form. The drug has been shown to undergo extensive first-pass metabolism, within the intestinal mucosa, into an equally pharmacologically active metabolite, ezetimibe glucuronide (EZEG), with both drugs being repeatedly subjected to enterohepatic recycling. In the first place, the C-t data of EZE and EZEG, obtained from a BE study in healthy subjects, are treated together and PK modeling is performed on total EZE concentrations (parent and metabolite data combined). In the subsequent study, population analysis is also performed separately for EZE and EZEG concentrations, through the construction of a joint population PK model that allows for the simultaneous description of the two active agents.

Since both agents undergo extensive enterohepatic recycling, the core of both studies is to build EHC-based models that not only include an additional re-distribution component, but also provide a more physiological representation for the parameters and processes related to EHC. In this vein, extensive modeling has been conducted to account for the EHC process observed for both EZE and its active metabolite and a diverse set of approaches is implemented in modeling of this process. Finally, in line with the previous analyses, as a secondary aim of both studies, the potential contribution of several covariates was examined in order to extract any useful information for EZE pharmacotherapy.

B. Methods

B.1. Analyzed Drugs and Study Designs

As described above, five separate analyses were performed; the first three concerned drugs administered via the inhaled route and the latter two an orally administered active agent. The two widely used inhaled combinations, fluticasone propionate/salmeterol and budesonide/formoterol combinations administered via different dry powder inhalation devices, were initially investigated. Subsequently, the complex metabolism and distribution kinetics of the cholesterol absorption inhibitor ezetimibe was explored, either as total drug concentrations, or by considering both the parent drug and its active metabolite.

Plasma C-t data of each drug, therefore, obtained from four different comparative pharmacokinetic studies, were analyzed using population and NCA PK approaches. The studies were performed on healthy subjects or patient population groups, who received either a test or reference formulation, under fasting conditions. These PK studies followed a single dose, two-sequence, two- or four-period, crossover design, while an activated charcoal scheme was also co-administered, in certain cases, in order to prevent the absorption from the gastrointestinal tract. The studies were in compliance with the ICH E6 Good Clinical Practice Guidance and followed the principles of Helsinki Declaration. They were approved by National Ethics Committees and the competent regulatory authorities. A more detailed description on the protocol information of each study is presented in the relevant chapter of 'Results' section.

B.2. Population PK Analysis

The main goal of this work was to apply PK modeling approaches in order to further characterize the absorption and disposition kinetics of the drugs following either inhaled or oral administration, as well as, to detect potential factors that may affect their PK performance. Since all the datasets derived from comparative PK studies implementing a crossover design, plasma C–t data from both T and R products and the different treatment periods were pooled together and incorporated in the analysis by setting the 'treatment' and 'period' effects as potential covariates in the final dataset. Similar methodologies in population PK analyses have been already proposed in previously published studies (Fradette et al, 2005; Panhard & Mentre, 2005).

The population PK analysis was performed using a non-linear mixed effects modeling approach (Sheiner and Beal, 1983; Bonate, 2005). The Stochastic Approximation Expectation Maximization algorithm, implemented in Monolix software, was used for the estimations of the population PK parameters. The algorithm settings were left to the default values; the maximum numbers of SAEM stochastic (k1) and cooling (k2) iterations did not exceed 500 and 200, respectively, whereas a simulated annealing version of SAEM was used to estimate the population parameters (i.e., the variances were constrained to decrease or increase slowly during the first iterations of SAEM). No burning iterations were tested and the number of Markov chains was set equal to unity. Finally, the Monte-Carlo sizes for the prediction distribution graphic, visual predictive check plots, and the log-likelihood estimation were set to 100, 500 and 20,000, respectively.

Missing concentration data and those below the lower limit of quantitation (BLQ), were either omitted from the analysis or treated as censored data, replaced by the lower limit of quantitation (LLOQ) value of the bioanalytical method, using the relevant software setting. In some cases, however, not all missing concentrations in the obtained datasets could be treated as censored data, due to computational reasons. In these cases, truncation of the dataset was performed, based on the plethora of missing values and information regarding the elimination half-life of the respective drug.

A step-by-step procedure was followed to find the PK model that could satisfactorily describe the C-t profile of each drug. At first, the analysis focused on the selection of the most appropriate structural model. Typical one-, two-, and three-compartment models with different drug input kinetics were initially evaluated. However, since most of the analyzed drugs exhibited a rather complex PK behavior, these conventional models were proven inadequate to describe the C-t profiles of drugs in most cases, and thus, models of increasing complexity had to be constructed. These newly developed models were encoded through a system of ordinary differential equations (ODE) in the model translator MLXTRAN of Monolix® software.

During the model building procedure, different initial values were tested for the fixed effects. Random initial values or values derived from published data were tested and the estimated model PK parameters were evaluated and compared. The ‘fixed’ option, in the initialization frame of Monolix, was also used during the initial model optimization

process for some of the PK parameters. The individual pharmacokinetic parameters were assumed to follow log-normal distribution, whereas a logit model was also implemented in special cases in order to force a PK parameter to be constrained on a zero to one scale.

Along the structural model construction, the statistical model was further embodied in the PK model, accounting for the between-subject variability (BSV), the inter-occasion (IOV) and residual variability. Between-subject variability was assumed to follow log-normal distribution as well, for all PK parameters. The variability in PK parameters between the different study periods, IOV, was also evaluated, whereas various residual error models (constant, proportional, exponential, and combined) were tested in order to describe the RUV of the structural model. Finally, potential correlations between the random effects of the PK parameters were also assessed for their contribution in the final model, using the goodness-of-fit criteria described below.

Accordingly, for the evaluation of the best PK model, before the addition of any covariate effect, goodness-of-fit criteria in addition to the plausibility and stability of the model were examined. In this context, numerical and graphical selection criteria, as well as the physiological soundness of the estimated PK parameters were considered. Models were, therefore, compared using the commonly used numerical selection criteria of statistical significance: -2LL (-2 log likelihood), AIC and BIC. To statistically distinguish between the nested models, the likelihood ratio test based on the reduction of -2LL value was used, while AIC and BIC were used to discriminate between nonhierarchical models. A reduction greater than 3.84 from the base or previous model to the current model was designated as statistically significant at $p<0.05$. The precision of model predicted estimates through the inspection of their percent relative standard errors (RSE%), as well as their BSV and residual error values were also taken into consideration.

In addition to the above, evaluation of the goodness-of-fit plots was also performed during model selection. With respect to the visual inspection of graphical criteria: (a) the adequacy of fitting of the model predicted estimates to the individual C-t data was assessed for each model, (b) individual predicted (IPRED) and population predicted (PPRED) plasma concentrations were directly compared to the observed data, (c) the amount of bias was assessed by plotting the individual weighted residuals (IWRES) and the normalized prediction distribution errors (NPDE) *versus* the individual predicted (IPRED) concentrations, and (d) the distributions of random effects were compared to the

theoretical normal. Finally, visual predictive checks plots (VPCs) were also performed to evaluate the predictive ability of the model, where the 95% CIs around the 10^{th}, 50^{th}, and 90^{th} prediction percentiles from 500 simulated datasets were overlaid to the 10^{th}, 50^{th}, and 90^{th} percentiles of the observed data, binned using the theoretical sampling times. The most parsimonious model with the lowest values of the numerical information criteria and the best goodness-of-fit plots was finally chosen.

Following the determination of the best structural model for each drug, various covariates were tested for their contribution in the model. The investigated covariates included patient demographic characteristics such as gender, age, body weight (BW), height and body mass index (BMI), disease state and in some cases clinical and laboratory measurements, such as the forced expiratory volume in 1 second (FEV1) values, liver function descriptors, serum creatinine, bilirubin, albumin, hemoglobin and urea blood levels. The effects of the different administered products (test or reference) and treatment periods, defined as 'treatment' and 'occasion' effects, were also assessed as potential covariates. In all cases, the continuous covariates were examined either untransformed or centered around their 'mean' value. Allometric scaling with a standardized body weight of 70 kg as the size descriptor and fixed exponents (1 for the central and peripheral volume of distribution and 0.75 for clearance) was also evaluated.

A combination of forward addition and backward elimination methods was implemented for the exploration of all potential covariates on reducing the between-subject-variability and improving goodness-of-fit criteria of the final model. Covariates were initially tested by a forward selection method starting with a univariate analysis, which assessed the effect of each covariate on the model parameters separately, followed by a sequential addition of all important covariates. This step allowed, in the first place, for the identification of covariates which might have significant impact on the PK variability. After completing this step, the backward elimination method was further applied. A stepwise procedure was followed that involved the initial inclusion of all covariates in the model and the progressive deletion of non-significant covariates using the pre-defined model selection criteria. The removal of each covariate should improve the model numerical criteria (e.g. a decrease in the −2LL by at least 3.84) and parameters precision, and the process was repeated until no further improvement of the model was possible. Significance levels of 5% were considered in all procedures. Finally, the selection of the

best final model was based on the selection criteria described above and the significance and physiological soundness of each covariate.

The entire computational work was implemented in sequential versions of Monolix® software v.4.2 - v.2016R1 (Lixoft, Orsay France).

B.3. Non-compartmental Analysis - Bioequivalence

Using the data from the above studies, a non-compartmental analysis was also performed, for the characterization of the rate and extent of systemic exposure of the drugs. The estimated PK parameters referred to the area under the concentration–time curve from time zero to the last sampling point or the last measurable concentration, whichever occurs earlier (AUCt), the area under the C–t curve from time zero extrapolated to infinity (AUCinf), the first recorded maximum plasma concentration value (Cmax), and the time (Tmax) at which Cmax occurs. AUCt was calculated using the linear trapezoidal rule. Values for AUCinf, were calculated as AUCt + Clast/λz, where Clast is the last quantifiable concentration and λz refers to the apparent terminal elimination rate constant. The latter was determined by a least squares regression analysis applied to the terminal log-linear phase of the C-t curve. Descriptive statistics (arithmetic mean, standard deviation, coefficient of variation, median and range) were also calculated for these PK parameters.

The non-compartmental analysis was further extended by performing a BE assessment on the obtained PK parameters for the two products under comparison. In this respect, two of the above parameters, the AUCt and Cmax estimates were assessed according to the current EMA guideline on the investigation of bioequivalence by applying a general linear model (analysis of variance, ANOVA) (EMA CHMP, 2010). The data were transformed prior to analysis using a logarithmic transformation. The 90% CIs around the geometric mean ratios (GMR) of T over R formulation (T/R) were constructed using the residual error from ANOVA model. The two products under comparison were considered bioequivalent if the 90% CIs for the log-transformed values of both AUCt and Cmax were lying within the predetermined equivalence range of 80.00–125.00% (EMA, 2010). All the effects used in the ANOVA model (sequence, subject within sequence, period and formulation) were considered as fixed. The entire computational work of the non-

compartmental analysis was implemented in the pharmacokinetic software package WinNonlin® v.5.0.1 (Pharsight Corp, Menlo Park, CA).

In general, the same methods for both non-compartmental and compartmental analyses, as described above, were applied in all studies. Special characteristics and deviations from the described methodologies can be found in the relevant sections of each study, presented within the 'Results' section below.

C. Results

C.1. Inhaled Drugs

C.1.1. Study 1: Inhaled Fluticasone/Salmeterol combination in healthy subjects, in the presence of activated charcoal.

C.1.1.1 Introduction

As reported previously, co-administration of inhaled corticosteroids with long-acting β_2-agonists is usually the treatment of choice for patients with severe COPD and asthma, since they can provide both an anti-inflammatory and a bronchodilator activity (Chrystyn, 2007; Kirby et al., 2001; Labiris and Dolovich, 2003). One such combination is the fluticasone propionate/salmeterol incorporated in dry powder inhalers, as well as other oral inhalation devices (Fenton and Keating, 2004; Jenkins et al., 2009).

Fluticasone propionate (Figure C.1.1) is a potent inhaled corticosteroid which has been shown to exert an important anti-inflammatory activity within the lung (Crim et al., 2001), while salmeterol (Figure C.1.1) is an effective β_2-adrenergic agonist, able to provide a sustained relief from bronchoconstriction following inhalation (Verberne and Fuller, 1998). It has been shown that for an optimal pharmacodynamic interaction, these two agents should reach the target cells together and in adequate concentrations (Nelson et al., 2003).

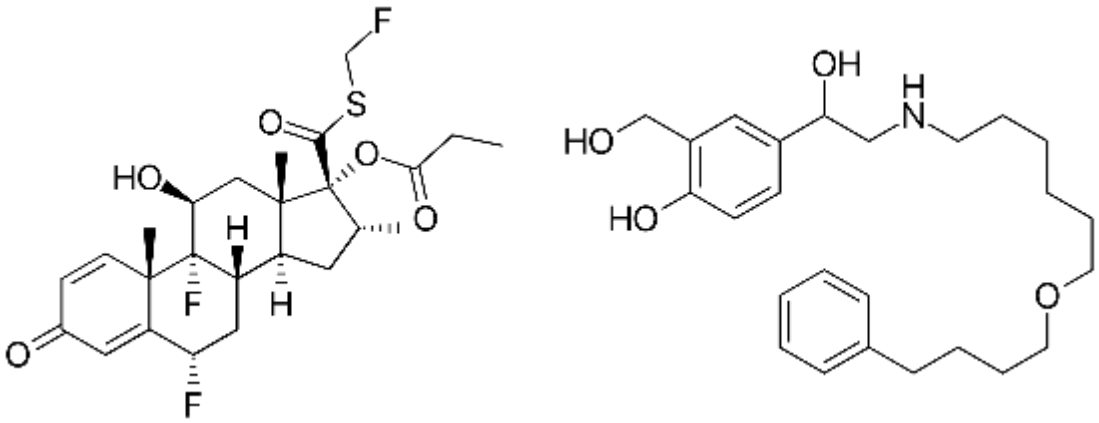

Figure C.1.1. Molecular structures of fluticasone propionate (left) and salmeterol (right).

FLP is a potent anti-inflammatory agent with a favorable ratio of topical to systemic activity (Lawrence et al., 1997). It is an androstane glucocorticosteroid with high lipophilicity, high selectivity and affinity for the glucocorticoid receptors (Crim et al., 2001). Importantly, it is not appreciably absorbed from the gastrointestinal tract; therefore, the fraction of the inhaled fluticasone propionate dose delivered to the lungs is considered as the primary source available for systemic absorption (Lawrence et al., 1997). On the

basis of available data from numerous clinical trials and an extended clinical use, inhaled fluticasone propionate offers an effective treatment option for the management of asthma and other respiratory diseases, with the potential of an enhanced safety profile (Holliday et al., 1994). In the recommended doses, it has been shown not to cause clinically significant effects on pituitary-adrenal function, bone metabolism and attainment of adult height in children. However, higher doses have been associated with systemic absorption and side effects (Lawrence et al., 1997).

SAL is a β2-adrenergic agonist which acts locally in the lung by providing a long-lasting (ca. 12 h) bronchodilation (Johnson et al., 1993). SAL offers effective protection against histamine-induced bronchoconstriction, by decreasing airway resistance and improving the ventilation of patients (Mahler et al., 1999; Ricciardolo et al., 2015). However, similarly to other β2-adrenoceptor agonists, the use of inhaled SAL has been associated with dose-related cardiovascular and systemic effects such as increased heart rate, palpitations, tremor and changes in plasma glucose and potassium levels (Guhan et al., 2000). Since the main adverse effects of inhaled SAL relate to its systemic exposure, knowledge of its pharmacokinetics is important for increasing drug's safety. At the same time, investigation of the pharmacokinetics of inhaled SAL may serve as a valuable tool for determining its lung deposition and bioavailability, thus providing useful information for optimizing drug delivery.

Due to the combined action, knowledge of the PK properties following co-administration of FLP and SAL is highly important. Previous studies have shown that after inhalation the absolute bioavailability of FLP is 10–30%, while oral bioavailability of inhaled FLP is negligible (less than 1%) due to both low absorptions from the gastrointestinal tract and high hepatic first-pass metabolism (Mollmann et al., 1998; Reynolds et al., 2005; Singh et al., 2003). Similarly, following administration of SAL via inhalation, plasma concentrations of the drug are very low or even undetectable (Cazzola et al., 2002; Nelson et al., 2003). The pharmacokinetics of SAL and FLP, when administered concomitantly through the same inhaler, are very similar to those of the two agents when administered separately and no pharmacokinetic interaction between the two agents occurs (Kirby et al., 2001; Reynolds et al., 2005).

The purpose of this study was to explore the pharmacokinetics of inhaled FLP and SAL after concomitant administration in healthy male and female subjects. The C-t data were

obtained from a BE study on two DPIs. Initially, a conventional non-compartmental methodology was applied. Furthermore, extensive population PK analysis was applied to FLP and SAL. In this context, several structural and residual error models were tested to find the one that described best the plasma C-t data of FLP and SAL. Also, the population PK analysis examined various subject demographic characteristics to elucidate the variability of the PK parameters.

C.1.1.2 Methods

C.1.1.2.1 Study design and volunteers

Plasma C-t data were obtained from a single dose, two-sequence, two-period, crossover 2x2 BE study using two dry powder inhalers: the traditional multi-dose (Fluticasone/Salmeterol via Diskus® 500/50 mcg/inhalation, GSK) and a novel single-dose device (Fluticasone/Salmeterol via Elpenhaler® 500/50 mcg/inhalation, ELPEN) under fasting conditions. Both devices are currently commercially available in various European countries. A wash-out period of 8 days was set between each treatment to allow for the complete removal of the drug from the body.

The study was performed in compliance with ICH E6 Good Clinical Practice Consolidated Guidance, by 3S-Pharmacological Consultation & Res. Srl in Romania. Sixty healthy male and female subjects were enrolled in the study. All subjects were informed about the purpose, protocol, and risks of the study and a written consent form was provided by each participant before entering the study. The subjects aged between 18 to 45 years and met the inclusion criteria, such as BMI within 19-29 kg/m^2, good general health, no clinically significant or relevant abnormalities of medical history, normal physical examination or laboratory values, non-smokers and non-lactating women. The main exclusion criteria included intolerance or hypersensitivity to the study drugs, hospitalization or donation of $\geq$450 mL of blood within two months prior to study initiation, intake of any medication two weeks prior to dosing, history of bronchial asthma or other bronchospastic conditions, positive AIDS or hepatitis B/C tests results etc. Vital signs, measured before and after the study drugs administration in each study period, were analyzed and all reported adverse effects were recorded. Finally, 57 subjects completed the study and further analyzed. The three subjects who were considered as drop-outs referred to either positive pregnancy or alcohol test results.

On the treatment days, after at least 10 hours of fasting, each subject received either one dose of Elpenhaler® 500/50 mcg/inhalation (Test formulation, T) or one dose of Diskus® 500/50 mcg/inhalation (Reference formulation, R), according to the randomization plan. Activated charcoal was co-administered at specified time points in order to prevent any absorption from the gastrointestinal tract. More specifically, it was administered 2 minutes pre-dosing and at 2, 60, 120 and 180 minutes post-dose. Blood samples (of 5 mL each) were collected before drug administration (time 0) and at 10, 20, 30, 45 min and 1, 1.33, 1.67, 2, 2.5, 3, 3.5, 4, 5, 6, 7, 8, 10, 12, 16, 24, 36, 48 and 72 hours post-dose. After the eight days of the washout period, the subjects received the alternate formulation, and blood samples were again drawn and analyzed using the same procedures.

C.1.1.2.2 Assay methodology

The identification and quantification of FLP and SAL in plasma were performed by validated Liquid Chromatography / Mass Spectrometry (LC-MS/MS) methods, showing adequate sensitivity, precision, accuracy, specificity, and linearity. The lower limits of quantification were 1.500 pg/mL and 2.500 pg/mL for SAL and FLP, respectively (Silvestro et al., 2012).

C.1.1.2.3 Pharmacokinetic analysis

C.1.1.2.3.1 Non-compartmental pharmacokinetic analysis

Initially, the PK parameters of FLP and SAL were evaluated using non-compartmental methods (WinNonlin® v.5.0.1 / Pharsight Corp, Menlo Park, CA). The non-compartmental analysis was performed according to the methodologies described in the Methods section, and the following PK parameters were calculated: AUCt, AUCinf, Cmax, Tmax and λz, along with their descriptive statistics (arithmetic mean, standard deviation, coefficient of variation, median and range).

The conventional non-compartmental analysis was extended by performing a BE assessment of the estimated PK parameters, AUCt and Cmax according to the methodology proposed by the European Medicines Agency (EMA, 2010). Data from the 57 subjects, who completed all periods of the study, were included in the statistical analysis. The entire computing work was implemented in WinNonlin® v.5.0.1 (Pharsight Corp, Menlo Park, CA).

C.1.1.2.3.2 Population pharmacokinetic analysis

The population PK analysis was performed using a non-linear mixed effects modeling approach. Due to the fact that the data refer to a 2x2 crossover design, the C-t data of the T and R products were pooled together and the 'treatment' was set as a covariate. This procedure was followed separately for FLP and SAL. The population PK analysis was in line with other published works (Dubois et al, 2012; Fradette et al, 2005; Karlsson and Sheiner 1993; Panhard and Mentre, 2005).

Several structural models were evaluated which included one-, two-, and three-compartment models. Absorption kinetics was assumed to be either first-order or bolus since these types of kinetics had also been reported in the literature for FLP and SAL. The choice of first order absorption kinetics was selected based on previous findings from other published studies (Rohatagi et al, 1996; Simon et al., 1998; Wu et al., 2008; Xu et al., 2010). Oral absorption rate constant was also excluded from both models due to the co-administration of activated charcoal which prohibited any systemic absorption from the gastrointestinal tract.

In all cases, elimination was considered to take place in the central compartment and follow first-order kinetics. The structural PK models were parameterized in terms of the absorption rate constant (ka), apparent clearance (CL/F), apparent intercompartmental clearance (Q/F), apparent volume of drug distribution of the central (V_c/F) and the peripheral compartment(s) (e.g. V_p/F for the two-compartment model); the term F refers to the bioavailable fraction of dose. The between-subject variability in the PK parameters was assumed to follow log-normal distribution. The possibility of covariance between the PK parameters was assessed. The effect of each product (T and R) on PK parameters was evaluated through the inclusion of the treatment as a covariate. Several residual error models (constant, proportional, exponential, and combined) were examined to describe the unexplained variability of the structural model.

A step-by-step procedure was applied to find the model that best describes the available FLP and SAL plasma C-t data. All models were tested in terms of the methodologies described in the Methods section, implementing both numerical and graphical goodness-of-fit criteria. After the appropriate structural model for each drug was identified, several covariates were tested. The covariates examined in this study referred to subject specific characteristics and in particular: gender, age, body weight, height, and BMI. Each

covariate was assessed either alone or in combination with other covariates, using a combination of forward addition and backward elimination methodologies. Finally, the selection of the best model was based on the model selection criteria described above and on the significance and physiological soundness of each covariate.

All population analyses were applied to the entire set of data of the 57 subjects who completed the study. Missing concentration data which were below the lower limit of quantitation were modeled as censored data using the appropriate setting in Monolix®. In case of FLP all censored observations (i.e., up to the last sampling point 72 h) were replaced with the LLOQ value (2.5 pg/mL). For SAL, not all missing data could be treated as censored, due to computational reasons. Thus, any missing observations up to 16 h were modeled as censored and were replaced by the LLOQ value (1.5 pg/mL). It should be mentioned that other missing concentration data (i.e., not lower than the limit of quantitation) were treated with the typical methodology, namely, using the 'missing' option of the software.

C.1.1.3 Results

A total of 57 male and female subjects finally completed the study and were included in the PK analysis. The mean age of subjects was 30 years (18-44 years), mean height was 171 cm (154-190 cm), mean BW was 71.6 kg (50-98 kg), and mean BMI was 24.3 kg/m^2 (19.2-29 kg/m^2). Seven non-serious adverse events were recorded in the study; three of moderate and four of mild intensity. According to the clinical study report, there were no statistically significant differences in the incidence of adverse events between the T and R treatment.

C.1.1.3.1 Non-compartmental pharmacokinetic analysis

The mean plasma C-t curves of FLP and SAL after a single inhaled dose of the T and R formulations are shown in Figure C.1.2(A) and C.1.2(B), respectively.

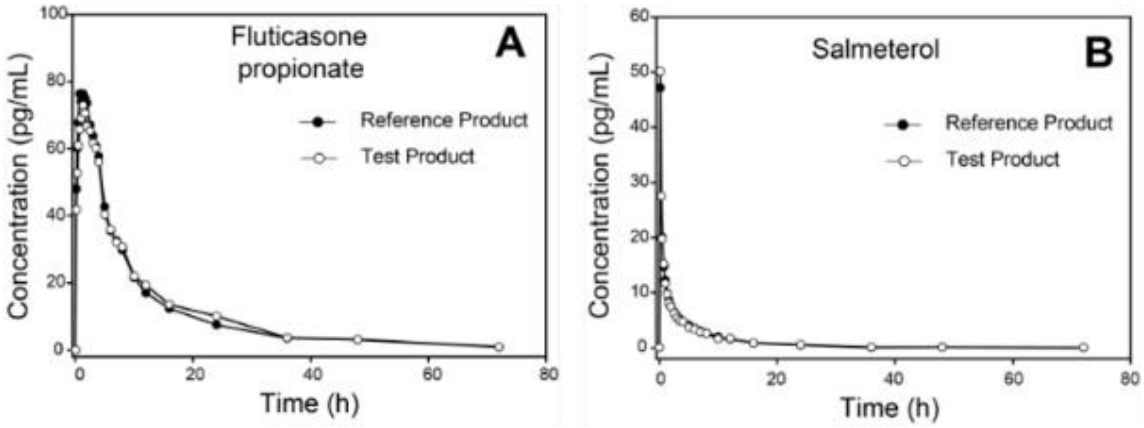

Figure C.1.2. Mean plasma concentration - time profiles of fluticasone propionate (A) and salmeterol (B) for the test and reference dry powder inhalers.

The mean PK parameters (i.e. AUCt, AUCinf, Cmax, Tmax, and λz) accompanied by their statistical descriptive criteria (mean, SD, CV%, median, minimum, and maximum) are summarized in Table C.1.1 for FLP and Table C.1.2 for SAL. For FLP, the peak concentration was 82.62 pg/mL for the T and 88.36 pg/mL for the R product. In the case of SAL, the Cmax values were 50.38 pg/mL and 47.17 pg/mL, for the T and R inhalers, respectively. Also, comparable values between the two tested formulations were obtained for AUCt for both FLP (T: 801.29 pg/mL/h vs. R: 785.10 pg/mL/h) and SAL (T: 79.36 pg/mL/h vs. R: 78.37 pg/mL/h). Besides, the derived CV% values were between 40-60% for almost all PK parameters for the two dry powder inhalers and active substances. In addition, both products exhibited similar mean terminal slope values for FLP (T: λz=0.064

h^{-1} vs. R: $\lambda z=0.075\ h^{-1}$) and SAL (T: $\lambda z=0.122\ h^{-1}$ vs. R: $\lambda z=0.121\ h^{-1}$) (Tables C.1.1 and C.1.2).

Table C.1.1. Pharmacokinetic parameters and statistical descriptive criteria for the plasma concentration-time data of inhaled fluticasone propionate (T and R products).

PK parameter [x]	Mean	SD [y]	CV% [z]	Median	Min	Max
Test						
AUCt (pg/mL/h)	801.293	391.837	48.901	712.057	319.698	2215.581
Cmax (pg/mL)	82.616	32.611	39.473	77.112	28.901	162.751
AUCinf (pg/mL/h)	917.493	426.157	46.448	779.859	332.714	2287.245
Tmax (h)	1.417	-	-	1.333	0.500	4.000
λz (h^{-1})	0.064	0.037	57.860	0.057	0.014	0.249
Reference						
AUCt (pg/mL)	785.100	522.574	66.561	681.769	99.371	3596.052
Cmax (pg/mL)	88.361	35.211	39.849	83.395	35.740	226.911
AUCinf (pg/mL/h)	863.396	552.464	63.987	782.419	125.134	3879.131
Tmax (h)	1.197	-	-	1.000	0.167	3.500
λz (h^{-1})	0.075	0.044	58.024	0.061	0.028	0.260

[x] AUCt: area under the concentration-time curve from time zero to the last quantifiable sample; Cmax: the first recorded maximum plasma concentration value; AUCinf: area under the concentration-time curve from time zero extrapolated to infinity; Tmax: the time at which Cmax occurs; λz: apparent terminal elimination rate constant.
[y] Standard deviation.
[z] Coefficient of variation in %.

Table C.1.2. Pharmacokinetic parameters and statistical descriptive criteria for the plasma concentration-time data of inhaled salmeterol (T and R products).

PK parameter	Mean	SD	CV%	Median	Min	Max
Test						
AUCt (pg/mL/h)	79.358	40.066	50.488	75.773	7.803	226.869
Cmax (pg/mL)	50.377	20.491	40.676	47.258	16.862	104.599
AUCinf (pg/mL/h)	105.431	59.184	56.136	94.116	9.725	356.014
Tmax (h)	0.177	-	-	0.167	0.167	0.750
λz (h^{-1})	0.122	0.124	100.996	0.101	0.015	0.923
Reference						
AUCt (pg/mL)	78.368	37.512	47.867	66.782	9.213	172.378
Cmax (pg/mL)	47.171	24.061	51.009	40.616	9.299	147.611
AUCinf (pg/mL/h)	102.130	51.088	50.023	83.048	12.527	236.574
Tmax (h)	0.167	-	-	0.167	0.167	0.167
λz (h^{-1})	0.121	0.092	76.250	0.110	0.021	0.590

The PK parameters for FLP and SAL were further analyzed following the BE assessment procedure of the EMA (EMA, 2010). The results are listed in Table C.1.3. In case of FLP, the percent GMR of AUCt was 107.3%, while the 90% CI ranged from 96.22% to 119.66%. For SAL, the relevant estimates were 100.9% and 88.43-115.14%. The estimated statically power of the study was found to be 95.73% and 87.37%, for FLP and SAL, respectively. The coefficient of variation of the within-subject variability was 36% for FLP and 44% for SAL.

Table C.1.3. Bioequivalence results for the fluticasone propionate and salmeterol study.

Pharmacokinetic parameters	**GMR (%) [w]**	**Lower 90% CI [x]**	**Upper 90% CI**	**Statistical power (%) [y]**	**Residual CV% [z]**
	Fluticasone propionate				
AUCt (pg/mL/h)	107.3	96.22	119.66	95.73	36%
Cmax (pg/mL)	92.84	85.13	101.25	99.45	28%
	Salmeterol				
AUCt (pg/mL/h)	100.9	88.43	115.14	87.37	44%
Cmax (pg/mL)	110.51	99.74	122.44	97.3	34%

[w] GMR refers to the geometric mean ratio of the test over reference PK metric.
[x] The 90% confidence interval (90% CI) around the GMR.
[y] Statistical power of the study computed using: the estimated GMR, the residual error of the study, level of significance 5%, a number of 57 subjects, and a 2x2 clinical design.
[z] The percent values of the coefficient of variation (CV%) of the residual error.

Table C.1.3 also quotes the BE results for Cmax. For FLP, the GMR value was 92.84% (90% CI: 85.13-101.25%), whereas for SAL the GMR was found equal to 110.51% (90% CI: 99.74-122.44%). The statistical power values were 99.45% for FLP and 97.3% in case of SAL. Finally, the coefficients of variation values of the within-subject variability were 28% for FLP and 34% for SAL.

C.1.1.3.2 Population pharmacokinetic analysis

In case of all different datasets, a plethora of program executions took place in order to examine as many as possible combinations of conditions at each step of analysis. Many different models and scenarios were tested even starting from poor initial PK parameters estimates. Apart from the visual inspection of the individual C-t plots for FLP and SAL, the selection of the final model was based on the criteria described in the 'Methods' section (Bonate, 2005; Gabrielsson and Weiner, 2007). Obviously, not all results can be presented, but only some representative model program executions along with the corresponding numerical criteria and some basic goodness-of-fit plots.

In case of FLP, a first order absorption and elimination process were tested in 1-, 2- and 3-compartment models. The 1-compartment model (Figure C.1.3) was inadequate in describing the elimination process of FLP (Table C.1.4).

Figure C.1.3. Schematic representation of the 1-compartment PK model for inhaled FLP. *Key:* ka, first-order absorption constant; V, volume of distribution; CL, clearance.

Table C.1.4. Goodness of fit criteria for the 1-compartment PK model for inhaled FLP.

Observed vs individual predicted concentrations plot	VPC plot
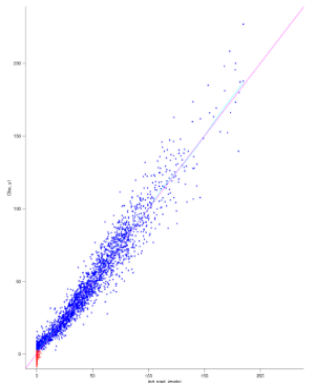	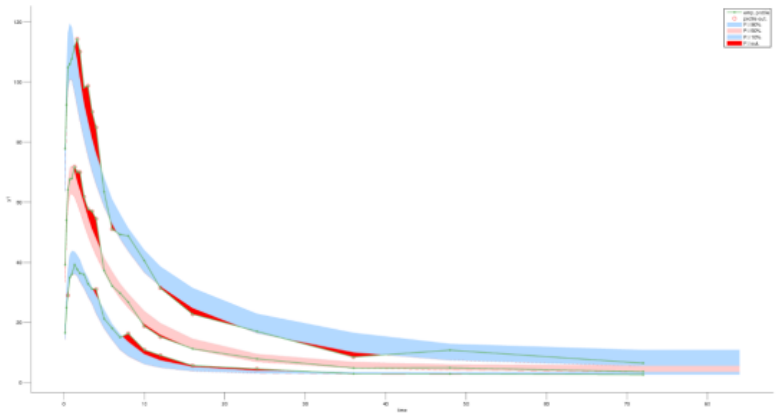

Numerical criteria: -2LL, 17612.23; AIC, 17646.23; BIC, 17692.74

Similar results were also obtained for the 3-compartment model (Figure C.1.4) who failed to describe satisfactorily the distribution and elimination processes of the drug (Table C.1.5).

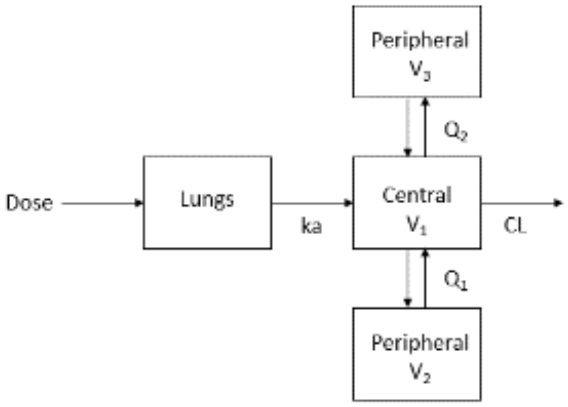

Figure C.1.4. Schematic representation of the 3-compartment PK model for inhaled FLP. *Key:* V_1, volume of distribution of the central compartment; V_2, volume of distribution of the peripheral compartment 1; V_3, volume of distribution of the peripheral compartment 2; Q_1 and Q_2, inter-compartmental clearances.

Table C.1.5. Goodness of fit criteria for the 3-compartment PK model for inhaled FLP.

Observed vs individual predicted concentrations plot	**VPC plot**
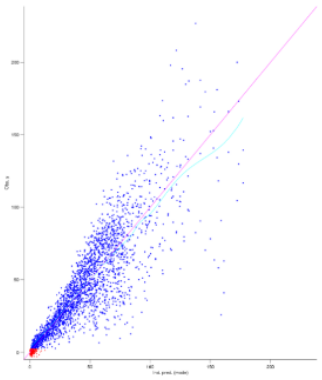	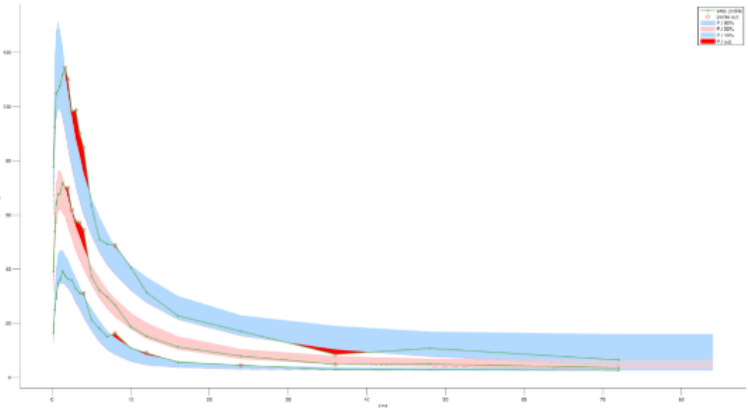

Numerical criteria: -2LL, 19271.75; AIC, 19303.75; BIC, 19347.53

Finally, the structural model that was best fitted to the C-t data was a two-compartment model with first order absorption and elimination kinetics (Figure C.1.5, Table C.1.6).

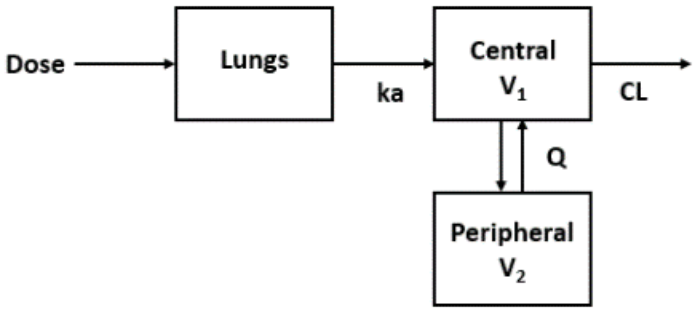

Figure C.1.5. Schematic representation of the final 2-compartment PK model for inhaled FLP.

Table C.1.6. Goodness of fit criteria for the 2-compartment PK model for inhaled FLP.

Observed vs individual predicted concentrations plot	VPC plot
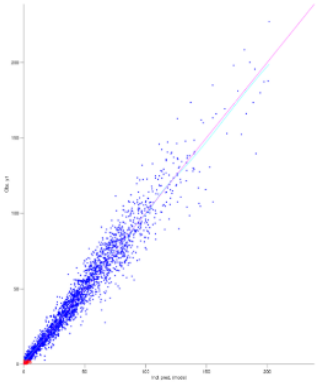	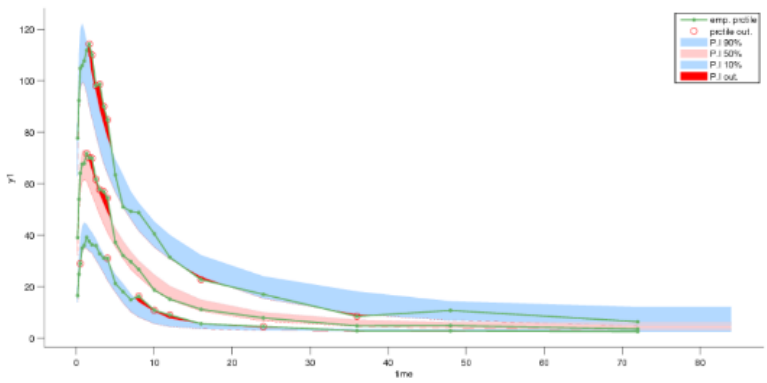

Numerical criteria: -2LL, 17236.49; AIC, 17290.49; BIC, 17364.36

The inclusion in the 2-compartment model of weight as a significant covariate in certain PK parameters further improved the performance of the final model. The estimates of the population parameters of FLP, their BSV% values, along with their RSE% estimates for each parameter are listed in Table C.1.7.

Table C.1.7. Fluticasone propionate population pharmacokinetic parameters for the final best model. *Key*: ka = first order absorption rate constant (h^{-1}); F = Fraction of bioavailable dose; V_1/F = Apparent volume of drug distribution (L) of the central compartment; V_2/F = Apparent volume of drug distribution (L) of the peripheral compartment; Q/F = Inter-compartmental clearance of the drug (L/h); CL/F = Drug clearance (L/h); *a* and *b* = Residual error parameters for the combined error model (Eq.4); RSE% = Relative standard error of the calculation of the population pharmacokinetic estimate; BSV% = between subject variability.

Parameter	Mean (RSE%)	BSV% (RSE%)
ka (h^{-1})	3.87 (8)	21.23 (33)
CL/F (L/h)	659 (8)	39.19 (16)
V_1/F (L)	5,690 (7)	30.37 (15)
V_2/F (L)	5,550 (23)	45.64 (50)
Q/F (L/h)	259 (12)	31.87 (31)
Covariates effects		
Body weight on Ka [y]	0.0215 (19) ($p = 1.4 \cdot 10^{-7}$)	-
Body weight on Q/F [y]	0.0207 (30) ($p = 0.00086$)	-
Body weight on V_2/F [y]	0.0315 (35) ($p = 0.0048$)	-
Residual error model		
a	1.91 (5)	-
b	0.117 (3)	-
Numerical criteria		
-2LL: 17195.45	AIC: 17255.45	BIC: 17337.54

[y] The covariate of 'weight' was centered around the mean weight.

The estimated mean first order absorption rate constant for the study population was 3.87 h^{-1}, the mean apparent clearance was equal to 659 L/h and the mean apparent inter-compartmental clearance equal to 259 L/h. The apparent volume of distribution of the central compartment V_1 was 5,690 L and that of the peripheral compartment equal to 5,550 L. The residual error model that led to the optimum performance was a combined (i.e. additive & proportional) model:

$$C_{ij} = f_{ij} + (a + b \cdot f_{ij}) \cdot \varepsilon_{ij} \qquad \text{(Eq. 4)}$$

where C_{ij} is the j_{th} observed concentration (of either FLP or SAL) for the i_{th} individual, *a* and *b* are the parameters of the residual error model, f_{ij} is the j_{th} model predicted value for i_{th} subject, and ε_{ij} is the random error which is assumed to be normally distributed with mean 0 and variance 1. Also, any combination of covariance terms between the PK parameters did not lead to better fittings or significant correlations between the PK parameters.

The 'treatment' effect was not found to be a significant ($p>0.05$) covariate on any PK parameter, while body weight (i.e., mass) was found significant on ka ($p=1.4\cdot10^{-7}< 0.05$), Q/F ($p=0.00086<0.05$) and V_2/F ($p=0.0048< 0.05$). The model functions for the covariates are:

$$Q/F = \theta_1 \cdot \exp\left(0.0207 \cdot (BW - Mean\,BW)\right) \quad \text{(Eq. 5)}$$

$$Ka = \theta_2 \cdot \exp\left(0.0215 \cdot (BW - Mean\,BW)\right) \quad \text{(Eq. 6)}$$

$$V_2/F = \theta_3 \cdot \exp\left(0.0315 \cdot (BW - Mean\,BW)\right) \quad \text{(Eq. 7)}$$

where the term θ_1 refers to the typical apparent inter-compartmental clearance estimate for a subject with the 'mean' body weight, θ_2 reflects the typical first order absorption rate constant and θ_3 the typical apparent volume of distribution of the peripheral compartment. Equations 5-7 reveal that ka, Q/F and V_2/F rise with the increase of the BW. The correlation plots of weight with the above PK parameters are presented in Figure C.1.6 below.

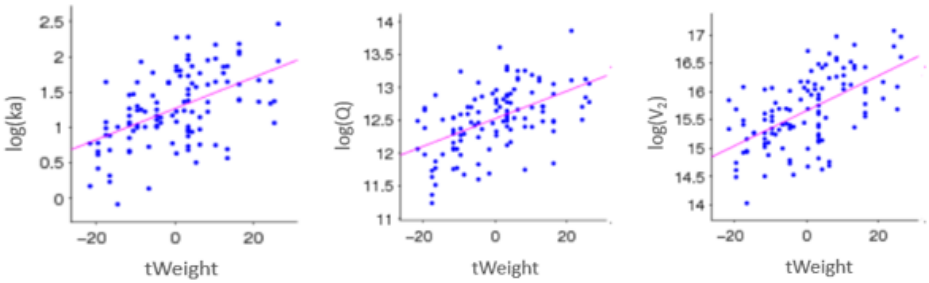

Figure C.1.6. Covariate correlation plots of weight versus ka, Q/F and V_2/F.

The residual error parameters for the combined error model (Eq. 4) were: a=1.91 and b=0.117. Finally, the BSV% estimates were found to exhibit moderate to relatively high values which ranged approximately from 16% to 50% (Table C.1.7).

Figures C.1.7 and C.1.8 illustrate the predicted vs. observed concentration values, as well as the individual weighted residuals (IWRES) and normalized prediction distribution errors (NPDE) *versus* the individual predicted concentrations (IPRED) for the final population PK model of inhaled FLP. An adequate degree of linearity can be observed in all plots.

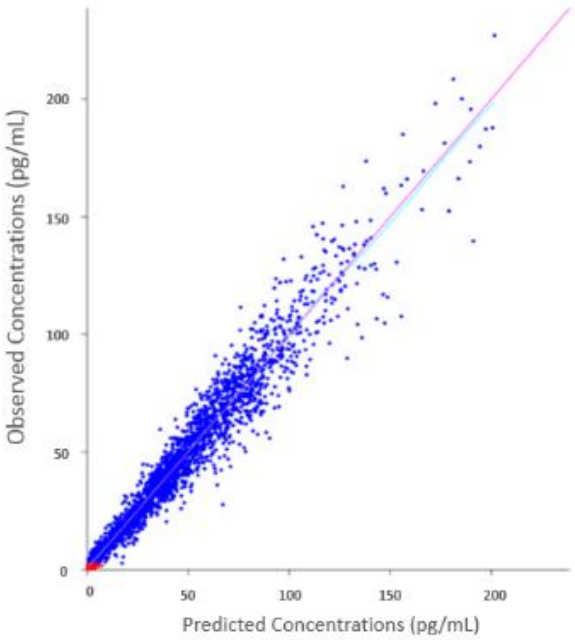

Figure C.1.7. Graphical representation of the individual predicted – observed plasma concentration values for the final PK model of inhaled Fluticasone propionate. The diagonal red line represents the line of unity, namely, of the ideal situation.

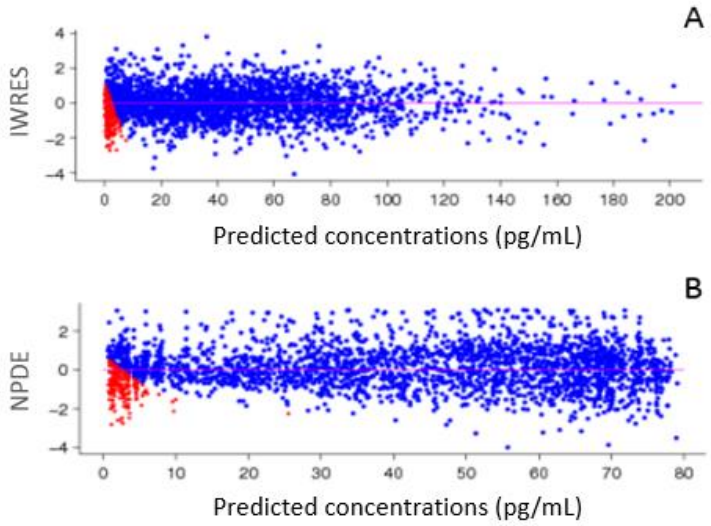

Figure C.1.8. Graphical representation of: (A) the IWRES *vs* IPRED concentrations, and (B) the NPDE *vs* the IPRED concentrations, for the final best model of inhaled FLP.

The VPC of the final model is also depicted in Figure C.1.9, showing a good predictability of the observed data from the model.

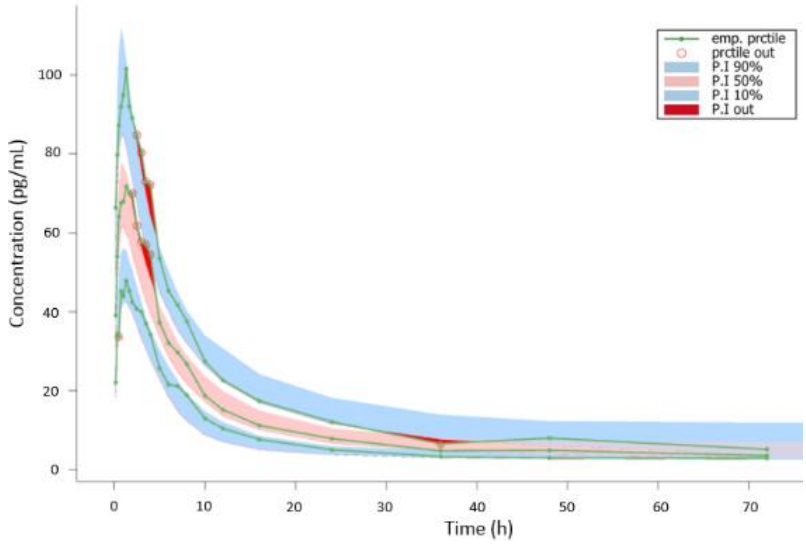

Figure C.1.9. Visual predictive check of the final model for FLP. *Key*: Solid lines refer to the 10th, 50th, and 90th percentiles of the empirical data; Shaded areas refer to the 95% prediction intervals around each theoretical percentile; red circles and areas denote the outlier data.

For SAL, a similar procedure was followed, testing 1-, 2- and 3-compartment models, with first-order absorption and elimination, for their performance. Initially, the 1-compartment model with first-order absorption (Figure C.1.10) failed to describe the very fast absorption of SAL from the lungs, as well as to adequately characterize its slower elimination process (Table C.1.8).

Figure C.1.10. Schematic representation of the 1-compartment PK model with first-order absorption for inhaled SAL.

Table C.1.8. Goodness of fit criteria for the 1-compartment PK model with first-order absorption for inhaled SAL.

Observed vs individual predicted concentrations plot	**VPC plot**
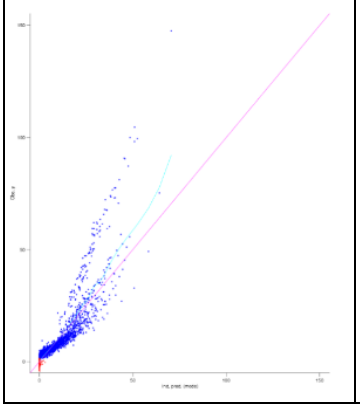	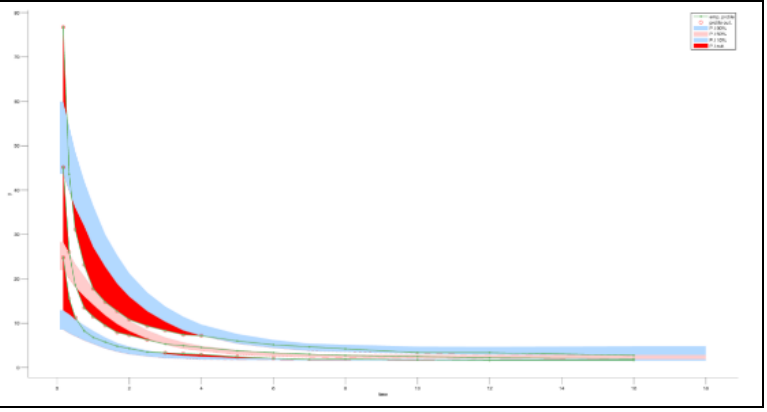

Numerical criteria: -2LL, 11343.84; AIC, 11365.84; BIC, 11395.94

Very high values for the absorption rate estimate were obtained, suggesting that the very fast pulmonary absorption of the drug could be better described by bolus kinetics, i.e like an intravenous bolus administration, also in accordance with previous reported data for SAL absorption from the lungs (Cazzola et al., 2002). The 1- and 3-compartment models tested again showed inadequate fitting and increased numerical criteria (Figures C.1.11 & C.1.12, Tables C.1.9 & C.1.10).

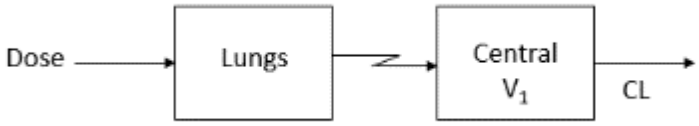

Figure C.1.11. Schematic representation of the 1-compartment PK model with bolus absorption kinetics for inhaled SAL.

Table C.1.9. Goodness of fit criteria for the 1-compartment PK model with bolus absorption kinetics for inhaled SAL.

Observed vs individual predicted concentrations plot	**VPC plot**
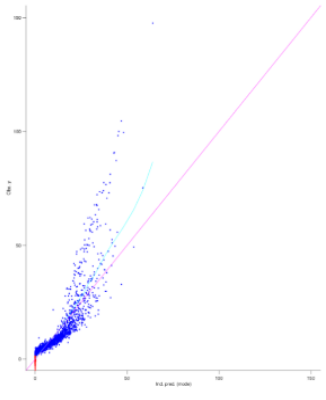	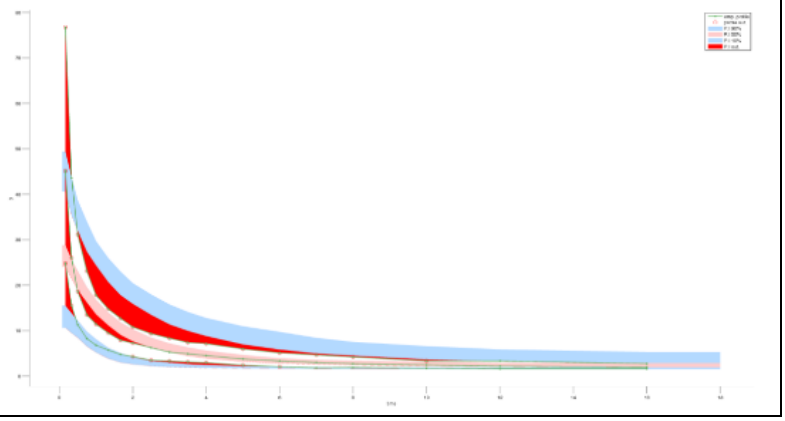

Numerical criteria: -2LL, 11485.59; AIC, 11501.59; BIC, 11523.48

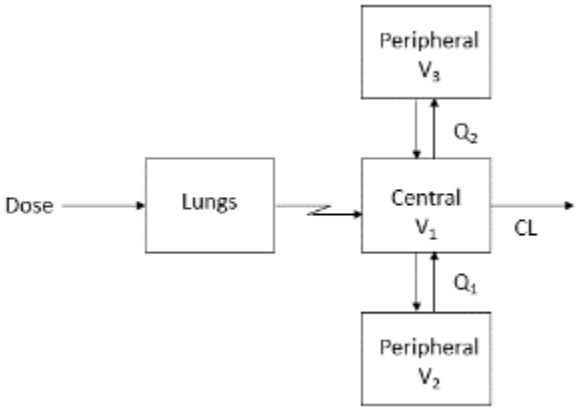

Figure C.1.12. Schematic representation of the 3-compartment PK model with bolus absorption kinetics for inhaled SAL.

Table C.1.10. Goodness of fit criteria for the 3-compartment PK model with bolus absorption kinetics for inhaled SAL.

Observed vs individual predicted concentrations plot	VPC plot
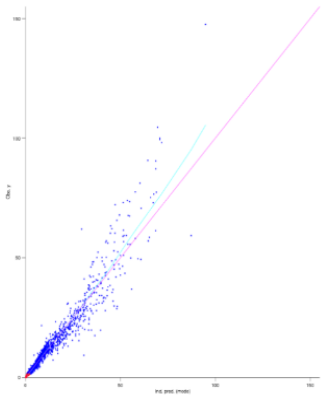	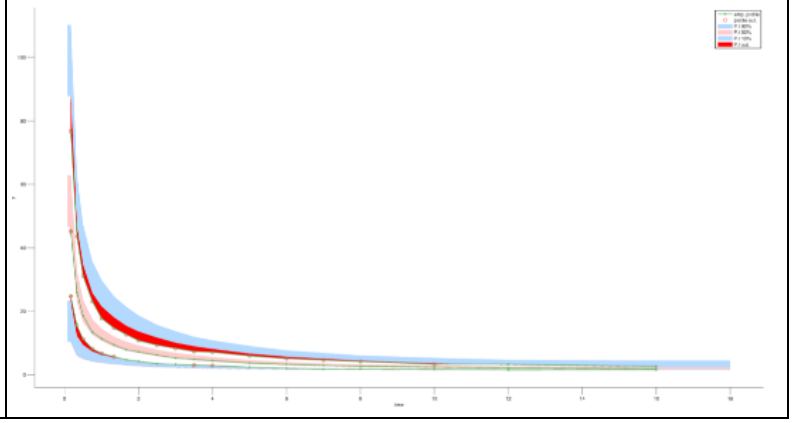

Numerical criteria: -2LL, 7652.81; AIC, 7682.81; BIC, 7723.86

The final best model was obtained when a two-compartment disposition model was used, assuming very rapid absorption kinetics (like intravenous bolus) and first-order elimination kinetics (Figure C.1.13, Table C.1.11).

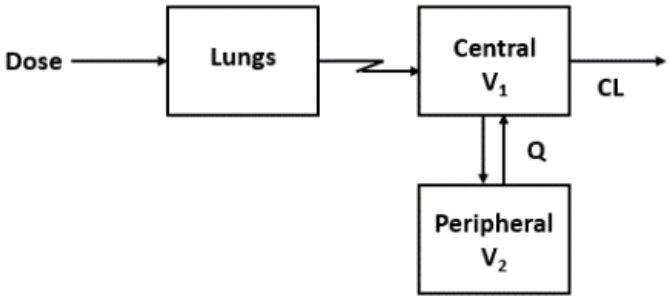

Figure C.1.13. Schematic representation of the 2-compartment PK model with bolus absorption kinetics for inhaled SAL.

Table C.1.11. Goodness of fit criteria for the 2-compartment PK model with bolus absorption kinetics for inhaled SAL.

Observed vs individual predicted concentrations plot	**VPC plot**
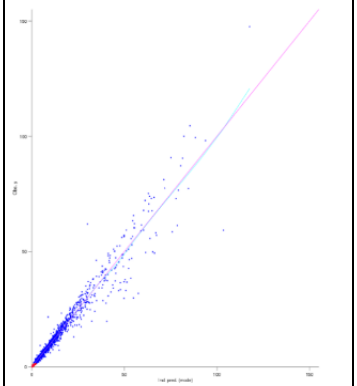	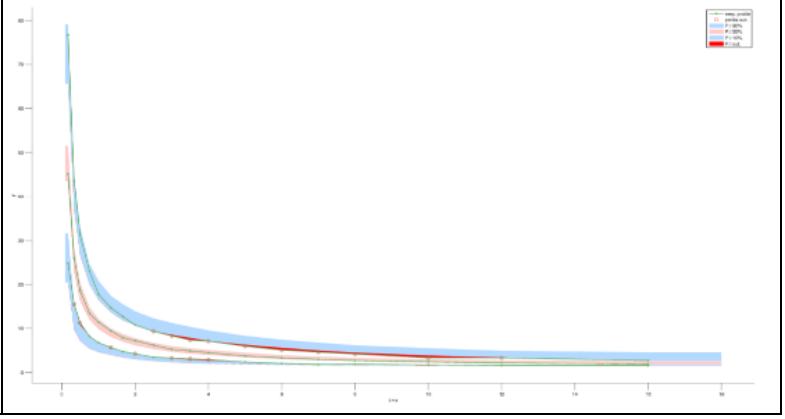

Numerical criteria: -2LL, 7584.73; AIC, 7606.73; BIC, 7636.83

Similar to FLP, a combined (additive & proportional) error model was found to describe best the residual variability, while the inclusion of gender as a significant covariate in the elimination parameter (CL/F) further improved the final model. The estimated population parameters and the BSV% values along with their RSE% are quoted in Table C.1.12.

Table C.1.12. Salmeterol population pharmacokinetic parameters for the final best model.

Parameter	Mean (RSE%)	BSV% (RSE%)
CL/F (L/h)	678 (7)	26.34 (31)
V_1/F (L)	891 (9)	36.76 (14)
V_2/F (L)	2,570 (7)	27.29 (12)
Q/F (L/h)	1,270 (8)	35.88 (12)
Covariates effects		
Gender on CL/F [y]	-0.235 (33) (p = 0.0024)	-
Residual error model		
a	0.2 (4)	-
b	0.125 (3)	-
Numerical criteria		
-2LL: 7326.46	AIC: 7372.46	BIC: 7435.39

[y] Male was considered as the 'control' group.

The mean apparent clearance was found to be 678 L/h, the apparent volumes of distribution were 891 L and 2,570 L for the central and the peripheral compartment, respectively. The estimated apparent inter-compartmental clearance was found equal to 1,270 L/h. As in the case of FLP, the 'treatment' effect was not found to be significant (p>0.05) for any parameter. However, for the C-t data of this study, gender was found to exert a significant effect on CL/F (Eq. 8):

$$\mathrm{CL/F} = \theta_4 \cdot \exp(-0.235) \qquad \text{(Eq. 8)}$$

where θ_4 refers to the typical population PK parameter estimate for the male subjects. In other words, male subjects were found to exhibit about 21% higher clearance compared with females. The boxplot in Figure C.1.14, shows a visual representation of the relationship between SAL clearance and gender.

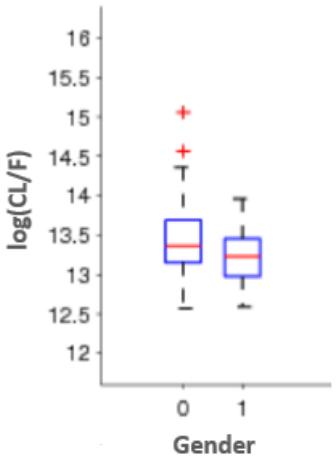

Figure C.1.14. Boxplot for the visualization of the relationship between SAL clearance and the categorical covariate of gender. The boxes represent the observations from the 25th percentile (Q1) to 75th percentile (Q3). The red line within the box represents the median. The points beyond the inter-quartile range (IQR) and which are within 1.5 times the IQR constitute the whiskers. Points beyond the whiskers qualify to be outliers and are represented with red crosses. Males were considered as the 'control' group (0).

The residual error parameters for the combined error model (Eq. 4) were *a*=0.2 and *b*=-0.125 (Table C.1.12). In the same context, the BSV% estimates were found to exhibit moderate to relatively high values ranging approximately from 26% to 37%. Figure C.1.15 illustrates the predicted vs. observed concentration values for the final population PK model of SAL, showing adequate degree of linearity.

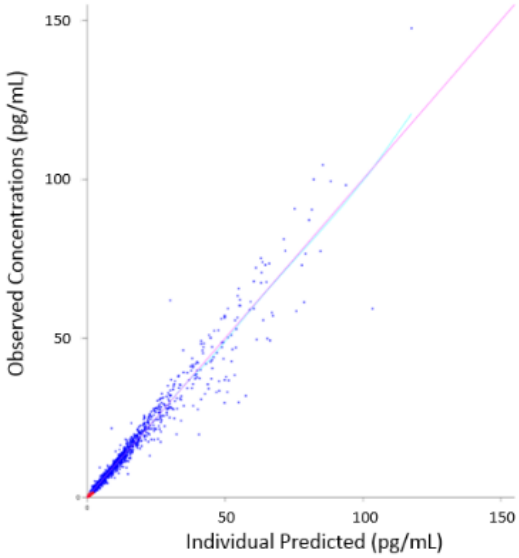

Figure C.1.15. Individual predicted – observed plasma concentration values in case of the final population model of inhaled SAL. The diagonal red line represents the line of unity, namely, of the ideal situation.

Two other goodness-of-fit plots, IWRES and NPDE *versus* IPRED concentrations (Figure C.1.16), also showed a satisfactory distribution of the residual errors of the model around zero.

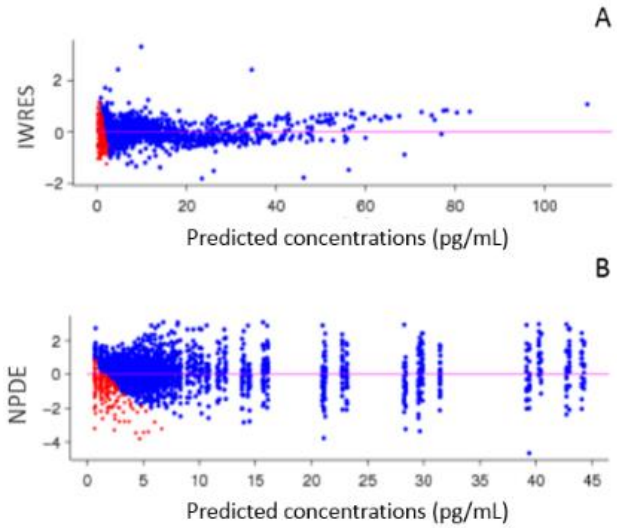

Figure C.1.16. Graphical representation of: (A) the IWRES *vs* IPRED concentrations, and (B) the NPDE *vs* IPRED concentrations, for the final best model of inhaled Salmeterol. The red points refer to censored data.

Finally, the VPC of the final model of SAL is depicted in Figure C.1.17. The predictions from the model described adequately the observed high and median concentration profiles of the inhaled agent.

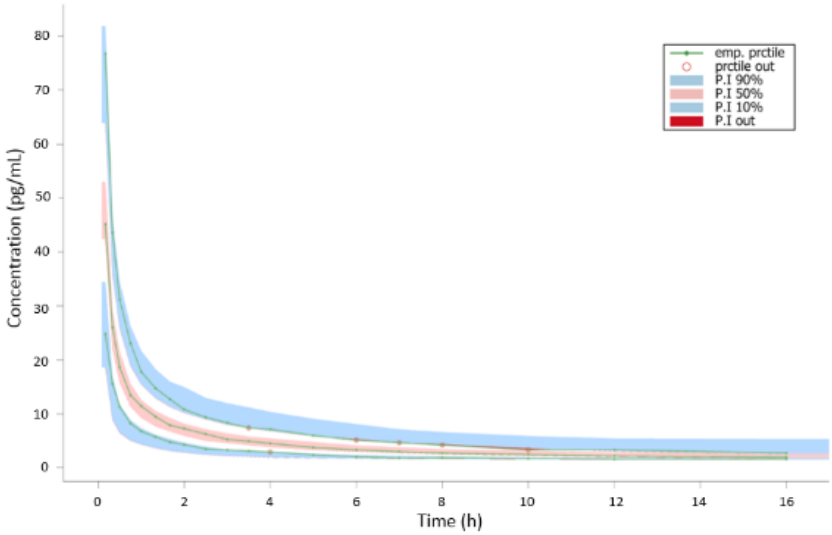

Figure C.1.17. Visual predictive check of the final model for inhaled SAL. *Key*: Solid lines refer to the 10th, 50th, and 90th percentiles of empirical data; Shaded areas refer to the 95% prediction intervals around each theoretical percentile; red circles and areas denote the outlier data.

C.1.1.4 Discussion

Fluticasone propionate and salmeterol are two very valuable compounds for the treatment of COPD. Therefore, knowledge of the PKs of these two drugs, as well as the factors which might affect them is of special importance. The objective of this study was to

explore the PKs of the combination FLP/SAL, when co-administered via inhalation, using data from two dry powder inhalers.

The individual C-t data analyzed in this work were obtained from a 2x2 crossover BE study. Plasma drug levels were low for both agents, with Cmax values up to around 80 pg/mL for FLP and 50 pg/mL for SAL (Fig. C.1.2). The limited systemic absorption is consistent with previously published data, where especially in the case of SAL very low plasma levels were reached following inhalation of therapeutic doses (Cazzola et al., 2002; Mollmann et al., 2001). Visual inspection of the plasma C-t profiles of FLP and SAL (Fig. C.1.2) reveals a similar general profile. It should not be disregarded that these plasma C-t data can only be ascribed to the systemic absorption of the two drugs through the lungs, since gastrointestinal absorption cannot occur due to the co-administration of activated charcoal.

Initially, a non-compartmental PK analysis was applied to the FLP and SAL C-t data in order to estimate the basic PK parameter estimates of the studied sample of volunteers (Tables C.1.1 and C.1.2). Data from periods I and II of the BE study were combined into one group for each drug; thus, a dataset of 57 individuals was available for FLP and SAL. This manipulation was feasible since both treatments (at period I and II) were held under exactly the same conditions. Tables C.1.1 and C.1.2 reveal that similar PK estimates (e.g. Cmax, AUCt, AUCinf etc.) were obtained for the T and R products. The PK parameters were generally in agreement with previously reported values (Cazzola et al., 2002; Mollmann et al., 2001). Peak plasma concentrations of FLP were achieved between 1 to 2 hours following inhalation, while the absorption of SAL was much faster with maximum drug concentrations observed within 10 minutes after inhalation.

The BE results for the FLP and SAL data utilized in this analysis are listed in Table C.1.3. These results indicate that the two dry powder inhalers are bioequivalent, since in all cases the 90% CI for AUCt and Cmax lie within the acceptance interval of 80-125% (EMA, 2010). It is worth mentioning that BE is proved despite the high within-subject variability (ranges from 28% to 44%) of the drug. Also, the derived statistical power for each PK parameter is well above the limiting value of 80%.

Apart from typical non-compartmental analysis, a population PK analysis was also applied to the C-t data of FLP and SAL. Data for the T and R products were combined,

while period (i.e., occasion) and treatment (i.e., T or R) effect were considered as covariates in the population models. Thus, a dataset of 114 individuals was available for analysis in the case of both FLP and SAL. Many runs using several scenarios such as a variety of structural and error models, initial estimates, combination of covariates, were examined. The evaluation the results obtained were made using the goodness-of-fit criteria (visual inspections of several types of plots and statistical criteria) presented in the 'Methods' section.

The C-t data of FLP, obtained following a single inhaled administration in the presence of activated charcoal, were best described by a two-compartment model with first-order absorption and elimination kinetics (Figure C.1.5). A similar model for FLP has also been suggested in the literature (Krishnaswami et al., 2005; Wu et al., 2008). A one-compartment disposition model has been also described in the literature for fluticasone propionate (Rohatagi et al., 1996; Simon et al., 1998; Xu et al., 2010). Perhaps, this divergence might be attributed to the different sample size of the trials and the health status (healthy or asthmatic) of the study participants. The data, we analyzed in this study, came from a BE study where 57 healthy volunteers are analyzed. In contrast, the studies of Rohatagi et al., Simon et al., and Xu et al., 2010 included asthmatic patients where the FLP kinetics are potentially different.

The estimates of the population PK parameters, their BSV% values, along with their RSE% estimates are quoted in Table C.1.7. It should be noted here that previous studies have shown that for lipophilic substances, as in case of FLP, pulmonary dissolution acts in essence as the rate limiting step in the entire process of pulmonary absorption (Hochhaus et al., 1997). Thus, the so-called in this study as absorption rate constant (i.e., Ka), is actually is hybrid parameter representing both slow dissolution of the lipophilic FLP in the lungs and its passing through the alveolar-capillary interface. In the current study, the pulmonary dissolution and absorption were considered as a single process that was described by a single PK estimate, i.e., the absorption rate constant. The latter is in accordance with other published studies (Rohatagi et al., 1996; Simon et al., 1998; Wu et al., 2008; Xu et al., 2010).

It is worth mentioning that until now, the PK models appeared in the literature have treated fluticasone propionate and salmeterol, assuming simple first order absorption kinetics. It is therefore acknowledged that the current models are, like any model, only a

simplification of the true pulmonary behavior. These models could of course be extended with the incorporation of intravenous data and the acquisition of more evidence regarding the physiology and the complex underlying absorption processes.

Another point that requires special attention is the fact that due to slow dissolution of FLP in the lungs and the non-existence of intravenous data, there is a difficulty to distinguish whether this situation is flip-flop kinetics or not. In our study, the estimate of ka (3.87 h^{-1}), was considered to reflect truly the absorption rate constant, since it is quite close to the reported ka value (4.07 h^{-1}) in the more recent study of Xu et al. which utilizes a simpler PK model applied to 32 asthmatic patients (Xu et al., 2010). Besides, our estimated ka value is also close to the ka estimate (2.79 h^{-1}) reported in the study of Wu et al. where a two-compartment model fitted to the C-t data of 14 healthy subjects (Wu et al., 2008).

The derived FLP volume of distribution for the central and the peripheral compartments were found to be equal to 5,690 L and 5,550 L for V_1 and V_2, respectively (Table C.1.7). It should be stated that in the study of Xu et al. (in 32 asthmatic patients), the apparent volume of distribution was found to be even larger, namely, 9,800 L (Xu et al., 2010). Even though a direct comparison of the pharmacokinetic behavior of FLP between asthmatic patients and healthy volunteers cannot be easily performed, this study confirms the extensive distribution of FLP into tissues which appears to be consistent with the high lipid solubility and tissue binding of the drug (Harrison et al., 2003; Thorsson et al., 1997). The extensive distribution of FLP may be the reason for its delayed elimination from the body. The latter is reflected on the fact that FLP plasma concentrations can be detected for more than 24 h after inhalation.

This population analysis also examined the significance of several covariates on the PK parameters. Initially, it should be stated that ‘treatment’ and ‘period’ effect were not found to exert a significant impact on any PK parameter at the 5% significance level. This finding, that ‘treatment’ effect was not found to be significant, is in line with the results derived from the BE study which suggests that administration of the two inhaled formulations will result in similar pharmacokinetic profiles for FLP. For the remaining tested covariates, only body weight (centered around mean) was found to significantly influence ka ($p=1.4\cdot10^{-7}<0.05$), inter-compartmental clearance ($p=0.00086<0.05$) and peripheral volume of distribution ($p=0.0048<0.05$) (Table C.1.7). These findings suggest that as body weight increases, absorption rate, drug inter-compartmental clearance and

peripheral volume of distribution also rise. Fluticasone propionate appears to be restricted to the extracellular space and the extravascular distribution of the drug could be facilitated by the increased fluid associated with an increased body weight. The latter may explain the high volume of distribution estimates found in this study. Also, a literature search revealed that a gender effect on volume of distribution and clearance has been reported, but these data come from a study which did not include healthy subjects, but asthmatic patients (Simon et al., 2008). Again in asthma patients, two other studies did not identify any differences between male and female subjects (Xu et al., 2010).

The increase in FLP absorption rate with higher body weight might be attributed to a larger lung size, which offers a wider absorption surface. Besides, the estimated increase in Q/F as body weight rises seems reasonable due to the physicochemical properties of FLP and the physiologic effect of weight. A similar effect of body weight on Q/F has been reported for propofol (which is also a lipophilic drug) using allometric scaling (Knibbe et al., 2005). Nevertheless, it should be reminded that the current population PK analysis was applied to a relatively homogenous sample of subjects, since it comes from a BE study. An increased sample size and a more heterogeneous pool of subjects would carry more information regarding the effect of covariates.

In case of SAL, visual inspection of the mean C-t plot reveals that its peak plasma levels are reached almost instantaneously. In particular, Tmax estimates are observed almost 10 min (Table C.1.2) after inhalation. The best fitting results were obtained when a two-compartment disposition model was used assuming very rapid absorption kinetics (like intravenous bolus) and first-order elimination kinetics from the central compartment (Figure C.1.13). In order to verify our findings, population PK analysis was also applied assuming first-order input. The latter led to very high ka estimates equal to $2.22 \cdot 10^5$ h^{-1} (data not shown). For this reason, it was decided to consider an instantaneous absorption in order to be able to estimate more accurately the remaining parameters. Besides, the rapid absorption of SAL is in agreement with literature reports (Cazzola et al., 2002). The choice between one- and two-compartment models was based on the C-t fittings and goodness-of-fit criteria.

The apparent volume of distribution of SAL for the central compartment was large (891 L) and it was found even higher for the peripheral compartment (2,570 L), Table C.1.12.

These findings indicate an extensive distribution of SAL within the body, which can ascribed to its high lipophilicity.

A gender effect was found on CL/F (Table C.1.12). Males were found to have higher parameter values for these PK parameters compared to female subjects. The gender effect on clearance might be attributed to the higher enzymatic capacity of men to metabolize SAL and a difference in lung deposition between males and females (Cazzola et al., 2002). Again, in accordance with the results from the BE study, the 'treatment' effect was not found to exert a significant impact on any PK parameter of SAL at the 5% significance level. This finding implies that administration of either T or the R product would lead to similar PK profiles of SAL.

The plots of individual predicted – observed concentration values, for FLP and SAL, reveal that the data are mostly randomly distributed around the line of identity (Fig. C.1.7 & C.1.15). This finding implies a good agreement between the observed and the model predicted drug plasma concentrations for the two models. Furthermore, no trend was observed in the diagnostic plots of IWRES and NPDE *versus* the IPRED concentrations for both FLP and SAL (Fig. C.1.8 & C.1.16). The individual weighted residues were almost symmetrically distributed around zero.

Finally, the goodness-of-fit of the final models was evaluated by visual predictive checks (Figure C.1.9 & C.1.17). Even though, some observations lie outside the 5^{th} or 95^{th}, the majority of them is within. The large concentration values of FLP and SAL are in line with the descriptive statistical criteria quoted in Tables C.1.1 and C.1.2. For example, the Cmax (pg/mL) estimates of FLP range from 28.9 to 162.7 for the test product and from 35.7 to 226.9 in case of the reference dry powder inhaler. We should also bear in mind that a number of 114 observations correspond to each time-point.

C.1.1.5 Conclusions

The purpose of this study was to explore the pharmacokinetics in healthy male and female subjects of FLP and SAL after concomitant administration using data from two dry powder inhalers. Classic non-compartmental approaches, as well as, population pharmacokinetic analyses were applied separately to FLP and SAL. The classic PK analysis allowed the estimation of the individual Cmax, AUCt, AUCinf, Tmax, λz values as well as their descriptive statistics. In a second step, a BE assessment was applied to the estimated PK parameters of the two dry powder inhalers, which showed their bioequivalence. According to the population pharmacokinetic analysis, a two-compartment model was found to best describe the C-t data of FLP assuming first-order absorption and elimination kinetics from the central compartment. In case of SAL, the best results were found when a two-compartment disposition model was used assuming very rapid absorption kinetics (like intravenous bolus) and first-order elimination kinetics from the central compartment. For both FLP and SAL situations, a combined residual error model led to the optimum performance.

C.1.2. Study 2: Inhaled Salmeterol in asthma patients, in the absence of activated charcoal.

C.1.2.1 Introduction

In the present study, the PK analysis of salmeterol is extended to an asthma patient group, in order to further investigate the influence of airway state on the pharmacokinetics of inhaled salmeterol. The data used for this analysis came from a two sequence, four-period, crossover bioequivalence study in asthma patients receiving the FLP/SAL combination via two different inhalation devices. FLP levels were not measured in the study and instead of them, the systemic exposure of cortisol was determined as a safety measure related to fluticasone treatment. Another important difference of this study compared to the previous one is the absence of an activated charcoal scheme, which allowed the gastrointestinal absorption of SAL following inhalation and enabled us to examine the total systemic exposure of the drug.

In accordance with "Study 1", a non-compartmental and a population PK analysis were applied to SAL C–t data. The novelty of this work relies on the following issues: a) to reveal the pharmacokinetics of inhaled salmeterol in asthma patients, and try to determine the fraction of inhaled salmeterol that is absorbed through the gastrointestinal tract, b) to apply population pharmacokinetic analysis as a surrogate for bioequivalence investigation of two medicinal products, c) to investigate and identify demographic characteristics (e.g., gender, body weight) and study related factors (e.g., period, treatment) as potential covariates influencing the pharmacokinetics of inhaled salmeterol.

C.1.2.2 Methods

C.1.2.2.1 Study design and Subjects

Salmeterol plasma C–t data were obtained from a single dose, two sequence, four- period, crossover (2×4) bioequivalence study using two DPIs of the FLP/SAL xinafoate combination: the multi- dose Seretide® Diskus™ (250/50 μg/inhalation, GlaxoSmithKline (GSK), Brentford, UK) and a single- dose device Rolenium® Elpenhaler® (250/50 μg/inhalation, ELPEN Pharmaceuticals, Attica, Greece) under fasting conditions. In the bioequivalence study, instead of fluticasone propionate levels, cortisol plasma levels were determined as a measure of safety related to the fluticasone treatment. A washout period of 5 days was set between each treatment to allow for the

complete removal of salmeterol from the body and to prevent carryover effects. The study was performed in accordance with ICH E6 Good Clinical Practice Consolidated Guidance and the Declaration of Helsinki, by 3S–Pharmacological Consultation and Research (Harpstedt, Germany).

Forty- eight controlled or partly controlled (according to the GINA 2009 classification of Level Asthma Control) asthma male and female patients, with varying degrees of symptoms severity, were enrolled in the study. All patients were informed about the purpose, protocol and potential risks of the study and each participant signed a written consent form before entering the study. The subjects were aged between 18 and 65 years and met the inclusion criteria specified in the study protocol, such as BMI within 18.5–30 kg/m^2, controlled or partly controlled asthma with mild to moderate exacerbations, regular asthma therapy with inhaled glucocorticosteroids (except fluticasone) alone or in combination with longacting β2agonist bronchodilators, (except salmeterol), absence of other than respiratory diseases, non- smokers, non- pregnant and non- lactating women. The main exclusion criteria referred to intolerance or hypersensitivity to the study drugs or lactose, poor clinical asthma control, hospitalization for any other reason or donation of ≥450 ml of blood within 2 months prior to study initiation, any recent history of drug or alcohol abuse, upper respiratory tract infection within 6 weeks prior to the study, electrocardiographic (ECG) changes or any clinical significant abnormalities, positive AIDS or hepatitis B/C tests results. Vital signs, measured before and after the study drugs administration in each study period, were analyzed and all reported adverse effects were recorded. Three subjects were considered as drop- outs due to positive pregnancy test results, concomitant medication or personal reasons.

Therefore, 45 subjects completed the study and their salmeterol C–t data were analyzed and included in our study. On the treatment days, after at least 8 h of fasting, each patient received either one dose of Rolenium® Elpenhaler® 250/50 μg/inhalation (T product) or one dose of Seretide® Diskus™ 250/50 μg/ inhalation (R product), according to the randomization scheme. Activated charcoal, for gastrointestinal absorption blockade, was not co- administered in order to compare the total systemic exposure of salmeterol and to investigate the safety of the drug in the real treatment conditions. Blood samples (6 ml each) were collected before drug administration (i.e. time 0) and at 2, 4, 7, 10, 15, 30 and 45 min, as well as at 1, 1.33, 1.67, 2, 2.5, 3, 3.5, 4, 5, 6, 7, 9, 12, 16, 24, 36, 48, and 72 h

post- dose. The elimination half- life of salmeterol is 5.5 h (Serevent Diskus, 2014), which implies that most of the drug (ca. 90%) will be removed from the body within 27.5 h after its administration. However, blood samples were collected at 36, 48 and 72 h post-dose and analyzed to confirm the complete elimination of the drug after 24 h. After 5 days of the washout period, patients received the alternate product and blood samples were again drawn and analyzed using the same procedures. The entire procedure was repeated for each subject since the study had a fully replicate design.

C.1.2.2.2 Assay methodology

The identification and quantification of salmeterol in plasma were performed by a validated LC–MS/MS method, showing adequate sensitivity, precision, accuracy, specificity and linearity. Separations were performed on a reversed phase column Ascentis Phenyl, 10 cm × 2.1 mm, 5 μm (Merck), in isocratic conditions using a mobile phase composition of 90% acetonitrile and 10% ammonium acetate 15 mM in water, with a flow rate of 1 ml/min. The utilized technique was a re- validated version of the previously published method (Silvestro et al., 2012). The LLOQ for salmeterol was 1.00 pg/ml.

C.1.2.2.3 Pharmacokinetic analysis

C.1.2.2.3.1 Non- compartmental pharmacokinetic analysis

For the purposes of the study, the salmeterol C–t data were initially analyzed using non-compartmental pharmacokinetic approaches. The PK parameters of salmeterol (AUCt, AUCinf, Cmax, Tmax and λz) were calculated and a bioequivalence assessment between the two inhalation devices was further performed on the two main PK parameters (AUCt and Cmax) using the previously described methodology (Methods Section).

C.1.2.2.3.2 Population pharmacokinetic analysis

The population PK analysis was applied to the entire set of data of the 45 subjects who completed all four periods of the bioequivalence study, providing a final dataset of 180 C–t profiles for the analysis. Again plasma C–t data from both T and R products were incorporated in the analysis by setting the ‘treatment’ and ‘period’ effects as potential covariates.

The first stage of the analysis included the determination of the structural model. In this context, one- and two- compartment models were evaluated. Due to the fact that

activated charcoal was not co-administered, apart from the pulmonary absorption of salmeterol, a systemic absorption from the GI tract was also expected to be present. Therefore, the kinetics of salmeterol absorption was modeled in a way capable of describing the parallel pulmonary and GI absorption. An Mlxtran code was created incorporating the two parallel absorption processes of salmeterol, namely, the very rapid (like IV bolus) kinetics of the pulmonary absorption, as described in the previous study and the potential first- order kinetics for the GI absorption. In addition, the relative fraction of the administered dose absorbed via the lungs (R_L) was included as a term into the model. Estimation of R_L allowed also the knowledge of the remaining amount of salmeterol which is capable of being absorbed through the GI (R_{GI}), since the two parameters were assumed to be complementary and their sum to equal to unity. Thus, in the case of the one- compartment model, the structural PK model was parameterized in terms of the apparent first- order absorption rate constant (ka), R_L (or equivalently R_{GI}), the apparent volume of distribution (V/F), and the apparent systemic drug clearance (CL/F), where the term F refers to the bioavailable fraction of dose. For the two- compartment model, the PK parameters incorporated in the model were ka, R_L, CL/F, the apparent volume of drug distribution of the central (Vc/F) and the peripheral (Vp/F) compartments, as well as the apparent inter- compartmental clearance (Q/F).

The individual pharmacokinetic parameters and the BSV values were assumed to follow log- normal distribution. In all cases, elimination was considered to take place in the central compartment following first- order kinetics. Several residual error models were tested, whereas IOV was also evaluated. Finally, the possibility of covariance between the PK parameters was assessed and the effect of the administered product (test or reference) on PK parameters was evaluated through the inclusion of the 'treatment' as an additional component in the model.

Different initial values, including random or values from previously published data were tested and the estimated model PK parameters were evaluated and compared. The 'fixed' option, in the initialization frame of Monolix, was also used during the initial model optimization process for some of the PK parameters (i.e. Vc/F, Vp/F) where the level of PK estimates was not known.

BLQ data were treated as censored data using the appropriate setting of the software and were replaced by the LLOQ value of the bioanalytical method (1 pg/ml). However, not all

missing data up to 72 h of sampling could be treated as censored, for computational reasons. The latter arose from the fact that almost all drug was eliminated from the body at 24 h (the elimination half-life is 5.5 h) and after this time point the vast majority of concentration data were missing (Serevent Diskus, 2014). Therefore, truncation at 36 h was applied, while any missing observations up to 36 h were treated as censored, whereas C–t data after 36 h were omitted.

For the evaluation of the best final PK model, numerical and graphical selection criteria, as well as the physiological soundness of the PK estimates were taken into consideration. After determining the best model, patient covariates were also tested for their contribution into the final model. The investigated covariates included patient demographic characteristics such as gender, age, body weight, height and BMI, the treatment period and formulation effects.

C.1.2.3 Results

The salmeterol C–t data of the 45 male and female patients, who completed the four periods of the study, were included in the PK and statistical analysis. Since FLP levels were not measured in this study, modeling was only performed for the salmeterol data. The mean age of the study population was 45 years (age range 23–64 years), mean BW 75.1 kg (range 52–100 kg), mean height 168 cm (range 150–187 cm) and mean BMI was 26.5 kg/m^2 (range 18.9–29.9 kg/m^2). The tolerability of both products was acceptable, since a total of 13 adverse events were recorded in 10 patients; namely, 7 (R: 3, T: 4) were of mild intensity and 6 (R: 4, T: 2) characterized of moderate intensity. No serious adverse event occurred during treatment with either the T or R products. Also, no statistically significant difference in the incidence of adverse events between the two treatments was observed. The subjects that encountered these adverse events completely recovered before the end of the study. No clinically significant abnormalities on physical examination, vital sign measurements or electrocardiographic recordings were reported.

C.1.2.3.1 Non - compartmental pharmacokinetic analysis

The mean salmeterol C–t profiles following a single administration of the T and R products to the 45 patient volunteers are presented in Figure C.2.1.

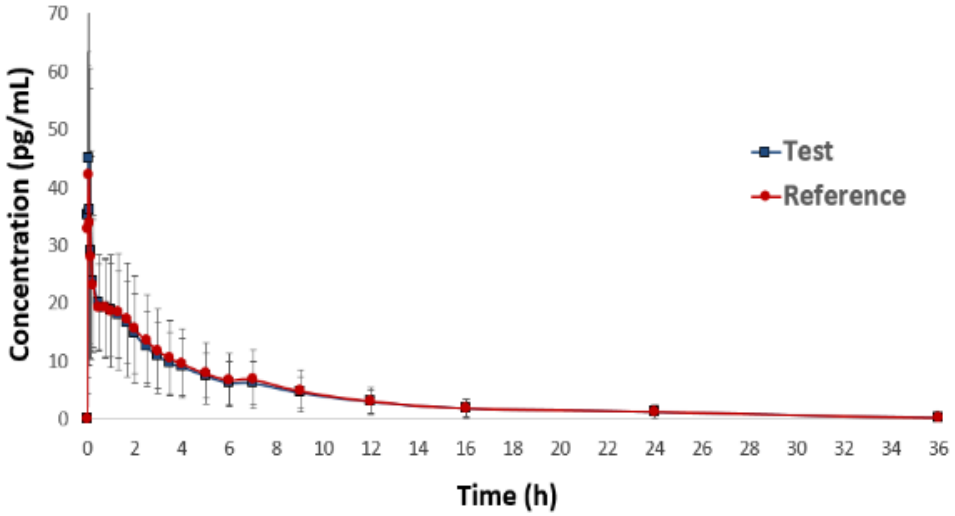

Figure C.2.1. Mean plasma C-t profiles of salmeterol for the test and reference DPIs. The error-bars refer to the standard deviation of the concentration values at each time-point.

Despite the wide time-range of the sampling period, it is evident that the plasma C–t profile of inhaled SAL shows a biphasic time course. The second lesser peak observed between 1-2 hours post-dose in the C–t profile suggests a parallel pulmonary and GI absorption for inhaled SAL, which can be attributed to the absence of oral activated charcoal. This is further supported by the fact that in similar conditions, such a behavior was not observed for inhaled SAL in the previous study, where activated charcoal had been co-administered. Table C.2.1 summarizes the estimates of the PK parameters (AUCt, AUCinf, Cmax, Tmax and λz) of salmeterol accompanied by their descriptive statistics, namely, mean, SD, CV%, median, minimum and maximum.

Table C.2.1. Pharmacokinetic parameters and statistical descriptive criteria for the plasma concentration-time data of inhaled salmeterol (T and R products).

PK parameter	Mean	SD	CV%	Median	Min	Max
Test						
AUCt (pg/mL/h)	136.333	84.509	62.0	115.029	28.530	622.572
Cmax (pg/mL)	47.897	30.090	62.8	40.473	10.959	135.164
AUCinf (pg/mL/h)	156.041	90.414	57.9	133.733	43.608	655.111
Tmax (h)	0.240	-	-	0.067	0.033	1.667
λz (h^{-1})	0.096	0.048	50.3	0.092	0.032	0.294
Reference						
AUCt (pg/mL)	140.502	100.959	71.9	119.725	38.923	883.011
Cmax (pg/mL)	46.543	30.935	66.5	37.639	9.976	131.266
AUCinf (pg/mL/h)	160.726	107.254	66.7	137.039	46.096	919.744
Tmax (h)	0.411	-	-	0.067	0.033	2.000
λz (h^{-1})	0.102	0.051	49.9	0.099	0.008	0.288

The mean Cmax, AUCt, AUCinf and λz values of the T product appear quite close to those of the R product. The Tmax of the R product is 1.7 times slower than that of T. The derived CV% values ranged from 49.9% to 71.9% for all PK parameters. Subsequently, a bioequivalence assessment was performed for the AUCt and Cmax estimates, quoted in Table C.2.1, following the EMA methodology (EMA, 2010). These results are listed in Table C.2.2.

Table C.2.2. BE results for SAL administered via two different dry powder inhalers.

Pharmacokinetic parameters	GMR(%)	Lower 90% CI	Upper 90% CI	Statistical power (%) [a]
AUCt (pg/mL/h)	97.96	92.88	103.32	100.00
Cmax (pg/mL)	106.71	95.97	118.66	94.08

[a] Statistical power of the study computed using: the estimated GMR, the residual error of the study, level of significance 5%, a number of 45 subjects, and a 2x4 clinical design.

For both PK parameters, the 90% CIs were within the acceptance range of 80–125%, indicating that the two products are bioequivalent. The point estimates of the GMR(%) of AUCt was 97.96%, while the 90% CI ranged from 92.88% to 103.32%. With regard to Cmax, the GMR(%) value was 106.71% with a 90% CI ranging from 95.97% to 118.66%. In addition, no significant sequence, treatment or period effects were observed for any PK parameter of salmeterol.

C.1.2.3.2 Population pharmacokinetic analysis

A total of 180 (= 4 periods × 45 subjects) C–t profiles of SAL were included in the dataset for the population PK analysis. As reported above, careful examination of the individual spaghetti plots of SAL (Figure C.2.2) revealed the presence of secondary concentration peaks indicative of a parallel pulmonary and oral absorption process.

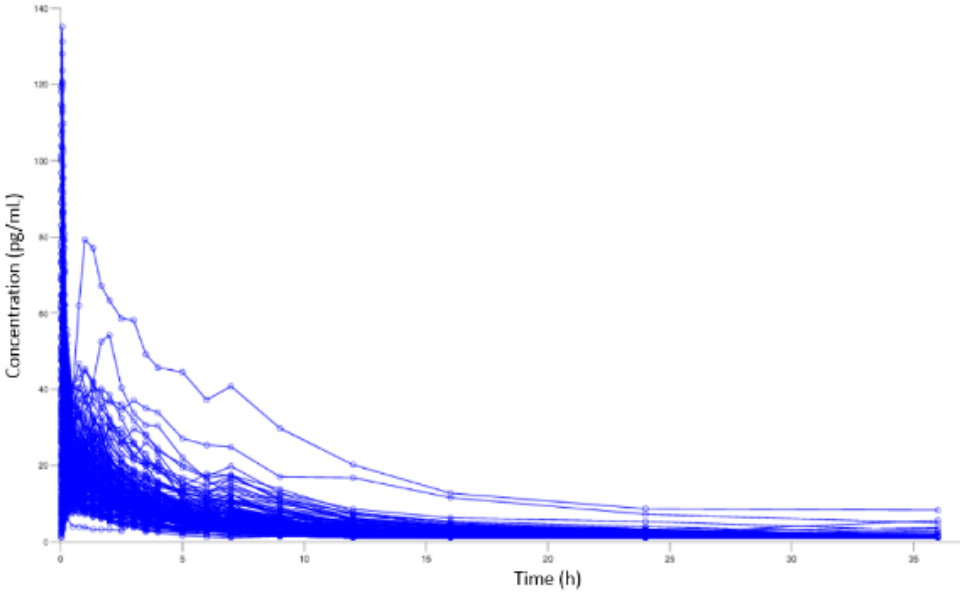

Figure C.2.2. Spaghetti plots of single inhaled dose of SAL in the absence of activated charcoal in asthma patients (n = 180).

Initially, the simple 2-compartment model with bolus absorption, developed for SAL in the previous study, was tested (Figure C.2.3). This model, however, could not satisfactorily describe the kinetics of SAL in the absence of charcoal and capture the dual absorption of the drug (Table C.2.3).

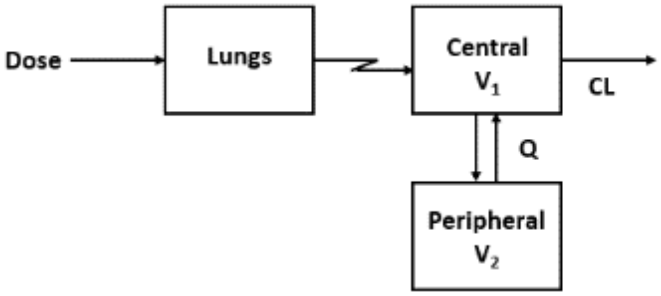

Figure C.2.3 Schematic representation of the 2-compartment PK model with bolus absorption kinetics for inhaled SAL.

Table C.2.3. Goodness of fit criteria for the 2-compartment PK model with bolus absorption kinetics for inhaled SAL.

Observed vs individual predicted concentrations plot	VPC plot
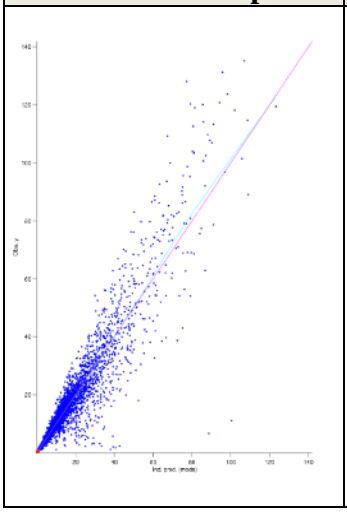	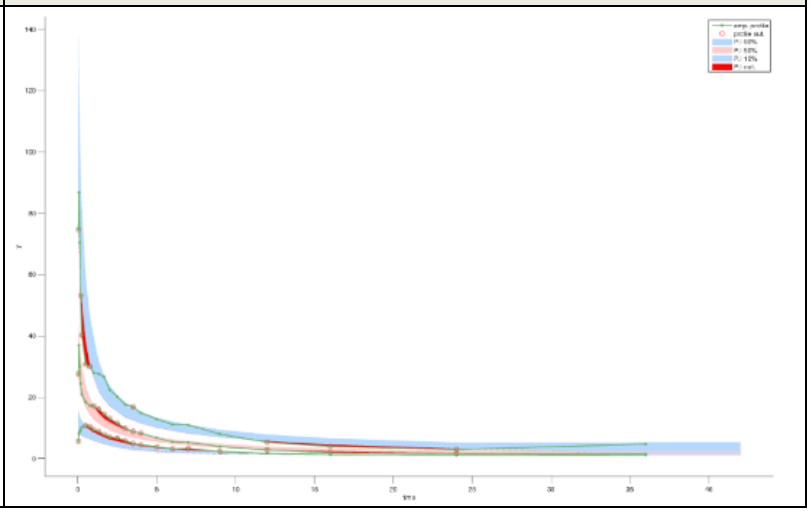

Numerical criteria: -2LL, 19869.17; AIC, 19895.17; BIC, 19936.67

Therefore, many different scenarios were examined and diverse Mlxtran codes were developed in an effort to describe more closely the complex absorption kinetics of inhaled SAL. Finally, SAL plasma concentrations were best described by a two-compartment disposition model combining two parallel absorption processes, a first order absorption from the GI and a very rapid absorption (like IV bolus) from the lungs. Elimination was considered to take place in the central compartment following first order kinetics. Figure C.2.4 depicts the structural model of the pharmacokinetics of salmeterol following inhaled administration in the absence of activated charcoal. The performance of the model is summarized in Table C.2.4.

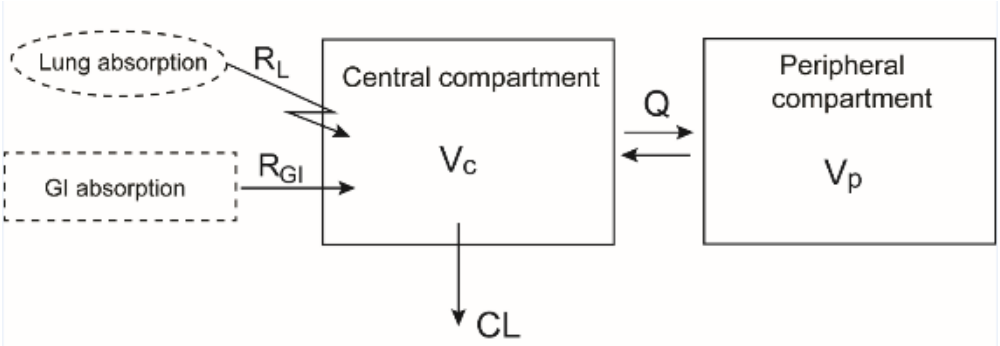

Figure C.2.4. Structural representation of the two - compartment model used to describe the pharmacokinetics of salmeterol after inhalation in the absence of activated charcoal. Two input sources are shown: lung and GI absorption. A relative part of the drug (R_L) is absorbed via the lungs, while the remaining part (R_{GI}) is finally swallowed and deposited in the GI.

Table C.2.4. Goodness of fit criteria for the two-compartment PK model with parallel bolus and first-order absorption kinetics for inhaled SAL.

Observed vs individual predicted concentrations plot	VPC plot
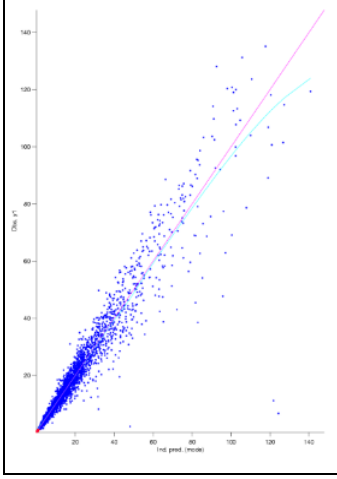	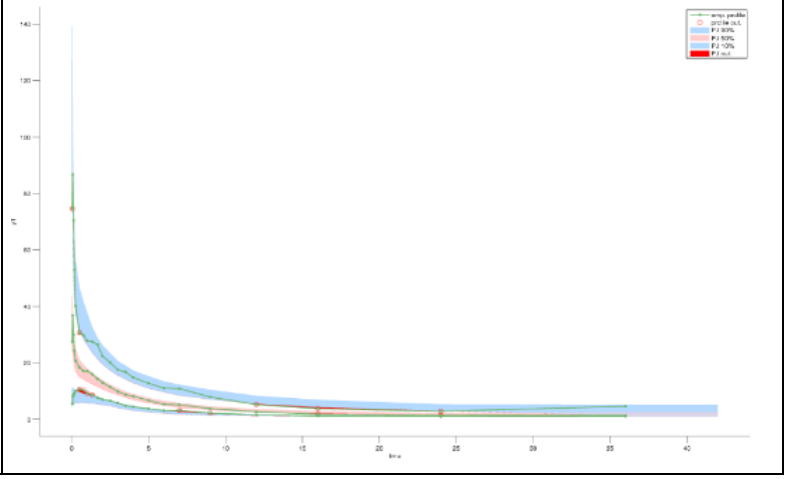

Numerical criteria: -2LL, 17748.92; AIC, 17786.92; BIC, 17847.58

Inclusion of some significant covariates, such as the gender, allometric weight and a treatment effect on certain PK parameters in the final model, further improved its performance. Finally, the best PK model for SAL was parameterized in terms of the GI absorption rate constant (ka), apparent volume of distribution in the central (Vc/F) and the peripheral (Vp/F) compartment, as well as apparent clearance (CL/F) and inter-compartmental clearance (Q/F). The relative fraction of dose swallowed and deposited at the GI (R_{GI}) was also set as a parameter estimated by the optimization process. The residual error model that led to the optimum performance was a proportional error model:

$$C_{ij} = f_{ij} + b \cdot f_{ij} \cdot \varepsilon_{ij} \qquad \text{(Eq. 9)}$$

where Cij is the j^{th} observed concentration of salmeterol for the i^{th} individual, fij is the j^{th} model predicted value for i^{th} subject, b is the parameter of the residual error model, and εij is the random error which is assumed to be normally distributed with mean 0 and variance 1. Any combination of covariance between the random effects of PK parameters did not lead to better fittings or significant correlations between the PK parameters. Table C.2.5 lists the estimates of the population parameters of salmeterol, their BSV% and RSE% estimates for each parameter.

Table C.2.5. Population PK parameters for the best population PK model applied to SAL data. *Key*: R_{GI} = relative fraction of dose undergoing swallowing and being deposited to the GI tract.

Parameter	Mean (RSE%)	BSV% (RSE%)
ka (h^{-1})	0.33 (6)	43.69 (11)
R_{GI}	0.87 (1)	9.32 (11)
CL/F (L/h)	392 (10)	43.69 (12)
Vc/F (L)	177 (11)	73.19 (12)
Vp/F (L)	3,160 (9)	60.69 (12)
Q/F (L/h)	340 (9)	63.88 (12)
Covariates effects		
Gender on CL/F [a]	-0.31 (41) (p = 0.016)	-
Treatment on Vc/F [b]	-0.17 (40) (p = 0.013)	-
Allometric weight on Vp/F[c]	1	-
Residual error model		
b	0.16 (1)	-
Numerical criteria		
-2LL: 17541.93	AIC: 17583.93	BIC: 17650.98

[a] Male was considered as the 'control' group.

[b] The Reference product was considered as the 'control' group.

[c] Allometric scaling exponent fixed at value "1".

The estimated first order GI absorption rate constant was 0.33 h^{-1}, the relative fraction of dose absorbed from the GI was 0.87, the apparent clearance was equal to 392 L/h and the mean apparent inter-compartmental clearance was 340 L/h. The population values of the apparent volume of distribution of the central compartment and peripheral compartment were equal to 177 and 3160 L, respectively. Relatively high BSV% values were observed for almost all estimated PK parameters, which ranged from 9% to 73%.

Gender was found to be a significant covariate on CL/F (p = 0.016), with male patients exhibiting about 27% higher clearance values compared with females. A comparison of the main pharmacokinetic parameters between male and female subjects also shows a higher exposure of women to the drug compared to men, further supporting the above finding (Table C.2.6).

Table C.2.6. Mean values of the main PK parameters for the plasma C-t data of inhaled SAL between male and female subjects.

Pharmacokinetic parameters	Male Subjects (n = 20) [a]	Female Subjects (n = 28)	% Difference [b]
Cmax (pg/mL)	38.69	54.04	33.11
AUCt (pg/mL/h)	111.35	160.07	35.90
AUCinf (pg/mL/h)	131.77	179.67	30.76
		Overall	33.26

[a] The term 'n' refers to the number of subjects (either male or female).

[b] Difference values for each parameter derive from the equation: % Difference = [(Females – Males) / (Females + Males)/2] x 100.

Body weight was also found to be a significant covariate on Vp/F. The latter was implemented by using an allometric relationship between Vp/F and body weight (normalized by a fixed value of 70) and setting fixed the allometric exponent at unity. Finally, a 'treatment' effect (T or R product) was observed on Vc/F. Therefore, the model functions for the covariates are:

$$CL/F = \theta_1 \cdot \exp(-0.31) \quad \text{(Eq. 10)}$$

$$Vc/F = \theta_2 \cdot \exp(-0.17) \quad \text{(Eq. 11)}$$

where θ_1 refers to the typical apparent drug clearance estimate for the male subjects and θ_2 refers to the typical apparent volume of distribution of the central compartment for the reference product. The 'period' effect was not found to be a significant ($p > 0.05$) covariate on any PK parameter. Figure C.2.5 shows the correlation between Gender vs. CL/F and Treatment vs. Vc/F depicted in boxplots.

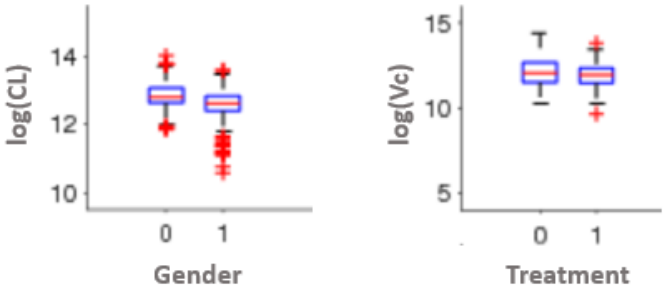

Figure C.2.5. Boxplots showing the relationship between SAL clearance and gender (left) and the apparent volume of distribution of the central compartment and treatment (right). The boxes represent the observations from the 25th percentile (Q1) to 75th percentile (Q3). The red line represents the median. The points beyond the IQR and within 1.5 times the IQR constitute the whiskers. Points beyond the whiskers qualify to be outliers and are represented with red crosses. Male subjects and the reference product were considered as the 'control' groups (0).

Goodness-of-fit plots for the final model are depicted in Figures C.2.6-C.2.8. Figure C.2.6 illustrates the individual predicted SAL concentrations *versus* their observed concentration values for the final population PK model.

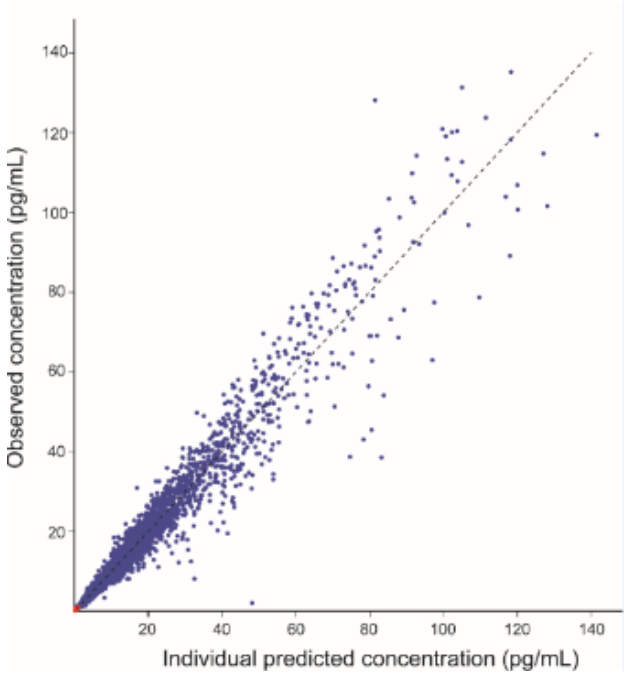

Figure C.2.6. Observed salmeterol plasma concentrations *versus* the individual predicted concentration values from the population pharmacokinetic model of inhaled SAL. The diagonal dashed line represents the line of unity, namely, the ideal situation. Points in red color refer to the missing data due to censoring.

As shown in Figure C.2.6, there is a reasonable agreement between the predicted and observed concentrations. The overall distribution of points around the line of unity looks random and roughly symmetric. This is also supported by the balanced distribution around the zero line in the IWRES and NPDEs versus predicted concentration plots in Figure C.2.7.

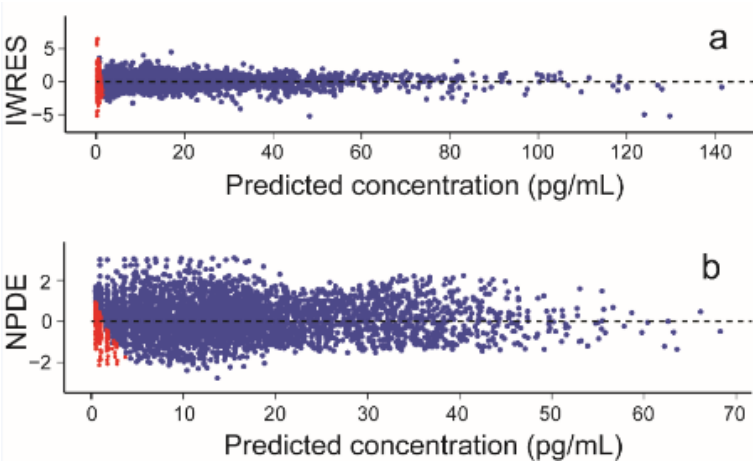

Figure C.2.7. Graphical representation of: (a) the IWRES *vs* IPRED concntations and (b) the NPDE *vs* IPRED concentrations for the final model of salmeterol. Points in red color refer to the missing data due to censoring.

Finally, the VPC plot is presented in Figure C.2.8. The observed concentrations seem to be reproduced adequately by the model, indicating that the utilized structural/error models are appropriate for describing the plasma C–t profile of salmeterol.

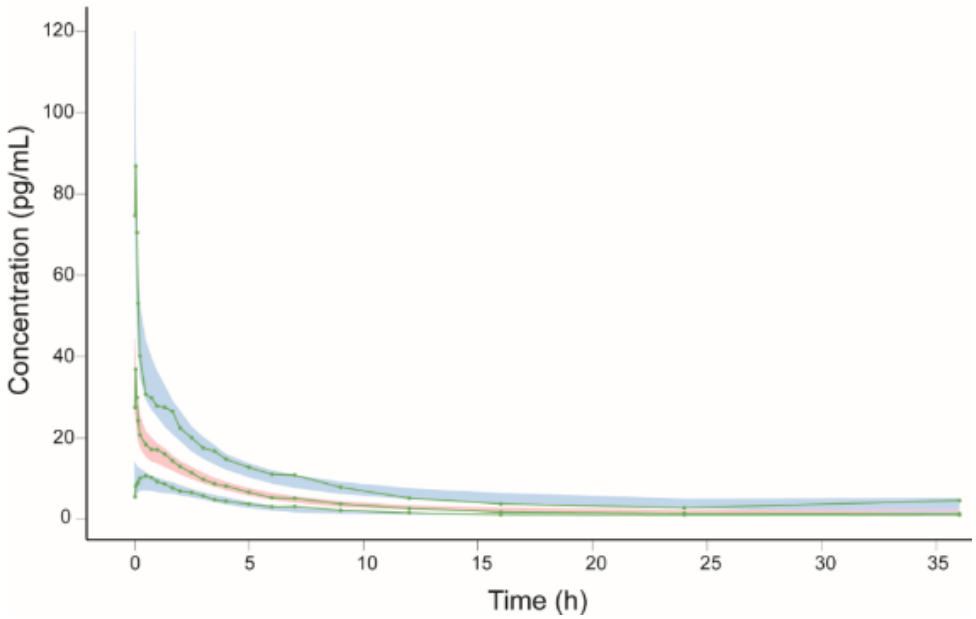

Figure C.2.8. Visual predictive check of the final model for salmeterol. *Key*: Solid lines refer to the 10th, 50th, and 90th percentiles of the empirical data; Shaded areas refer to the 95% prediction intervals around each theoretical percentile; red circles and areas denote the outlier data.

C.1.2.4 Discussion

It can generally be considered that the airway disease state of asthma patients may alter the pulmonary disposition and absorption of salmeterol, similarly to that observed with other β2-agonists (Lipworth and Clark, 1997; Vaisman et al., 1987). However, relatively limited data have been published on the PK behavior of salmeterol. Thus, the aim of this study was to investigate the salmeterol pharmacokinetics in patients with controlled or partly controlled asthma after inhalation by two different dry powder devices.

C.1.2.4.1 Non-compartmental pharmacokinetic analysis

In the first part of our study, the C–t data obtained from the 45 patients, completing all four periods of the bioequivalence study, were analyzed using the classic non-compartmental PK methodology. The blood sampling scheme was considered appropriate to adequately characterize salmeterol pharmacokinetics after a single inhaled administration. Another important point is that highly variable C-t profiles were observed among the 45 subjects (Figure C.2.1). Likely contributors to this variation are the inclusion of asthma patients with varying degrees of symptom severity, the high variability associated with patients' inhalation and the inadequate understanding of device-administration interactions (Smaldone, 2005). In addition, other factors that contribute to this high variability may refer to subjects' pharmacokinetics, namely differences in absorption, distribution and elimination processes. Possible differences in demographic characteristics, such as gender, age and body weight among the treated population may also be considered as additional sources of variation. Despite this high variability, similar PK parameters (Cmax, AUCt, AUCinf, Tmax, λz) were obtained for the two products under evaluation (Table C.2.1). The estimated PK parameters were generally in agreement with previously reported values (Cazzola et al., 2002; Kempsford et al., 2005), as well as with the results from our previous PK study in healthy volunteers.

The results of the bioequivalence assessment for the two inhalers (T, R) are listed in Table C.2.2. Based on these results, it can be concluded that the two products are bioequivalent in terms of the extent and rate of absorption; this finding permits one to conclude that the two dry powder inhalers lead to comparable total systemic drug exposure. For both PK parameters (AUCt and Cmax), the 90% CIs lie within the acceptance interval of 80–125% (EMA, 2010).

C.1.2.4.2 Population pharmacokinetic analysis

In the second part of the study, the same C–t data were analyzed in terms of population PK methodology. Our aim was not limited to providing a description of the subjects' C–t profiles, but also to provide an in-depth analysis of salmeterol kinetics. In this vein, the argument made in this work aims at: a) discussing the structural model, b) unveiling the complex mechanisms of lung absorption, as well as the parallel absorption from the GI, c) highlighting the relative fraction of dose absorbed either through the lungs or the GI tract, d) commenting on the large salmeterol volume of distribution, e) justifying the existence of possible covariates, and finally f) commenting on the evaluation of the intermediate and final models.

C.1.2.4.2.1 On the structural model

Data from the 45 subjects and the four periods of the study for both products (T and R) were pooled together, producing a dataset of 180 C-t profiles for the analysis. Several combinations were examined, including a variety of structural and error models, different absorption kinetics and initial estimates. Finally, a two-compartment disposition model with first-order absorption from the GI and very rapid absorption (like an IV bolus) from the lungs was found to describe successfully the plasma salmeterol C–t data in asthma patients, with elimination from the central compartment following first order kinetics (Figure C.2.4). It should be mentioned that a two-compartment disposition model was also developed for salmeterol in our previous PK study, where healthy subjects received a single dose of inhaled salmeterol in the presence of activated charcoal. Besides, similar two-compartment PK models have been also described for the disposition kinetics of other β2-agonists, including formoterol (Derks et al., 1997), albuterol (Anderson et al., 1998; Maier et al., 2007), batefenterol (Ambery et al., 2015) and vilanterol (Goyal et al., 2014).

C.1.2.4.2.2 Parallel absorption – Complex mechanisms

In our study, following a single inhaled administration of salmeterol, the plasma C–t profiles showed a two-peak pattern with a very short-lived, high peak concentration within the first 10 min after inhalation and a lower second peak concentration, occurring at 30–90 min. It is generally considered that the fraction of dose reaching the airways is absorbed systemically in the same way as an intravenous dose, while the swallowed fraction of an inhaled SAL dose is absorbed similarly to an oral formulation (Cazzola et al., 2002;

Harrison et al., 2011). The very rapid absorption from the respiratory system is in accordance with previous findings where absorption can only occur through the lungs (Anderson et al., 1998; Grekas et al., 2014). The second concentration peak observed in the later phase indicates a slower absorption process, which can be mainly attributed to the swallowed portion of drug finally absorbed from the GI. The assumption that the second concentration peak primarily characterizes gastrointestinal absorption of SAL is further supported by findings in PK studies of other inhaled β2-agonists (Derks et al., 1997; Dhand et al., 1999).

Besides, it has been suggested that for lipophilic substances, such as salmeterol, delayed pulmonary dissolution may lead to a prolonged pulmonary absorption and also contribute to the later absorption phase observed for salmeterol (Horhota et al., 2015; Weber and Hochhaus, 2015). Likewise, the presence of flip-flop kinetics in the later absorption phase and a possible mismatching of the estimated oral absorption rate constant with the disposition parameters cannot be excluded as well. The so-called, in this study, oral absorption rate constant, is actually a hybrid parameter expressing both slow dissolution of the remaining drug in the lungs and oral absorption from the GI. In our analysis, the pulmonary dissolution and GI absorption were described by a single PK parameter (Krishnaswami et al., 2005; Liang and Derendorf, 1998). However, the delayed drug absorption from the lungs is not believed to contribute to a great extent to the second absorption phase of salmeterol. This is further supported by the absence of a second peak concentration in the C–t profile of salmeterol in the presence of activated charcoal in a previous study.

It is, therefore, acknowledged that the estimated absorption PK parameters (e.g. ka and R_{GI}) approximate the underlying more complex drug absorption kinetics. Irrespective of the complexity of the absorption process, the structural model should be able to describe the two parallel pulmonary and gastrointestinal absorption processes.

C.1.2.4.2.3 Relative absorption from lungs and gastrointestinal system

It is evident that the systemic drug levels of salmeterol result from the absorption from both the respiratory epithelium and the GI tract, with a variable contribution of each absorption site among the patients. The estimated RGI value was equal to 87%, which implies that the remaining fraction of the administered dose absorbed via the lungs was

around 13%. This low RL value implies that most of the inhaled drug does not undergo pulmonary absorption, but is deposited (either after swallowing or from the mucociliary clearance) in the GI tract and can enter the general circulation. This finding is in line with other literature studies which showed that, even with an optimal inhalation condition, most of the drug (60–90%) is impacting the oropharynx and the upper airways and is subsequently swallowed, with a much smaller fraction (10–20%) reaching the lungs (Cazzola et al., 2002; Lipworth, 1996). For example, following inhalation of salbutamol, another β2-adrenergic agonist, most of the dose (60–80%) was found to be delivered to the oropharynx and hence to the gut after swallowing, whereas not more than 20% of the dose was deposited in the lungs (Newnham et al, 1993). It has been also reported that the mean total lung deposition of radiolabeled terbutaline in ten asthmatics, using a dry powder inhaler, was in the range 9.1%–16.8% of the inhaled dose (Newman et al, 1991), while similar results have been reported for salbutamol, using another dry powder inhaler device, with a range of 11.7%–16.1% of the inhaled dose deposited in the lungs (Pitcairn et al, 1994). In line with the above reports, the estimated RGI value of 87% in our study suggests a high gut deposition of inhaled SAL in asthma patients.

C.1.2.4.2.4 Volume of distribution

The apparent volume of distribution of SAL was large for both the central (117 L) and the peripheral (3,160 L) compartment (Table C.2.5). After absorption from the lungs, it is likely that salmeterol rapidly distributes into tissues and membranes due to its high lipophilicity (Kirby et al., 2001). In a disposition study in laboratory animals, radioactive salmeterol was widely distributed throughout the body tissues in rats and dogs following intravenous and oral administration (Manchee et al., 1993). In that study, the salmeterol volume of distribution was significantly greater than the total body water in both species and indicated high tissue uptake of the drug. Furthermore, even though a direct comparison of the PK behavior of salmeterol between asthma patients and healthy volunteers cannot easily be performed, this study confirms the extensive distribution of salmeterol into tissues observed in healthy volunteers. Finally, CL/F and Q/F were also high for salmeterol. Similar values for both parameters have also been reported for another inhaled β2-agonist, (R)-albuterol (Maier et al., 2007).

C.1.2.4.2.5 The role of covariates

A gender effect was found on CL/F (Table C.2.5). Males were found to exhibit about 27% higher clearance values compared with female subjects. This difference is also depicted when comparing the three main PK parameters (Cmax, AUCt, AUCinf) between male and female subjects (Table C.2.6). Comparison of these parameters shows that male subjects have about a 30–35% lower Cmax, AUCt and AUCinf values compared with the females. The gender effect on clearance might be attributed to the higher enzymatic capacity of men to metabolize salmeterol, as well as possible differences in lung deposition between males and females (Cazzola et al., 2002).

A similar gender effect on salmeterol clearance has been also observed in our previous study in healthy volunteers, where women exerted a lower capability to eliminate salmeterol than men by 21%. Body weight, in terms of an allometric relationship, was also found to significantly influence the volume of distribution of the peripheral compartment (Table C.2.5). It appears that salmeterol, due to its high lipophilicity, distributes to the extravascular space of body, and this distribution can be further facilitated with an increased body weight. Significant effects of gender and body weight on disposition parameters, CL/F and apparent volumes of distribution (of the central and two peripheral compartments), have been also reported for a new long acting β2-agonist, PF-00610355 (Diderichsen et al., 2013). It should be mentioned that in the final model, the 'period' effect was not found to be a significant ($p > 0.05$) covariate on any PK parameter. The 'treatment' effect (i.e. T or R) was found to be significant only in the case of Vc/F; however, no physiological meaning can be ascribed to this finding, since drug formulation cannot be related to the volume of distribution. This absence of correlation between the administered products and the PK parameters is in accordance with the obtained bioequivalence results, which suggest that administration of the two inhaled products will result in similar PK behavior for salmeterol.

To this point, it should be stated that, since the original purpose of the clinical study was the investigation of the bioequivalence between two medicinal products, a relatively homogenous sample of subjects, in terms of demographic characteristics, was used in the study and were further included in our population PK analysis. In any case, the present analysis was still capable of identifying the role of body weight and gender on salmeterol pharmacokinetics. An increased sample size and a more heterogeneous group of subjects

could provide better information for the potential covariate effects. In addition, other physiological or physical factors, such as lung function parameters, drug particle size distribution and patient status, could potentially explain part of the remaining variability in the estimated PK parameters, however, no such kind of information were available in the current analysis.

C.1.2.4.2.6 Model evaluation

The evaluation of the intermediate and final population PK models was made using several principles such as goodness-of-fit criteria, visual inspections of plots and the physiological soundness of the PK values. Some representative goodness-of-fit plots of the final PK model are shown in Figures C.2.6–C.2.8. In Figure C.2.6, the individual predicted salmeterol concentration values were compared directly with the observed data. The distribution of points around the line of identity appears to be random and roughly symmetric, which implies a good agreement between the observed and the model predicted drug plasma concentrations. The two diagnostic graphs with IWRES and NPDE presented in Figure C.2.7 further support this finding. In both cases, no actual trend was observed and the data were almost symmetrically distributed around zero.

Finally, the goodness-of-fit of the final model was evaluated by a VPC plot (Figure C.2.8). The VPC was performed on the basis of 500 model-based simulations in order to evaluate the model's performance. Visual inspection of the VPC plot reveals that most of the time the three empirical percentiles (median, 10% and 90%) were within the relevant confidence intervals of the simulated percentiles, despite the large variability of the data. We cannot also disregard the fact that a number of 180 observations correspond to each time-point, while the C–t data used in the analysis derived from a patient population with varying degrees of asthma severity. Overall, the obtained plots indicate that the developed model allows for an adequate description of the pharmacokinetics of salmeterol following administration via inhalation.

C.1.2.5 Conclusions

The aim of this study was to investigate the pharmacokinetics of inhaled salmeterol in asthma patients using two different dry powder inhalers. A classic non-compartmental and a population PK modeling approach were applied to a set of C–t data of 45 patients participating in a 2 × 4 bioequivalence study. The population PK analysis led to the same finding with regard to equivalence of the PK parameters of the two inhalation devices. The plasma C–t profiles generally showed a two-peak pattern with a very early Cmax, which is followed by a lower second peak. For this reason, the salmeterol C–t data were modeled assuming parallel lung absorption (very rapid like an IV bolus) and a slower first order absorption. The population PK analysis showed that a two-compartment PK model, with parallel (GI and lung) absorption describes successfully the C–t profile of salmeterol in asthma patients. Elimination was considered to take place in the central compartment following first order kinetics. The relative amount of dose absorbed via the lungs was around 13%, which indicates that most of the drug is swallowed and deposited in the GI. Women were found to exert less capability to eliminate salmeterol than men, while body weight was found to be an important covariate for the volume of distribution of the peripheral compartment. A proportional residual error model led to the optimum performance.

C.1.3. Study 3: Inhaled Budesonide/Formoterol combination in asthma patients, in the presence of activated charcoal.

C.1.3.1 Introduction

Another drug combination successfully incorporated in dry powder inhalers is the budesonide/formoterol combination. These two drugs have played a central role in the management of moderate-to-severe asthma or other pulmonary diseases. Numerous randomized, double-blind clinical studies have shown that co-administration of the two agents is significantly more effective than each drug alone in improving airway function, controlling asthma symptoms, and reducing the risk of exacerbations; thus, providing a favorable therapeutic ratio compared to other treatment options (Cazzola et al., 1995; Lattore et al., 2015).

Budesonide, is one of the most commonly used inhaled corticosteroids, with a proven efficacy record and a well-known safety profile (Figure C.3.1).

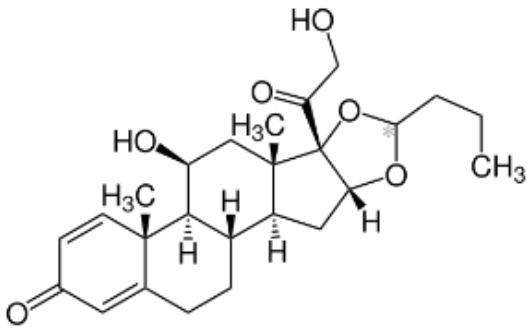

Figure C.3.1. Chemical structure of budesonide.

The drug acts by decreasing airway hyper-responsiveness and the number of inflammatory cells and mediators present in the airways of patients with asthma, treating not only the symptoms of asthma, but also the underlying cause of the disease (Szefler, 1999). The safety and efficacy profiles of inhaled BUD reflect the associated PK and pharmacodynamic properties (Derendorf et al., 2006). In the literature there are studies that describe the BUD plasma levels after inhaled administration (Grekas et al., 2014), however, relatively few studies have identified its pulmonary absorption and systemic disposition characteristics. Inhaled budesonide reaches the systemic circulation either by direct absorption through the lungs or via gastrointestinal absorption of the drug that is inadvertently swallowed. Since BUD is a moderately lipophilic compound, it undergoes rapid uptake into the airway mucosa (Donnelly and Seale, 2001), while evidence suggests

that fatty acid conjugates of the drug are formed and retained within the lung on inhalation, providing a slow-release depot of free drug (Jendbro et al., 2001). This reversible esterification has been shown to prolong the anti-inflammatory activity of BUD, allowing for a once-daily treatment regimen (Szefler, 1999).

Formoterol, on the other hand, is a highly potent, selective β2-adrenoceptor agonist, with a rapid onset and prolonged duration of bronchodilatory action (Figure C.3.2).

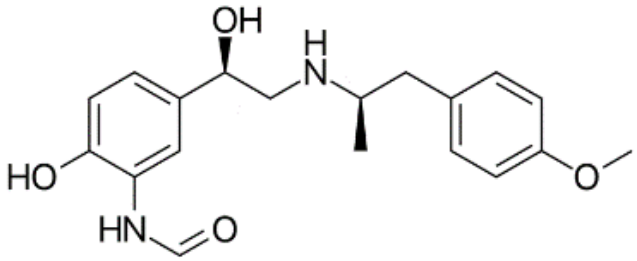

Figure C.3.2. Chemical structure of formoterol.

Following inhalation, the drug causes relaxation of the bronchial smooth muscles and pulmonary artery vasodilation, improves airway muscle function, and increases mucus clearance (Cazzola et al., 1995). A significant bronchodilatory effect is already detected at 1 min after inhalation of a therapeutic dose which persists for at least 12 h. Formoterol has a predictable adverse event profile, including headache, tremor, palpitations, and decreased serum potassium, which is directly related to its total systemic exposure (Lecaillon et al., 1999). The drug has been shown to demonstrate complex absorption and distribution characteristics, i.e., absorption from different sites, enterohepatic recirculation, etc. (Lecaillon et al., 1999). However, its systemic time course following inhalation has not been adequately described, due to the very low (in the level of pg/mL) concentrations reached following inhalation of therapeutic doses, and PK data of formoterol in plasma or blood of humans are sparse in the published literature (Derks et al., 1997; Grekas et al., 2014; Lecaillon et al., 1999).

The aim of the present investigation was, therefore, to explore the absorption and disposition kinetics of the BUD/FOR combination delivered via the single-dose DPI Pulmoton® Elpenhaler® (400/12 μg/inhalation, ELPEN Pharmaceuticals) compared with the multi-dose DPI Symbicort® Turbuhaler® (400/12 μg/inhalation, AstraZeneca) in asthma male and female patients. For this purpose, C-t data, obtained from a BE study with the two DPIs, were analyzed using non-compartmental and population

compartmental approaches. The non-compartmental analysis was implemented for the initial characterization of the rate and extent of systemic exposure of inhaled BUD and FOR. Nevertheless, the main goal of this study was to apply population PK modeling in order to investigate the complex absorption and disposition characteristics of the two drugs following inhalation, as well as to determine the role of potential covariates on the variability of the PK parameters.

C.1.3.2 Methods

C.1.3.2.1 Study design and Subjects

Plasma C-t data of BUD and FOR were obtained from a single dose, two-sequence, two-period, crossover 2x2 BE study using two fix combination dry powder inhalers: Symbicort® Turbuhaler® (Budesonide/Formoterol 400/12 mcg/inhalation, AstraZeneca) and Pulmoton® Elpenhaler® (Budesonide/Formoterol 400/12 mcg/inhalation, ELPEN Pharmaceuticals), under fasting conditions. The study was performed in controlled and partly controlled asthma patients, while activated charcoal was co-administered, with a certain scheme, in order to prevent absorption of the two drugs from the gastrointestinal tract. A washout period of 6 days was set between the two treatment periods, in order to ensure the complete removal of the drugs from the body and prevent any carry-over effect during the second study period. The study was in compliance with the ICH E6 Good Clinical Practice Guidance and was conducted according to the principles of Helsinki Declaration. It was approved by the Romanian National Ethics Committee and the competent regulatory authorities.

One hundred controlled or partly controlled asthma patients, according to the Global Initiative for Asthma (GINA) 2009 classification of Level Asthma Control, with mild to moderate exacerbations at medical history, were enrolled in the study. All subjects were informed about the purpose and potential risks of the study, and a written consent form was obtained by each study participant before enrollment. Male and female patients were considered eligible for inclusion in the study, if they met the following criteria: age between 18 to 65 years, BMI within 18.5-30 kg/m^2, no intolerance or hypersensitivity to study drugs, lactose or other milk proteins, absence of cardiovascular or other than respiratory disease, non-pregnant and non-lactating women. In subjects qualified for regular controller asthma therapy, normal asthma therapy was kept constant throughout the entire study period, except if they had been treated with the study drug combination.

In the latter case, patients had to switch to an equivalent treatment at least 1 week before the initiation of the study. All participants had to be medication-free for at least 12 hours and salbutamol-free for 6 hours before study initiation. Patients were excluded from the study if they had poor asthma control and frequent exacerbations in the past year, participation in another clinical trial in the last three months, hospitalization or donation of ≥450 mL of blood within two months prior to study initiation, upper respiratory tract infection or history of other relevant pulmonary disease, renal or hepatic insufficiency, positive AIDS or hepatitis B/C tests results, and alcohol or drug abuse. Vital signs measurements and clinical examinations were performed before and after the study drugs administration in each study period, and all reported adverse effects were recorded and evaluated.

On the treatment days, after at least 8 hours of fasting, each subject received either one dose of Pulmoton® Elpenhaler® 400/12 μg/inhalation (T product) or one dose of Symbicort® Turbuhaler® 400/12 μg/inhalation (R product), according to the randomization scheme. An activated charcoal scheme was administered 2 minutes pre-dosing, and at 2 min, 1, 2, and 3 hours post-dose in order to block any absorption from the gastrointestinal tract. Blood samples (of 6 mL) were collected before drug administration (time 0) and at 1, 3, 5, 10, 15, 30, 45 min and 1, 1.33, 1.67, 2, 2.33, 2.67, 3, 4, 5, 6, 8, 12, 16, 24, 36, and 48 hours post-dose. Following the six days of washout period, patients received the alternate formulation and the same procedures were followed, as in the first study period.

C.1.3.2.2 Assay methodology

The quantification of FOR was performed in all the collected plasma samples up to 48 h post-dose, whereas BUD plasma concentrations were determined up to 24 h. Two separate LC-MS/MS methods were developed and applied for the analysis of each drug which were firstly presented in a previous study (Grekas et al., 2014). Both analytical techniques were validated and presented adequate sensitivity, precision, accuracy, specificity, and linearity. The LLOQ values were 5.000 pg/ml for BUD and 0.300 pg/mL for FOR (Grekas et al., 2014).

C.1.3.2.3 Pharmacokinetic analysis

C.1.3.2.3.1 Non-compartmental pharmacokinetic analysis

Budesonide and formoterol C-t data were, initially, analyzed using non-compartmental methods and the following PK parameters were calculated: AUCt, AUCinf, Cmax, Tmax and λz. Descriptive statistics were also calculated for these PK parameters. Bioequivalence assessment was also performed on the primary PK parameters (AUCt and Cmax) following the current methodology proposed by the European Medicines Agency (EMA, 2010), described previously.

C.1.3.2.3.2 Population pharmacokinetic analysis

Data for both drugs were further analyzed using a compartmental population PK methodology. A non-linear mixed effects model approach was applied separately for each drug and the entire computational work has been implemented in Monolix® 2016R1 software (Lixoft, Orsay France). Data for each drug obtained from the different treatment periods and administered products (T and R) were pooled together setting 'period' and 'treatment' effects as potential covariates in the final dataset. Finally, a dose of 320 mcg instead of 400 mcg was considered for BUD and 9mcg instead of 12mcg for FOR. The latter correction was in accordance with the relevant drug products information, since these two doses (i.e., 320 mcg and 9 mcg) are the actually delivered doses through the mouthpiece during inhalation (Symbicort, 2016).

Initially, the analysis focused on the selection of the most appropriate structural model for each drug and thus, typical one-, two-, and three-compartment models with different drug input kinetics were investigated. However, since both drugs (BUD and FOR) exhibited rather complex PK profiles following inhaled administration, conventional models were proven inadequate to describe the kinetics of the two drugs and structural models of increasing complexity had to be constructed. The developed models were encoded through an ordinary differential equation system in the model translator MLXTRAN of Monolix® software.

In particular, in the case of FOR a plateau or a second lower peak was observed at around four hours post-dose in the majority of C-t profiles (Figure C.3.3).

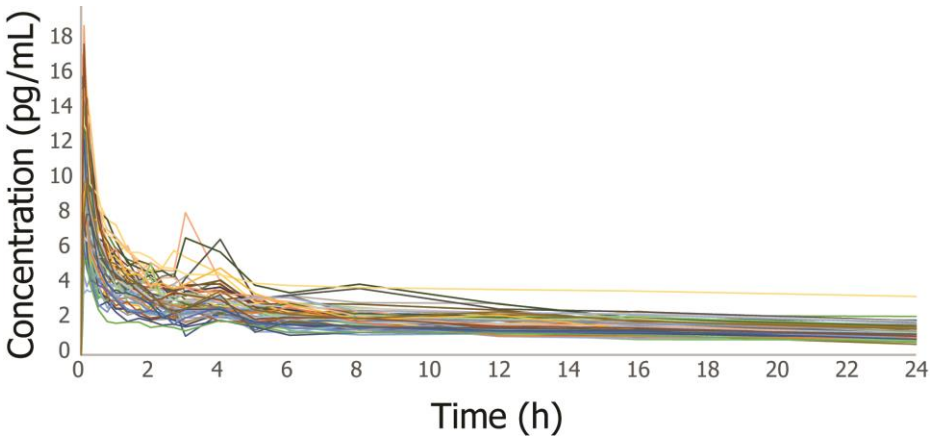

Figure C.3.3. Individual concentration-time profiles of FOR in plasma of 90 asthma patients after a single inhaled dose of formoterol fumarate from two dry powder inhalers.

Since the activated charcoal scheme was administered up to three hours in the present study, gastrointestinal absorption of the swallowed part of the inhaled dose was excluded, and the observed second peak was attributed to an enterohepatic circulation process, known to occur in the case of FOR. For this reason, PK models capable of describing this re-distribution process within the body were developed. Different scenarios were tested, including multi-compartment models with additional GI and GB compartments consisting the enterohepatic loop, application of bolus, first- and zero-order kinetics or sine function models for bile release, different time intervals for gallbladder emptying, presence or absence of fecal elimination, etc. Absorption from the lungs, as well as elimination from the central and/or GI compartments were assumed to follow first-order kinetics.

Similarly, BUD also required the development of a more complex PK model, in order to describe its multiphasic lung absorption processes. The choice of two parallel lung absorption processes for BUD has been also previously suggested by Weber and Hochhaus (Weber and Hochhaus, 2013). A parallel fast and slow pulmonary absorption process was, therefore, incorporated in the PK model. Single- or double-input processes, pulmonary depot sub-compartments, transit absorption compartment models with first- and zero-order rate constants, Erlang-type transit compartments, and time-dependent absorption were also evaluated during model development. Accordingly, oral absorption was excluded due to the co-administration of the activated charcoal scheme. One-, two-, and three-compartment models, were investigated for the distribution kinetics of BUD. In all cases, elimination was considered to take place in the central compartment and follow first-order kinetics.

The between-subject variability was assumed to follow log-normal distribution for all PK parameters of FOR. In case of BUD, in addition to log-normal distribution, a logit-transformation was also implemented in certain PK parameters constrained to be on a zero to one scale. Inter-occasion variability was considered, while the possibility of correlation between the random effects of the PK parameters was also assessed. Various statistical models (constant, proportional, exponential, and combined) describing the random residual variability of the structural models were considered.

Following the determination of the best structural model for each drug, various covariates were tested for their contribution in the model, including: BW, gender, age, height, BMI, asthma disease state, and baseline FEV1 measurements, the period and formulation effects. Candidate models for BUD and FOR were assessed in terms of model statistical criteria, as well as visual inspection of goodness-of-fit plots and simulation-based diagnostics. PK parameter estimates were required to be physiologically plausible and had to remain stable when significant digits and initial parameter estimates were altered.

C.1.3.3 Results

Finally, 90 subjects were included in the non-compartmental and population PK analyses since ten volunteers withdrew from the study. A number of 59% of the enrolled subjects had controlled asthma. Three subjects were considered as dropouts referring to positive pregnancy test results and seven patients presented very low or undetectable plasma drug levels in the majority of their samples. The demographic characteristics of the enrolled subjects along with their descriptive statistics are listed in Table C.3.1. Forty-three non-serious adverse events (headaches, vomiting and dizziness) were recorded in the study: 32 of moderate and 11 of mild intensity were equally distributed between the two treatments. No deaths or any other significant adverse events were recorded and all volunteers completely recovered before the termination of the study.

Table C.3.1. Descriptive statistics of demographic characteristics of the enrolled subjects.

	Age (years)	Weight (kg)	Height (cm)	BMI (kg/m^2)
Mean	46.85	73.26	166.61	26.40
SD	11.51	11.50	9.03	3.59
CV %	24.6	15.7	5.4	13.6
Minimum	19	50	150	18.7
Maximum	65	97	192	30.0
Range	46	47	42	11.3

C.1.3.3.1 Non-compartmental pharmacokinetic analysis

The observed mean plasma concentrations of FOR and BUD *versus* time, following a single inhaled dose from T and R, are presented in Figures C.3.4(A) and C.3.4(B), respectively. Despite the increased variability following inhaled administration, quite similar drug C-t profiles were obtained for the two DPI products.

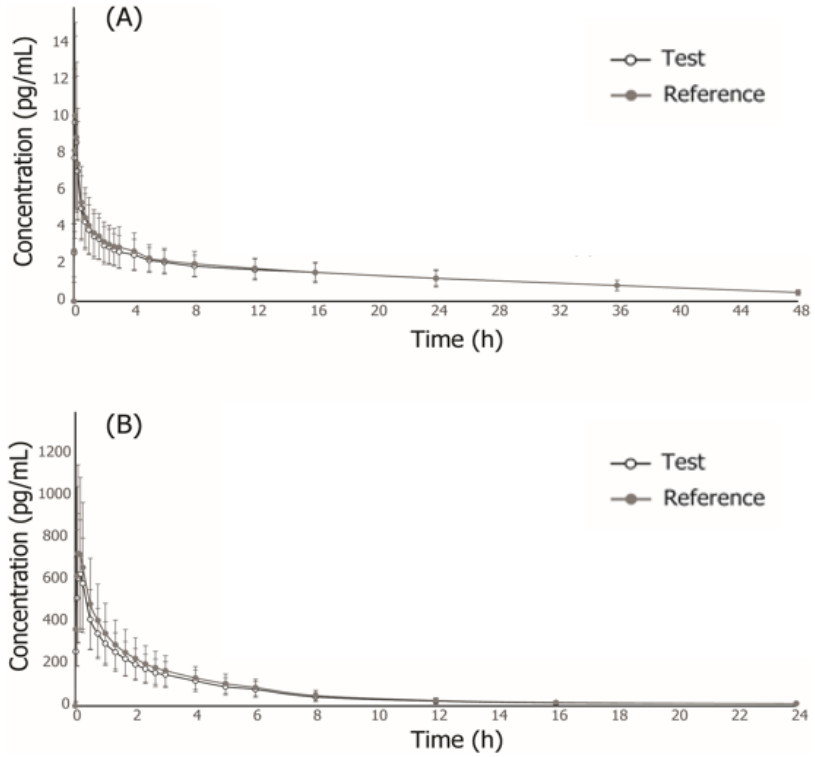

Figure C.3.4. Mean plasma concentration - time profiles of formoterol (A) and budesonide (B) for the test and reference DPIs. The error-bars refer to the standard deviation of the concentration values at each time-point.

The calculated mean PK parameters (i.e. AUCt, AUCinf, Cmax, Tmax, and λz) accompanied by their statistical descriptive criteria are summarized in Table C.3.2 for FOR and Table C.3.3 for BUD. Comparable values between the two tested formulations were obtained for Cmax, AUCt and AUCinf for both drugs. The derived CV% values

ranged from 25.6 to 47.9% for the estimated PK parameters of FOR and from 37.9 to 64.5% for PK parameters of BUD.

Table C.3.2. Pharmacokinetic parameters and statistical descriptive criteria for the plasma concentration-time data of inhaled FOR (R and T products) in 90 asthma patients.

PK parameter	Mean	SD	CV%	Median	Min	Max
Reference						
AUCt (pg/mL/h)	69.417	19.729	28.4	68.018	21.805	117.249
Cmax (pg/mL)	10.356	4.962	47.9	9.288	2.272	33.977
AUCinf (pg/mL/h)	83.513	21.703	26.0	81.787	35.840	148.372
Tmax (h)	-	-	-	0.083	0.05	0.5
λz (h^{-1})	0.040	0.010	25.6	0.040	0.016	0.065
Test						
AUCt (pg/mL)	67.523	20.666	30.6	69.632	26.141	145.293
Cmax (pg/mL)	10.117	4.630	45.8	8.86	3.371	25.797
AUCinf (pg/mL/h)	81.432	22.831	28.0	81.728	35.106	173.926
Tmax (h)	-	-	-	0.083	0.05	0.5
λz (h^{-1})	0.040	0.010	25.8	0.040	0.016	0.069

Table C.3.3. Pharmacokinetic parameters and statistical descriptive criteria for the plasma concentration-time data of inhaled BUD (R and T products) in 90 asthma patients.

PK parameter	Mean	SD	CV%	Median	Min	Max
Reference						
AUCt (pg/mL/h)	1769.415	759.655	42.9	1613.058	191.131	4159.821
Cmax (pg/mL)	818.993	411.144	50.2	800.775	109.588	2214.556
AUCinf (pg/mL/h)	1844.653	789.637	42.8	1690.863	208.889	4366.584
Tmax (h)	-	-	-	0.167	0.05	1.00
λz (h^{-1})	0.169	0.064	37.9	0.162	0.056	0.343
Test						
AUCt (pg/mL)	1541.628	617.343	40.1	1406.357	478.144	3366.919
Cmax (pg/mL)	709.483	277.298	39.1	725.356	182.660	1568.544
AUCinf (pg/mL/h)	1614.704	655.631	40.6	1454.959	523.423	3579.876
Tmax (h)	-	-	-	0.167	0.05	1.00
λz (h^{-1})	0.180	0.116	64.50	0.166	0.060	0.984

The primary PK parameters, C_{max} and AUC_t, for BUD and FOR were further analyzed following the BE assessment methodology of the EMA guideline (EMA, 2010). For both drugs, the percent GMRs of C_{max} and AUC_t estimates, along with the 90% CIs are within the acceptance range of 80-125%, indicating that the two products are bioequivalent (Tables C.3.4 and C.3.5).

Table C.3.4. Bioequivalence results for FOR administered via two DPIs (T and R).

Pharmacokinetic parameters	GMR(%)	Lower 90% CI	Upper 90% CI	Statistical power (%) [a]
AUCt (pg/mL/h)	96.62	93.46	99.89	100.00
Cmax (pg/mL)	98.38	91.10	106.24	99.89

[a] Statistical power of the study computed using: the estimated GMR, the residual error of the study, level of significance 5%, a number of 90 subjects, and a 2x2 clinical design.

Table C.3.5. Bioequivalence results for BUD administered via two DPIs (T and R).

Pharmacokinetic parameters	GMR(%)	Lower 90% CI	Upper 90% CI	Statistical power (%)
AUCt (pg/mL/h)	89.78	83.18	96.90	99.90
Cmax (pg/mL)	91.30	84.01	99.22	99.68

C.1.3.3.2 Population pharmacokinetic analysis

In total, 180 (=2 periods x 90 patients) C-t profiles were used for the population PK analysis and model building of each drug. As reported in the 'Methods' section, both FOR and BUD presented complex absorption and disposition kinetics following inhaled administration, with the classic one-, two-, and three- compartment models proven inadequate to describe the available C-t data. Therefore, MLXTRAN codes were developed for each drug and further assessed for their performance.

C.1.3.3.2.1 Formoterol

In the case of FOR, visual inspection of the spaghetti plot (Figure C.3.5) revealed second smaller concentration peaks within 3-5 hours post-dose. The contribution of absorption of the swallowed fraction of dose from the GI tract was excluded due to the concomitant administration of activated charcoal; thus, the second peak is most probably attributed to an enterohepatic recirculation of FOR.

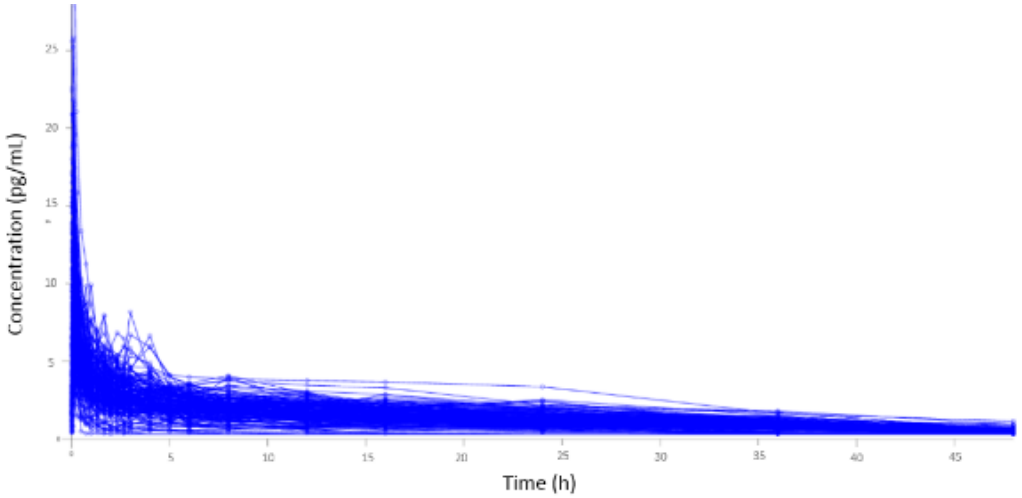

Figure C.3.5. Spaghetti plot of FOR following a single inhaled administration in 180 subjects.

A conventional 2-compartment model with first-order absorption was found inadequate to fit this complex re-circulation process (Table C.3.6). Similarly, 1- and 3-compartment models incorporating first-order or bolus kinetics for drug absorption also failed to describe FOR PKs following inhalation.

Table C.3.6. Performance of a conventional 2-compartment PK model with first-order absorption for the description of the pharmacokinetics of inhaled FOR.

Observed vs individual predicted concentrations plot	**VPC plot**
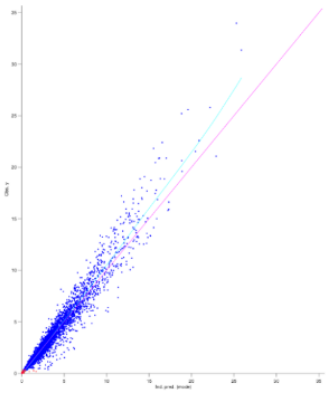	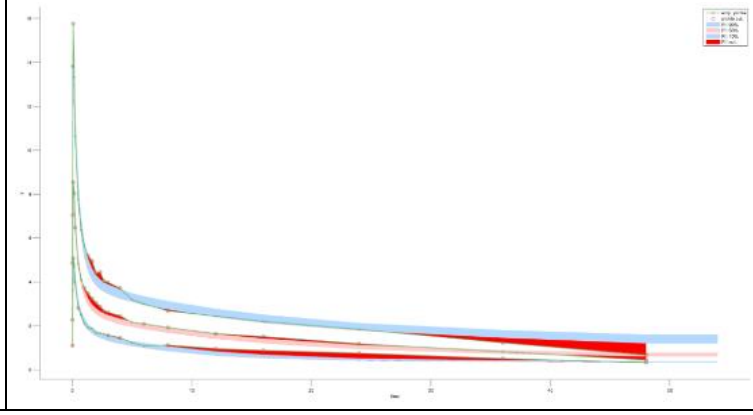

Numerical criteria: -2LL, 8435.66; AIC, 8489.66; BIC, 8577.89

Taking into account prior information on the EHC of formoterol and based on the above results, it was evident that an EHC component should be included in the final model. In this vein, different scenarios for the description of EHC of FOR were tested. In all cases, the structural model of FOR included a two-compartment disposition model linked to a lung and a gallbladder (GB) compartment. An additional GI compartment was implemented in certain cases, between the central and GB compartments, creating an enterohepatic re-circulation loop. In these models, several treatments were applied for GB

emptying, which was assumed to release bile either directly to the central compartment or to the GI compartment. Among others, the inclusion of a sine function model for the description of EHC (Figure C.3.6) was capable of providing an oscillatory bile release, however, it could not provide the required flexibility in terms timing and duration of the re-circulation process (Table C.3.7).

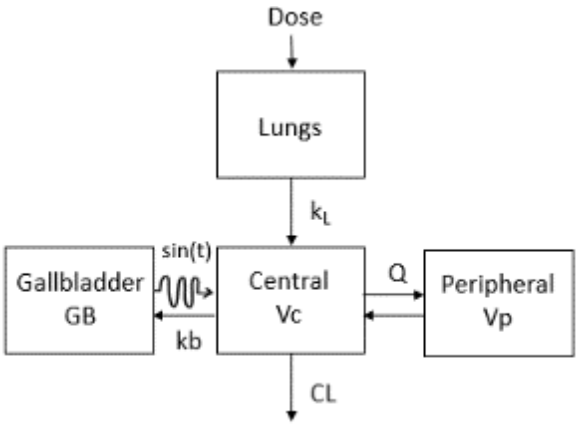

Figure C.3.6. Schematic representation of a two-compartment model with sine function for the description of EHC of inhaled FOR. *Key*: k_L = first-order absorption rate constant from the lungs; k_b = transfer rate constant to the gallbladder; sin(t) = sine function for bile release from the gallbladder.

Table C.3.7. Performance of a 2-compartment PK model with sine function for the description of EHC of inhaled FOR.

Observed vs individual predicted concentrations plot	**VPC plot**
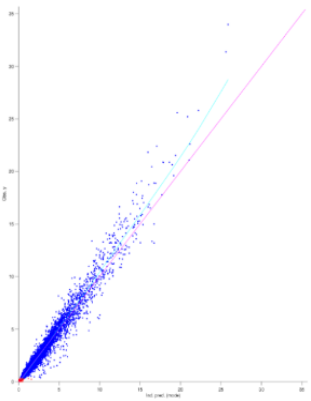	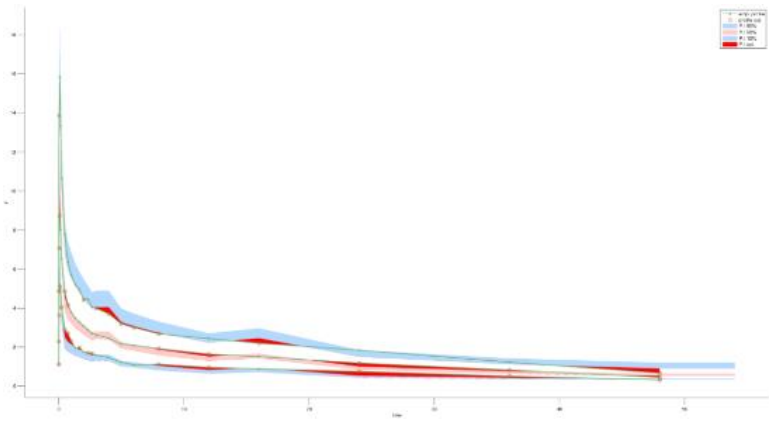

Numerical criteria: -2LL, 8404.11; AIC, 8444.11; BIC, 8509.06

Finally, inhaled FOR kinetics was best described by a structural model consisting of a two-compartment disposition model linked to a lung compartment, as well as to serial GB and GI compartments for the description of the EHC process (Figure C.3.7).

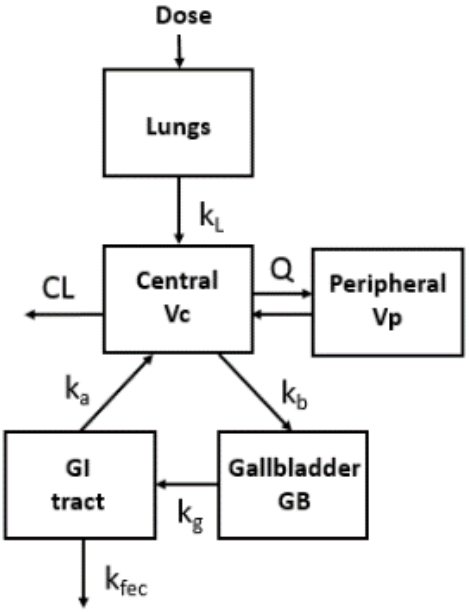

Figure C.3.7. Schematic diagram of the final two-compartment model used to describe the PKs of FOR after inhalation with activated charcoal. Compartments: lung compartment (1), central compartment (2), peripheral (3), gallbladder (4) and gastrointestinal compartment (5) for the enterohepatic re-circulation process. *Key*: k_L = first-order absorption rate constant from the lungs; k_b = transfer rate constant to the gallbladder; k_g = excretion rate constant from the GB to the GI tract; k_a = absorption rate constant from the GI tract; k_{fec} = fecal elimination rate constant.

In the EHC loop, the two additional compartments (i.e., GB and GI) were linked by first-order kinetics and a gallbladder emptying time interval, based on the time of the second peak observed in the C-t plot, i.e. between 2-5 hours post-dose. The EHC process was modeled by introducing a first-order rate constant (k_b) describing the drug transfer from the central compartment to the GB compartment. When gallbladder emptying occurred, FOR was introduced to the GI compartment and was reabsorbed into the central compartment. First-order absorption from the GI compartment was initiated at 3 hours post-dose, since then was the termination of the co-administered activated charcoal scheme. Elimination was considered, for both the central and the GI compartments, to follow first-order kinetics. The population parameter estimates of the final PK model of FOR, along with the BSV% and RSE% values are listed in Table C.3.8.

Table C.3.8. Population parameters for the final best PK model applied to FOR data. *Key*: k_L = first-order rate constant for lung absorption (h^{-1}); k_b = transfer rate constant to the GB (h^{-1}); k_g = excretion rate constant from GB to GI (h^{-1}); k_a = absorption rate constant from the GI tract (h^{-1}); k_{fec} = fecal elimination rate constant (h^{-1}).

Parameter	Mean (RSE%)	BSV% (RSE%)
k_L (h^{-1})	14.8 (3)	15.08 (23)
Vc/F (L)	619 (4)	32.30 (14)
Vp/F (L)	1,130 (4)	36.65 (10)
Q/F (L/h)	2,350 (6)	48.89 (10)
CL/F (L/h)	93 (3)	24.66 (9)
k_b (h^{-1})	0.37 (5)	48.31 (8)
k_g (h^{-1})	0.70 (8)	61.83 (15)
k_a (h^{-1})	0.26 (6)	48.89 (13)
k_{fec} (h^{-1})	0.01 (14)	88.42 (20)
PK Random Effects Correlation		
Vp/F - Q/F	0.74 (11)	-
Residual error model		
a	0.12 (7)	-
b	0.15 (2)	-
Numerical criteria		
-2LL: 8251.26	AIC: 8311.26	BIC: 8407.05

The PK estimates of the final best model were the following: absorption rate constant through the lungs (k_L) = 14.8 h^{-1}, apparent volume of distribution of the central compartment (Vc/F) = 619 L, apparent volume of distribution of the peripheral compartment (Vp/F) = 1,130 L, apparent clearance from the central compartment (CL/F) = 93 L/h, inter-compartmental clearance (Q/F) = 2,350 L/h, transfer rate constant from the central compartment to bile (k_b) = 0.37 h^{-1}, excretion rate constant from the gallbladder to the intestine (k_g) =0.7 h^{-1}, GI absorption rate constant (k_a) = 0.26 h^{-1}, and fecal elimination rate constant (k_{fec}) = 0.01 h^{-1}. It is reasonable that only "apparent" PK parameters could be estimated in the present study, since only inhaled administration was performed and not intravenous administrations. For this reason, the term F was included, referring to the bioavailable fraction of dose. BSV% estimates were found to exhibit moderate to high values, which ranged approximately from 15% to 88%. The RSE% values, obtained for both PK and BSV% estimates, were relatively low (3-23%), indicating that the model parameters were precisely estimated (Table C.3.8). The residual error model that led to the optimum performance was a combined error model consisting of an additive component α and multiplicative coefficient *b*:

$$C_{ij} = f_{ij} + (a + b \cdot f_{ij}) \cdot \varepsilon_{ij} \quad \text{(Eq. 12)}$$

where C_{ij} is the j_{th} observed concentration of FOR for the i_{th} individual, a and b are the parameters of the residual error model, f_{ij} is the j_{th} model predicted value for i_{th} subject, and ε_{ij} is the random error which is assumed to be normally distributed with mean 0 and variance 1. The residual error parameters for the combined error model (Eq. 12) were: α=0.12 and b=0.15. Finally, a significant correlation of the random effects between the two PK parameters, Vp/F and Q/F (corr = 0.74) was incorporated in the final model, as it lead to better fittings and improved numerical criteria. No effect of gender, age, body weight, height and BMI on FOR estimated PK parameters was found, and no difference in the performances of the two DPIs, or between the different treatment periods was observed.

Goodness-of-fit plots for the final PK model of FOR are depicted in Figures C.3.8-C.3.10. Figure C.3.8 shows the individual predicted concentrations *versus* the observed concentration values for the final population PK model of inhaled FOR. A symmetric distribution of points around the line of unity is observed, showing an adequate degree of linearity and a reasonable agreement between the model predicted and observed concentrations.

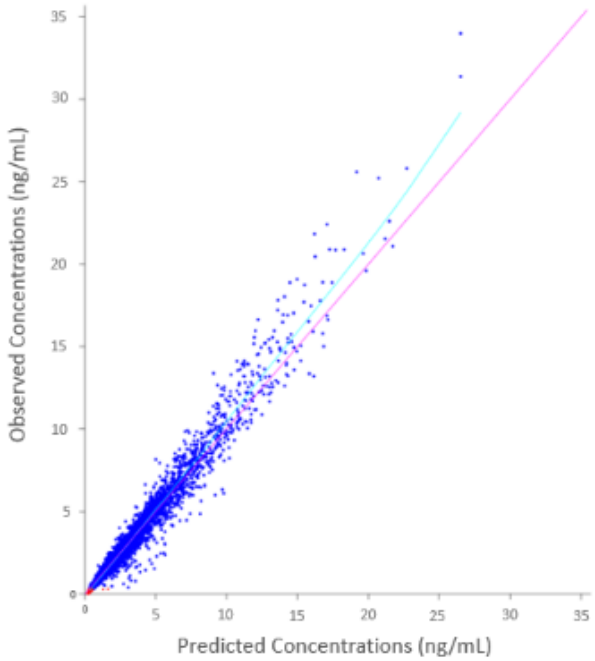

Figure C.3.8. Observed concentrations *versus* individual predicted concentration values for the final population model of FOR. The diagonal red line represents the line of unity, namely, the ideal situation.

In line with the above, the IWRES and the NPDE versus the IPRED concentrations, illustrated in Figure C.3.9(A, B), also show a balanced distribution around the zero line, indicating that the combined (proportional and additive) error model provided adequate description of the residual error.

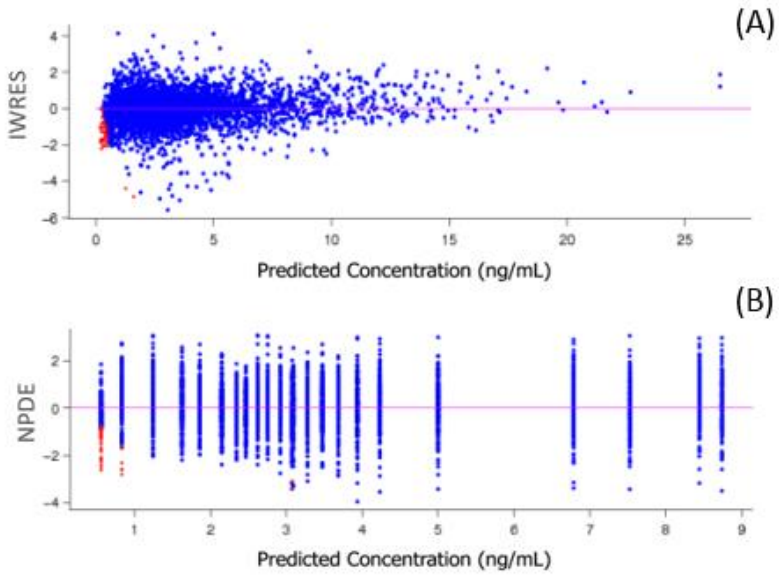

Figure C.3.9. Graphical representation of (A) the IWRES and (B) the NPDE *versus* the IPRED concentrations for the final model of inhaled FOR. Points in red color refer to the censored data.

Finally, Figure C.3.10 presents the VPC plot obtained for the final model of FOR.

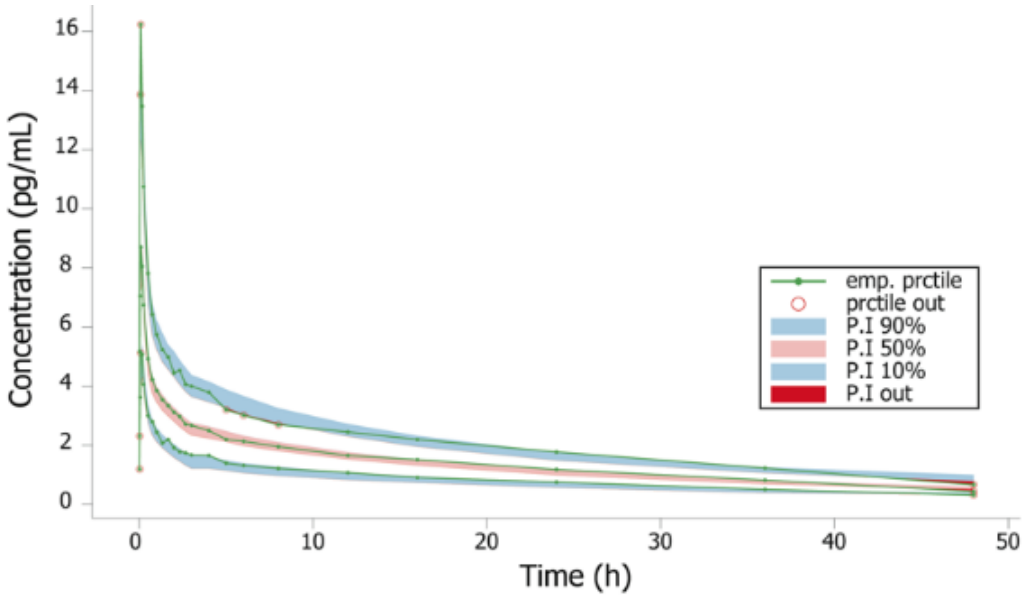

Figure C.3.10. VPC of the final model for inhaled FOR. *Key*: Solid lines refer to the 10th, 50th, and 90th percentiles of the empirical data; Shaded areas refer to the 95% prediction intervals around each theoretical percentile; red circles and areas denote the outlier data.

The predictions from the model described adequately the observed high and median concentration profiles of the compound, suggesting that the utilized structural/error

models were appropriate for describing the plasma C-t profiles of FOR following inhalation.

C.1.3.3.2.2 Budesonide

Accordingly, the spaghetti plot obtained for inhaled BUD is shown in Figure C.3.11.

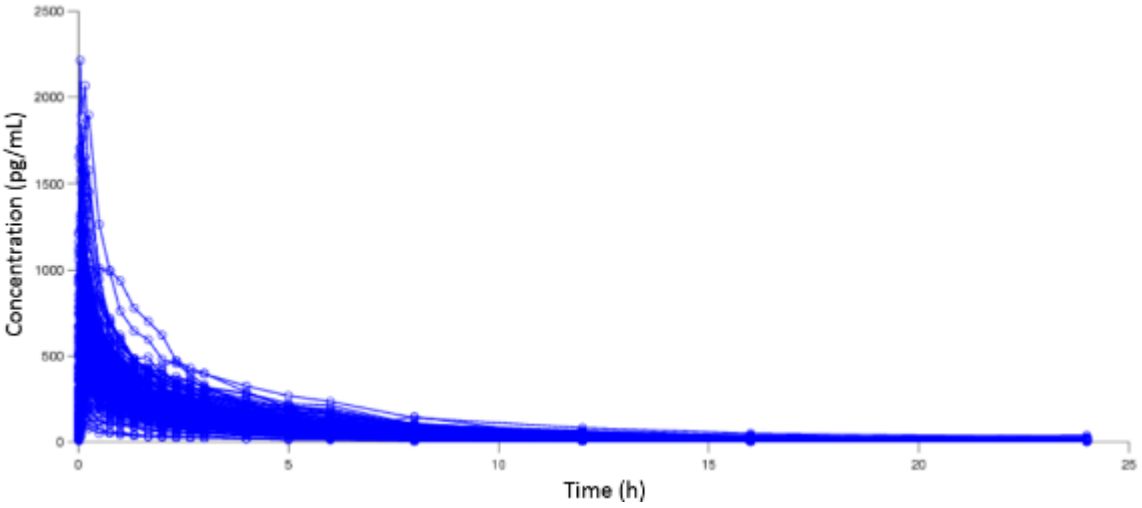

Figure C.3.11. Spaghetti plots following a single dose of inhaled BUD in 180 subjects.

Similarly to FOR, a 2-compartment model was chosen for BUD disposition, and the following general categories of absorption kinetics were evaluated. Initially, conventional models including first-order (Table C.3.9) or bolus (Table C.3.10) kinetics failed to describe the drug's complex absorption characteristics.

Table C.3.9. Performance of a conventional 2-compartment PK model with first-order absorption for the description of the pharmacokinetics of inhaled BUD.

Observed vs individual predicted concentrations plot	**VPC plot**
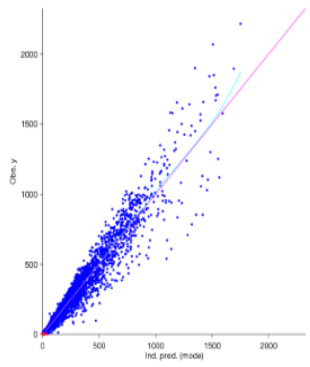	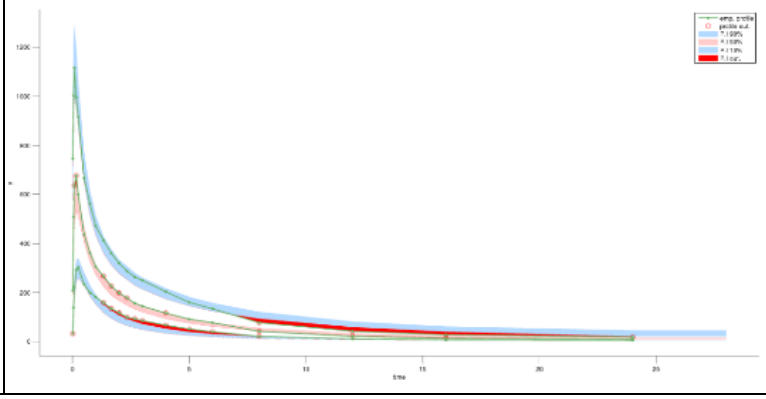

Numerical criteria: -2LL, 38071.58; AIC, 38099.58; BIC, 38144.28

Table C.3.10. Performance of a conventional 2-compartment PK model with bolus absorption kinetics for the description of the pharmacokinetics of inhaled BUD.

Observed vs individual predicted concentrations plot	VPC plot
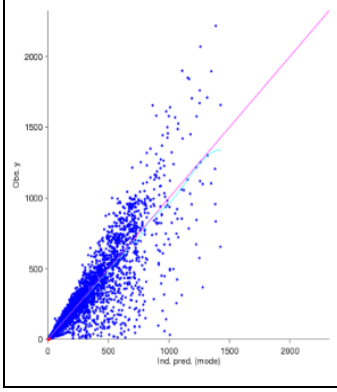	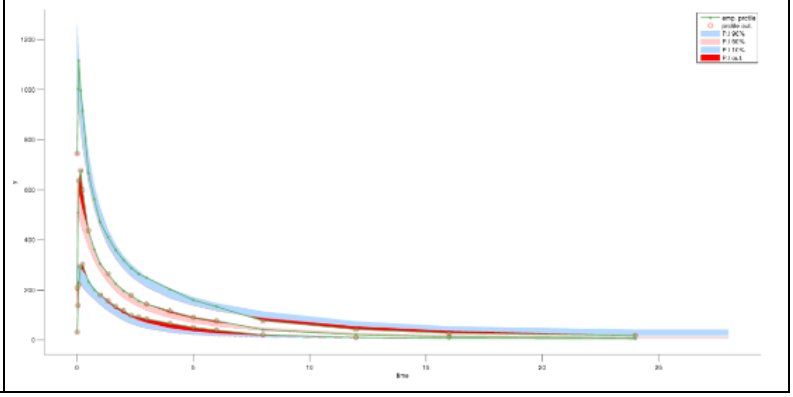

Numerical criteria: -2LL, 40183.59; AIC, 40205.59; BIC, 40240.72

Taking into consideration the physiological characteristics of pulmonary absorption, as well as prior information regarding the pre-systemic conjugation of BUD within the lung, focus was placed on more complex models for the description of absorption kinetics, with different approaches tested during model development. A combination of first-order and Erlang distribution model using a variable number of transit compartment to account for the delayed absorption of BUD (Figure C.3.12) was also evaluated, but failed to capture the parallel absorption of the drug through the lungs (Table C.3.11).

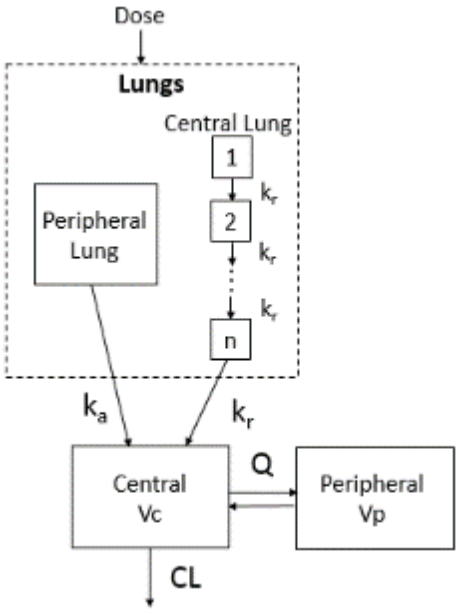

Figure C.3.12. Representation of the 2-compartment model with the combination of first-order kinetics (ka) and Erlang distribution as an absorption model, simulated as a linear chain of identical compartments connected by an identical exiting rate constant (kr).

Table C.3.11. Performance of the 2-compartment PK model with first-order and Erlang distribution for the description of absorption of inhaled BUD.

Observed vs individual predicted concentrations plot	VPC plot
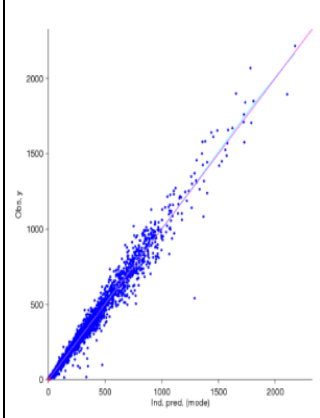	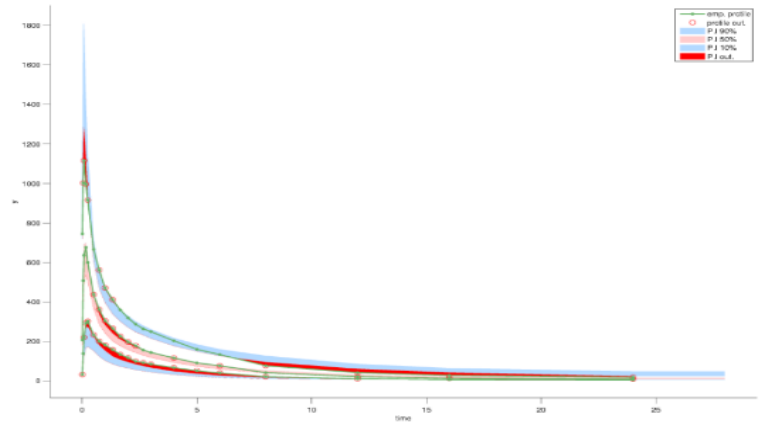

Numerical criteria: -2LL, 40183.59; AIC, 40205.59; BIC, 40240.72

The final best model was obtained when a two-compartment disposition model was connected with two lung absorption compartments providing two parallel first-order absorption processes (Figure C.3.13, Table C.3.12).

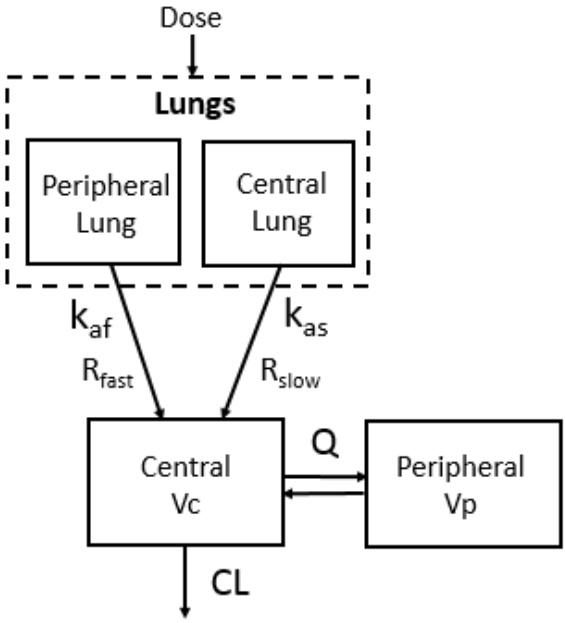

Figure C.3.13. Schematic diagram of the final two-compartment model used to describe the pharmacokinetics of BUD after inhalation with activated charcoal. Compartments: central lung compartment, peripheral lung compartment, central compartment and peripheral compartment. Two different first-order input rates (fast and slow) were considered for lung absorption of inhaled BUD, with a relative fraction of the inhaled dose (R_{fast}) absorbed rapidly via the lungs and another fraction (R_{slow}) showing a delayed absorption. *Key*: k_{af} = fast first-order absorption rate constant from the lungs (h^{-1}); k_{as} = slow first-order absorption rate constant from the lungs (h^{-1}); R_{fast} = relative fraction of dose absorbed rapidly from the lungs; R_{slow} = relative fraction of dose absorbed slowly from the lungs.

Table C.3.12. Performance of the 2-compartment PK model with two parallel first-order rate constants for the description of absorption of inhaled BUD.

Observed vs individual predicted concentrations plot	VPC plot
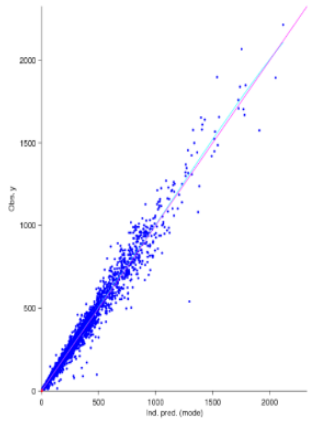	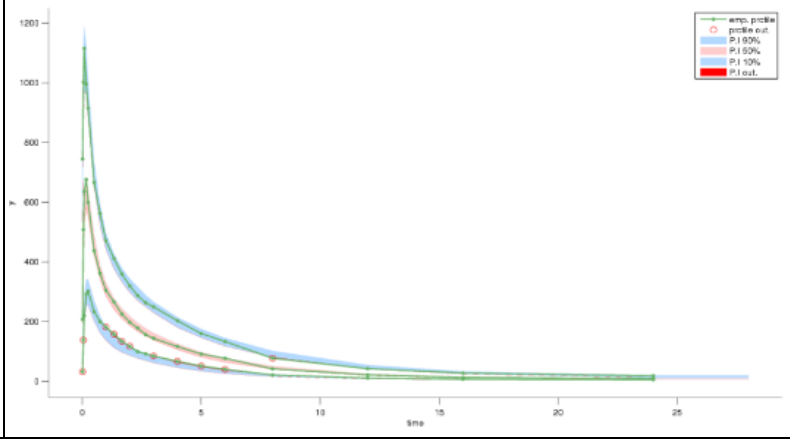

Numerical criteria: -2LL, 35643.92; AIC, 35695.92; BIC, 35778.94

In the final model, therefore, in order to account for the two parallel first-order absorption processes, the lung was composed of two absorption compartments to describe the 'fast' and 'slow' absorption of inhaled BUD. Elimination was assumed to take place in the central compartment following first-order kinetics.

Following the inclusion of some significant covariates and correlations of the random effects between certain PK parameters, Table C.3.13 summarizes the estimates of the population parameters of the final model, along with their BSV% and RSE% values.

Table C.3.13. Population parameters for the final PK model applied to the budesonide data. *Key*: k_{af} = fast first-order lung absorption rate constant (h^{-1}); k_{as} = slow first-order lung absorption rate constant (h^{-1}); R_{slow} = relative fraction of dose absorbed slowly from the lungs; z = the ratio of dose fractions absorbed either fast (R_{fast}) or slowly (R_{slow}) through the lungs (i.e. R_{fast}/R_{slow}); *a* and *b* = residual error parameters for the combined error model.

Parameter	Mean (RSE%)	BSV% (RSE%)
k_{af} (h^{-1})	19.7 (8)	72.34 (12)
k_{as} (h^{-1})	0.11 (11)	51.38 (12)
R_{slow}	0.67 (3)	63.75 (17)
z	0.27 (5)	49.72 (11)
Vc/F (L)	228 (3)	28.24 (10)
Vp/F (L)	182 (6)	35.77 (10)
Q/F (L/h)	254 (6)	50.90 (10)
CL/F (L/h)	154 (3)	22.79 (9)
PK Random Effects Correlation		
k_{af} - R_{slow}	0.45 (38)	-
Vp/F - Q/F	0.84 (6)	-
Covariates effects		
Gender on k_{as} [a]	-0.58 (23) ($p = 1.6 \cdot 10^{-5}$)	-
Gender on Vp/F [a]	0.22 (28) (p = 0.00031)	-
Residual error model		
a	0.90 (18)	-
b	0.13 (2)	-
Numerical criteria		
-2LL: 35521.6	AIC: 35581.63	BIC: 35677.41

[a] Males were considered as the 'control' group.

The structural PK model was parameterized in terms of the fast (k_{af} = 19.7 h^{-1}) and slow (k_{as} = 0.11 h^{-1}) lung absorption rate constants, the relative fraction of dose absorbed slowly (R_{slow} = 0.67) through the lungs and the R_{fast}/R_{slow} ratio (z = R_{fast}/R_{slow} = 0.27), where R_{fast} refers to the fraction of dose absorbed rapidly through the lungs. Besides, the remaining model parameters are the apparent volume of distribution in the central (Vc/F = 228 L) and peripheral (Vp/F = 182 L) compartments, the apparent inter-compartmental clearance (Q/F = 254 L/h), and the apparent clearance (CL/F = 154 L/h). A combined additive and proportional error model (Eq. 12) was also used to describe the residual unexplained variability. The estimated residual error parameters were: α=0.90 and *b*=0.13. A significant correlation of the random effects between Vp/F - Q/F (corr = 0.84) and k_{af} - R_{slow} (corr = 0.45) was found and included in the final model. BSV% values ranged from 22% to 72%, while RSE% values remained relatively low ranging from 9 to 17% for all the estimated parameters (Table C.3.13).

Gender was found to be a significant covariate on k_{as} and Vp/F (Eqs. 13 and 14), with male subjects exhibiting a faster absorption for the slow lung absorption phase of BUD and lower peripheral distribution compared to females (Figure C.3.14).

$$k_{as} = \theta_1 \cdot \exp(-0.58) \quad \text{(Eq. 13)}$$

$$Vp/F = \theta_2 \cdot \exp(0.22) \quad \text{(Eq. 14)}$$

where θ_1 and θ_2 refer to the typical population PK parameter estimates for male subjects.

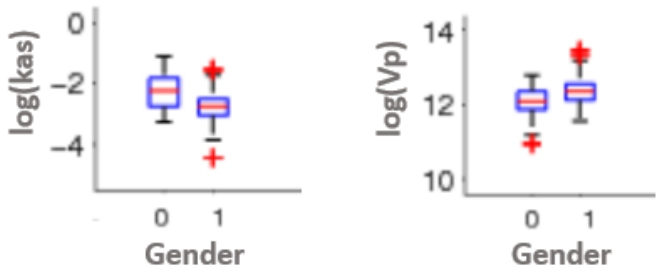

Figure C.3.14. Boxplots showing the relationship between FOR slow absorption rate constant (left) and the apparent volume of distribution of the peripheral compartment (right) with gender. The boxes represent the observations from the 25th percentile (Q1) to 75th percentile (Q3). The red line within the box represents the median. The points beyond the IQR and which are within 1.5 times the IQR constitute the whiskers. Points beyond the whiskers qualify to be outliers and are represented with red crosses. Males were considered as the 'control' group (0).

No 'treatment', 'period' or any other covariate effect was found to be significant ($p > 0.05$) on any other PK parameter. Goodness-of-fit plots for the final PK models of BUD are shown in Figures C.3.15-C.3.17.

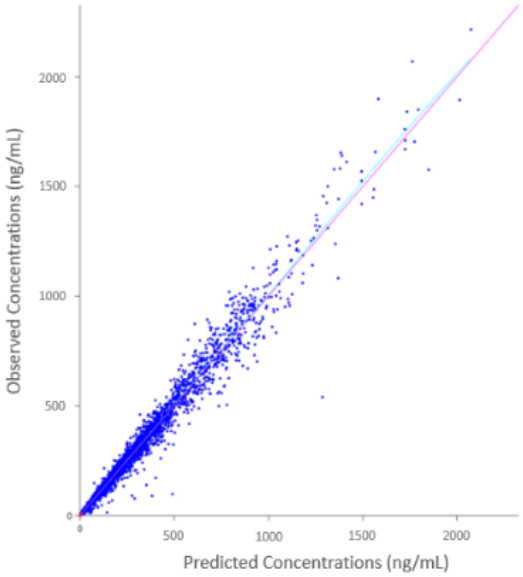

Figure C.3.15. Individual predicted *versus* observed concentrations from the population PK model of BUD. The diagonal red line represents the line of unity, namely, the ideal situation.

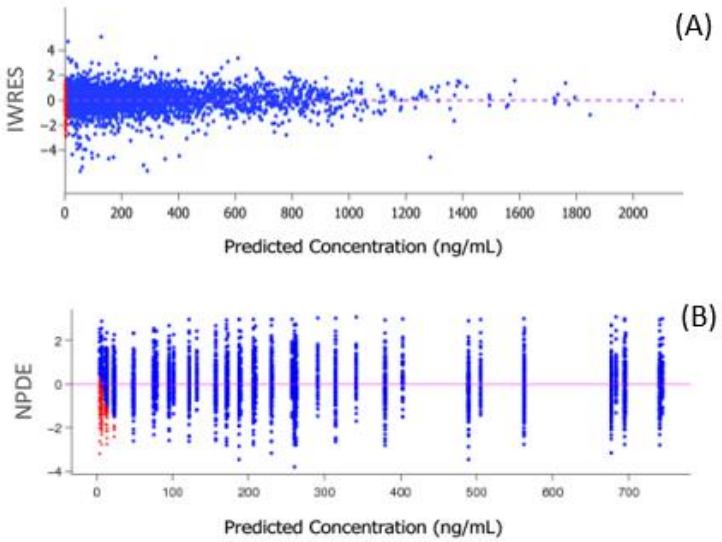

Figure C.3.16. Graphical representation of (A) the IWRES and (B) the NPDEs *versus* the IPRED concentrations for the final PK model of inhaled BUD. Points in red color refer to the censored data.

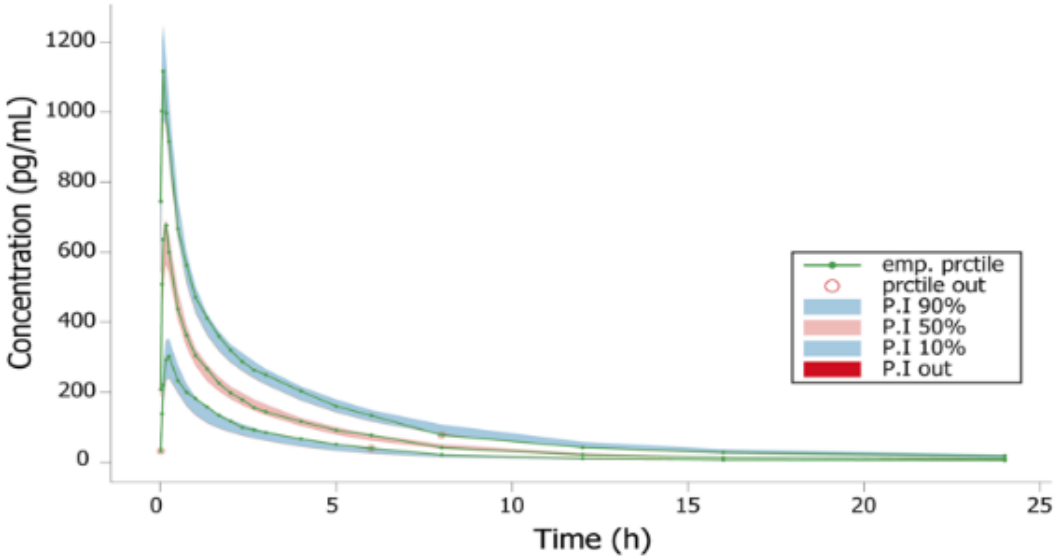

Figure C.3.17. VPC of the final model for inhaled BUD. *Key*: Solid lines refer to the 10th, 50th, and 90th percentiles of the empirical data; Shaded areas refer to the 95% prediction intervals around each theoretical percentile; red circles and areas denote the outlier data.

As in the case of FOR, a symmetric distribution of points around the line of unity is observed in all cases, in addition to a satisfactory simulation and predictability of the observed concentrations by the final PK model.

C.1.3.4 Discussion

The study aimed at investigating the pharmacokinetics of the inhaled combination BUD/FOR in an asthma patient group in order to elucidate the absorption and disposition characteristics of these two drugs. In this respect, a standard non-compartmental PK approach and a population PK modeling methodology were applied.

C.1.3.4.1 Non-compartmental pharmacokinetic analysis

The non-compartmental approach was applied initially to the available C-t data in order to get the estimates of some basic PK parameters. Even though low plasma drug levels were obtained in both cases, the high sensitivity of the bioassays allowed the accurate quantification and characterization of the PK profiles of both FOR and BUD. It is worth mentioning that the C-t levels reflected solely the initial pulmonary absorption, since the gastrointestinal absorption of the swallowed fraction, following inhaled administration, has been blocked by the co-administration of an activated charcoal scheme (Mobley and Hochhaus, 2001).

Peak plasma concentrations of BUD were achieved within 30 minutes following inhalation, while the lung absorption of FOR was even faster with maximum drug concentrations in most subjects found within 5-10 minutes. Short absorption half-lives have been also reported for both drugs in previous studies in asthma patients and healthy volunteers (Donnelly and Seale, 2001; Derks et al., 1997). This is in accordance with the moderately lipophilic character of both molecules, found to be readily dissolved in human bronchial secretions and rapidly absorbed across the lung epithelium (Edsbäcker and Johansson, 2006; Cote et al., 2009). The primary PK parameters of BUD and FOR were calculated separately for each DPI product (T or R), and were further compared in terms of BE assessment, according to the currently proposed EMA methodology (EMA, 2010).

C.1.3.4.2 Population pharmacokinetic analysis

Visual inspection of the plasma C-t profiles of BUD and FOR revealed rather complex absorption and distribution characteristics that could not be explained by the classic non-compartmental analysis. For this reason, the primary aim of this study was to develop population PK models able to describe the entire time profiles of inhaled BUD and FOR. A dataset of 180 individual C-t profiles was used for the development of the two structural PK models. Data for the two DPI products from each study period were combined, by

considering the ‘period’ (i.e., occasion) and ‘treatment’ (i.e., T or R) effects as potential covariates.

C.1.3.4.2.1 Formoterol

In case of FOR, inspection of the individual C-t profiles (Fig. C.3.5) revealed either a plateau or small double concentration peaks, observed in most subjects between 3 to 5 hours post-dose. These lesser peaks, observed at later times, were considered to reflect the EHC of the drug, since gastrointestinal absorption of the swallowed fraction was excluded due to the co-administration of activated charcoal. Besides, it has been previously reported that, apart from renal excretion, formoterol glucuronide conjugates might be excreted via the bile, into the intestinal lumen and subsequently cleaved by the gut flora, resulting in reabsorption of the free drug by enterocytes and re-circulation through the liver (Lecaillon et al., 1999; Rosenborg et al., 1999). This finding was further supported by animal studies where, biliary excretion of FOR accounted for about 31-65% of an orally administered dose (Sasaki et al., 1982). Therefore, an enterohepatic re-circulation model was developed for inhaled FOR in our study, based on the above-mentioned physiological aspects of biliary excretion and re-circulation processes. Plasma C-t profiles were best described by a five-compartment model capable of simulating the processes of lung absorption, systemic disposition, tissue distribution of the drug and gallbladder emptying during the enterohepatic recycling and subsequent intestinal absorption and elimination. The final structural model consisted of a two-compartment disposition model linked to a lung absorption compartment and sequential gallbladder and GI compartments representing the EHC loop (Fig. C.3.7). For reasons of simplicity, the liver (as a well perfused organ) was considered part of the central compartment, while, metabolic and de-esterification reactions of FOR were omitted in the final model.

It should be mentioned that in actual physiological conditions, the EHC process is much more complicated and several PK models have been proposed for the proper characterization of the EHC process. Reported models for other drugs showing enterohepatic re-circulation either assumed continuous enterohepatic recirculation (Cremers et al., 2005), one or multiple secretions of bile using an on/off switch time interval (Funaki, 1999), time-dependent transfer from bile into gut (Kim et al., 2015), or implemented a sine function to describe periodic bile releases (Wajima et al., 2002). When more complicated methodologies were implemented in our case, the model was over-

parameterized and no reliable fits could be obtained. Nevertheless, in our study we investigated many of these possibilities.

Unlike conventional PK models, EHC models require the determination of additional rate parameters for the description of biliary excretion, intestinal absorption, fecal and urinary elimination of the active compound. Defining appropriate characteristics, such as the rate constants for the EHC loop, the 'lag-time' for the GI absorption and the gallbladder emptying time interval, was a key element during model construction. In our final model, the enterohepatic loop compartments were linked by first-order transport rate constants, while a lag-time of three hours was considered for the initiation of GI absorption, due to the presence of activated charcoal. Finally, a gallbladder emptying time interval between 2-5 hours post-dose was chosen, based on the observed secondary absorption peak in the individual plasma C-t profiles of FOR.

The estimates of the population PK parameters for the final PK model, their BSV% and RSE% values are listed in Table C.3.8. A high absorption rate constant (k_L = 14.8 h^{-1}) was estimated for FOR, which is in accordance with the small Tmax values (5-10 min) observed in the non-compartmental analysis, while the apparent volumes of distribution for the central (Vc/F = 619 L) and the peripheral compartments (Vp/F = 1,130 L) were in line the moderately lipophilic character of the drug and in agreement with previously reported values (Derks et al., 1997; van den Berg, 1999). Clearance of the drug from the central compartment (CL/F = 93 L/h) was determined to be somewhat smaller compared with other reported values (Derks et al., 1997), which may be partly explained by the addition of fecal elimination contributing to the total clearance of the drug. A moderate inter-individual variability was observed for most PK parameters of FOR. However, rate constants between the central and peripheral compartments and within the EHC loop varied largely within the study population, highlighting the increased inter-subject variability in the re-distribution processes.

In regards to the covariate model, no significant correlation was observed between the examined covariates and the PK parameters of FOR. Demographic characteristics, the effect of inhalation device, treatment period, and patient status were not found to influence systemic drug exposure of FOR. The goodness-of fit results showed that the model was able to provide sensible predictions of the observed values despite some difficulties in

capturing the EHC of FOR in some individuals and the increased variability attributed to the large sample size of the study population and the complexity of the EHC process.

C.1.3.4.2.2 Budesonide

At 10-15 min after BUD inhalation, a peak serum concentration was observed with a subsequent slower elimination of the drug (Figure C.3.11). The initial absorption phase was considered to reflect a rapid absorption of free BUD *via* the peripheral respiratory tract regions, while a much slower underlying absorption process, attributed to absorption of the drug from the central airways and the formation of BUD fatty acid conjugates within the lung, was considered to contribute to the slowly declining phase.

In general, drug absorption from the alveolar space (peripheral lung regions) is often assumed to be fast due to the high local perfusion, the large absorption surface area and the thin diffusion barrier. The moderately lipophilic character of BUD leads to high solubility in human bronchial secretions which in turn implies fast dissolution (within 6 min) and rapid absorption from the peripheral airways (Edsbäcker and Johansson, 2006). Conversely, in the conducting airways (central lung regions), absorption of inhaled drugs is found to be slower compared to the peripheral regions, due to less perfusion and thicker airway walls (Borghardt et al., 2015). Nevertheless, apart from a delayed absorption of the centrally deposited drug, a reversible fatty acid esterification of BUD within the airways, further contributes to the slowly absorbed fraction. Budesonide esterification process is both rapid (within 5 minutes) and reversible and greatly increases the lipophilicity and pulmonary retention of the drug. As the intracellular concentration of free BUD decreases, drug esters are hydrolyzed back to their active state providing a slow-release reservoir of free BUD in the lung over a period of several hours (Brattsand and Miller-Larsson, 2003; Edsbacker and Brattsand, 2002).

Taking into consideration the above physiological parameters, a two-compartment disposition model with two parallel first-order absorption processes (fast and slow) from the lungs was finally chosen for the description of the C-t profiles of inhaled BUD (Figure C.3.13). In the developed model, the dose of BUD was assumed to be divided into two different fractions deposited in the two kinetically different lung compartments, allowing explicitly for different absorption rate constants for drug absorption.

The estimates of the population PK parameters obtained for the final model, their BSV% and RSE% values are listed in Table C.3.13. A high absorption rate constant was estimated for the rapidly absorbed fraction (k_{af} = 19.6 h^{-1}), suggesting that lung is an efficient route of systemic absorption of BUD. Besides, the estimated slow absorption rate constant (k_{as} = 0.11 h^{-1}) accounted for the slowly absorbed fraction. The ratio of the relative fractions of dose absorbed either fast (R_{fast}) or slowly (R_{slow}) through the lungs (z) was equal to 0.27, suggesting that the main fraction of the inhaled dose was slowly absorbed through the lungs. This finding is further supported by previous studies indicating an increased central lung deposition of inhaled BUD from DPI inhalers, especially in asthma patients and reports showing that most of tissue budesonide remains esterified several hours after inhalation (Brattsand and Miller-Larsson, 2003; van den Brink et al., 2008). Although the underlying processes are much more complicated, the current approach affords a fair approximation of the underlying absorption process based on a numerically robust, parsimonious model along with the right combination of parameters. In any case, the parameters showing the greatest inter-individual variability for BUD were those describing the absorption from lungs, reflecting the great complexity and variability in lung absorption processes.

The derived BUD volumes of distribution for the central and the peripheral compartments were relatively small (Table C.3.13), which is in line with the intermediate lipophilicity of the drug (Borghardt et al., 2015) and broadly consistent with previously reported values (Thorsson et al., 2001; Hübner et al., 2005). In addition, the rapid clearance observed in our study further supports previous findings regarding the rapid systemic dilution and the limited nonspecific tissue retention of the intact, non-esterified BUD (Edsbäcker and Johansson, 2006). The observed small elimination half-life of the drug following inhalation also minimizes the possibility of 'flip-flop kinetics'. Indeed, many single- and repeated-dose PK studies after intravenous and inhaled administrations of BUD have confirmed the absence of difference in plasma kinetics between these (Edsbäcker and Brattsand, 2002).

Finally, the impact of several covariates on the estimated PK parameters was also examined in the case of BUD. Only gender was found to significantly influence k_{as} and the peripheral volume of distribution Vp/F, with men showing higher k_{as} values and lower peripheral volumes of distribution compared to female subjects. There is little available information about gender effects on pharmacokinetics, particularly regarding lung

absorption of inhaled drugs. The gender effect observed on k_{as}, in our case, might be attributed to a difference in total and regional lung deposition patterns between males and females and other anatomical and dynamic differences. For instance, the size of the lung is found to be larger in men compared to women, particularly in the upper and large conducting airways, offering a wider absorption surface in the more central lung regions (Kim et al., 1998). The effect of gender on peripheral volume of distribution is also in line with the lipophilic character of the drug. The higher body fat percentage in women compared to men may account for the observed higher peripheral volume of distribution of BUD in women. Nevertheless, since inhaled BUD reaches the site of action before it is absorbed systemically, it is not expected that these inter-gender differences will be accompanied by differences in the onset or intensity of therapeutic effect. No other covariate effect (weight, age, height, BMI, FEV1, asthma state, treatment and period) was observed for BUD pharmacokinetics.

C.1.3.5 Conclusions

The aim of the present study was to investigate the absorption and disposition kinetics of FOR and BUD in asthma patients, following a combined inhaled administration using two different dry powder inhalers. Initially, the application of a classic non-compartmental analysis and the subsequent BE assessment, allowed for the estimation of some basic PK parameters and showed the equivalence of the two inhalation products regarding the primary PK parameters for both agents. However, this study focused on the population PK analysis of the two inhaled drugs. In case of inhaled FOR, a PK model describing the enterohepatic re-circulation process of the drug was developed in asthma patients. For inhaled BUD, the incorporation of two parallel first-order absorption rate constants (fast and slow) for lung absorption in the PK model emphasized the importance of pulmonary anatomical features and underlying physiological processes during model development of inhaled drugs. Finally, men were found to exert higher values for the slow absorption rate constant of BUD and smaller peripheral volume of distribution compared to women.

C.2. Orally Administered Drugs

C.2.1. Study 4: Ezetimibe

C.2.1.1 Introduction

Ezetimibe (EZE, Figure C.4.1) is a widely used cholesterol absorption inhibitor indicated for the treatment of hypercholesterolaemia (Kosoglou et al., 2005).

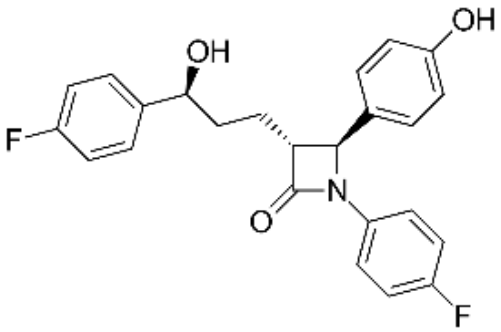

Figure C.4.1. Chemical structure of Ezetimibe.

The drug has been extensively studied in patients with primary hypercholesterolemia, homozygous familial hypercholesterolemia, or homozygous familial sitosterolemia, both as monotherapy (Bays et al., 2001; Dujovne et al., 2002) and in combination with other lipid-lowering agents, such as statins (Ballantyne et al., 2003) and fibrates (Sweeney & Johnson, 2007). Clinical trials have shown that administration of ezetimibe at a dose of 10 mg once daily produces a marked inhibition of cholesterol absorption by 54-65%, which results in approximately 17-20% reduction of plasma low-density lipoprotein cholesterol in mildly to moderately hypercholesterolemic subjects (Sudhop et al., 2002). The drug also shows a favorable safety profile, and has an adverse event profile similar to that of placebo, as demonstrated in numerous treated patients over the years (Patel et al., 2003).

Ezetimibe exerts its cholesterol-lowering activity by effectively blocking the intestinal uptake of dietary and biliary cholesterol, through the inhibition of apically localized sterol transporters in the small intestine (Jeu and Cheng, 2003; Nashimoto et al., 2017). Preclinical studies have shown that ezetimibe undergoes extensive glucuronidation via specific uridine glucuronosyltransferase isoenzymes to form an active glucuronide metabolite localized at the intestinal mucosa (van Heek et al., 1997; Van Heek et al., 2000). Therefore, the pharmacological activity of ezetimibe can be ascribed to both the parent drug and the metabolite, with conjugated ezetimibe being at least as potent an

inhibitor of intestinal cholesterol absorption as the free drug (Kosoglou et al., 2005; van Heek et al, 2000).

Following oral administration, EZE is rapidly absorbed and undergoes extensive first-pass metabolism (>95% glucuronidation) in the intestinal wall to form the pharmacologically active metabolite, ezetimibe phenolic glucuronide (EZEG), which accounts for approximately 80-90% of the total drug in plasma (Patrick et al., 2002). Clearance of EZE and EZEG from blood is not a straightforward process, and both drugs exhibit multiple peaks in their plasma concentration-time profiles (Patrick et al., 2002). These multiple peaks are attributed to an extensive EHC, in which both compounds are transported through portal vessels to the liver, where ezetimibe undergoes further glucuronidation and subsequent biliary secretion through the gallbladder back into the intestine (de Waart et al., 2009).

In the intestinal lumen, EZE conjugates undergo enzymatic hydrolysis and are rapidly and completely reconverted to the parent drug which is reabsorbed into the systemic circulation (Kosoglou et al., 2005). EHC continues to happen until the drug is completely cleared from the body (Malik et al., 2016). Approximately 78 and 11% of an administered EZE dose are excreted in feces and urine, respectively, with a terminal elimination half-life for both EZE and EZEG of approximately 22 hours (Jeu & Cheng, 2003; Patrick et al., 2002). Even though, the PKs of ezetimibe are complex and associated with high inter- and intra-individual variability, the EHC process has the potential to enhance the residence time of the compound in the intestinal lumen, thereby potentiating its cholesterol-lowering activity and allowing for once-daily dosing (Jeu and Cheng, 2003).

An insight into the EHC of drugs with extensive bile excretion is of crucial importance, since it may significantly affect their pharmacokinetics and prolong their pharmacological effect (Roberts et al., 2002). Characterization of EHC through classical pharmacokinetic methodologies is proved inadequate for the in-depth description of such complicated C-t profiles. Unlike non-compartmental analysis, a model-based approach allows for a better approximation of drugs' kinetics and enables a further characterization of the influence of this re-distribution process on PK parameters such as absorption, distribution, and clearance. To date, most published PK studies for EZE focused mainly in the determination of model-independent PK parameters, such as AUC, Cmax and $t_{1/2}$ (Kosoglou et al., 2005; Patrick et al., 2002). To the best of our knowledge, only one

compartmental model describing EZE PKs in humans is available in the literature (Ezzet et al., 2001), and thus data describing model-based parameters such as volumes of distribution, elimination and rate constants are sparse for ezetimibe. The limited use of population compartmental analysis in case of EZE could be attributed to the complex PK behavior of the drug and the high between-subject variability caused by the EHC process.

In order to increase our understanding on the clinical pharmacokinetics of enterohepatic recycling, the primary objective of this study was to develop a novel population PK model for the description of EZE kinetics. Using data from a crossover BE study, nonlinear mixed effects modeling was employed to develop a model for total ezetimibe (parent and glucuronide metabolite) based on physiological considerations. Since conventional PK models were inadequate for capturing the multiple peaks observed in the obtained C-t profiles, additional models were developed to incorporate an EHC component. As a secondary aim of this study, the potential contribution of several covariates was examined in order to extract any useful information for EZE pharmacotherapy.

C.2.1.2 Methods

C.2.1.2.1 Study Design and Subjects

The plasma concentration data used for model building were obtained from a BE study which employed a standard open-label, single-dose, randomized crossover design, in healthy adult subjects under fasting conditions. The study was in compliance with the Good Clinical Practice guidelines issued by the International Conference on Harmonization and was conducted according to the principles of the Declaration of Helsinki. The study protocol was reviewed and approved by the National ('Anveshhan') Independent Ethics Committee, and a written informed consent was obtained from each participant prior to enrolment in the study.

Thirty-six healthy, adult subjects were enrolled in the study. All participants underwent a physical examination, ECG evaluation and laboratory tests, and a thorough medical history review to ensure their health status. The inclusion criteria referred to male or female subjects aged between 18-45 years, within the normal weight range and BMI from 18.5 to 30 kg/m^2, absence of intolerance or hypersensitivity to the study drug or any of the excipients, non-pregnant and non-lactating women, subjects having negative urine screen for drugs of abuse and negative alcohol, HIV or hepatitis B/C tests. Participants

were excluded from study if they had a history, or presence, of significant cardiovascular or any other disease, any treatment which could alter hepatic enzyme function or any other prescribed medication during the last one month prior to study initiation, history or presence of significant alcoholism or drug abuse, smoking, asthma, urticaria or other significant allergic reaction. Volunteers were also excluded if they have donated ≥450 mL of blood within 3 months prior to study initiation or had a significant blood loss or other major illness.

In the treatment days, after at least 10 hours of overnight fasting, subjects were randomly allocated in two groups receiving either one dose of Ezetimibe 10 mg Tablets (Rafarm S.A. Athens, Greece) or Ezetrol® 10 mg Tablets (Merck Sharp & Dohme S.A.), administered orally with water. Fasting continued until 4 h after the initiation of drug administration, at which a standardized meal was served. Similar meals were also given at 8, 12, and 24 h post-dose. For each subject, 26 blood samples (each of 6.0 mL) were collected before dose and at 0.33, 0.67, 1.00, 1.33, 1.67, 2, 2.5, 3, 4, 4.5, 5, 5.5, 6, 6.5, 7, 8, 10, 12, 14, 16, 24, 36, 48, 72, and 96 hours post-dose. Samples were collected in pre-labeled vacutainer containing K_3-EDTA as anticoagulant and plasma was separated by centrifugation and stored at −80°C until the quantitative analysis. After a 14-day washout period, subjects received the alternate formulation and the same procedures were followed as in the first study period.

All study participants were monitored closely for potential adverse events, while clinical examinations and vital signs measurements (sitting blood pressure, oral body temperature, radial pulse rate and respiratory rate) were performed before and after drug administration in each study period. Baseline and post-study laboratory measurements, including hematology and biochemical parameters (serum creatinine, ALT, AST, bilirubin, urea, haemoglobin, and albumin) were also performed, and all reported adverse effects were recorded and evaluated.

C.2.1.2.2 Assay methodology

Plasma samples were assayed for EZE and EZEG using a validated LC-MS/MS method. Briefly, the analytes were extracted by a solid phase extraction process, which employed as internal standards ezetimibe D4 and ezetimibe phenoxy D4 glucurodine analogs, respectively. The separations were carried out using a BDS Hypersil analytical column

(C18, 250x4.6mm, 5µ) with the isocratic elution system of 35:65 % v/v of water containing 1mM ammonium acetate and acetonitrile:methanol (75:25% v/v), and a flow rate of 1 mL/min. The analytic method had a LLOQ of 0.1 ng/mL and calibration curve range of 0.1 ng/mL to 15.0 ng/mL. It presented adequate sensitivity, precision, accuracy, specificity, and linearity, with the intra-day coefficient of variation for the assay being below 3.89% and 1.67% for EZE and EZEG, respectively.

C.2.1.2.3 Population pharmacokinetic analysis

Both EZE and EZEG exhibit similar cholesterol-lowering activity and multiple peaks in their pharmacokinetic profiles. In this vein, the current population PK analysis was performed using the total EZE concentration-time data (i.e., the sum of unchanged EZE and EZEG). Similar methodologies in the treatment of EZE data and PK analysis have been suggested in previously published works (Chu et al., 2012; Ezzet et al., 2001).

A non-linear mixed effects modeling approach was applied to the obtained dataset using Monolix® 2016R1 (Lixoft, Orsay France). PK parameter estimates for total EZE concentrations were determined following sequential steps. In the first step, single- and multi-compartmental PK models with linear elimination were fitted to the obtained data to determine the best structural PK model. One-, two-, and three-compartment models with or without the presence of EHC were tested for their ability to describe the distribution and elimination processes of total EZE. Since multiple secondary peaks, indicative of the significant EHC of the drug, were observed in the mean and individual C-t profiles of subjects (Figure C.4.2(A) and C.4.2(B)), conventional PK models were proved inadequate to describe the complex re-circulation kinetics of the drug.

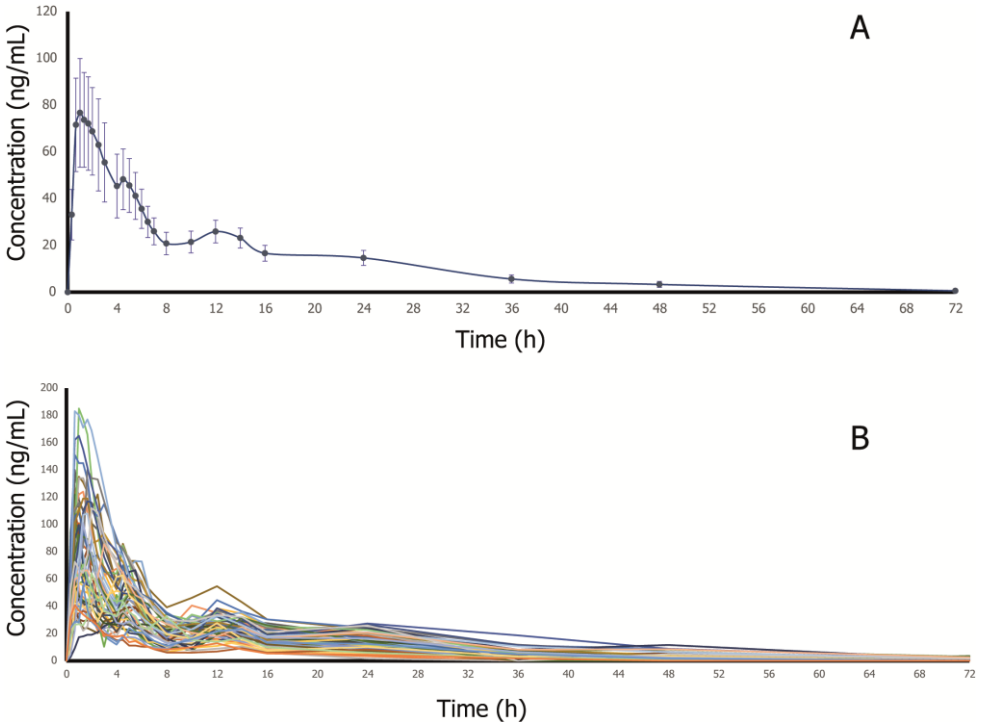

Figure C.4.2. Mean (A) and individual (B) C-t plots of total ezetimibe following a single oral dose of 10 mg Ezetimibe in 28 subjects. Data from both the two products (Rafarm S.A. & Merck Sharp Dohme S.A.) and both periods of administration are shown.

For this reason, more sophisticated user-defined models incorporating an EHC process were developed during model building. These models were encoded as ordinary differential equation systems using the custom-built model coding language MLXTRAN of Monolix® software. Four different categories of models of increasing complexity were investigated. A schematic representation of the types of models investigated in the current analysis is shown in Figure C.4.3.

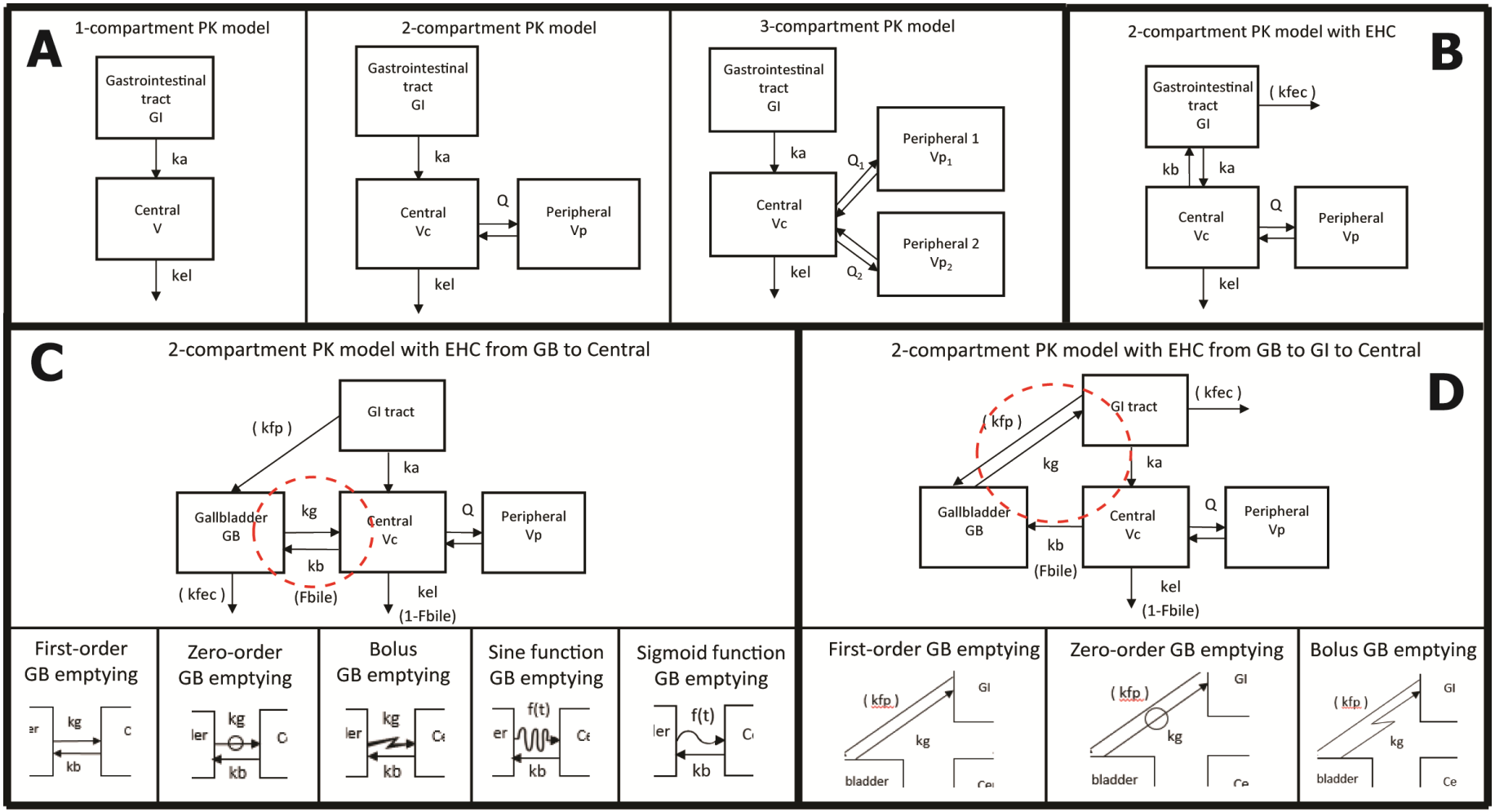

Figure C.4.3. General forms of the structural models examined for total Ezetimibe. The red circles highlight on the specific kinetics of the structural model and are described in the boxes next to each model. *Key*: kb = first-order transfer rate from the central compartment to the GB compartment; Fbile: fraction of dose transferred in the GB compartment; kg = switch function release rate constant from the GB to the GI compartment; kfp = first-order rate constant for first-pass metabolism; kel = first-order elimination rate constant; kfec: first-order rate constant for fecal elimination.

The first category (Fig. C.4.3(A)) included conventional one-, two-, and three-compartment models without the inclusion of an EHC process. In the second category (Fig. C.4.3(B)), a three-compartment model incorporating the EHC process occurring between the GI and central compartment was evaluated. The third category (Fig. C.4.3(C)) included four-compartment models, where an additional gallbladder compartment was introduced into the system - in that case EHC was described by a direct bile release from the GB compartment to the central compartment using different release kinetics. Finally, the fourth category (Fig. C.4.3(D)) included a four-compartment model, as in case of Fig. C.4.3(C), with the difference that the GB compartment was assumed to release drug into the GI compartment which was subsequently absorbed to the central compartment creating an EHC loop of three serial compartments.

In all tested PK model, the drug was presented into the GI compartment following oral administration, from which a fraction of dose (F) was absorbed by first-order process into the central compartment. The drug was either eliminated from the central compartment or transferred into the peripheral and redistribution compartments by first-order processes. All models were parameterized in terms of volumes of distribution for the central and peripheral compartments (Vc and Vp), inter-compartmental clearance (Q), and the first-order absorption and elimination rate constants (ka and kel). As bioavailability could not be quantified, since only data from an oral administration were available, the term F, referring to the bioavailable fraction of dose, was included to the estimated PK parameters, i.e., Vc/F, Vp/F, and Q/F, corresponding to their apparent values.

For the PK models with the EHC component, additional parameters describing the recirculation process had to be introduced. These parameters included a first-order rate constant describing the drug transfer from the central compartment to the GB compartment (kb) and an excretion rate constant simulating the bile release from the gallbladder (kg). The latter was also controlled by an intermittent switch function to account for the discontinuous GB emptying process. The choice of discontinuous bile release kinetics in the model was based on theoretical, as well as simulation studies which suggest that secondary peaks cannot be described by linear compartment systems with continuous cyclic transfer processes. For this reason, different scenarios were explored regarding the bile release kinetics, including bolus, first- or zero-order kinetics, time-dependent rate transfer, as well as sigmoid and sine function models which were able to

provide an oscillatory enterohepatic circulation. Several assumptions considering the time and duration (T_{GE}) of gallbladder emptying were also assessed for inclusion in the final model, along with the presence or absence of a smaller baseline bile release constant (kg*), a first-pass effect (kfp), fecal elimination (kfec), or a parameter describing the fraction of dose undergoing EHC (Fb).

At first, the GB emptying times and durations were considered as parameters, but in order to increase the accuracy of the other estimated PK parameters, these times were finally fixed. In most subjects, meal times were shown to trigger the timing of GB emptying, therefore, GB emptying times were standardized based on the intake of meals as defined in the study protocol (4, 8, 12, and 24h after drug administration) and the appearance of the secondary peaks in the obtained C-t plot. Different durations of GB empting (0.01, 0.5, 0.75, 1, and 1.5 h) were also tested, based on physiological criteria and previously reported values (Berg et al., 2013; de Winter et al., 2009; Sam et al., 2009).

The statistical model accounting for variability in EZE pharmacokinetics included parameters for BSV, IOV and RUV. All parameters were assumed to follow log-normal distribution, while logit-transformation was implemented for the PK parameters constrained to be on the 0-1 scale. Correlations of the random effects of the PK parameters and different error models for residual variability were also assessed using the likelihood ratio test.

Along the base model selection, the effect of certain covariates on model PK parameters was investigated. These included baseline demographic characteristics, such as body weight, age, height and BMI, as well as treatment effect, laboratory measurements obtained during screening tests, such as liver enzymes (AST and ALT), bilirubin (total, conjugated and free), serum creatinine, albumin, hemoglobin and urea. The impact of continuous covariates was tested according to allometric or linear relationships, either untransformed or centered around their ‘mean’ value.

Final model selection was based on goodness-of-fit numerical and graphical criteria in addition to the plausibility and stability of the model. PK parameter estimates were required to be physiologically plausible and a model had to remain stable when significant digits and initial parameter estimates were altered.

C.2.1.3 Results

Data from 28 male subjects were used in the population PK analysis. Demographic and biochemical parameters of the included population are presented in Table C.4.1.

Table C.4.1. Demographic and biochemical characteristics of the studied population (n = 28).

Continuous Characteristics	**Mean**	**Range (Min-Max)**
Age (y)	27	19-37
Body weight (Kg)	59.6	47.3-76.7
Height (cm)	165.4	152-176.5
Body mass index (Kg/m^2)	21.8	18.73-26.84
Serum creatinine (mg/dL)	0.7	0.59-0.93
Serum urea (mg/dL)	18.5	9.2-34.5
Serum albumin (gm/dL)	4.8	4.38-5.35
Aspartate aminotransferase (IU/L)	24.9	13.7-43.32
Alanine aminotransferase (IU/L)	23.8	8.2-45.1
Haemoglobin (g/dL)	13.7	12.2-16
Bilirubin total (mg/dL)	0.6	0.23-1.22
Bilirubin conjugated (mg/dL)	0.2	0.09-0.33
Bilirubin unconjugated (mg/dL)	0.4	0.14-0.9

The study medication was generally well tolerated and all volunteers completed the study procedures without any adverse effects. In total 1,508 concentration–time values were analyzed. A high proportion (around 95%) of concentrations below the LLOQ were found for the 96 h time-point and for this reason the dataset was truncated up to 72h. Figure C.4.2(A&B) displays the mean and individual plasma C-t profiles of total EZE which is indicative of the high variability encountered in the absorption and distribution processes among subjects.

Plasma concentrations of total EZE reach Cmax at around 1 hour after dosing, with all participants demonstrating multiple secondary peaks at around meal-times, consistent with the known EHC of the drug. Given this complex C-t profile, conventional 1-, 2- and 3-compartment models were proved inadequate to fit total EZE C-t data and describe the multiple concentration peaks observed in the C-t profile of the drug (Figure C.4.4, Table C.4.2).

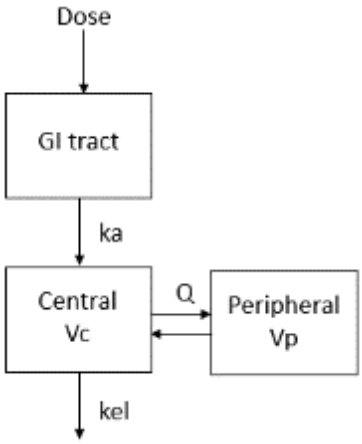

Figure C.4.4. Conventional 2-compartment model for total Ezetimibe.

Table C.4.2. Goodness of fit criteria for the 2-compartment model.

Observed vs individual predicted concentrations plot	VPC plot
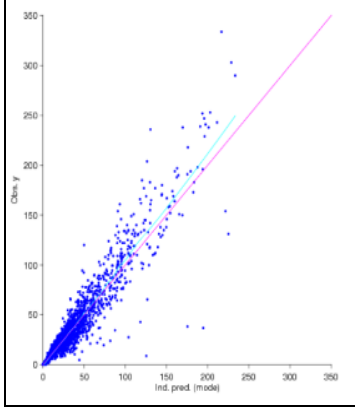	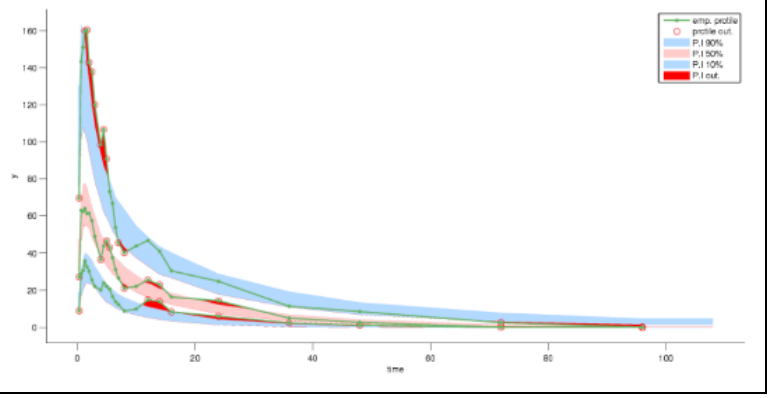

Numerical criteria: -2LL, 10999.45; AIC, 11025.45; BIC, 11053.10

As the feature of EHC was apparent in all study participants, a recirculation compartment was included a priori in the subsequent models. Prior information regarding the metabolism and disposition of EZE, as well as different methodologies regarding EHC kinetics proposed by previous studies, were considered during model development. In this respect, two main model categories were investigated; the first (Group A) considered GB release directly to the central compartment of drug, whereas the second category (Group B) followed a more physiologically realistic approach, by assuming GB release to the GI tract and then re-absorption of the drug back to its central compartment.

Starting with the simpler model configurations of Group A, different release kinetics, including bolus (instantaneous), zero- and first-order kinetics as well as sine and sigmoid functions were tested to describe bile release. The models with zero-order and bolus

release kinetics for GB emptying, shown in Figures C.4.5 and C.4.6, respectively, even though they were able to capture the multiple concentration peaks of total EZE profile, were considered inadequate in terms of fitting (Tables C.4.3 & C.4.4, respectively).

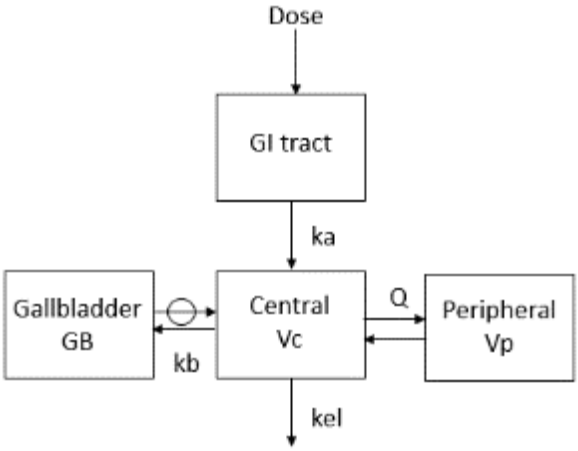

Figure C.4.5. Model category A1, GB release directly to the central compartment, zero-order bile release kinetics. *Key:* kb, first-order transfer rate constant from the central to GB compartment.

Table C.4.3. Goodness of fit criteria for category A1, GB release directly to the central compartment, zero-order bile release kinetics.

Observed vs individual predicted concentrations plot	**VPC plot**
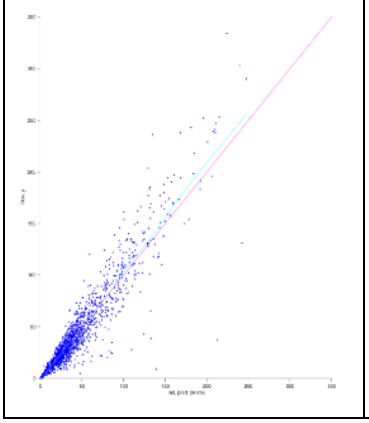	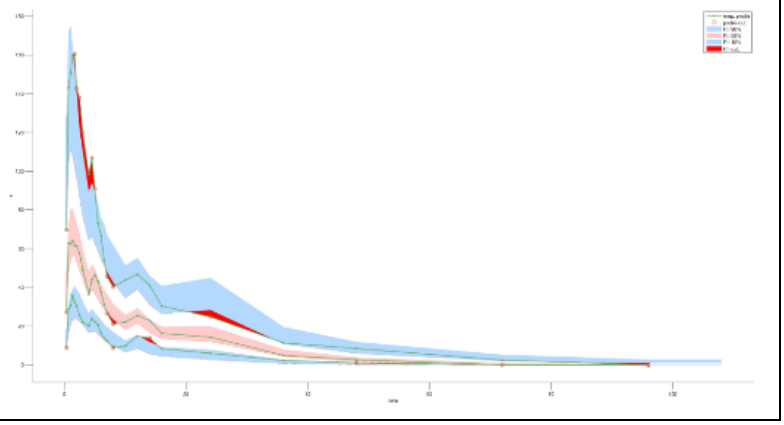

Numerical criteria: -2LL, 11504.70; AIC, 11538.70; BIC, 11574.86

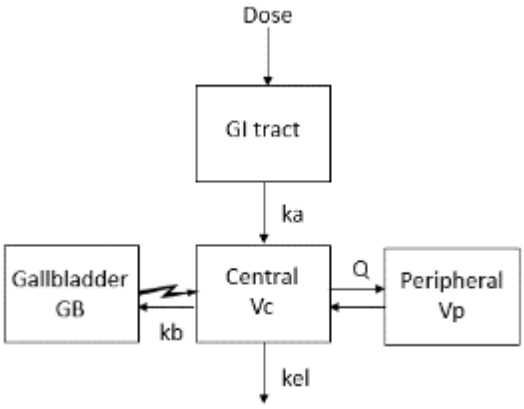

Figure C.4.6. Model category A2, GB release directly to the central compartment, bolus release kinetics for bile.

Table C.4.4. Goodness of fit criteria for category A2, GB release directly to the central compartment, bolus release kinetics for bile.

Observed vs individual predicted concentrations plot	**VPC plot**
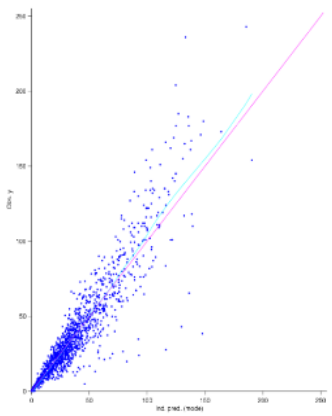	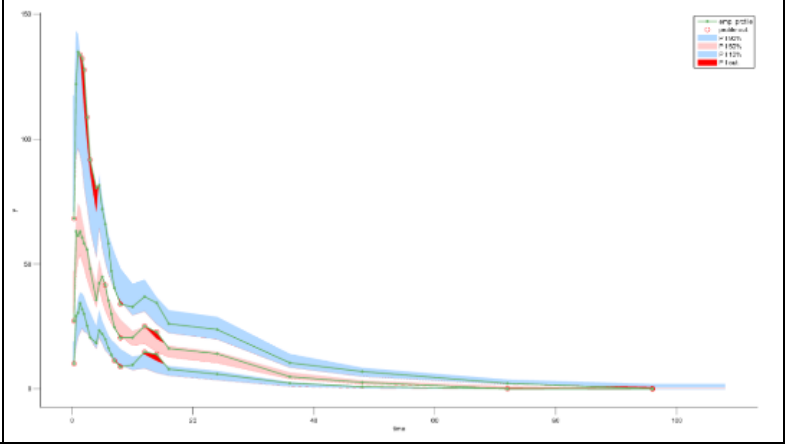

Numerical criteria: -2LL, 10080.48; AIC, 10110.48; BIC, 10140.86

In the case of sine function (Figure C.4.7), regular intervals of bile release were assumed which could not provide the required flexibility in terms of cycle's timing and duration in the model (Table C.4.5).

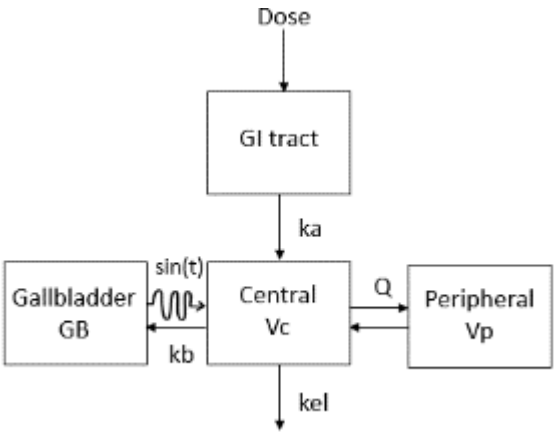

Figure C.4.7. Model category A3, GB release directly to the central compartment, sine function release kinetics for bile. *Key:* sin(t), sine function for bile release.

Table C.4.5. Goodness of fit criteria for category A3, GB release directly to the central compartment, sine function release kinetics for bile.

Observed vs individual predicted concentrations plot	VPC plot
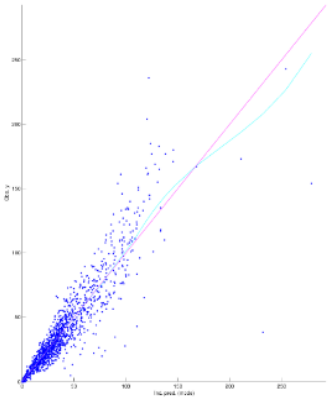	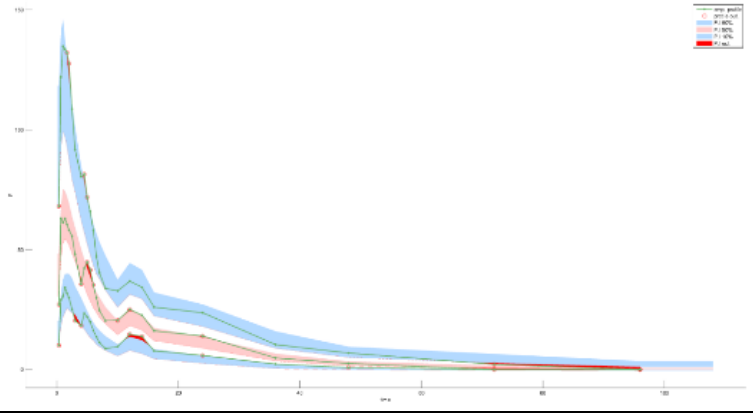

Numerical criteria: -2LL, 10052.75; AIC, 10086.75; BIC, 10121.18

Similarly to the sine function, the incorporation of a sigmoid function for the description of bile release (Figure C.4.8), also led to unsatisfactory model fitting (Table C.4.6).

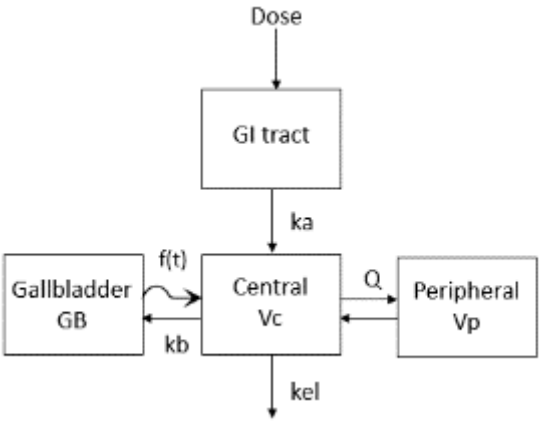

Figure C.4.8. Model category A4, GB release directly to the central compartment, sigmoid function release kinetics for bile. *Key:* f(t), sigmoid function for bile release.

Table C.4.6. Goodness of fit criteria for category A4, GB release directly to the central compartment, sigmoid function release kinetics for bile.

Observed vs individual predicted concentrations plot	**VPC plot**
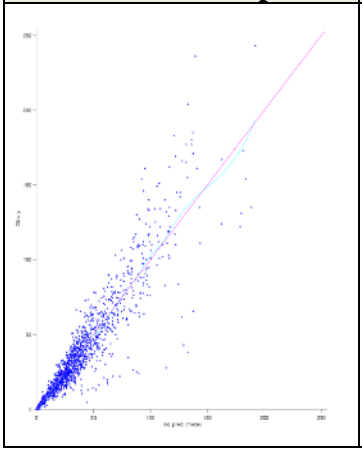	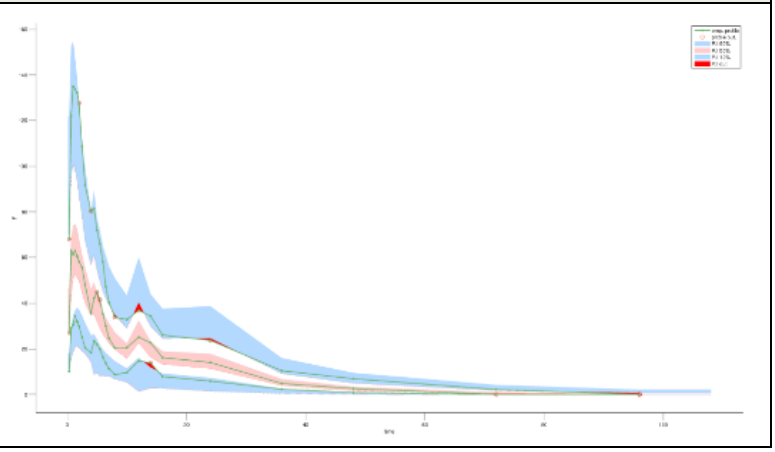

Numerical criteria: -2LL, 10090.09; AIC, 10128.09; BIC, 10166.57

In contrast to the above, first-order bile release kinetics (Figure C.4.9) provided a better fitting with a significant reduction in the numerical criteria compared to the previous models (Table C.4.7).

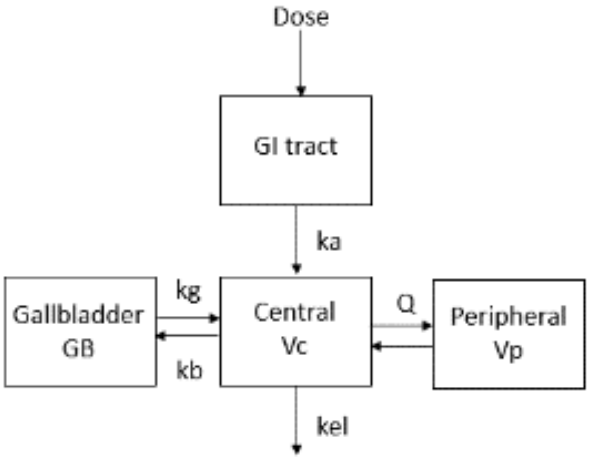

Figure C.4.9. Model category A5, GB release directly to the central compartment, first-order bile release kinetics. *Key:* kg, first-order rate constant for bile release.

Table C.4.7. Goodness of fit criteria for category A5, GB release directly to the central compartment, first-order bile release kinetics.

Observed vs individual predicted concentrations plot	VPC plot
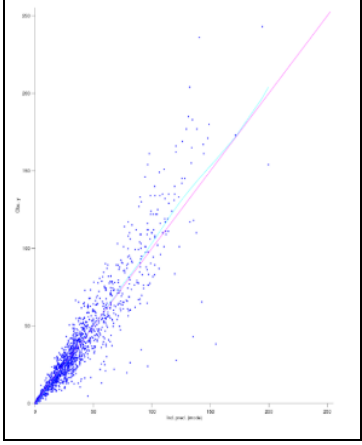	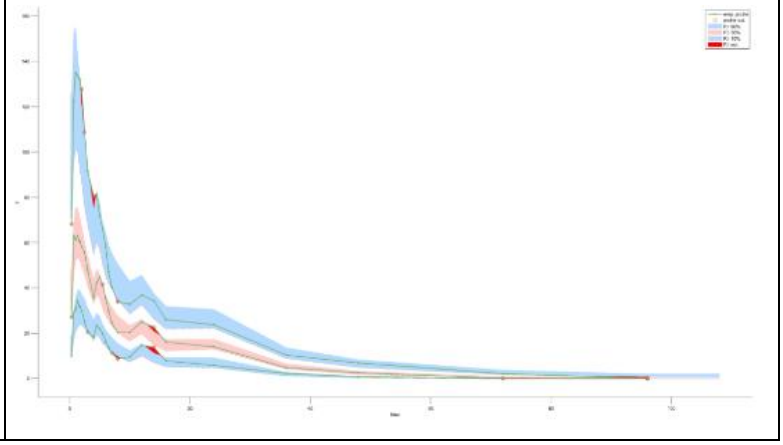

Numerical criteria: -2LL, 9899.99; AIC, 9933.99; BIC, 9968.42

Nevertheless, further improvement of fitting was attempted, proceeding to the models of Group B, where GB was assumed to release bile within the GI compartment. As sigmoid and sine functions were proved inappropriate for the description of bile release in our case, only zero-, first-order and bolus kinetics were tested for the description of bile release in Group B models. In this case, first- and zero-order bile release failed to adequately characterize the entire EHC process of the drug, with a significant weakness of both models to capture the first enterohepatic cycle of EZE, observed at around 4 hours post dose (Figures C.4.10 & C.4.11, Tables C.4.8 & C.4.9).

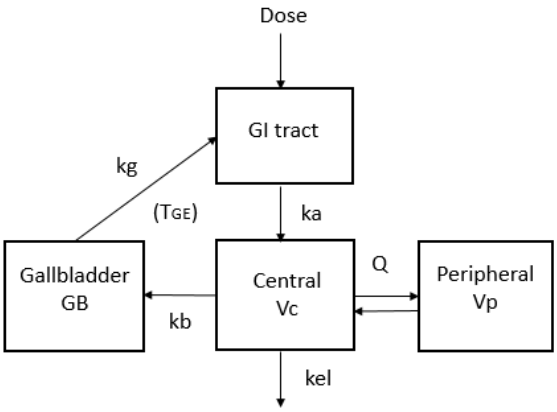

Figure C.4.10. Model category B1, GB release to the GI tract, first-order bile release kinetics.
Key: kg, first-order rate constant for bile release; T_{GE}, gallbladder emptying time intrval.

Table C.4.8. Goodness of fit criteria for category B1, GB release to the GI tract, first-order bile release kinetics.

Observed vs individual predicted concentrations plot	**VPC plot**
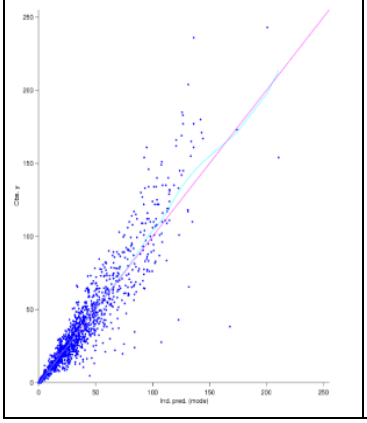	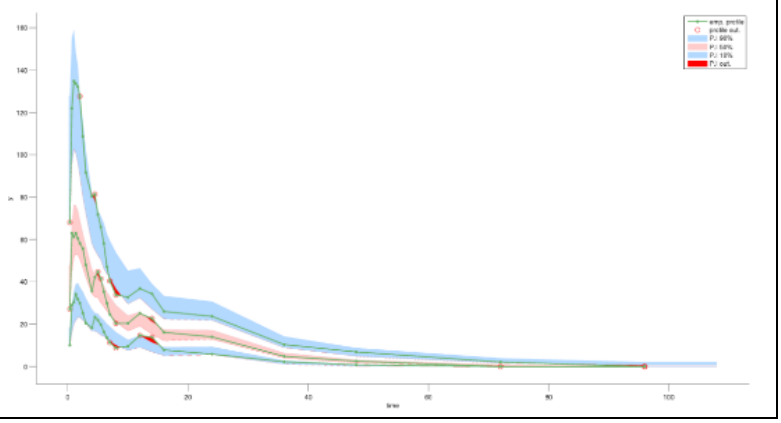

Numerical criteria: -2LL, 10124.43; AIC, 10158.43; BIC, 10192.86

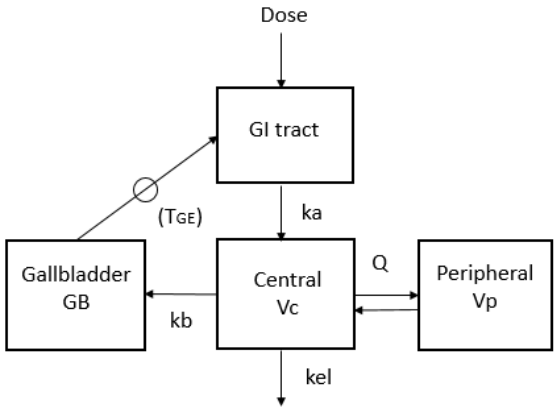

Figure C.4.11. Model category B2, GB release to the GI tract, zero-order bile release kinetics.

Table C.4.9. Goodness of fit criteria for category B2, GB release to the GI tract, zero-order bile release kinetics.

Observed vs individual predicted concentrations plot	**VPC plot**
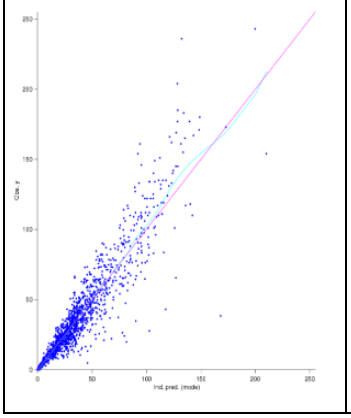	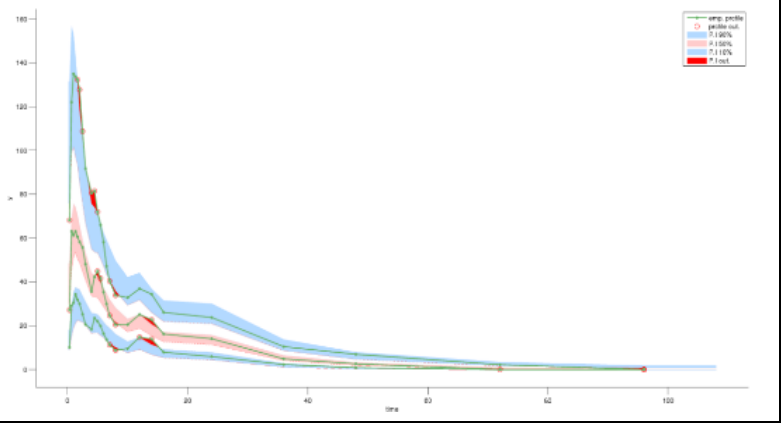

Numerical criteria: -2LL, 10186.99; AIC, 10216.99; BIC, 10247.37

Finally, a population PK model, incorporating an intermittent GB emptying to the GI tract described by bolus kinetics was able to simulate successfully the EHC process of total EZE (Figure C.4.12).

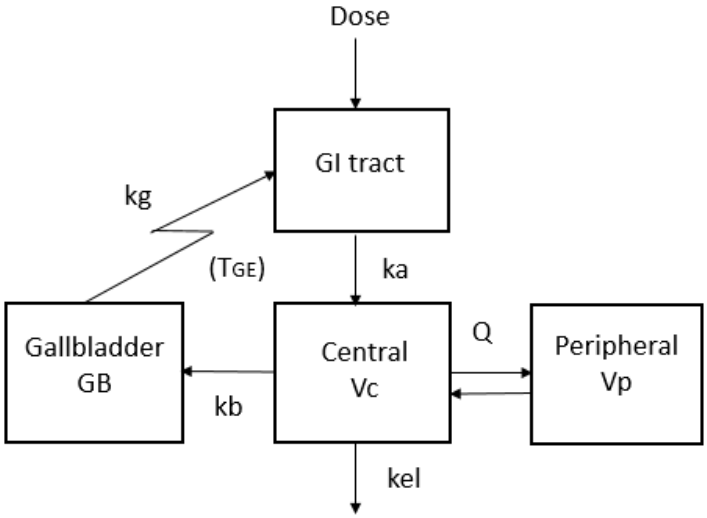

Figure C.4.12. The final enterohepatic recirculation model for total Ezetimibe. The lightning between the GB and GI compartments represent the bolus release of bile from the GB. *Key:* ka = first-order absorption rate constant; Vc = apparent volume of drug distribution of the central compartment; Vp = apparent volume of drug distribution of the peripheral compartment; Q = apparent inter-compartmental clearance of the drug; kb = first-order transfer rate from the central compartment to the GB compartment; kg = switch function release rate constant from the GB to the GI compartment; kel = first-order elimination rate constant.

As shown in Figure C.4.12, the structure of this model included four compartments: the central, peripheral, GI and GB compartments. The central compartment representing the blood and liver was reversibly connected to a peripheral tissue compartment. A hypothetical GB compartment introduced into the model and was linked to both the central and GI compartments creating the enterohepatic recirculation loop. The drug in the central compartment was either eliminated or transferred into the peripheral of GB compartment, following first-order kinetics. Following accumulation in the GB compartment, the drug was intermittently released from the GB to the GI compartment using a "very fast" first-order rate constant (like a bolus release), with fixed GB emptying times and duration. The drug was then re-absorbed from the GI tract to the central compartment with the same first-order rate constant as the administered oral dose. Elimination was considered to occur from the central compartment following first-order kinetics and accounted for both renal and fecal excretion.

Assuming all the kinetic processes, except bile release followed first-order kinetics, the set of ordinary differential equations for the PK model is described by Equations 15-20:

$$dA_1/dt = - ka \cdot A_1 + GBE \cdot k_{41} \cdot A_4 \quad \text{(Eq. 15)}$$

$$dA_2/dt = ka \cdot A_1 - (k_{23} + k_{24} + kel) \cdot A_2 + k_{32} \cdot A_3 \quad \text{(Eq. 16)}$$

$$dA_3/dt = k_{23} \cdot A_2 - k_{32} \cdot A_3 \quad \text{(Eq. 17)}$$

$$dA_4/dt = k_{24} \cdot A_2 - GBE \cdot k_{41} \cdot A_4 \quad \text{(Eq. 18)}$$

$$k_{23} = Q/Vc \quad \text{(Eq. 19)}$$

$$k_{32} = Q/Vp \quad \text{(Eq. 20)}$$

where, *An* represents the drug amount in the n^{th} compartment: (1) the gastrointestinal tract compartment; (2) the central compartment; (3) the peripheral compartment; (4) the gallbladder compartment, and k_{ij} are the absorption, elimination or transfer rate constants among the compartments. The term GBE is a switching criterion with values 0 or 1 which refer to the situations in the absence of GB emptying (GBE=0) or when GB emptying occurs (GBE=1). The initial conditions of all compartments were set to zero except *A1*, which is assumed to contain the entire EZE dose at zero time.

In this analysis, GB emptying was defined as a known intermittent process, with essentially complete emptying within each enterohepatic cycle. Based on the time of secondary peaks and the intake of food relative to dose, EHC was modeled to simulate three release times with the GB emptying described as a bolus impulse into the GI compartment. The duration of bile release was fixed at 0.75 h which approximates the mean GB emptying time in healthy individuals (Berg et al, 2013). Finally, the bile release rate constant (k_{41} or kg) was assumed to either equal to zero or was fixed to a high positive value (Sam and Joy, 2010), i.e., arbitrarily set at 21 h^{-1}, which eventually was found to provide the best model performance.

Additional assumptions were also made to aid in producing a model that would successfully minimize:

- the rate constants associated with each compartment were not affected by the recycling
- liver, being a well perfused organ, was considered as part of the central compartment in the final model.

- GB emptied completely at each cycle and the three EHC were exactly the same.
- EZE glucuronide was totally and rapidly hydrolyzed to free EZE in the gut immediately after bile release, followed by complete reabsorption of EZE.
- the recirculated drug was reabsorbed with the same first-order rate constant as the administered oral dose.
- fecal and renal elimination were incorporated in one drug elimination rate constant from the central compartment.

The parameter estimates for ka, Vc/F, Vp/F, Q/F, kb (or k_{24}), and kel that provided the best fit to the data set of each participant are summarized in Table C.4.10.

Table C.4.10. Population PK parameters for the final PK model applied to total ezetimibe data. *Key*: kb = first-order transfer rate from the central compartment to the gallbladder compartment (L/h); *a* and *b* = residual error parameters for the combined error model (Eq.21).

PK Parameter	Mean (RSE%)	BSV% (RSE%)
ka (h^{-1})	0.86 (9)	39.75 (19)
Vc/F (L)	50 (8)	31.76 (17)
Vp/F (L)	146 (10)	56.58 (15)
Q/F (L/h)	30.5 (15)	86.59 (16)
kb (h^{-1})	0.096 (12)	26.03 (88)
kel (h^{-1})	0.208 (7)	22.17 (31)
PK Random Effects Correlation		
Vc/F - Q/F	0.88 (11)	-
Residual error model		
a	0.32 (17)	-
b	0.29 (3)	-
Numerical criteria		
-2LL: 9720.90	AIC: 9750.90	BIC: 9781.28

Between-subject variability exhibited moderate values, ranging from 22-56% with the exception of inter-compartmental clearance (Q/F) in which %BSV value was 86%. Model parameters were considered to be precisely estimated with relatively low RSE% values obtained for both PK parameters and BSV% estimates (Table C.4.10). A correlation of the random effects between Vc/F and Q/F (corr = 0.88) was also incorporated in the final model, as it significantly decreased the numerical criteria and improved goodness-of-fit plots. Residual variability was described by a combined error model consisting of an additive component α and multiplicative coefficient *b*:

$$C_{ij} = f_{ij} + (a + b \cdot f_{ij}) \cdot \varepsilon_{ij} \quad \text{(Eq. 21)}$$

where C_{ij} is the j_{th} observed concentration of EZE for the i_{th} individual, a and b are the parameters of the residual error model, f_{ij} is the j_{th} model predicted value for i_{th} subject, and ε_{ij} is the random error which is assumed to be normally distributed with mean 0 and variance 1. The residual error parameters for the combined error model (Eq. 21) were: α=0.32 and b=0.29. No covariate effect including age, body weight, height and BMI or any of the biochemical laboratory measurements tested was found significant for the estimated PK parameters. Inter-occasion variability and treatment effects were also not found to be statistically significant on any PK parameter.

Model comparison of the different types of models tested was done using mainly the AIC estimates. In all cases, AIC values were lower for the models included enterohepatic compartments compared to those derived from the same model without such compartments. In particular, introduction of the EHC process in the final PK model for total EZE decreased AIC by 1,275 units relative to the relevant model (two-compartment) without enterohepatic recycling. Goodness-of-fit plots also demonstrate a desired performance of the final population PK model of total EZE (Figures C.4.13-C.4.15). A good agreement between the individual predicted and the observed concentrations is depicted in Figure C.4.13, showing an adequate degree of linearity.

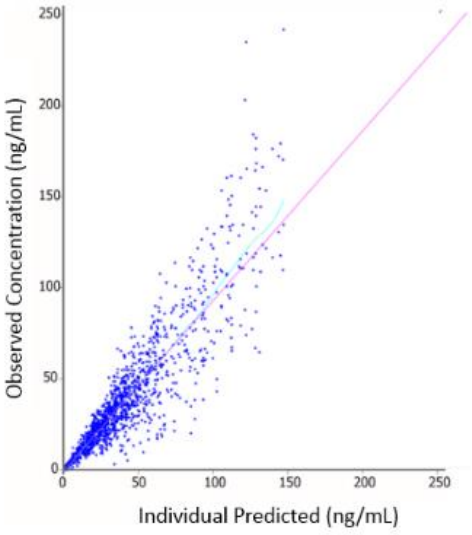

Figure C.4.13. Observed plasma concentrations *versus* the individual predicted concentration values from the population pharmacokinetic model of total Ezetimibe. The diagonal red line represents the line of unity, namely, the ideal situation.

Moreover, a symmetrical distribution with no significant trends can be observed when the IWRES or NPDEs were plotted *versus* the IPRED concentrations (Figure C.4.14). The bulk of residuals lie within the generally accepted range of ±2 units, indicating an acceptable description of the residual error by the combined error model.

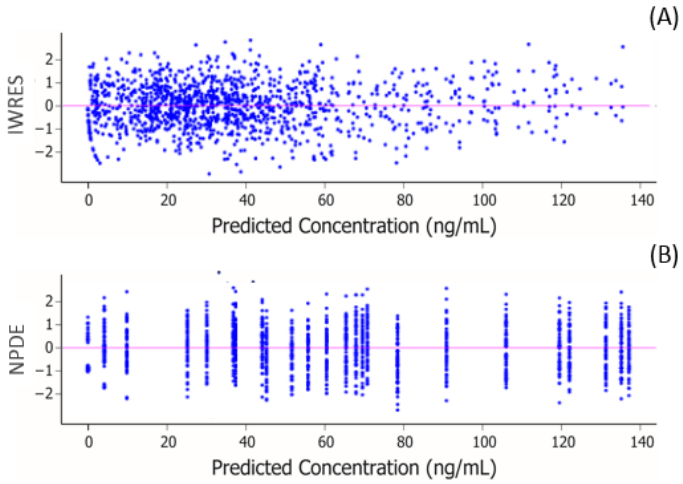

Figure C.4.14. Graphical illustration of: (A) the IWRES and (B) the NPDEs *versus* the IPRED concentrations for the final best model of total ezetimibe.

Finally, the VPC plot (Figure C.4.15) demonstrated that the majority of the observed plasma concentrations lied within the 10th and 90th percentiles of the simulated drug concentrations, providing a good description of mean tendency of the C-t data and an acceptable predictive ability of the final model.

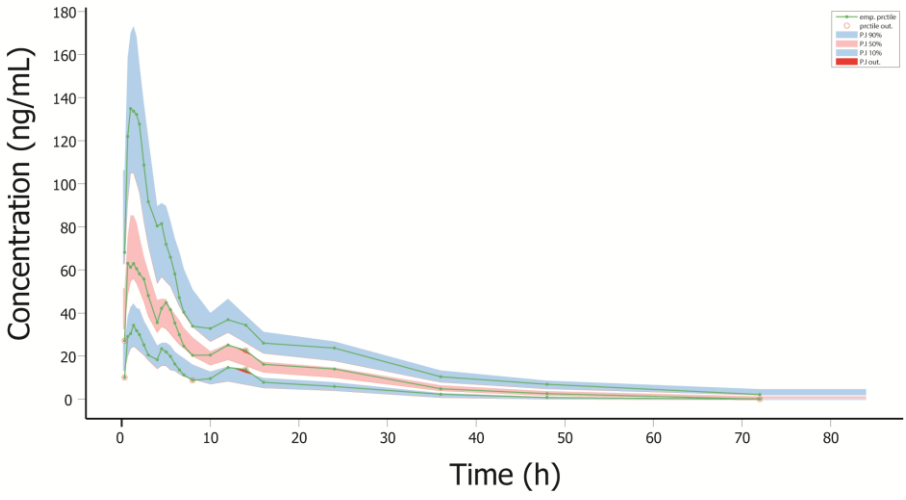

Figure C.4.15. VPC plot of the final model of total EZE. *Key*: Solid lines refer to the 10th, 50th, and 90th percentiles of the empirical data; Shaded areas refer to the 95% prediction intervals around each theoretical percentile; red circles and areas denote the outlier data.

The inclusion of additional parameters, such as a baseline bile release rate constant (kg*) during the fasting state (Shou et al., 2005), separate absorption (ka) and reabsorption (ka*)

rate constants from the GI (Strandgården et al., 2000), a first-pass effect (kfp) (Kim et al., 2015), or an additional parameter for the fraction of drug recycled in each EHC (Fb) (Shou et al, 2005) were also evaluated during model development, but did not lead to significant improvements of fitting and were not included in the final model. More complex models containing liver as a separate compartment were also considered (Kim et al., 2015), however, such an attempt has resulted in model over-parameterization and poor convergence (APPENDIX A).

C.2.1.4 Discussion

Following oral administration, EZE is rapidly absorbed by the intestine and extensively metabolized (>80%) to a pharmacologically active glucuronide conjugate. EZE alone has a molecular weight of over 400 g/mole and following glucuronidation, its molecular weight increases up to 580 g/mole, making both compounds prone to EHC. Previous studies have shown that EZE and EZEG are repeatedly delivered with bile into the intestinal lumen as a result of re-circulation, leading to an increased residence time of the drug to the site of action (Ezzet et al., 2001; Kosoglou et al., 2005). As evident in Fig. C.4.2, multiple secondary peaks are observed in the individual and mean C-t profiles of total EZE, with clear increases in plasma concentrations between 4-5, 11-13, and 23-25 hours post-dose in almost all subjects. This timing is consistent with food intake stimulating the emptying of the gallbladder.

In this respect, and to further expand our current understanding on metabolism and disposition of EZE, we developed a population PK model for the description of total EZE concentrations (parent and active metabolite), that could describe the enterohepatic recirculation of the drug and adequately characterize its complex disposition kinetics. The analysis was performed on the C-t data of 28 healthy subjects who participated in a BE study comparing two solid oral dosage forms of ezetimibe: Ezetimibe 10 mg Tablets (Rafarm S.A. Athens, Greece) *versus* Ezetrol® 10 mg Tablets (Merck Sharp & Dohme S.A.).

Modeling EHC has always been intricate and various models using different approaches have been investigated in our analysis to interpret the PK profile of total EZE (Okour and Brundage, 2017). The first models tested to describe EZE plasma profile were conventional models using variable number of compartments. One-, two-, and three-

compartment models were proven inadequate to capture the multiple concentration peaks observed in the C-t profile, as they did not consider for any recirculation process. Classical models were extended by a chain of compartments accounting for enterohepatic recirculation (Younis et al., 2009), however, these models did not consider the discontinuous pattern of bile release and the time elapsed during the recycling. Therefore, an appropriate time function had to be introduced in the PK model, accounting for the toggle nature of the GB emptying process.

In this sense, EHC models containing a variable number of compartments and different bile release kinetics, accommodating an irregular GB emptying were developed. Several treatments were applied for bile release kinetics, either directly to the central compartment or via the GI compartment. These included first-order (Berg et al., 2013), bolus (Jiao et al., 2007) or zero-order (Yau et al., 2009) release kinetics at a priori known times (e.g. time of food intake), or periodic bile release described by sine (Wajima et al., 2002) and sigmoid functions (Jain et al., 2011). Additional parameters for describing more adequately the EHC process were also considered but in most cases led in model over-parameterization and poor convergence (APPENDIX A).

Following several trials and based on physiological considerations, the basic structural model for EZE consisted of a 4-compartment disposition model including an enterohepatic recirculation loop added to the central compartment with instantaneously bile release at specific time intervals (Figure C.4.12). The recirculation loop was incorporated between the central and the GI compartment via the inclusion of a gallbladder compartment accounting for the accumulation of the drug in bile. A similar PK model for the description of total EZE concentrations in healthy subjects has been previously described by Ezzet and co-workers (Ezzet et al., 2001), however, the EHC component in that model was incorporated as a secondary input directly into the systemic circulation amounting to a percentage of the absorbed dose.

In the current model, EHC was simulated through multiple discharges of the GB compartment towards the intestine, and two circumstances were considered: i) absence of GB emptying during the fasting period and ii) presence of GB emptying around food intake. GB emptying was assumed to occur instantaneously at specific time intervals, where all the drug stored in the GB was released back to the intestine as a bolus impulse. This was achieved by using a first-order bile release constant fixed to a very large value

(kg = 21 h^{-1}), in addition to assuming a relatively short GB emptying duration (T_{GE} = 0.75 h). Each cycle was followed by another cycle of filling that proceeded until the next GB emptying triggered by the next meal and so on. As opposed to the sine or sigmoid functions, the use of switch on/off function for bile release provided more flexibility in terms of modeling the GB emptying process related to meal-times, providing the best physiological representation when compared to the rest modeling strategies. In the switch function release models, the rate constant controlling the GB emptying process is described by a piece-wise function (Okour and Brundage, 2017).

It is evident that models incorporating EHC can rapidly gain in complexity and may present parameter identifiability problems and numerical difficulties. Accordingly, in our case, to overcome such problems and keep a minimum model complexity, some parameters regarding EHC had to be fixed. Therefore, even though parameters, such as the bile release rate constant and the time and duration of GB emptying, were initially allowed to be estimated and vary within and between subjects, for the sake of parameter interpretation and covariate analysis, their values were finally fixed. It is acknowledged that fixing parameters for a recirculation process is not always an easy task, as it can dangerously distort and bias the choice of reabsorption kinetics and estimation of other PK parameters (Abi Khalil et al., 1993). However, in our case, based on a strict meal-time protocol and physiological considerations regarding GB emptying, as well as a thorough investigation on the most suitable bile release kinetics, we were able to develop a parsimonious model with the desired numerical stability and predictive power.

The estimated population parameter ka suggests that EZE is relatively rapidly absorbed with a rate constant value indicative of the short Tmax values observed in the PK profiles and similar to previously reported values (Ezzet et al., 2001; Kosoglou et al., 2005). Relatively high apparent volumes of distribution and low clearance were also obtained for EZE, consistent with the extensive recycling of the drug (Colburn, 1982; Roberts et al., 2002; Smith et al., 2015). The fraction of drug excreted into the bile within each EHC (EHC%) could also be indirectly estimated using a previously proposed equation (Colom et al., 2014):

$$EHC\% = (kb / kb + kel) * 100 \quad \text{(Eq. 22)}$$

where, kb is the rate constant for the transfer of drug from the central towards the theoretical GB compartment and kel is the first-order elimination rate. The equation showed that about 30% of the amount absorbed is recirculated in each enterohepatic cycle, a fraction slightly higher than previously reported values of around 20% (Ezzet et al., 2001).

None of the tested covariates was found to be significant or to improve the numerical or graphical criteria of the final model. This may be partly attributed to the relatively homogenous population, which can constrain the ability of the model to unveil the signal of a covariate relationship. Enterohepatic recycling has been generally shown to be affected by several factors, such as patient characteristics and genetic variability, age- or gender-related effects, liver and kidney function, potential disease effects or co-medication (Roberts et al., 2002). However, our findings coincide with the literature evidence for EZE, where no significant effect of age, gender, and race have been reported; the latter implies that no dosage adjustment is necessary for patients with mild renal or hepatic impairment (Jeu and Cheng, 2003; Kosoglou et al., 2005).

C.2.1.5 Conclusions

The aim of this study was to apply population PK modeling in order to describe the C-t data of total EZE and furthermore to elaborate on the enterohepatic recirculation models. In order to achieve in this task several different forms of EHC pharmacokinetic models were developed and evaluated. Eventually, total EZE was best described by a four-compartment model where EHC was modeled through the inclusion of an additional gallbladder compartment that released drug at specific time-intervals in agreement with food administration. This modeling approach led to the development of a novel population PK model for total EZE which is sufficiently realistic from a PK and physiological point of view. This model was found to accurately estimate the relevant PK parameters of total EZE, as well as to adequately characterize the enterohepatic recycling process of the drug and accommodated all secondary peaks observed in the profile.

C.2.2. Study 5: Joint PK model of Ezetimibe and its active metabolite

C.2.2.1 Introduction

Similarly to our previous study, most pharmacokinetic analyses so far have been applied to the total EZE concentrations, defined as the sum of unconjugated ezetimibe (i.e. unchanged parent drug) and ezetimibe-glucuronide (Kosoglou et al., 2004, 2005), with only one compartmental analysis using total EZE concentrations being available in the literature (Ezzet et al., 2001). However, since both EZE and EZEG are found to be pharmacologically active, a joint PK modeling of the parent drug and the metabolite could be also performed.

EZEG accounts for the majority (80-90%) of total ezetimibe concentrations measured in human plasma (Patrick, 2002; Jeu 2003). The major metabolic pathway for ezetimibe consists of glucuronidation of the 4-hydroxyphenyl group by the uridine 5′-diphosphate-glucuronosyltransferase isoenzymes UGT1A1, UGT1A3 and UGT2B15, to form ezetimibe-glucuronide in the intestine and liver (Ghosal et al., 2004; Kosoglou et al., 2005).

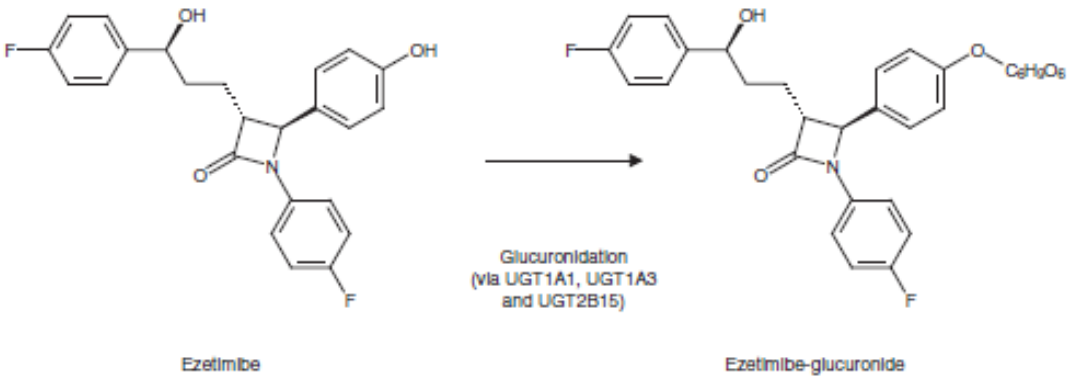

Figure C.5.1. Molecular structure of ezetimibe and ezetimibe-glucuronide before and after glucuronidation with uridine 5'-diphosphate-glucuronosyltransferase (UTG) isoenzymes.

Thereafter, the parent drug and its conjugated metabolite are transported through portal vessels to the liver where ezetimibe undergoes further glucuronidation and subsequent biliary secretion into the intestine. The phenolic glucuronide product undergoes enzymatic hydrolysis in the intestinal lumen, delivering parent compound back to absorption site, where it can be reabsorbed (van Heek et al, 1997). EZE and EZEG concentrations are found to rapidly decline and then increase, with plasma concentration-versus-time profiles of both drugs exhibiting multiple peaks consistent with enterohepatic recycling (Kosoglou et al., 2005; van Heek et al., 2000). As shown in the mean and individual C-t plots of EZE

and EZEG in Figure C.5.2, multiple secondary peaks were also observed in our study for both drugs at around 4 to 6, 10 to 12 and 22 to 24 h post dose. These times corresponded to the approximate time of meals, which are known to stimulate bile release from the gallbladder and significantly affect the enterohepatic recirculation of drugs.

Mean and Individual C-t profiles of EZE	Mean and Individual C-t profiles of EZEG
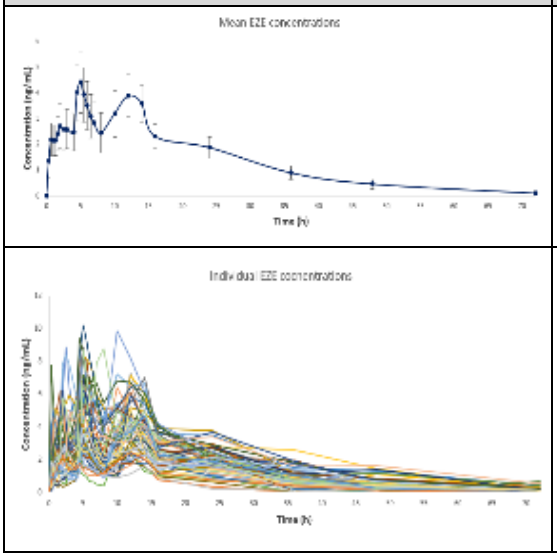	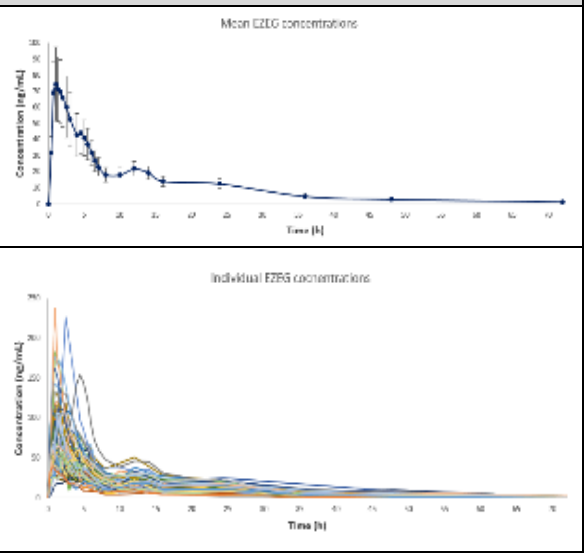

Figure C.5.2. Mean and individual C-t profiles of ezetimibe and ezetimibe-glucuronide in plasma following a 10mg single-dose oral administration.

Subsequently, plasma concentrations decline slowly, with drug concentrations of conjugated and unconjugated ezetimibe being quantifiable until 24 to 48 h post-dose. (Patrick et al., 2002). Similar results have been observed in previous studies, suggesting that the pharmacokinetics of both ezetimibe and its active metabolite are highly affected by this complex re-distribution process (Ezzet et al., 2001; Jeu and Cheng, 2003).

This study aimed, therefore, to develop the first joint population pharmacokinetic model for the description of the absorption and disposition kinetics of ezetimibe (EZE) and its active metabolite ezetimibe-glucuronide (EZEG). Since both agents are found to be repeatedly delivered to the intestinal wall by enterohepatic recycling (Patrick et al., 2002), an enterohepatic recirculation process was considered per se for both drugs during model development. In this respect, different structural models were developed and compared based on their predictive performance and adequate characterization of the underlying physiological processes.

C.2.2.2 Methods

The plasma concentration data used for the current analysis came from the same comparative PK study described in the previous Chapter. This was a standard open-label, single-dose, randomized crossover BE study, in 36 healthy adult subjects receiving either one dose of Ezetimibe 10 mg Tablets (Rafarm S.A. Athens, Greece) or Ezetrol® 10 mg Tablets (Merck Sharp & Dohme S.A.), under fasting conditions. Fasting continued until 4 h after the initiation of drug administration, at which a standardized meal was served, also given at 8, 12, and 24 h post-dose. In total 26 blood samples were collected from each participant, starting before drug administration and up to 96 hours post-dose.

In this analysis, all logarithmically transformed plasma C-t data of EZE and its glucuronide metabolite EZEG were analyzed simultaneously. For modeling purposes, ezetimibe doses and plasma EZE and EZEG concentrations were converted to molar equivalents (nmol/L) by dividing them by their molecular weight (EZE 409.4 g/mol; EZEG 585.5 g/mol), and then were recalculated back to ng/mL in results. The data of both drugs were then fitted together in one model using the nonlinear mixed-effect modeling software program Monolix (version 2016R1, Lixoft, France). As previously, data below the limit of quantification were treated as missing data and were excluded from the analysis.

Since both agents are known to undergo enterohepatic recycling, and based on the multiple peaks observed in both drugs' C-t profiles (Figure ##), EHC modeling was intrinsically incorporated in models for both agents, by presuming a hypothetical gallbladder compartment accounting for the intermittent redistribution process. Models were written as ordinary differential equations systems using the custom-built model coding language MLXTRAN of Monolix® software.

Different PK models of increasing complexity were constructed and compared for their performance. These included one-, two- and three-compartment distribution models for the parent and the metabolite, first-pass metabolism in the GI tract, the presence of one or two bile release compartments, bile release to the GI tract or directly to the central compartments of drugs along with different bile release kinetics (first-order or bolus) in each case, variant times and durations of gallbladder emptying and an additional fecal elimination from the GB or the GI compartment. In addition, the presence of a dose apportionment parameter for first-pass metabolism ('*Fp*') as well as a direct inter-

conversion between the parent and metabolite compartments and/or through the GB compartment were tested for potential improvements in the final model.

In principle, in most PK models, the drug was presented into the gastrointestinal lumen following oral administration, from which a fraction (F) of dose was absorbed by first-order process into the parent or metabolite central compartment. Thereafter, the two agents were either eliminated from their central compartments, transferred into their peripheral compartments or underwent enterohepatic recirculation, via a gallbladder compartment, which released intermittently drug back to the GI or the central drug compartments.

All models were basically parameterized in terms of absorption rate constants (ka), apparent volumes of distribution (V), intercompartmental clearances (Q) and elimination rate constants (kel). As bioavailability (F) could not be quantified, volumes of distribution and intercompartmental clearances corresponded to their apparent values - that is, Vcp/F, Vpm/F, Qp/F, etc. For the EHC component of the model, the additional parameters included the first-order constants for re-distribution of drugs (km and kmb), and bile release rate constants (kg1 and kg2). The latter where either allowed to be estimated as first-order rate constants, or were fixed to a very high value (e.g. 20 h^{-1}) in order to simulate the bolus impulse of gallbladder emptying. As in the previous model developed for total ezetimibe, bile release was further controlled by an intermittent switch function to account for the discontinuous bile release from the gallbladder. Several assumptions considering the time and duration of gallbladder emptying were also assessed. These assumptions were based on the study protocol information regarding the standardized meal intake (4, 8, 12, and 24h after drug administration), the appearance of the secondary peaks in the obtained C-t plots, as well as physiological considerations regarding gallbladder function.

PK parameters were assumed to follow log-normal distribution, while logit-transformation was implemented to force certain parameters to be constrained on a 0-1 scale (e.g., $0 \leq Fp \leq 1$). Between-subject, inter-occasion and residual unexplained variability were also included in the final model, while correlations of the random effects of the PK parameters and the effect of certain covariates on model PK parameters were investigated. The covariates tested included baseline demographic characteristics, such as body weight, age, height and BMI, the treatment formulation effect, and laboratory

measurements obtained during screening tests, such as liver enzymes (AST and ALT), bilirubin (total, conjugated and free), serum creatinine, albumin, hemoglobin and urea.

Final model selection was based on the previously described goodness-of-fit statistical criteria and visual predictive check plots in addition to the robustness of the model and the physiological plausibility of the estimated PK parameters.

C.2.2.3 Results

In total 28 subjects were used in the current population PK analysis, providing 56 C-t profiles for each drug. The spaghetti plots for EZE and EZEG shown in Figure C.5.3 (A and B), respectively, reveal the increased complexity and variability of the analyzed datasets.

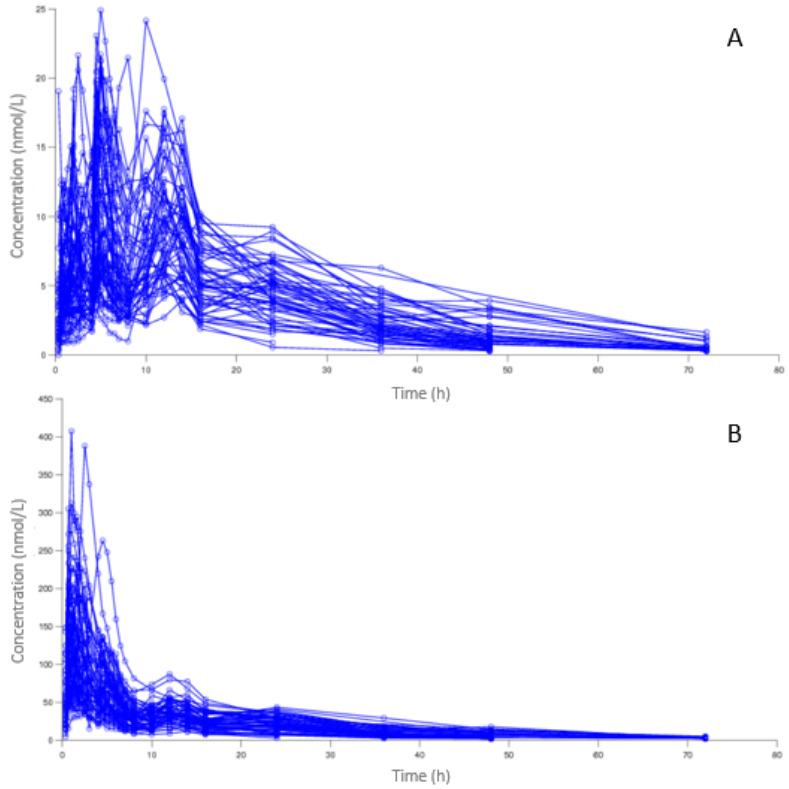

Figure C.5.3. Spaghetti plots of EZE (A) and EZEG (B) following a single oral administration of 10mg ezetimibe in healthy subjects under fasting conditions (n= 28).

In order to elaborate these erratic PK profiles, various approaches were investigated during model development. As the simple 1-, 2- and 3-compartment models could not adequately describe the data of EZE and EZEG, more complex models had to be

constructed. The first category of models tested included 2-compartment disposition models for both drugs, without the presence of first-pass metabolism within the GI tract (Model A, Figure C.5.4). However, this type of models failed to describe the PKs of the two drugs and were unable to minimize successfully (Table C.5.1).

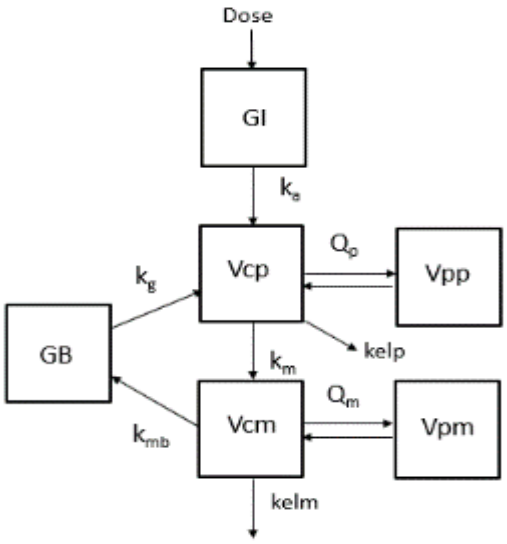

Figure C.5.4. Schematic representation of the joint population PK model for EZE and EZEG, without first-pass metabolism (Model A). *Key:* Vcp/Vcm, and Vpp/Vpm, volumes of distribution of the central and peripheral compartments for the parent and the metabolite, respectively; Qp and Qm, inter-compartmental clearances for the parent and the metabolite; km, first-order transformation constant of the parent to metabolite; kg, bile release first-order constant; kmb, first-order transfer constant of the metabolite to the GB compartment; kelp and kelm, first-order elimination constants for the parent and the metabolite, respectively.

Table C.5.1. Goodness of fit criteria for Model A (joint model without first-pass metabolism).

Observed vs individual predicted concentrations plot	VPC plots
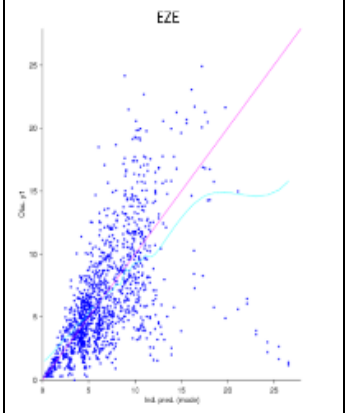	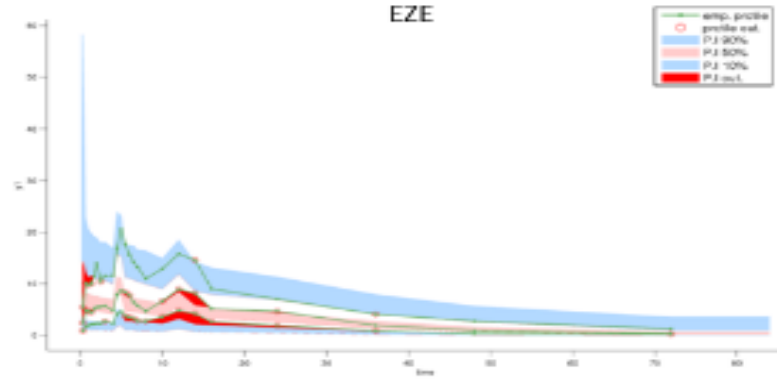
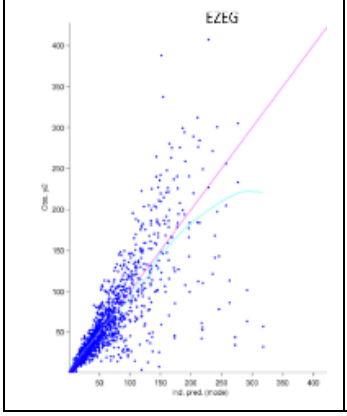	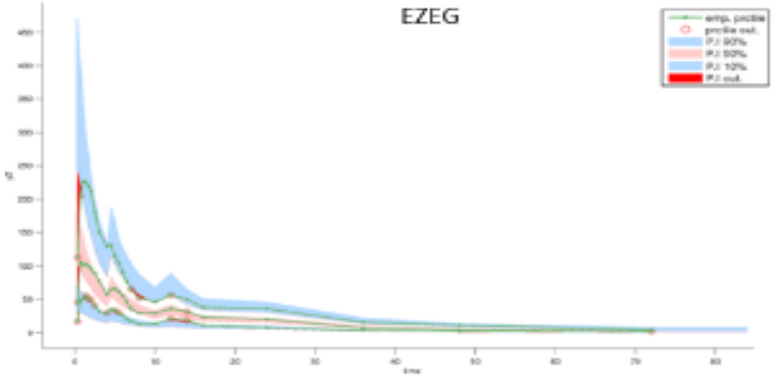

Numerical criteria: -2LL, 17566.29; AIC, 17622.29; BIC, 17679.00

Therefore, confirming pre-existent knowledge on EZE pharmacokinetics, the addition of pre-systemic metabolism in the GI tract greatly enhanced the model fitting with a significant improvement of the statistical criteria. In the following steps, therefore, a first-pass effect was incorporated as an intrinsic factor in all the developed models and further investigation focused mainly on the description of the EHC process of the two drugs. Initially, EHC was described by a loop of 4 compartments including the GI tract, the two central compartments and the gallbladder, which was assumed to deliver bile as bolus release back to the GI tract, where the two drugs could be re-absorbed to the central compartments by first-order processes (Figure C.5.5, Table C.5.2).

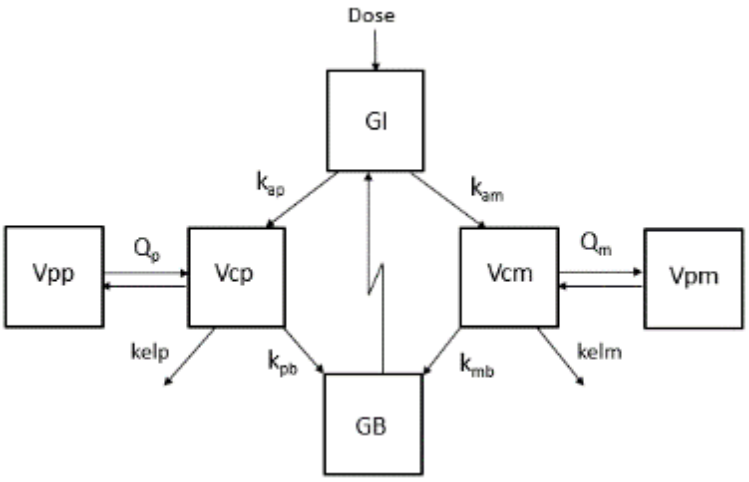

Figure C.5.5. Schematic representation of the joint population PK model for EZE and EZEG, with first-pass metabolism, GB emptying to GI (Model B). The lightning between the GB and GI compartments represent the bolus release of bile from the GB. *Key:* kap and kam, first-order absorption constants for the parent and the metabolite; kpb and kmb, first-order transfer constants of the parent and the metabolite to the GB compartment.

Table C.5.2. Goodness of fit criteria for Model B (joint model with first-pass metabolism, GB release bile to the GI).

Observed vs individual predicted concentrations plot	**VPC plots**
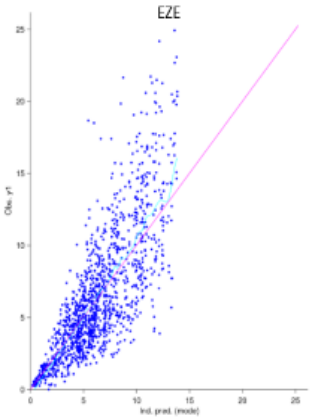	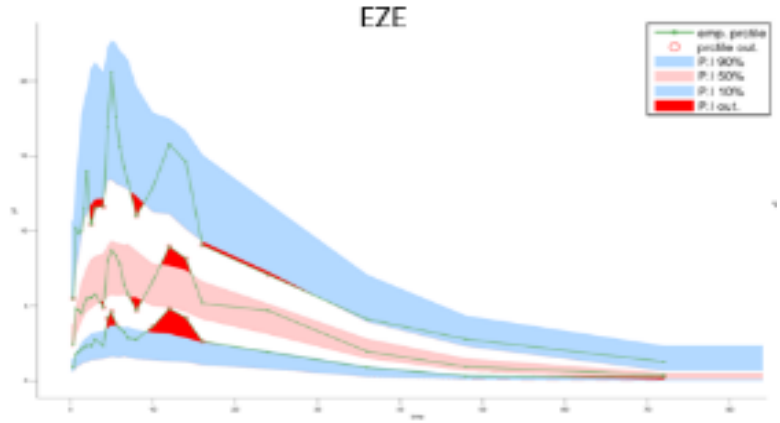
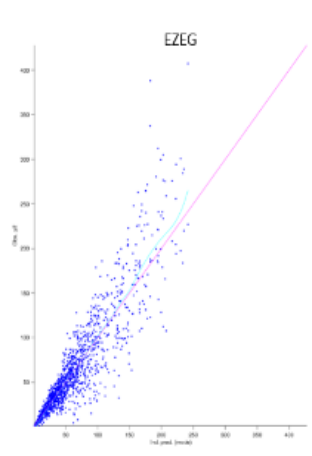	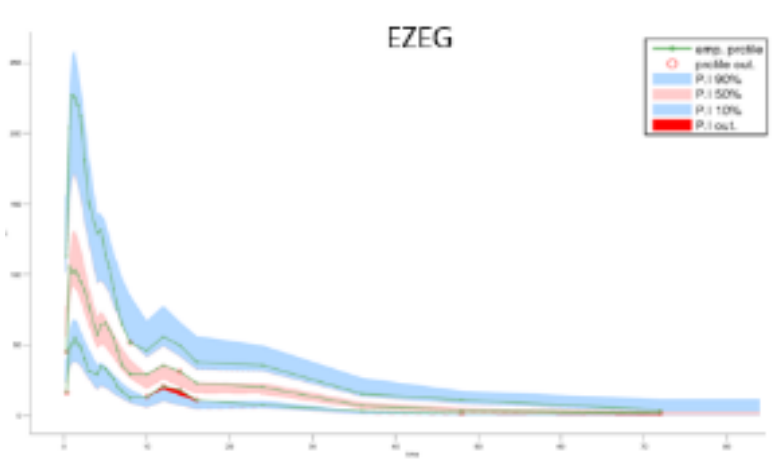

Numerical criteria: -2LL, 16650.45; AIC, 16706.45; BIC, 16763.16

Even though the addition of a first-pass effect led to a 900-U decrease in BIC and significantly improved model fitting in case of EZEG, these models were found unable to capture the EHC of EZE. For this reason, another approach for EHC was utilized, with the inclusion of two separate GB compartments for each drug, which directly released bile back to the central compartments by first-order processes (Figure C.5.6, Table C.5.3).

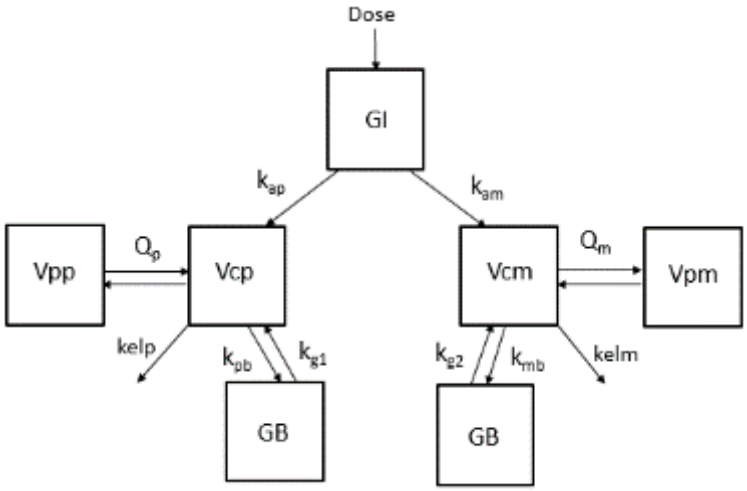

Figure C.5.6. Schematic representation of the joint population PK model for EZE and EZEG, with first-pass metabolism, 2 GB compartments, GB emptying to central compartments (Model C). *Key:* kpb and kmb, first-order transfer constants of the parent and metabolite to the GB; kg1 and kg2, bile release first-order constants for the parent and the metabolite.

Table C.5.3. Goodness of fit criteria for Model C (joint model with first-pass metabolism, 2 GB compartments, GB release bile to the central compartments).

Observed vs individual predicted concentrations plot	VPC plots
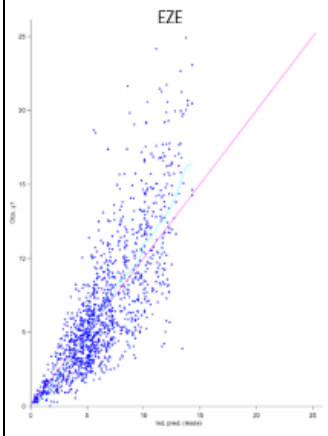	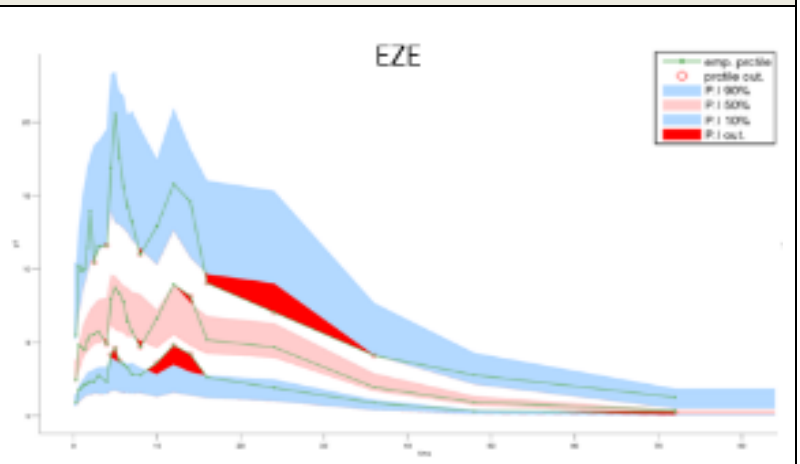
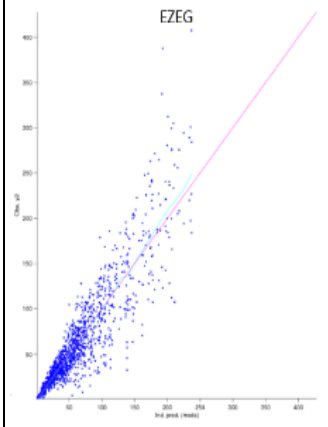	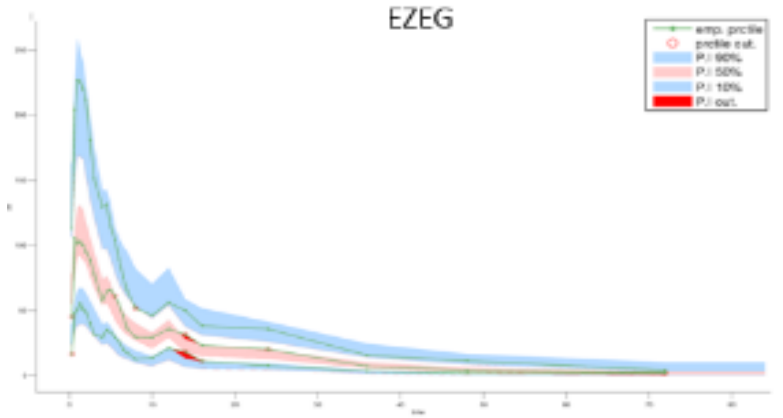

Numerical criteria: -2LL, 17073.90; AIC, 17141.90; BIC, 17210.76

Description of EHC through the incorporation of a first-order release from the GB compartments directly to the central compartments of the drugs allowed the characterization of the secondary peaks seen in both drugs plasma concentration profiles, however, a misfit of the model was still observed in the case of EZE, in addition to an increase in the numerical criteria.

Following a thorough model investigation, and testing different assumptions regarding EHC process, finally, a 6-compartment PK model coupled with an EHC re-distribution loop, incorporating a direct transformation of the parent drug into its metabolite and re-circulation via a GB compartment, was found to best describe the EZE and EZEG data simultaneously. Its structural representation is shown in Fig. C.5.7, along with the definition of related parameters.

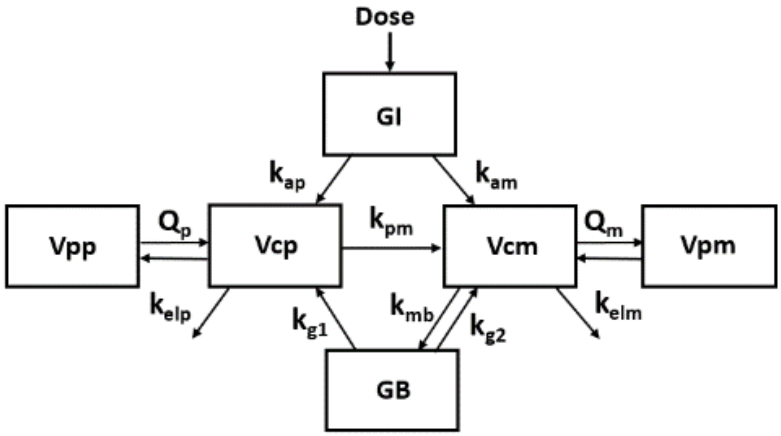

Figure C.5.7. Schematic representation of the final joint population PK model for EZE and EZEG. *Key:* kap and kam, first-order absorption constants for the parent and the metabolite; kpm, first-order transformation constant of the parent to metabolite; kmb, first-order transfer constant of the metabolite from the central to the GB; kg1 and kg2, bile release first-order constants for the parent and the metabolite.

In line with previous reports on EZE pharmacokinetics, a first-pass effect within the GI tract has been considered: the dose not only enters into the parent compartment at a rate 'kap' but also enters into the metabolite compartment at a rate 'kam'. Then, the parent drug is either eliminated from the system with a clearance constant 'kelp', distributed to a peripheral compartment, or is transformed into its metabolite (EZEG) by a first-order process. Accordingly, EZEG was cleared from the system by a constant 'kelm', distributed to its peripheral compartment or transferred to the gallbladder compartment, which at certain time points emptied back into the central compartments of both EZE and EZEG. All drug transfers between compartments were modeled as first-order processes, while biliary secretion was further controlled by a switch function able to simulate the intermittent process of GB emptying. The set of ordinary differential equations for the PK model is described by Equations 23-32:

$$dA_1/dt = - kap \cdot A_1 - kam \cdot A_1 \quad \text{(Eq. 23)}$$

$$dA_2/dt = kap \cdot A_1 - (k_{25}+k_{23}+kelp) \cdot A_2 + k_{52} \cdot A_5 + GBE \cdot k_{42} \cdot A_4 \quad \text{(Eq. 24)}$$

$$dA_3/dt = kam \cdot A_1 - (k_{36}+k_{34}+kelm) \cdot A_3 + k_{63} \cdot A_6 + k_{23} \cdot A_2 + GBE \cdot k_{43} \cdot A_4 \quad \text{(Eq. 25)}$$

$$dA_4/dt = k_{34} \cdot A_3 - GBE \cdot (k_{42} \cdot A_4 + k_{43} \cdot A_4) \quad \text{(Eq. 26)}$$

$$dA_5/dt = k_{25} \cdot A_2 – k_{52} \cdot A_5 \quad \text{(Eq. 27)}$$

$$dA_6/dt = k_{36} \cdot A_3 – k_{63} \cdot A_6 \quad \text{(Eq. 28)}$$

$$k_{25} = Qp/Vcp \quad \text{(Eq. 29)}$$
$$k_{52} = Qp/Vpp \quad \text{(Eq. 30)}$$

$$k_{36} = Qm/Vcm \quad \text{(Eq. 31)}$$
$$k_{63} = Qm/Vpm \quad \text{(Eq. 32)}$$

where, *An* represents the drug amount in the n^{th} compartment: (1) the gastrointestinal tract compartment; (2) the central compartment of the parent drug; (3) the central compartment of the metabolite; (4) the gallbladder compartment; (5) the peripheral compartment of the parent drug; (6) the peripheral compartment of the metablite, and k_{ij} are the absorption, elimination or transfer rate constants among the compartments. The term GBE is a switching criterion with values 0 or 1 which refer to the situations in the absence of GB emptying (GBE=0) or when GB emptying occurs (GBE=1). The initial conditions of all compartments were set to zero except *A1*, which is assumed to contain the entire EZE dose at zero time.

Three bile release periods (at 4, 11 and 21 hours post-dose) were considered for EZEG, whereas the low plasma levels of EZE after 20 hours post-dose allowed for the inclusion of only the first two cycles for the parent drug (e.g. 4 and 11 hours post-dose). The duration of bile release in each enterohepatic cycle was fixed at 0.75 h, which approximates the mean GB emptying time in healthy individuals (Berg et al, 2013). Elimination of both drugs was considered to occur from the central compartments following first-order kinetics and accounted for both renal and fecal excretion. The population parameter estimates of the joint PK model of EZE and EZEG, along with their BSV% and RSE% values are listed in Table C.5.4.

Table C.5.4. Population PK parameters for the final joint model applied to EZE and EZEG data. *Key*: kap and kam = first-order absorption rate constant of the parent and the metabolite (h^{-1}); km = first-order transfer rate from the parent compartment to the metabolite compartment (L/h); kg1 and kg2 = first-order constants for bile release into the parent and metabolite compartments (h^{-1}); kmb = first-order transfer rate from the metabolite compartment to the GB compartment (L/h); *b1* and *b2* = residual error parameters for the proportional error model.

PK Parameter	Mean (RSE%)	BSV% (RSE%)
kap (h^{-1})	0.19 (12)	66.88 (14)
kam (h^{-1})	0.49 (8)	43.13 (15)
Vcp/F (L)	223 (5)	22.06 (19)
Vpp/F (L)	698 (8)	42.22 (15)
Qp/F (L/h)	957 (14)	80.09 (15)
km (h^{-1})	0.19 (6)	15.69 (31)
kelp (h^{-1})	0.033 (18)	39.64 (44)
kg1 (h^{-1})	1.44 (10)	53.66 (15)
Vcm/F (L)	43.4 (8)	35.99 (16)
Vpm/F (L)	118 (15)	84.79 (15)
Qm/F (L/h)	19.4 (19)	118.76 (15)
kmb (h^{-1})	0.24 (10)	44.95 (19)
kg2 (h^{-1})	0.49 (7)	16.31 (41)
kelm (h^{-1})	0.27 (9)	40.76 (17)
PK Random Effects Correlation		
kam – Vcm/F	0.36 (52)	-
Vpm/F - Qm/F	0.89 (6)	-
Residual error model		
b1	0.37 (2)	-
b2	0.30 (2)	-
Numerical criteria		
-2LL: 16609.98	AIC: 16673.98	BIC: 16738.79

Between-subject variability for the estimated parameters of this joint model exhibited moderate values, ranging from 15-53% with the exception of inter-compartmental clearances (Q/F) in which BSV% values were over 80%. In addition, the relatively low RSE% values obtained for all estimates, indicated that all PK parameters could be precisely estimated, suggesting a satisfactory model fitting. A correlation of the random effects between kam-Vcm/F (corr = 0.36) and Vpm/F-Qm/F (corr = 0.89) was also included in the final model, as it significantly improved the goodness-of-fit criteria. A proportional error model with a multiplicative coefficient b was used for both the parent drug and the metabolite:

$$C_{ij} = f_{ij} + b \cdot f_{ij} \cdot \varepsilon_{ij} \qquad \text{(Eq. 33)}$$

where C_{ij} is the j_{th} observed concentration of EZE of EZEG for the i_{th} individual, b is the parameter of the residual error model, f_{ij} is the j_{th} model predicted value for i_{th} subject, and

ε_{ij} is the random error which is assumed to be normally distributed with mean 0 and variance 1. The residual error parameters for the proportional error model (Eq. 33) were: *b1*=0.37 and *b2*=0.30, for EZE and EZEG, respectively. Finally, no covariate effect including age, body weight, height, BMI and any of the biochemical laboratory measurements tested, or treatment and period effects, was found to significantly affect the estimated PK parameters.

Model selection was based on the statistical and graphical criteria described in the Methods section. Goodness-of-fit plots of the final model for the two agents are presented in Figures C.5.8-C.5.11. Figure C.5.8(A, B) depicts the individual predicted EZE and EZEG concentrations vs their observed concentration values for the final population PK model. For both EZE and EZEG, an adequate degree of linearity can be observed between the predicted and observed concentrations.

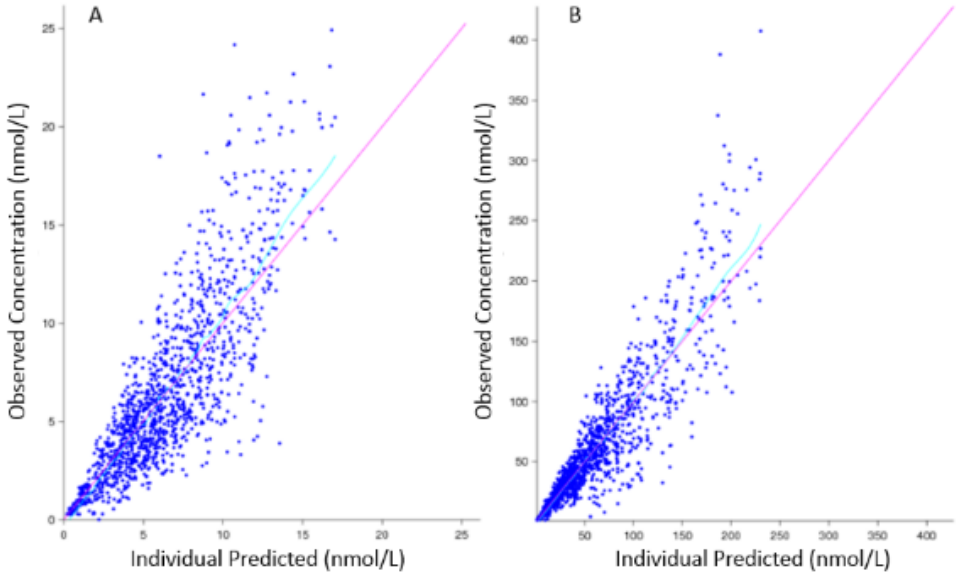

Figure C.5.8. Observed plasma concentrations *versus* the individual predicted concentration values from the joint population pharmacokinetic model of EZE (A) and EZEG (B). The diagonal red line represents the line of unity, namely, the ideal situation.

The balanced distribution around the zero line observed in the individual weighted residuals and normalized prediction distribution errors vs the individual predicted concentration plots presented in Figures C.5.9 and C.5.10, respectively, also suggests that the proportional error model chosen in the final model provided an adequate description of the model residual error for both drugs. The IWRES and NPDEs appear to be randomly distributed around 0 and within the required boundaries.

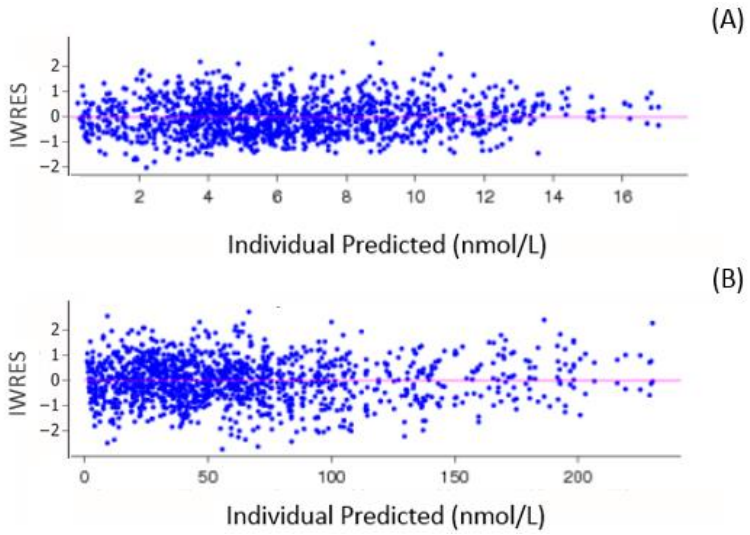

Figure C.5.9. Graphical representation of the IWRES *versus* the IPRED concentrations for the final joint model of EZE (A) and EZEG (B). The horizontal red line represents the zero line, namely, the ideal situation.

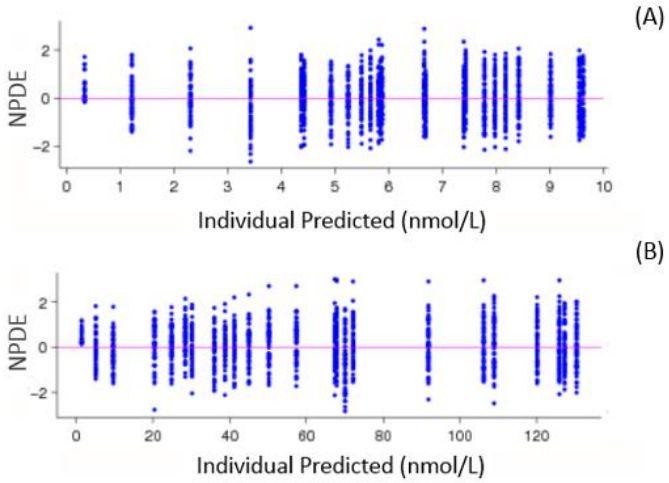

Figure C.5.10. Normalized prediction distribution errors versus the individual predicted concentrations for the final joint model of EZE (A) and EZEG (B). The horizontal red line represents the zero line, namely, the ideal situation.

Finally, Figure C.5.11(A, B) represents the visual predictive check plots obtained for each compound.

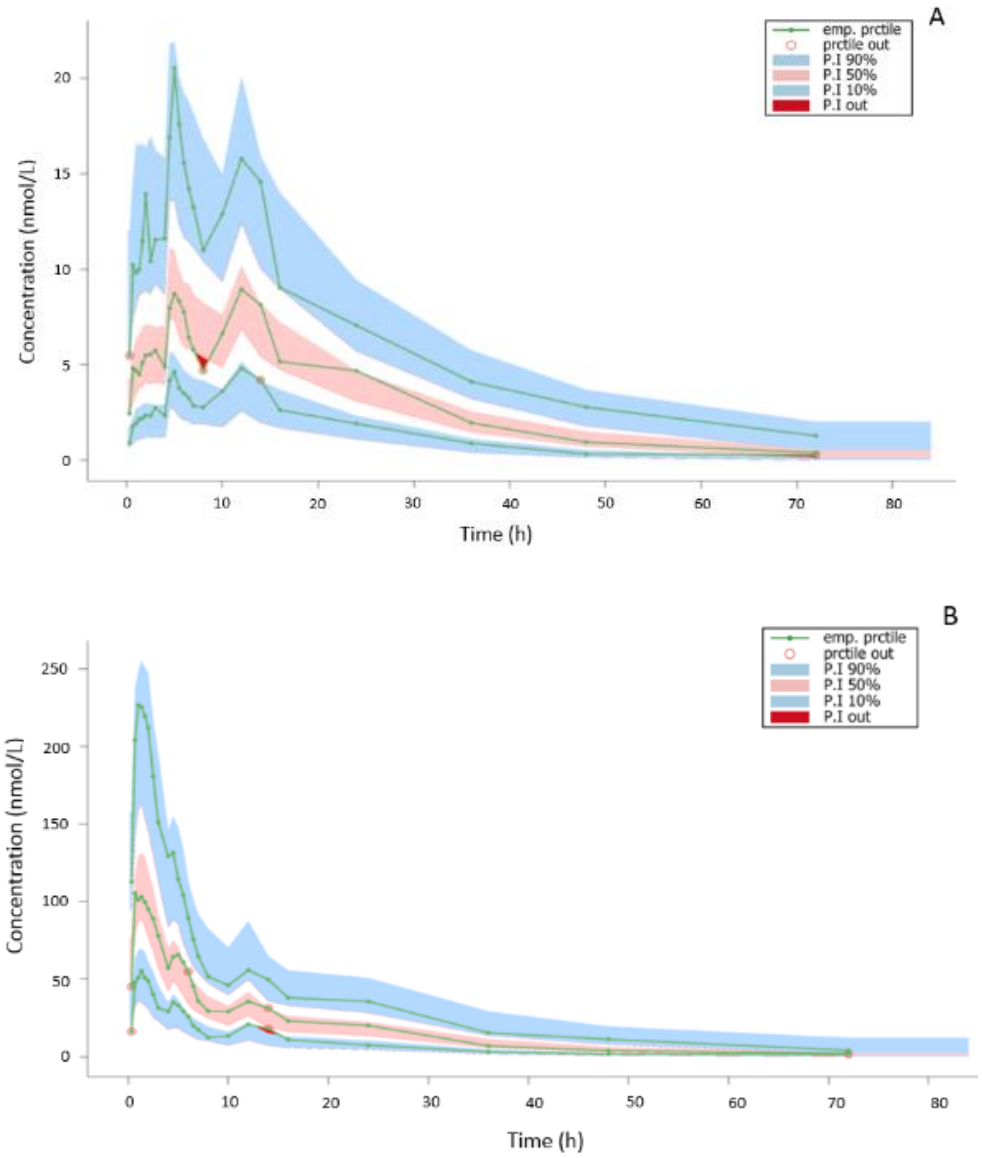

Figure C.5.11. Visual predictive check plots of the final joint PK model for EZE (A) and EZEG (B). *Key*: Solid lines refer to the 10th, 50th, and 90th percentiles of the empirical data; Shaded areas refer to the 95% prediction intervals around each theoretical percentile; red circles and areas denote the outlier data.

The predictions from the model described adequately the observed high and median concentration profiles of both molecules. However, the model seems to predict less well the low concentration-time profiles, with a slight under-prediction of the second enterohepatic cycle at around 10-13 h post-dose for both the parent drug and the metabolite. It is noteworthy though that some of these misfits might be explained by some atypical individual profiles, which drive the lower observed percentile estimates.

Additional investigations included the application of a first-pass dose apportionment parameter in the final model, with an estimated fraction (Fp) of the dose leading to the parent drug and the remaining fraction (1-Fp) leading to the metabolite, prior to reach the plasma (Figure C.5.12).

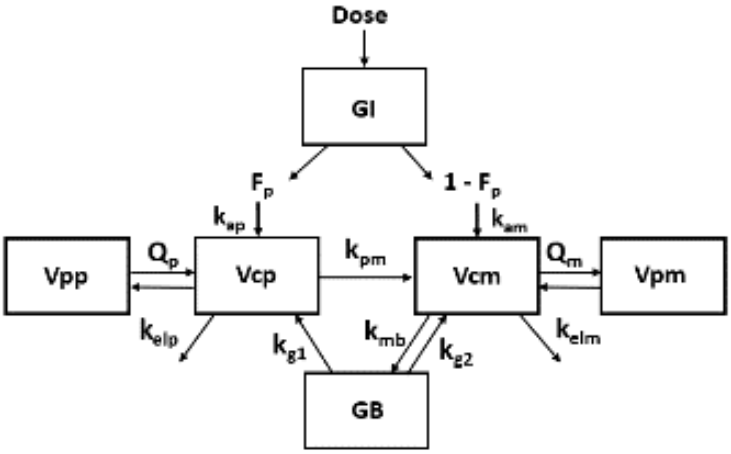

Figure C.5.12. Schematic representation of the final joint model with dose apportionment. *Key:* Fp, fraction of parent drug reaching systemic circulation after absorption.

This model was also able to adequately fit to the data and provide physiologically reasonable estimates (Table C.5.5). The fraction of dose leading to the parent drug (Fp) was estimated at 19%, which is in line with bibliographic reports, suggesting that EZEG contributes to approximately 80-90% of the total drug in plasma (Patrick et al., 2002; Jeu and Cheng, 2003; Kosoglou et al., 2005). However, for reasons of simplicity and to avoid the risk of over-parameterization and potential estimation difficulties, the most parsimonious model without the 'Fp' parameter was finally selected.

Table C.5.5. Goodness of fit criteria for Model D (final joint model with dose apportionment).

Observed vs individual predicted concentrations plot	VPC plots
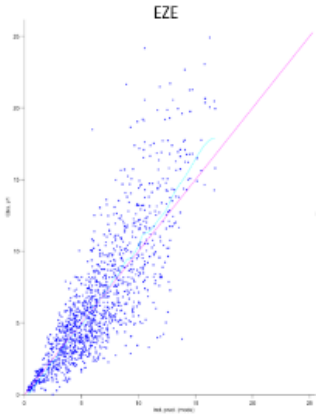	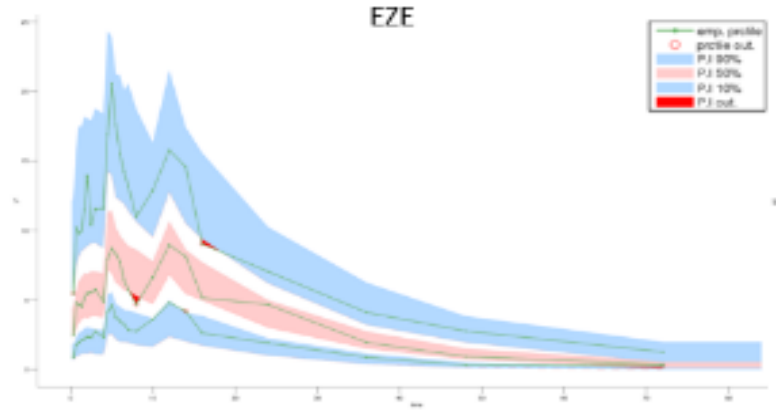
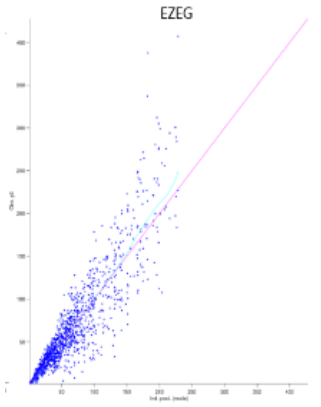	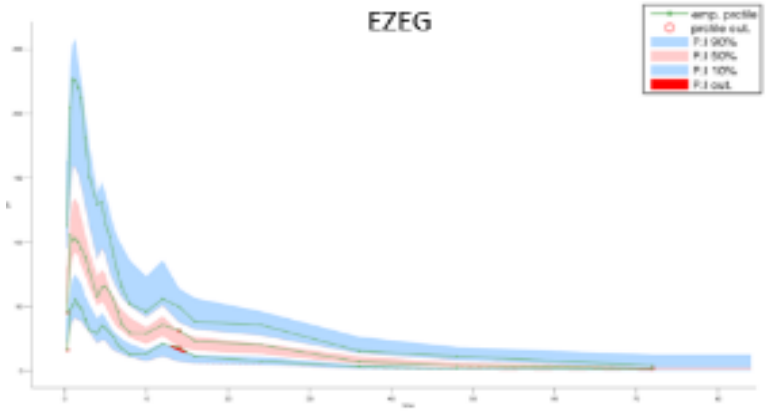

Numerical criteria: -2LL, 16792.74; AIC, 16860.74; BIC, 16929.61

Accordingly, the addition in the final model of a direct inter-conversion process, fecal elimination or 1- and 3-compartment disposition models for EZE and EZEG, was also not associated with better fit of the data, leading to either non-convergence of the model or over-parameterization.

C.2.2.4 Discussion

EZE exhibits a complex PK profile as it is shown to undergo EHC via conversion to its active metabolite EZEG and back-transformation to the parent drug through repeated biliary excretion (Malik et al., 2016). Therefore, PK analysis by traditional 1- or 2-compartmental models could not adequately describe the erratic PKs of the two drugs and appropriately characterize their metabolism and elimination processes. As such, a more sophisticated joint model that could incorporate both compounds simultaneously and describe their EHC was developed. Previous population models for EZE suffer from the drawback of describing the PKs and EHC of EZE and EZEG as a single agent, using total ezetimibe concentrations, defined as the sum of the two drugs (Ezzet et al., 2001). Even though, the two compounds exert a similar pharmacological activity and pharmacokinetic behavior (van Heek et al., 2000), the simultaneous modelling of EZE and EZEG concentrations, described in the present analysis, presents a physiologically more realistic aspect for the disposition of the two drugs and adequately reflects the complex absorption and EHC processes associated with EZE dosing in healthy individuals. In addition to the information obtained from single-agent PK models, joint models may also account for the uncertainties in the data and allow feedback from the metabolite data to the parent drug data to influence the estimation (Bertrand et al., 2011). Hence, this study proposes an improved joint 6-compartment model for EZE and its metabolite EZEG, which incorporates a physiologically realistic time-varying gallbladder emptying process as an integral EHC component of the two drugs.

Different structural models, implementing diverse approaches regarding the metabolism and disposition processes of the two drugs were developed and assessed for their performance. The first type of models evaluated, did not included first-pass metabolism in the gut and failed to describe the PKs of both drugs. The first-pass effect allowed to capture the early bump observed in the metabolite data, which could not be otherwise specified. Bertrand et al. also showed that adding a first-pass effect in their model allowed to fit metabolite concentrations that appeared quicker or at the same time as the parent drug (Bertrand et al., 2011). In the subsequent models, therefore, first-pass metabolism was intrinsically incorporated in the structural model and different approaches describing the EHC of the two drugs were applied.

Finally, the most appropriate model able to fit the available data was a multi-compartment model with first-pass metabolism and the incorporation of an additional compartment simulating the intermittent gallbladder emptying process during enterohepatic recycling. The model included a series of 6 compartments: gut, central (EZE), peripheral (EZE), central (EZEG), peripheral (EZEG), and a gallbladder compartment with bile release triggered at specific time intervals. In this model, following first-pass metabolism and absorption into the central compartments, drugs were eliminated by first-order processes or distributed into peripheral compartments or the gallbladder. The inter-conversion between EZE and EZEG was assumed to occur through the gallbladder compartment, via transformation of the parent drug to its glucuronide metabolite, and thereafter biliary secretion of parent EZE and its metabolite back into circulation. Gallbladder was assumed to directly deliver drug back into the central compartments by first-order processes, with gallbladder emptying simulated to coincide with the time of the secondary peaks observed in the C-t plots and the intake of food relative to the dose.

It is recognized that such models, however, can rapidly gain in complexity and present parameter identifiability problems and numerical difficulties in terms of estimation. To solve the issue, it was important to identify the parameters or "apparent" parameters that could be estimated, and for the sake of parameter interpretation or covariate analysis, it was deemed necessary to make some assumptions on some of the parameters (e.g., fixing one parameter to a given value) (Bertrand et al., 2011). In this vein, a limited number of assumptions was made in this joint parent-metabolite EHC model, as follows: i) all minor metabolic pathways were disregarded as the major metabolic pathway of EZE is the phenyl glucuronidation to its main primary metabolite, EZEG; ii) the time and duration of gallbladder emptying were fixed to certain values, based on mealtimes and considerations regarding gallbladder physiology; iii) three enterohepatic cycles were considered for EZEG (i.e. at 4, 11 and 21 hours), whereas in the case of EZE the very low plasma levels of the drug allowed for the inclusion of only the first two cycles (i.e. at 4 and 11 hours); and finally, iv) the fraction of dose excreted from the GB was hypothesized to be directly delivered to the central compartments of the drugs instead of the GI tract. This model, although less physiological, is parsimonious because it incorporates all the underlying processes of hydrolysis and re-absorption in one step, facilitating model fitting and PK parameters estimation.

Population mean estimates obtained for the final model for EZE and EZEG were found to be physiologically plausible and similar to literature values. The fixed effects of the final model could be precisely estimated with low RSE% values obtained for all PK parameters, whereas a relatively moderate inter-subject variability was observed in most PK parameters with BSV% values ranging from 15-53%. Also for all these models, it is noteworthy that only "apparent" parameters could be estimated. Estimating the actual values of PK parameters requires that both the parent drug and the metabolite be given by the intravenous route in addition to the oral administration of the parent compound (Bertrand et al., 2011). No significant covariate effect was also found on the estimated PK parameters. The inclusion of a relatively small number of subjects, derived from a healthy and relatively homogenous population usually enrolled in bioequivalence studies, as well as increased model complexity, may account for the absence of a significant covariate effect in our analysis. In any case, EZE pharmacokinetics has been shown not to be significantly influenced by age, gender, race or the presence of renal or hepatic abnormalities in previous studies (Kosoglou et al., 2005).

The multiple peaks arising from EHC for both EZE and EZEG were well characterized in the current model. The evaluation tests, including graphical analysis and the predictive checks show that the final model could describe the data satisfactorily. The final PK model was determined to be the most adequate based on successful minimization of the log-likelihood function and visual inspection of the diagnostic plots. Goodness-of-fit plots showed that observations and predictions were always spread randomly around the identity line for both active compounds. Visual predictive check plots also revealed a good agreement between the simulated and observed concentrations at all sampling time points, indicating that the estimations of the pharmacokinetic parameters are reasonable and the model provides a good description of the mean tendency of EZE and EZEG concentrations.

Overall, the population approach enabled us to estimate mean the pharmacokinetic parameters, interindividual variability, and residual variability as well as to evaluate for potential covariate effects on EZE pharmacokinetics in healthy individuals. The most striking aspect of our compartmental analysis is the development of joint EHC model for both EZE and EZEG concentrations that could sufficiently describe the complex pharmacokinetic behavior of both drugs simultaneously. The developed PK model was

based on physiological considerations of the EHC process as well as prior information on EZE pharmacokinetics. It would be of clinical value to extend the use of this EHC model to other population groups, including patients with hypercholesterolemia or those receiving EZE therapy with other concomitant medications and patients of different age or ethnicity, and further evaluate potential clinical applications of the current EHC model.

C.2.2.5 Conclusions

In the present study we were able to develop a joint PK model for ezetimibe and its main active metabolite ezetimibe-glucuronide, which could adequately describe the complex pharmacokinetics of both drugs in healthy individuals. This is one of the first attempts to develop a population PK model with EHC for both drugs simultaneously. The application of this model has provided greater understanding to the relationship between EZE and EZEG enterohepatic recirculation and its influence on the disposition kinetics of the two agents. Moreover, the obtained PK estimates and population variability in model parameters have ascertained previously reported values, and can provide an insight into the differences in EZE pharmacokinetics between healthy individuals, as well as to unveil the impact of covariate effects from other sources of pharmacokinetic variability. Finally, the proposed model may provide a valuable approach for planning future pharmacokinetic/pharmacodynamic studies and help to further elucidate the manner in which EZE and its glucuronidated metabolite contribute to the overall clinical effects of EZE therapy, including cholesterol-lowering activity and potential side effects.

D. Discussion

In this thesis, the pharmacokinetic data from four studies were analyzed which were reflected on seven separate population pharmacokinetic analyses. The first five concerned inhaled drugs demonstrating complex absorption and disposition characteristics, whereas the latter two dealt with an orally administered drug showing noteworthy enterohepatic recirculation properties.

The first project of this work (**Chapter C.1.1**) referred to the investigation of the pharmacokinetics of two inhaled drugs, the corticosteroid fluticasone propionate and the β2-adrenergic agonist, salmeterol. Pulmonary targeting is a desired characteristic for successful inhaled drugs. Even though inhalation therapy aims at the local action of drugs within the lung, systemic exposure may also occur and relate to the appearance of serious adverse effects. Therefore, knowledge of the systemic kinetic behavior of such drugs, as well as determination of potential factors which might affect this behavior are of great importance. At the same time, characterization of the pharmacokinetics of inhaled FLP and SAL may serve as a valuable tool for determining their lung deposition and bioavailability, thus providing useful information for optimizing pulmonary drug delivery. In this vein, C-t data obtained from a single-dose BE study using two dry powder inhalers with the FLP/SAL combination were used for the analysis. This study was performed in healthy subjects with a concomitant administration of an activated charcoal scheme, in order to limit gastrointestinal absorption of the swallowed part.

A simple two-compartment model assuming first-order absorption and elimination kinetics from the central compartment was found to best describe the C-t data of inhaled FLP. The population analysis was also able to unveil the significance of body weight on certain PK parameters, including the lung absorption rate constant (ka), the inter-compartmental clearance (Q/F) and the peripheral volume of distribution (Vp/F). These findings suggested that as body weight increases, all the three PK parameters were positively influenced. A combined residual error model led to the optimum performance, providing satisfactory goodness-of-fit criteria for the final PK model. In case of SAL, the best results were obtained when a two-compartment disposition model was used, assuming very rapid absorption kinetics (like intravenous bolus) and first-order elimination kinetics from the central compartment. Again a combined error model was chosen for the description of residual variability in the model, based on statistical and goodness-of-fit criteria. A gender effect was found on SAL clearance, with male subjects exhibiting about 21% higher clearance of the drug compared to the females. Finally, and

in accordance with the results obtained from the BE analysis, 'treatment' (T or R product) was not found to exert a significant effect on any PK parameter of either SAL or FLP. Besides, the classic NCA allowed initially the estimation of some basic PK parameters (Cmax, AUCt, AUCinf, Tmax, λz) and the assessment of comparative bioavailability of the two drugs from the two inhalation devices. Part of this work has been published in the journal *European Pharmaceutical Sciences*, under the title 'Population pharmacokinetics of fluticasone propionate/salmeterol using two different dry powder inhalers'.

In order to further investigate the impact of airway state on the pharmacokinetics of inhaled SAL, in our second study (**Chapter C.1.2**), the PK analysis of SAL was extended to an asthma patient group. In fact, it is generally considered that the airway state of asthma patients may play a significant role in the efficacy of inhaled therapy, by altering the pulmonary deposition of inhaled drugs, thus, leading to sub-therapeutic drug levels (Lipworth and Clark, 1997; Vaisman et al., 1987). As in the previous study, non-compartmental and mainly population PK methodologies were applied to the available SAL dataset. The data used for this analysis came from a BE study comparing the kinetics of the FLP/SAL combination from two different inhalation devices in asthma patients. In this study, however, the absence of an activated charcoal scheme allowed for both pulmonary and gastrointestinal absorption of SAL, which enabled us to determine the total systemic exposure of the drug following inhalation and further characterize its lung deposition. Our aim, therefore, was not limited in providing a description of the subjects' C–t profiles, but also to perform an in-depth analysis of SAL kinetics, unveiling the complex mechanisms of parallel pulmonary and GI absorption following inhalation.

As expected, the absence of activated charcoal led to plasma C-t profiles of inhaled SAL demonstrating a two-peak pattern, with a very early first concentration peak, attributed to the pulmonary absorption, followed by a lower secondary peak, as a result of GI absorption of the swallowed part. The population PK analysis in this study showed that a two-compartment PK model, with a parallel very fast absorption (like an i.v. bolus administration) through the lung and a slower first-order absorption from the GI tract was found to describe successfully the kinetics of inhaled SAL. Elimination was considered to take place in the central compartment following first-order kinetics. In addition to the description of absorption, disposition and elimination kinetics, the model also allowed for the estimation of the relative amount of dose absorbed through the lungs. This was

estimated to be at around 13%, suggesting that most of the drug is not absorbed through the lungs, but is deposited (either after swallowing or due to the pulmonary mucociliary clearance) in the GI tract, where it can enter the systemic circulation. This finding was in line with previous literature data showing that, even with optimal inhalation conditions, most of the drug (80–90%) is impacting the oropharynx and the upper airways and is subsequently swallowed, with a much smaller fraction (10–20%) reaching and being absorbed through the lungs (Cazzola et al., 2002; Lipworth, 1996).

Irrespectively of the complexity of the parallel absorption processes, the structural model was able to describe the pharmacokinetics of inhaled SAL, highlighting the relative fraction of dose absorbed through the lungs. Finally, the model was also able to justify the existence of a gender effect on SAL clearance. Again, as in the first study, women were found to exert less capability to eliminate SAL than men, with a 27% higher clearance values observed in male participants compared to the females. This difference was further substantiated through the comparison of the three main PK parameters (Cmax, AUCt, AUCinf) between male and female subjects, which showed 30-35% lower drug exposure in men compared to women. Body weight, in terms of an allometric relationship with the volume of distribution of the peripheral compartment (Vp/F) was also included in the final model, whereas, a 'treatment' effect (i.e. T or R) was found to be significant in the case of the volume of distribution of the central compartment (Vc/F). However, no physiological meaning can be ascribed to this finding, since drug formulation cannot rationally be related to the volume of distribution. Overall, evaluation of the final population PK model, based on goodness-of-fit criteria and the physiological soundness of the estimated PK parameters, indicated that the developed model allowed for an adequate characterization of inhaled SAL pharmacokinetics in asthma patients. Part of this work has been published in the journal *Biopharmaceutics and Drug Disposition*, under the title 'Pharmacokinetic analysis of inhaled salmeterol in asthma patients: Evidence from two dry powder inhalers'.

The third study of this thesis (**Chapter C.1.3**) further investigated the absorption and disposition kinetics of inhaled drugs. In this case, another inhaled combination was studied the corticosteroid budesonide and the β2-adrenergic agonist formoterol. For this purpose, C-t data of the inhaled combination, obtained from a BE study in asthma patients, comparing two different dry powder inhalers, were analyzed using non-compartmental

and population PK methodologies. As in the first study, an activated charcoal scheme had been also used in this case, in order to prevent GI absorption of the drugs. Similarly to the previous cases, the main goal of this analysis was to apply population PK modeling in order to characterize the complex absorption and disposition kinetics of the two drugs following inhalation, as well as to evaluate the impact of certain factors on the performance of model parameters.

Visual inspection of the obtained plasma C-t profiles of BUD and FOR revealed rather complex absorption and distribution characteristics for both drugs. In case of the inhaled BUD, conventional PK models could not adequately describe the complex pulmonary absorption processes of the drug. In this context, two separate lung absorption phases were considered for BUD, based on anatomical features of the lung and the known reversible fatty acid esterification of the drug within the airways. Taking into consideration this physiological background, a two-compartment disposition model with two parallel (fast and slow) first-order absorption rate constants from the lungs was finally chosen for the description of BUD C-t profiles. In this model, the dose of BUD was assumed to be divided into two different fractions, deposited into two kinetically different lung compartments, allowing explicitly for different absorption rate constants for drug absorption through the lung. Elimination of the drug was assumed to occur from the central compartment, following first-order kinetics. The final PK model suggested that men were shown to exert higher values for the slow absorption rate constant (k_{as}) and smaller peripheral volume of distribution (Vp/F) compared to women. Nevertheless, since inhaled BUD reaches the site of action before its systemic absorption, even though these correlations improved model performance, it is not expected that these inter-gender differences will be accompanied by any significant clinical effect.

Moving forward with the analysis of inhaled FOR, the obtained plasma C-t profiles revealed either a plateau or a smaller second concentration peak, between 3 to 5 hours post-dose in most subjects. Based on previous knowledge on FOR pharmacokinetics, and since GI absorption was excluded due to the presence of activated charcoal, these secondary peaks (occurring much later than the termination of the administration of charcoal) were considered to reflect an enterohepatic re-cycling process of the drug.

Therefore, an EHC model was developed for inhaled FOR, based on physiological considerations regarding gallbladder function and biliary excretion. Formoterol C-t

profiles were best described by a five-compartment model, consisting of a two-compartment disposition model linked to a lung absorption compartment and sequential gallbladder and GI compartments, capable of simulating the re-distribution process of enterohepatic recycling. The compartments within the enterohepatic loop were linked by first-order kinetics, and a gallbladder emptying time interval was assumed between 2-5 hours post-dose. A lag-time of three hours for the initiation of GI absorption was also considered, due to the administration of activated charcoal up to this time. Renal elimination was assumed to occur from the central compartment following first-order kinetics, whereas since EHC also involves significant fecal elimination, it was more physiologically relevant to consider both of these processes in the final model. Fecal excretion was, therefore, incorporated as an additional elimination process, assumed to occur through the GI compartment, following first-order kinetics, as well. In regards to the covariate model, none of the examined factors (demographic characteristics, inhalation device, treatment period, patient status) was found to influence the systemic drug exposure of inhaled FOR. Finally, the goodness-of fit criteria showed that the model was able to provide sensible predictions of the observed data, despite the increased complexity of the EHC process. Part of this work has been published in the journal *Pulmonary Pharmacology & Therapeutics*, under the title 'On the pharmacokinetics of two inhaled budesonide/formoterol combinations in asthma patients using modeling approaches'.

An in-depth description and characterization of the complex enterohepatic re-circulation process was also the subject of the following investigation (**Chapter C.2.1**). In this study, the available C-t data of ezetimibe, a cholesterol absorption inhibitor showing extensive biliary excretion and EHC (Patrick et al., 2002; Kosoglou et al., 2005), were analyzed using model-based methodologies. An insight into the EHC of drugs with considerable biliary excretion is of crucial importance, since this re-distribution process may significantly affect their systemic exposure and potentiate, thereby, their pharmacological activity or create toxic effects (Roberts et al., 2002). Therefore, in order to increase our understanding on the clinical pharmacokinetics of enterohepatic recycling, a thorough investigation of different EHC models was conducted using the total EZE concentrations (parent drug and glucuronide metabolite). The data used for the analysis derived from a crossover BE study comparing two oral formulations of EZE, and nonlinear mixed effects modeling was applied to develop a novel population PK model.

Since conventional PK models were inadequate of capturing the multiple peaks observed in total EZE C-t profiles, more sophisticated models were built to properly incorporate the EHC component. In this sense, EHC models with a variable number of compartments, accommodating a GB emptying process were constructed. Different bile release kinetics were evaluated during model development, including bolus, first-, and zero-order kinetics in pre-determined time periods, as well as sine and sigmoid functions providing a periodic bile release pattern.

Eventually, a gallbladder-based EHC model was developed, taking into account the physiological aspects of the hepatobiliary system. Total EZE concentrations were best described by a four-compartment model where EHC was modeled through the inclusion of a gallbladder compartment that released instantaneously drug into the GI compartment during specific time intervals, coinciding with meal intake. The proposed model consists of the gut, central, peripheral and gallbladder compartments, where EHC is assumed to be a re-distribution process that emanates from the central compartment. For simplicity reasons and to avoid over-parameterization of the model, fecal elimination was incorporated to the total elimination rate constant, placed to the central compartment and assumed to follow first-order kinetics. In terms of modeling, this means that the rate constant controlling the transfer of drug for the EHC process was considered as a distribution rate constant rather than a fraction of the elimination rate constant. The final model was found to be sufficiently realistic from a PK and physiological point of view and accurately characterize the enterohepatic recycling process of the total EZE concentrations. The fraction of drug excreted within each EHC (%EHC) could also be indirectly estimated from the PK parameters of the final model, using (Eq. 22) and was found to be around 30% of the total amount absorbed, a fraction slightly higher than previously reported values.

A secondary objective of this project was to evaluate clinical characteristics and environmental factors for their significance on the model performance. As the number of tested covariates was large, a multi-step covariate data analysis was performed. However, none of the tested covariates, was found to be significant or to improve the numerical or graphical criteria of the final model, which coincides with previous literature reports regarding ezetimibe pharmacokinetics (Jeu and Cheng, 2003; Kosoglou et al., 2005). Although the developed model, provided the advantage of being more physiological than

other empirical models and was found adequate in predicting the characteristics associated with EHC of total EZE concentrations, it did not include a representation of the extensive first-pass metabolism of EZE following its oral administration.

Oral ezetimibe is subjected to >80% glucuronidation within the intestinal mucosa to form the pharmacologically active glucuronyl-derivative (EZEG) (Kosoglou et al., 2005; Patrick et al., 2002). EZEG accounts for the majority (80-90%) of drug measured in human plasma, with the parent drug constituting only 10% of the entire drug-related material. The two drugs are also found to repeatedly pop in and out of the systemic circulation, exhibiting multiple peaks in their C-t profiles, consistent with enterohepatic recycling (Kosoglou 2005).

The last study of this thesis (**Chapter C.2.2**) aimed, therefore, to extend the investigation of EZE pharmacokinetics, by developing a joint population PK model for the description of both EZE and EZEG kinetics, simultaneously. Based on previous knowledge and visual inspection of the C-t profiles of drugs, first-pass metabolism and enterohepatic recirculation for both drugs were incorporated *per se* during model development. In this respect, different structural models were developed and compared based on their predictive performance and adequate characterization of the underlying physiological processes. This analysis finally proposed an improved joint model for EZE and its active metabolite EZEG, which was able to elaborate first-pass metabolism within the gut and a physiologically realistic gallbladder emptying process as an integral EHC component of the two drugs. The model included the following compartments: gut, central EZE, peripheral EZE, central EZEG, peripheral EZEG, and a gallbladder compartment with bile release triggered at specific time intervals. Inter-conversion between EZE and EZEG was assumed to occur via the gallbladder compartment, through transformation of the parent drug to its glucuronide metabolite, and thereafter, biliary secretion of both drugs back into their central compartments. Gallbladder emptying was assumed to follow first-order kinetics and to coincide with the time of food intake according to the study protocol. As in the case of total EZE PK model, no significant covariate effect was found on the estimated PK parameters of both drugs. The multiple peaks arising from EHC for both EZE and EZEG were well characterized. The most striking aspect of this compartmental analysis, however, was the development of the first joint EHC model for EZE and EZEG

that could sufficiently describe the complex pharmacokinetic behavior of both drugs simultaneously.

E. Conclusions

The overall goal of this work was to investigate and characterize the complex absorption and disposition processes of drugs showing special PK characteristics. Population PK modeling enabled us to patternize the kinetic behavior of these drugs, estimate their PK parameters, their inter-individual and residual variability, and unveil the impact of potential covariates on their performance.

The first part of this thesis focused on the exploration of the unique pulmonary pharmacokinetic characteristics of certain inhaled drugs in an attempt to gain more understanding on the factors affecting their clinical performance and contributing to the purpose of acquiring an optimum inhalation therapy. In the first study, analysis of the fluticasone/salmeterol DPI combination, administered in healthy subjects, in the presence of activated charcoal, led to a two-compartment disposition model for both drugs with first-order absorption kinetics for FLP and bolus absorption kinetics for SAL. A significant impact of body weight was found on absorption (ka) and distribution (Q/F and Vp/F) parameters of inhaled FLP, with these PK parameters increasing as body weight increases. In case of SAL a significant gender effect on clearance was evident, with male subjects exhibiting about 21% higher clearance of the drug compared to the females.

Analysis of SAL was further extended to an asthma patient population group, who received SAL via inhalation, in the absence of activated charcoal this time, which allowed for both pulmonary and gastrointestinal absorption of the drug. Analysis of those data also led to a two-compartment disposition model, however, in this case absorption kinetics were described by a parallel very fast (like bolus) absorption through the lung and a slower first-order absorption from the GI tract. The model allowed for the estimation of the relative amount of dose absorbed through the lungs, found to be around 13%, suggesting that most of the drug is not absorbed through the lungs, but is deposited (either after swallowing or due to the pulmonary mucociliary clearance) in the GI tract. Also the model further justified the existence of a gender effect on SAL clearance, by showing that women exerted about 27% less capability to eliminate SAL than men.

The other inhaled drug combination analyzed referred to the budesonide/formoterol combination administered via dry powder inhalers in asthma patients, in the presence of activated charcoal. In the case of inhaled BUD, a two-compartment disposition model with two parallel (fast and slow) first-order absorption processes from the lung was finally

chosen, which suggested that most of inhaled BUD is slowly absorbed through the lungs, possibly attributed to the reversible esterification and formation of a slow-release reservoir of the drug within the lungs. The model also unveiled the presence of some inter-gender differences in the absorption (k_{as}) and distribution (Vp/F) processes, however, of no significant clinical value. Finally, analysis of inhaled FOR data revealed the presence of enterohepatic recirculation of the drug. Therefore, a five-compartment model capable of incorporating this EHC process was developed, including both renal and fecal elimination, as well as, enterohepatic re-cycling through a gallbladder and a GI compartment linked by first-order processes. The model was based on physiological considerations regarding gallbladder function and highlighted the importance of food on biliary excretion.

Likewise, the two latter studies, in the second part of the thesis, provided us a with greater understanding of the enterohepatic re-circulation process and its influence on the disposition kinetics of drugs. In the case of total ezetimibe concentrations, following a thorough investigation of different EHC models, drug concentrations were best described by a four-compartment model, where EHC was modeled through the inclusion of a gallbladder compartment that released instantaneously drug into the GI compartment during specific time intervals, influenced by food intake. The fraction of drug excreted within each enterohepatic cycle was also estimated and found to be around 30% of the total amount absorbed, corroborating previously reported values.

In the final study, analysis of ezetimibe drug concentrations was further extended to include the extensive first-pass metabolism of the drug following oral administration, through the joint modeling of both the parent ezetimibe and its active glucuronide metabolite. This analysis finally proposed the first joint population model for EZE and EZEG, incorporating first-pass metabolism and a physiologically realistic EHC component for both drugs. Inter-conversion between EZE and EZEG and EHC were assumed to occur via a gallbladder compartment, through transformation of the parent drug to its glucuronide metabolite, and thereafter, biliary secretion of both drugs back into their central compartments by first-order processes, coinciding with food intake. No significant covariate effect was found in either model, which confirmed previous findings.

It is certainly acknowledged that the current models are, like any model, only a simplification of the true pharmacokinetic behavior. These models can of course be extended in future studies with the incorporation of *in vitro* and additional

pharmacokinetic or pharmacodynamic data, in order to provide a more integrated knowledge of drugs' characteristics, the systemic exposure and their final clinical outcome. It would also be of clinical value to extend the use of these PK models, by incorporating information from other population groups, such as patients, subjects of different age or ethnicity, or those receiving concomitant medications.

List of Literature References

Abi Khalil, F., Hanocq, M., & Dubois, J. (1993). A new method to estimate parameters of pharmacokinetics with enterohepatic circulation. *Eur J Drug Metab Pharmacokinet,* 18: 131–139.

Al-Numani, D. Colucci, P. Ducharme, M.P. (2015). Rethinking bioequivalence and equivalence requirements of orally inhaled drug products, *AJPS,* 10: 461–471.

Ambery, C. L., Wielders, P., Ludwig‐Sengpiel, A., Chan, R., & Riley, J. H. (2015). Population pharmacokinetics and pharmacodynamics of GSK961081 (Batefenterol), a muscarinic antagonist and b2-agonist, in moderate-to-severe COPD patients: Substudy of a randomized trial. *Drugs R D*, 15: 281-291.

Anderson, P. J., Zhou, X., Breen, P., Gann, L., Logsdon, T. W., Compadre, C. M., & Hiller, F. C. (1998). Pharmacokinetics of (R,S)-albuterol after aerosol inhalation in healthy adult volunteers. *J. Pharm. Sci.*, 87: 841-844.

Apiou-Sbirlea, G., Newman, S., Fleming, J., Siekmeier, R., Ehrmann, S., Scheuch, G., … Hickey, A. (2013). Bioequivalence of inhaled drugs: Fundamentals, challenges and perspectives. *Ther Deliv.,* 4: 343-367.

Ariel, A., Altraja, A., Belevskiy, A., Boros, P.W., Danila, E., Fležar, M., Koblizek, V., Fridlender, Z.G., Kostov, K., Krams, A., Milenkovic, B., Somfay, A., Tkacova, R., Tudoric, N., Ulmeanu, R., Valipour, A. (2018) Inhaled therapies in patients with moderate COPD in clinical practice: current thinking. *Int J of COPD,* 13: 45–56.

Atkins, P.J. (2005). Dry powder inhalers: an overview. *Respir Care,* 50(10): 1304-12.

Ballantyne, C. M., Houri, J., Notarbartolo, A., Melani, L., Lipka, L. J., Suresh, R., ... Veltri, E. P. (2003). Effect of ezetimibe coadministered with atorvastatin in 628 patients with primary hypercholesterolemia: a prospective, randomized, double-blind trial. *Circulation, 107*(19): 2409-2415.

Barber, P., Robertson, D. (2012). Pharmacodynamics and pharmacokinetics. Essentials of Pharmacology for Nurses – Chapter 1. McGraw-Hill Education (UK), 216 pages.

Bartels, C., Looby, M., Sechaud, R., & Kalser, G. (2013). Determination of the pharmacokinetics of glycopyrronium in the lung using a population pharmacokinetic modeling approach. *Br. J. Clin. Pharmacol.*, 76: 868-879.

Bauer, L.A. (2013). Applied Clinical Pharmacokinetics. Second Edition 2008 by The McGraw-Hill Companies, Inc. Behar, J. Physiology and pathophysiology of the biliary tract: the gallbladder and sphincter of Oddi - a review, ISRN Physiol. 83763015.

Bays, H. E., Moore, P. B., Drehobl, M. A., Rosenblatt, S., Toth, P. D., Dujovne, C. A., ... Veltri, E. P. (2001). Effectiveness and tolerability of ezetimibe in patients with primary hypercholesterolemia: pooled analysis of two phase II studies. *Clin. Ther., 23*(8): 1209-1030.

Benet, L.Z, Zia-Amirhosseini, P. (1995). Basic principles of pharmacokinetics. *Toxicol Pathol*, 23(2): 115-23.

Berg, A. K., Mandrekar, S. J., Ziegler, K. L., Carlson, E. C., Szabo, E., Ames, M. M., ... Reid, J. M. (2013). Population Pharmacokinetic Model for Cancer Chemoprevention With Sulindac in Healthy Subjects. *J. Clin. Pharmacol.*, 53(4): 403-412.

Bertrand, J., Laffont, C.M., Mentré, F., Chenel, M., Comets, E. (2011). Development of a complex parent-metabolite joint population pharmacokinetic model. *AAPS J.*, 13(3): 390-404.

Bhagwat, S., Schilling, U., Chen, M.J., Wei, X., Delvadia, R., Absar, M., Saluja, B., Hochhaus, G. (2017). Predicting Pulmonary Pharmacokinetics from In Vitro Properties of Dry Powder Inhalers. *Pharm Res*, 34(12): 2541-2556.

Bonate, P.L. (2005). Pharmacokinetic–Pharmacodynamic Modeling and Simulation Hardcover — 1 Edition (October 20, 2005). s.l. Springer 978-1-4419-9485-1.

Bonate, P.L. and Howard, D.R. (2005). Pharmacokinetics in Drug Development: Clinical Study Design and Analysis. Springer Science & Business Media, 628 pages

Borghardt, J.M., Weber, B., Staab, A., Kloft, C. (2015) Pharmacometric models for characterizing the pharmacokinetics of orally inhaled drugs, *AAPS J*., 17(4): 853–870.

Borghardt, J. M., Weber, B., Staab, A., Kunz, C., Formella, S., & Kloft, C. (2016). Investigating pulmonary and systemic pharmacokinetics of inhaled olodaterol in healthy volunteers using a population pharmacokinetic approach. *Br. J. Clin. Pharmacol.*, 81: 538-552.

Brattsand, R., Larsson, A.M. (2003). The role of intracellular esterification in budesonide once-daily dosing and airway selectivity. *Clin. Ther.* 25: C28–C41.

Bruton, L., Parker, K., Blumenthal, D., Buxton, I. (2008). *Goodman & Gilman's* Manual of Pharmacology and Therapeutics, by The McGraw-Hill Companies, Inc.

Callejas, S.L., Biddlecombe, R.A., Jones, A.E., Joyce, K.B., Pereira, A.I., Pleasance, S. (1998). Determination of the glucocorticoid fluticasone propionate in plasma by automated solid-phase extraction and liquid chromatography–tandem mass spectrometry. *J. Chromatogr. B,* 718: 243–250.

Cazzola, M., Matera, M.G., Santangelo, G., Vinciguerra, A., Rossi, F., D'Amato, G. (1995). Salmeterol and formoterol in partially reversible severe chronic obstructive pulmonary disease: a dose-response study. *Respir. Med.*, 89(5): 357–362.

Cazzola, M., Testi, R., & Matera, M. G. (2002). Clinical pharmacokinetics of salmeterol. *Clin Pharmacokinet*, 41: 19‐30.

Chrystyn, H., (2007). The Diskus™: a review of its position among dry powder inhaler devices. *Int. J. Clin. Pract.*, 61: 1022–1036.

Chu, N. N., Chen, W. L., Xu, H. R., & Li, X. N. (2012). Pharmacokinetics and safety of ezetimibe/simvastatin combination tablet: an open-label, single-dose study in healthy Chinese subjects. *Clin Drug Investig, 32*(12): 791-798.

Colburn, W.A. (1982). Pharmacokinetic and biopharmaceutic parameters during enterohepatic circulation of drugs. *J. Pharm. Sci., 71*(1): 131-133.

Colom, H., Lloberas, N., Andreu, F., Caldés, A., Torras, J., Oppenheimer, F., ... Grinyó, J.M. (2014). Pharmacokinetic modeling of enterohepatic circulation of mycophenolic acid in renal transplant recipients. *Kidney Int, 85*(6): 1434-1443.

Comets, E., Verstuyft, C., Lavielle, M., Jaillon, P., Becquemont, L., Mentré, F., (2007). Modelling the influence ofMDR1 polymorphismon digoxin pharmacokinetic parameters. *Eur. J. Clin. Pharmacol*. 63: 437–449.

Cote, C., Pearle, J.L., Sharafkhaneh, A., Spangenthal, S. (2009). Faster onset of action of formoterol versus salmeterol in patients with chronic obstructive pulmonary disease: a multicenter, randomized study. *Pulm. Pharmacol. Ther.,* 22(1): 44–49.

Cremers, S., Schoemaker, R., Scholten, E., den Hartigh, J., König-Quartel, J., van Kan, E., Paul, L., de Fijter, J. (2005). Characterizing the role of enterohepatic recycling in the interactions between mycophenolate mofetil and calcineurin inhibitors in renal transplant patients by pharmacokinetic modeling. *Br. J. Clin. Pharmacol.*, 60(3): 249–256.

Crim, C., Pierre, L.N., Daley-Yates, P.T., (2001). A review of the pharmacology and pharmacokinetics of inhaled fluticasone propionate and mometasone furoate. *Clin. Ther.*, 23: 1339–1354.

Csikesz, N.G., Gartman, E.J., (2014). New developments in the assessment of COPD: early diagnosis is key. *Int. J. Chron. Obstruct. Pulmon. Dis*., 9: 277–286.

Derendorf, H. (1997). Pharmacokinetic and pharmacodynamic properties of inhaled corticosteroids in relation to efficacy and safety. *Respir Med*. 91A: 22-28.

Derendorf, H., Nave, R., Drollmann, A., Cerasoli, F., Wurst, W. (2006). Relevance of pharmacokinetics and pharmacodynamics of inhaled corticosteroids to asthma. *Eur. Respir. J.*, 28: 1042–1050.

Derks, M.G.M., van den Berg, B.T.J., van der Zee, J.S., Braat, M.C.P., & van Boxtel, C. J. (1997). Biphasic effect‐time courses in man after formoterol inhalation: Eosinopenic and hypokalemic effects and inhibition of allergic skin reactions. *J. Pharmacol. Exp. Ther.*, 283: 824‐832.

de Waart, D.R., Vlaming, M.L., Kunne, C., Schinkel, A.H., & Oude Elferink, R.P. (2009). Complex pharmacokinetic behavior of ezetimibe depends on abcc2, abcc3, and abcg2. *Drug Metab Dispos, 37*(8): 1698-1702.

de Winter, B.C., van Gelder, T., Sombogaard, F., Shaw, L.M., van Hest, R.M., & Mathot, R.A. (2009). Pharmacokinetic role of protein binding of mycophenolic acid and its glucuronide metabolite in renal transplant recipients. *J Pharmacokinet Pharmacodyn, 36*(6): 541-564.

Dhand, R., Goode, M., Reid, R., Fink, J. B., Fahey, P. J., & Tobin, M. J. (1999). Preferential pulmonary retention of (S) ‐ albuterol after inhalation of racemic albuterol. *Am J Respir Crit Care Med*, 160: 1136 ‐ 1141.

Dhillon, S., and Kiren Gill, K. (2006) *Chapter 1*. Clinical Pharmacokinetics. Basic pharmacokinetics. Pharmaceutical Press.

Diderichsen, P.M., Cox, E., Martin, S.W., Cleton, A., & Ribbing, J. (2013). Characterizing systemic exposure of inhaled drugs: Application to the long ‐ acting b2 ‐ agonist PF ‐ 00610355. *Clin Pharmacokin*, 52: 443 ‐ 452.

Dobrinska, M.R. (1989). Enterohepatic Circulation of Drugs. *J. Clin. Pharmacol.,* 29(7): 577–580.

Donnelly, R., Seale, J.P. (2001). Clinical pharmacokinetics of inhaled budesonide, *Clin. Pharmacokinet.,* 40(6): 427–440.

Dubois, A., Gsteiger, S., Balser, S., Pigeolet, E., Steimer, J.L., Pillai, G., Mentré, F., (2012). Pharmacokinetic similarity of biologics: analysis using nonlinear mixed-effects modeling. *Clin. Pharmacol. Ther.,* 91: 234–242.

Dujovne, C.A., Ettinger, M.P., McNeer, J.F., Lipka, L.J., LeBeaut, A.P., Suresh, R., ... Veltri, E.P. (2002). Efficacy and safety of a potent new selective cholesterol absorption inhibitor, ezetimibe, in patients with primary hypercholesterolemia. *Am J Cardiol*, *90*(10): 1092-1097.

Ehrhardt, C. (2017). Inhalation Biopharmaceutics: Progress Towards Comprehending the Fate of Inhaled Medicines. *Pharm Res*, 34(12): 2451–2453.

Edsbacker, S., Brattsand, R. (2002). Budesonide fatty-acid esterification: a novel mechanism prolonging binding to airway tissue. Review of available data, *Ann. Allergy Asthma Immunol*., 88: 609–616.

Edsbäcker, S., Johansson, C.J. (2006). Airway selectivity: an update of pharmacokinetic factors affecting local and systemic disposition of inhaled steroids. *Basic Clin. Pharmacol. Toxicol.,* 98: 523–536.

European Medicines Agency, (2010). Committee for medicinal products for human use (CHMP): Guideline on the investigation of bioequivalence. London, 20 January 2010 Doc. Ref.: CPMP/EWP/QWP/1401/98 Rev. 1/ Corr **.

Ezzet, F., Krishna, G., Wexler, D. B., Statkevich, P., Kosoglou, T., & Batra, V. K. (2001). A population pharmacokinetic model that describes multiple peaks due to enterohepatic recirculation of ezetimibe. *Clin. Ther.*, *23*(6): 871-885.

Fabozzi, F.J., Focardi, S.M., Rachev, S.T., and Arshanapalli, B.G. (2014). The Basics of Financial Econometrics: Tools, Concepts, and Asset Management Applications. Appendix E. Model Selection Criterion: AIC and BIC. John Wiley & Sons, Inc. Published

Falk, J.A., Minai, O.A., Mosenifar, Z., (2008). Inhaled and systemic corticosteroids in chronic obstructive pulmonary disease. *Proc. Am. Thorac. Soc.,* 5: 506–512.

Fenton, C., Keating, G.M., (2004). Inhaled salmeterol/fluticasone propionate: a review of its use in chronic obstructive pulmonary disease. *Drugs,* 64: 1975–1996.

Food and Drug Administration, (1999). Guidance for Industry Population Pharmacokinetics U.S. Department of Health and Human Services. February 1999

Food and Drug Administration, (2003). Guidance for Industry Bioavailability and Bioequivalence Studies for Orally Administered Drug Products — General Considerations U.S. Department of Health and Human Services. March 2003 Revision 1.

Fradette, C., Lavigne, J., Waters, D., Ducharme, M.P., (2005). The utility of the population approach applied to bioequivalence in patients: comparison of 2 formulations of cyclosporine. *Ther. Drug Monit.,* 27: 592–600.

Frijlink, H.W., De Boer, A.H., (2004). Dry powder inhalers for pulmonary drug delivery. *Expert Opin. Drug Deliv*., 1: 67–86.

Funaki, T. (1999). Enterohepatic circulation model for population pharmacokinetic analysis. *J. Pharm. Pharmacol*., 51: 1143–1148.

Gabrielsson, J., Weiner, D., (2007). Pharmacokinetic and Pharmacodynamic Data Analysis: Concepts and Applications. 4th edition. Swedish Pharmaceutical Press (s.l.).

Gabrielsson, J., and Weiner, D. (2012). Non-compartmental Analysis-Chapter 16., Computational Toxicology: Volume I, Methods in Molecular Biology, vol. 929, Brad Reisfeld and Arthur N. Mayeno (eds.)Springer Science-Business Media.

Gao, Y., Shao, J., Jiang, Z., Chen, J., Gu, S., Yu, S., ... Jia, L. (2014). Drug enterohepatic circulation and disposition: constituents of systems pharmacokinetics. *Drug Discov Today, 19*(3): 326-340.

Gerritsen, J., Koeter, G. H., Postma, D. S., Schouten, J. P., & Knol, K. (1989). Prognosis of asthma from childhood to adulthood. *Am Rev Respir Dis,* 140: 1325 - 1330.

Ghosal, A., Hapangama, N., Yuan, Y., Achanfuo-Yeboah, J., Iannucci, R., Chowdhury, S., Alton, K., Patrick, J.E. and Zbaida S. (2004). Identification of human UDP-glucuronosyltransferase enzyme(s) responsible for the glucuronidation of ezetimibe (Zentia). *Drug Metab Dispos*, 32(3): 314-320.

Goyal, N., Beerahee, M., Kalberg, C., Church, A., Kilbride, S., & Mehta, R. (2014). Population pharmacokinetics of inhaled umeclidinium and vilanterol in patients with chronic obstructive pulmonary disease. *Clin Pharmacokinet*, 53: 637 - 648.

Greenblatt, D.J., von Moltke, L.L., Harmatz, J.S., and Shader, R.I. (2002). Pharmacokinetics, Pharmacodynamics and Drug Disposition - Chapter 38. *Neuropsychopharmacology: The Fifth Generation of Progress.* Lippincott, Williams, & Wilkins, Philadelphia, Pennsylvania.

Grekas, N., Athanassiou, K., Papataxiarchou, K., Savu, S. R., & Silvestro, L. (2014). Pharmacokinetic study for the establishment of two inhalation treatments containing budesonide plus formoterol. *J. Pharm. Pharmacol*., 66: 1677 - 1685.

Guhan, A. R., Cooper, S., Oborne, J., Lewis, S., Bennett, J., & Tattersfield, A. E. (2000). Systemic effects of formoterol and salmeterol: A dose-response comparison in healthy subjects. *Thorax*, 55: 650 ‑ 656.

Harrison, T.W., Tattersfield, A.E. (2003). Plasma concentrations of fluticasone propionateand budesonide following inhalation from dry powder inhalers by healthy andasthmatic subjects. *Thorax*, 58: 258–260.

Harrison, L.I., Novak, C.C., Needham, M.J., & Ratner, P. (2011). Comparative pulmonary function and pharmacokinetics of fluticasone propionate and salmeterol xinafoate delivered by two dry powder inhalers to patients with asthma. *J Aerosol Med Pulm Drug Deliv*, 24: 245 ‑ 252.

Hassett, D.J., Borchers, M.T., Panos, R.J., (2014). Chronic obstructive pulmonary disease (COPD): evaluation fromclinical, immunological and bacterial pathogenesis perspectives. *J. Microbiol*., 52: 211–226.

Hendeles, L., Daley-Yates, P., Hermann, R., De Backer, J., Dissamayake, S., Horhota, S.T. (2015). Pharmacodynamic studies to demonstrate bioequivalence of oral inhalation products. *AAPS J*., 17: 758–768.

Hochhaus, G., Möllmann, H., Derendorf, H., Gonzalez-Rothi, R.J. (1997). Pharmacokinetic/pharmacodynamic aspects of aerosol therapy using glucocorticoids as a model. *J. Clin. Pharmacol.*, 37: 881–892.

Holliday S.M., Faulds, D., Sorkin, E.M. (1994). Inhaled fluticasone propionate. A review of its pharmacodynamic and pharmacokinetic properties, and therapeutic use in asthma. Drugs, 47(2): 318-31.

Hochhaus, G., Horhota, S., Hendeles, L., Suarez, S., & Rebello, J. (2015). Pharmacokinetics of orally inhaled drug products. *AAPS J*., 17: 769 ‑ 775.

Horhota, S. T., van Noord, J. A., Verkleij, C. B., Bour, L. J., Sharma, A., Trunk, M., & Cornelissen, P. J. G. (2015). In vitro, pharmacokinetic, pharmacodynamic, and safety comparisons of single and combined administration of tiotropium and salmeterol in COPD patients using different dry powder inhalers. *AAPS J.*, 17: 871-880.

https://www.certara.com/software/pkpd-modeling-and-simulation/phoenix-winnonlin/?ap%5B0%5D=PKPD

Hübner, M., Hochhaus, G., Derendorf, H. (2005). Comparative pharmacology, bioavailability, pharmacokinetics, and pharmacodynamics of inhaled glucocorticosteroids. *Immunol. Allergy Clin. North Am.,* 25(3): 469–488.

Ibrahim, M., Verma, R., Garcia-Contreras, L. (2015). Inhalation drug delivery devices: technology update. *Med Devices (Auckl),* 12(8): 131-9.

Inclan, G., Suarez, E., Calvo, R., Aguirre, C., Macheras, P., Gazouli, M., Lukas, J.C. (2005). Bicompartmental kinetics of tobramycin analysed with a wide range of covariates. *Int J Antimicrob Agent*, 26(4):304-311.

Jain, L., Woo, S., Gardner, E. R., Dahut, W. L., Kohn, E. C., Kummar, S., ... Figg, W. D. (2011). Population pharmacokinetic analysis of sorafenib in patients with solid tumours. *Br. J. Clin. Pharmacol.*, *72*(2): 294-305.

Jendbro M., Johansson, C.-J., Strandberg, P., Falk-Nilsson, H., Edsbäcker, S. (2001). Pharmacokinetics of budesonide and its major ester metabolite after inhalation and intravenous administration of budesonide in the rat. *Drug Metab. Dispos*., 29: 769–776.

Jenkins, C.R., Jones, P.W., Calverley, P.M.A., Celli, B., Anderson, J.A., Ferguson, G.T., Yates, J.C., Willits, L.R., Vestbo, J., (2009). Efficacy of salmeterol/fluticasone propionate by GOLD stage of chronic obstructive pulmonary disease: analysis from the randomised, placebo-controlled TORCH study. *Respir. Res.*, 10, 59.

Jeu, L., & Cheng, J. W. (2003). Pharmacology and therapeutics of ezetimibe (SCH 58235), a cholesterol-absorption inhibitor. *Clin. Ther.*, *25*(9): 2352-2387.

Jiao, Z., Shen, J., Ding, J. J., Zhong, L. J., & Shi, X. J. (2007). Modified population pharmacokinetic model for enterohepatic circulation of mycophenolic acid and its application in a bioequivalence study. *Asian J Pharmacodyn Pharmacokin*, *7*(2): 153-160.

Johnson, M., Butchers, P.R., Coleman, R.A., Nials, A.T., Strong, P., Sumner, M.J., Whelan, C.J. (1993). The pharmacology of salmeterol. *Life Sci*., 52: 2131 - 2143.

Jusko, W.J. (2012). Use of Pharmacokinetic Data Below Lower Limit of Quantitation Values. *Pharm Res.*, 29(9): 2628–2631.

Karlsson, M.O., Sheiner, L.B., (1993). The importance ofmodeling interoccasion variability in population pharmacokinetic analyses. *J. Pharmacokinet. Biopharm*., 21: 735–750.

Kempsford, R., Handel, M., Mehta, R., De Silva, M., & Daley- Yates, P. (2005). Comparison of the systemic pharmacodynamic effects and pharmacokinetics of salmeterol delivered by CFC propellant and non- CFC propellant metered dose inhalers in healthy subjects. *Respir Med*, 99: S11- S19.

Kim, C.S., Hu, S.C. (1998). Regional deposition of inhaled particles in human lungs: comparison between men and women. *J. Appl. Physiol.*, 84(6): 1834–1844.

Kim, H.K. and Lee, S.D. (2005). Pathophysiology of Chronic Obstructive Pulmonary Disease. *Tuberc Respir Dis.*, 59(1): 5-13.

Kim, T.H., Shin, S., Landersdorfer, C.B., Chi, Y.H., Paik, S.H., Myung, J., Yadav, R., Horkovics-Kovats, S., Bulitta, J.B., Shin, B.S. (2015). Population pharmacokinetic modeling of the enterohepatic recirculation of fimasartan in rats, dogs, and humans, *AAPS J.*, 17(5): 1210–1223.

Kirby, S., Falcoz, C., Daniel, M.J., Milleri, S., Squassante, L., Ziviani, L., Ventresca, G.P., (2001). Salmeterol and fluticasone propionate given as a combination. Lack of systemic pharmacodynamic and pharmacokinetic interactions. *Eur. J. Clin. Pharmacol*., 56: 781–791.

Knibbe, C.A.J., Zuideveld, K.P., Aarts, L.P.H.J., Kuks, P.F.M., Danhof, M. (2005). Allometric relationships between the pharmacokinetics of propofol in rats, children and adults. *Br. J. Clin. Pharmacol*., 59: 705–711.

Krishnaswami, S., Möllmann, H., Derendorf, H., Hochhaus, G., (2000). A sensitive LC-MS:MS method for the quantification of fluticasone propionate in human plasma. *J. Pharm. Biomed. Anal*. 22: 123–129.

Krishnaswami, S., Hochhaus, G., Möllmann, H., Barth, J., Derendorf, H., (2005). Interpretation of absorption rate data for inhaled fluticasone propionate obtained in compartmental pharmacokinetic modeling. *Int. J. Clin. Pharmacol. Ther.* 43: 117–122.

Kosoglou T, Statkevich P, Fruchart JC, Pember LJ, Reyderman L, Cutler DL, Guillaume M, Maxwell SE, Veltri EP. Pharmacodynamic and pharmacokinetic interaction between fenofibrate and ezetimibe. *Curr Med Res Opin*, 20(8):1197-207.

Kosoglou, T., Statkevich, P., Johnson-Levonas, A. O., Paolini, J. F., Bergman, A. J., & Alton, K.B. (2005). Ezetimibe: a review of its metabolism, pharmacokinetics and drug interactions. *Clin Pharmacokinet, 44*(5): 467-494.

Labiris, N.R., Dolovich, M.B., (2003). Pulmonary drug delivery. Part II: the role of inhalant delivery devices and drug formulations in therapeutic effectiveness of aerosolized medications. *Br. J. Clin. Pharmacol*. 56: 600–612.

Latorrem M., Novelli, F., Vagaggini, B., Braido, F., Papi, A., Sanduzzi, A., Santus, P., Scichilone, N., Paggiaro, P. (2015). Differences in the efficacy and safety among inhaled corticosteroids (ICS)/long-acting beta2-agonists (LABA) combinations in the treatment of chronic obstructive pulmonary disease (COPD): role of ICS. *Pulm. Pharmacol. Ther.*, 30: 44–50.

Lavielle, M., Mentré, F., (2007). Estimation of population pharmacokinetic parameters of saquinavir in HIV patients with the MONOLIX software. *J. Pharmacokinet. Pharmacodyn.* 34: 229–249.

Lavorini, F. (2013). The challenge of delivering therapeutic aerosols to asthma patients. *ISRN Allergy.* 102418. eCollection 2013.

Lawrence, M., Wolfe, J., Webb, D.R., Chervinsky, P., Kellerman, D., Schaumberg, J.P., Shah, T. (1997). Efficacy of inhaled fluticasone propionate in asthma results from topical and not from systemic activity. *Am J Respir Crit Care Med*., 156(3Pt1): 744-51.

Lecaillon, J.B., Kaiser, G., Palmisano, M., Morgan, J., Della Cioppa, G. (1999). Pharmacokinetics and tolerability of formoterol in healthy volunteers after a single high dose of Foradil dry powder Inhalation via aerolizer™. *Eur. J. Clin. Pharmacol.*, 55: 131–138.

Liang, E., & Derendorf, H. (1998). Pitfalls in pharmacokinetic multicompartment analysis. *J Pharmacokinet Biopharm*, 26: 247-260.

Lipworth, B. J. (1996). Pharmacokinetics of inhaled drugs. *Br. J. Clin. Pharmacol.*, 42: 697-705.

Lipworth, B. J., & Clark, D. J. (1997). Effects of airway calibre on lung delivery of nebulised salbutamol. *Thorax,* 52: 1036-1039.

Lu, D., Lee, S.L., Lionberger, R.A., Choi, S., Adams, W., Caramenico, H.N., Chowdhury, B.A., Conner, D.P., Katial, R., Limb, S., Peters, J.R., Yu, L., Seymour, S., Li, B.S., (2015). International guidelines for bioequivalence of locally acting orally inhaled drug products: similarities and differences. *AAPS J.*, 17: 546–557.

Luiking, Y.C., Peeters, T.L., Stolk, M.F.J., Nieuwenhuijs, V.B., Portincasa, P., Depoortere I., van Berge Henegouwen, G.P, Akkermans, L.M. (1998). Motilin induces gall bladder emptying and antral contractions in the fasted state in humans, *Gut,* 42: 830–835.

, Karikas, G., Gazouli, M., Kalabalikis, P., Hatzis, T.,. (2004) Pharmacokinetics of teicoplanin in an ICU population of children and infants. *Pharm Res.* 21: 2074-2081.

Macheras, P., Lukas, J.C. (2003) Population pharmacokinetic/pharmacodynamic methods and their application: an introduction. *Pharmakeftiki,* 16: 65-68.

Mahler, D.A., Donohue, J.F., Barbee, R.A., Goldman, M.D., Gross, N.J., Wisniewski, M.E., … Anderson, W.H. (1999). Efficacy of salmeterol xinafoate in the treatment of COPD. *Chest,* 115: 957 ‐ 965.

Maier, G., Rubino, C., Hsu, R., Grasela, T., & Baumgartner, R. A. (2007). Population pharmacokinetics of (R) ‐ albuterol and (S) ‐ albuterol in pediatric patients aged 4–11 years with asthma. *Pulm Pharmacol Ther*, 20: 534 ‐ 542.

Malik, M. Y., Jaiswal, S., Sharma, A., Shukla, M., & Lal, J. (2016). Role of enterohepatic recirculation in drug disposition: cooperation and complications. *Drug Metab Rev*, *48*(2): 281-327.

Manchee, G.R., Barrow, A., Kulkarni, S., Palmer, E., Oxford, J., Colthup, P.V., … Tarbit, M.H. (1993). Disposition of salmeterol xinafoate in laboratory animals and humans. *Drug Metab Dispos*, 21: 1022 ‐ 1028.

Mertens, K.L., Kalsbeek, A., Soeters, M.R., Eggink, H.M. (2017) Bile Acid Signaling Pathways from the Enterohepatic Circulation to the Central Nervous System. *Front Neurosci.,* 7(11):617.

Mobley, C., Hochhaus, G., (2001). Methods to assess pulmonary deposition and absorption of drugs. *Drug Discov. Today*, 6: 367–375.

Möllmann, H., Wagner, M., Meilhm, B., Hochhaus, G., Barth, J., Stockmann, R., Krieg, M., Weisser, H., Falcoz, C., Derendorf, H., (1998). Pharmacokinetic and pharmacodynamic evaluation of fluticasone propionate after inhaled administration. *Eur. J. Clin. Pharmacol*., 53, 459–467.

Möllmann, H., Wagner, M., Krishnaswami, S., Dimova, H., Tang, Y., Falcoz, C., Daley-Yates, P.T., Krieg, M., Stöckmann, R., Barth, J., Lawlor, C., Möllmann, A.C., Derendorf, H., Hochhaus, G. (2001). Single-dose and steady-state pharmacokinetic and pharmacodynamic evaluation of therapeutically clinically equivalent doses of inhaled

fluticasone propionate and budesonide, given as Diskus® or Turbohaler® dry-powder inhalers to healthy subjects. *J. Clin. Pharmacol*., 41: 1329–1338.

Mould, D.R., and Upton, R.N. (2012). Basic Concepts in Population Modeling, Simulation, and Model-Based Drug Development. *CPT Pharmacometrics Syst Pharmacol.*, 1(9): e6.

Mould, D.R., and Upton, R.N. (2013). Basic Concepts in Population Modeling, Simulation, and Model-Based Drug Development—Part 2: Introduction to Pharmacokinetic Modeling Methods. *CPT Pharmacometrics Syst Pharmacol.*, 2(4): e38.

Murdoch, J. R., & Lloyd, C. M. (2010). Chronic inflammation and asthma. *Mutat Res*, (1–2): 24 - 39.

Nashimoto, S., Sato, Y., Takekuma, Y., & Sugawara, M. (2017). Inhibitory effect of ezetimibe can be prevented by an administration interval of 4 h between α-tocopherol and ezetimibe. *Biopharm Drug Dispos, 38*(4): 280-289.

Nelson, H.S., Chapman, K.R., Pyke, S.D., Johnson, M., Pritchard, J.N. (2003). Enhanced synergy between fluticasone propionate and salmeterol inhaled from a single inhaler versus separate inhalers. *J. Allergy Clin. Immunol.*, 112: 29–36.

Newman, S.P., Moren, F., Trofast, E., Talaee, N., & Clarke, S.W. (1991). Terbutaline sulphate Turbuhaler: Effect of inhaled flow rate on drug deposition and efficacy. *Int. J. Pharm.*, 74: 209 - 213.

Newnham, D. M., McDevitt, D.G., & Lipworth, B.J. (1993). Comparison of the extrapulmonary 2 - adrenoceptor responses and pharmacokinetics of salbutamol given by standard metered dose - inhaler and modified actuator device. *Br. J. Clin. Pharmacol.*, 36: 445 - 450.

Noreddin, A. (2012). Readings in Advanced Pharmacokinetics – Theory, Methods and Applications. Published by InTech Janeza Trdine 9, 51000 Rijeka, Croatia Copyright © 2012 InTech.

Northfield, T.C., Hofmann, A.F. (1975). Biliary lipid output during three meals and an overnight fast. I. Relationship to bile acid pool size and cholesterol saturation of bile in gallstone and control subjects. *Gut*, 16(1): 1–11.

Okour, M., & Brundage, R.C. (2017). Modeling Enterohepatic Circulation. *Curr Pharmacol Rep,* 3: 301-313.

Olsson, B., Bondesson, E., Borgström, L., Edsbäcker, S., Eirefelt Nelson, H.S., Chapman, K.R., Pyke, S.D., Johnson, M., Pritchard, J.N., (2003). Enhanced synergy between fluticasone propionate and salmeterol inhaled from a single inhaler versus separate inhalers. *J. Allergy Clin. Immunol.*, 112: 29–36.

Olsson, B., Bondesson, E., Borgström, L., Edsbäcker, S., Eirefelt, S., Ekelund, K., Gustavsson, L., Hegelund-Myrbäck, T., (2011). Pulmonary drug metabolism, clearance, and absorption-Chapter 2. In: Smyth, H.D.C., Hickey, A.J. (Eds.), Controlled Pulmonary Drug Delivery. Advances in Delivery Science and Technology, pp. 21–50.

Panhard, X., Mentré, F., (2005). Evaluation by simulation of tests based on non-linear mixed-effects models in pharmacokinetic interaction and bioequivalence cross-over trials. *Stat. Med.* 24: 1509–1524.

Papi, A., Brightling, C., Pedersen, S.E., Reddel, H.K. (2017). Asthma. *Seminar Published Online.*

Patel, J., Sheehan, V., & Gurk-Turner, C. (2003). Ezetimibe (Zetia): a new type of lipid-lowering agent. *Proc (Bayl Univ Med Cent), 16*(3): 354–358.

Patrick, J. E., Kosoglou, T., Stauber, K. L., Alton, K. B., Maxwell, S. E., Zhu, Y., ... Cayen, M. N. (2002). Disposition of the selective cholesterol absorption inhibitor ezetimibe in healthy male subjects. *Drug Metab Dispos, 30*(4): 430-437.

Pitcairn, G., Lunghetti, G., Ventura, P., & Newman, S. (1994). A comparison of the lung deposition of salbutamol inhaled from a new dry powder inhaler, at two inhaled flow rates. *Int. J. Pharm.*, 102: 11-18.

Pritchard, J.N. (2001). The influence of lung deposition on clinical response. *J Aerosol Med.* 14(1): S19-26.

Post, T.M., Freijer, J.I., Ploeger, B.A., Danhof, M., (2008). Extensions to the visual predictive check to facilitate model performance evaluation. *J. Pharmacokinet. Pharmacodyn.* 35: 185–202.

Reynolds, N.A., Lyseng-Williamson, K.A., Wiseman, L.R., (2005). Inhaled salmeterol/ fluticasone propionate. *Drugs*, 65: 1715–1734.

Ricciardolo, F.L., Blasi, F., Centanni, S., & Rogliani, P. (2015). Therapeutic novelties of inhaled corticosteroids and bronchodilators in asthma. *Pulm Pharmacol Ther*, 33: 1 ‑ 10.

Ritter, J.M., Lewis, L.D, Mant, T.G.K, Ferro, A. (2008). A textbook of Clinical Pharmacology and Therapeutics. Fifth Edition, Great Britain, Hodder Arnold.

Roberts, M.S., Magnusson, B. M., Burczynski, F. J., & Weiss, M. (2002). Enterohepatic circulation: physiological, pharmacokinetic and clinical implications. *Clin Pharmacokinet, 41*(10): 751-790.

Rohatagi, S., Bye, A., Falcoz, C., Mackie, A.E., Meibohm, B., Möllmann, H., Derendorf, H., (1996). Dynamic modeling of cortisol reduction after inhaled administration of fluticasone propionate. *J. Clin. Pharmacol*., 36: 938–941.

Rosenborg, J., Larsson, P., Tegnér, K., Hallström, G., (1999). Mass balance and metabolism of [$^{(3)}$H]-Formoterol in healthy men after combined i.v. and oral administration-mimicking inhalation. *Drug Metab. Dispos.* 27(10): 1104–1116.

Sakai, J,B. (2008). Practical Pharmacology for the Pharmacy Technician (Chapter 3). Lippincott Williams & Wilkins

Sam, W.J., Akhlaghi, F., & Rosenbaum, S. E. (2009). Population pharmacokinetics of mycophenolic acid and its 2 glucuronidated metabolites in kidney transplant recipients. *J. Clin. Pharmacol., 49*(2): 185-195.

Sam, W. J., & Joy, M. S. (2010). Population pharmacokinetics of mycophenolic acid and metabolites in patients with glomerulonephritis. *Ther Drug Monit., 32*(5): 594-605.

Sanders, M. (2007). Inhalation therapy: an historical review. *Prim Care Respir J,* 16: 71–81

Sasaki, H., Kamimura, H., Shiobara, Y., Esumi, Y., Takaichi, M., Yokoshima, T. (1982). Disposition and metabolism of formoterol fumarate, a new bronchodilator, in rats and dogs. *Xenobiotica*, 12: 803–812.

Savic, R., Lavielle, M., (2009). A new SAEM algorithm: performance in population models for count data. *J. Pharmacokinet. Pharmacodyn*., 36: 367–379.

Serevent Diskus. (2014). Product information, 2014.

Singh, S.D., Whale, C., Houghton, N., Daley-Yates, P., Kirby, S.M., Woodcock, A.A. (2003). Pharmacokinetics and systemic effects of inhaled fluticasone propionate in chronic obstructive pulmonary disease. *Br. J. Clin. Pharmacol.*, 55: 375–381.

Sheiner, L.B., Rosenberg, B., Melmon, K.L. (1972). Modelling of individual pharmacokinetics for computer-aided drug dosage. *Comput Biomed Res.*, 5(5): 411-59.

Sheiner, L.B., Beal, S.L., (1983). Evaluation of methods for estimating population pharmacokinetic parameters. III. Monoexponential model: routine clinical pharmacokinetic data. *J. Pharmacokinet. Biopharm.*, 11: 303–319.

Shou, M., Lu, W., Kari, P. H., Xiang, C., Liang, Y., Lu, P., ... Rodrigues, A. D. (2005). Population pharmacokinetic modeling for enterohepatic recirculation in Rhesus monkey. *Eur. J. Pharm. Sci., 26*(2): 151-161.

Silvestro, L., Savu, S.R., Savu, S.N., Tudoroniu, A., Tarcomnicu, I., (2012). Development of a sensitive method for simultaneous determination of fluticasone propionate and salmeterol in plasma samples by liquid chromatography–tandemmass spectrometry. *Biomed. Chromatogr.,* 26: 627–635.

Simon, N., Fuseau, E., Daley-Yates, P., (1998). Fluticasone propionate pharmacokinetics in asthma patients when administered alone or in combination to PAGE Abstracts of the Annual Meeting of the Population Approach Group in Europe. Poster Presentation.

Singh, S.D., Whale, C., Houghton, N., Daley-Yates, P., Kirby, S.M., Woodcock, A.A., (2003). Pharmacokinetics and systemic effects of inhaled fluticasone propionate in chronic obstructive pulmonary disease. *Br. J. Clin. Pharmacol.*, 55: 375–381.

Smaldone, G.C. (2005). Assessing new technologies: Patient-device interactions and deposition. *Respiratory Care,* 50: 1151-1158.

Smith, D. A., Beaumont, K., Maurer, T. S., & Di, L. (2015). Volume of Distribution in Drug Design. *J. Med. Chem., 58*(15): 5691-5698.

Strandgården, K., Höglund, P., Grönquist, L., Svensson, L., & Gunnarsson, P. O. (2000). Absorption and disposition including enterohepatic circulation of (^{14}C) roquinimex after oral administration to healthy volunteers. *Biopharm Drug Dispos., 21*(2): 53-67.

Sudhop, T., Lütjohann, D., Kodal, A., Igel, M., Tribble, D. L., Shah, S., ... von Bergmann, K. (2002). Inhibition of intestinal cholesterol absorption by ezetimibe in humans. *Circulation, 106*(15): 1943-1948.

Svartengren, K., Lindestad, P. A., Svartengren, M., Bylin, G., Philipson, K., & Camner, P. (1994). Deposition of inhaled particles in the mouth and throat of asthmatic subjects. *Eur Respir J*, 7: 1467-1473.

Sweeney, M. E., & Johnson, R. R. (2007). Ezetimibe: an update on the mechanism of action, pharmacokinetics and recent clinical trials. *Expert Opin Drug Metab Toxicol, 3*(3): 441-450.

Symbicort (2016), Summary of Product Characteristics, Symbicort Turbohaler 400/12, Inhalation Powder, AstraZeneca UK Limited.

Szefler, S.J. (1999). Pharmacodynamics and pharmacokinetics of budesonide: a new nebulized corticosteroid. *J. Allergy Clin. Immunol.*, 104: S175–S183.

Tena, A. F., & Clarà, P. C. (2012). Deposition of inhaled particles in the lungs. *Arch Bronconeumol.*, 48: 240-246.

Thakkar, K., Mhatre, S., Jadhav, M., Goswami, S., Shah, R., (2015). Pharmacokinetic studies for proving bioequivalence of orally inhaled drug products — critical issues and concepts. *Front. Pharmacol.*, 3 (6): 117.

Thorat, S., Mahajan, T., Meshram, S. (2015). Formulation and product development of dry powder inhalers: an overview. *World J Pharm Pharm Sci*, 4(11): 639-655

Thorsson, L., Dahlstrom, K., Edsbacker, S., Kallen, A., Paulson, J.,Wiren, J.E., (1997). Pharmacokinetics and systemic effects of inhaled fluticasone propionate in healthy subjects. *Br. J. Clin. Pharmacol*., 43: 155–161.

Thorsson, L., Edsbäcker, S., Källén, A., Löfdahl, C.G. (2001). Pharmacokinetics and systemic activity of fluticasone via Diskus and pMDI, and of budesonide via Turbuhaler. *Br. J. Clin. Pharmacol*., 52(5): 529–538.

Tozer, T.N. (1981). Concepts basic to pharmacokinetics. *Pharmacol. Ther.*, 12(1): 109-131.

Urso, R., Blardi, P., Giorgi, G. (2002). A short introduction to pharmacokinetics. *Eur Rev Med Pharmacol Sci*., 6(2-3): 33-44.

Usmani, O.S. (2015). Inhaled drug therapy for the management of asthma. *Prescriber*, 26(3,5): 23–25

Vaisman, N., Koren, G., Goldstein, D., Canny, G. J., Tan, Y. K., Soldin, S., & Pencharz, P. (1987). Pharmacokinetics of inhaled salbutamol in patients with cystic fibrosis versus healthy young adults. *J. Pediatr.*, 111: 914 ‑ 917.

van den Berg, B.T., Derks, M.G., Koolen, M.G., Braat, M.C., Butter, J.J., van Boxtel, C.J. (1999). Pharmacokinetic/pharmacodynamic modeling of the eosinopenic and

hypokalemic effects of formoterol and theophylline combination in healthy men, *Pulm. Pharmacol. Ther.,* 12(3): 185–192.

van den Brink, K.I., Boorsma, M., Staal-van den Brekel, A.J., Edsbäcker, S., Wouters, E.F., Thorsson, L. (2008). Evidence of the in vivo esterification of budesonide in human airways. *Br. J. Clin. Pharmacol*., 66(1): 27–35.

van de Moortele, T., Goerke, U., Wendt, C.H., Coletti, F. (2017) Airway morphology and inspiratory flow features in the early stages of Chronic Obstructive Pulmonary Disease. *Clin Biomech (Bristol, Avon)*, S0268-0033(17)30286-3.

van Heek, M., Farley, C., Compton, D. S., Hoos, L., Alton, K. B., Sybertz, E. J., & Davis, H. R. Jr. (2000). Comparison of the activity and disposition of the novel cholesterol absorption inhibitor, SCH58235, and its glucuronide, SCH60663. *Br J Pharmacol, 129*(8): 1748-1754.

van Heek, M., France, C. F., Compton, D. S., McLeod, R. L., Yumibe, N. P., Alton, K. B., ... Davis, H. R. Jr. (1997). *In vivo* metabolism-based discovery of a potent cholesterol absorption inhibitor, SCH58235, in the rat and rhesus monkey through the identification of the active metabolites of SCH48461. *J Pharmacol Exp Ther, 283*(1): 157-163.

Verberne, A.A.P.H., Fuller, R. (1998). An overview of nine clinical trials of salmeterol in an asthmatic population. *Respir. Med*., 92: 777–782.

Wagner, J.G. (1981). History of Pharmacokinetics. *Pharmac. Ther*., 12: 537-562.

Wajima, T., Yano, Y., Oguma, T. (2002). A pharmacokinetic model for analysis of drug disposition profiles undergoing enterohepatic circulation. *J. Pharm. Pharmacol*., 54(7): 929–934.

Weber, B., Hochhaus, G. (2013). A pharmacokinetic simulation tool for inhaled corticosteroids. *AAPS J.*, 15(1): 159–171.

Weber, B., & Hochhaus, G. (2015). A systematic analysis of the sensitivity of plasma pharmacokinetics to detect differences in the pulmonary performance of inhaled fluticasone propionate products using a model-based simulation approach. *AAPS J.*, 17: 999-1010.

Wu, K., Goyal, N., Stark, J.G., Hochhaus, G., (2008). Evaluation of the administration time effect on the cumulative cortisol suppression and cumulative lymphocytes suppression for once daily inhaled corticosteroids: a population modeling/simulation approach. *J. Clin. Pharmacol.*, 48: 1069–1080.

Xu, J., Nave, R., Lahu, G., Derom, E., Derendorf, H., (2010). Population pharmacokinetics and pharmacodynamics of inhaled ciclesonide and fluticasone propionate in patients with persistent asthma. *J. Clin. Pharmacol*., 50: 1118–1127.

Younis, I. R., Malone, S., Friedman, H. S., Schaaf, L. J., & Petros, W. P. (2009). Enterohepatic recirculation model of irinotecan (CPT-11) and metabolite pharmacokinetics in patients with glioma. *Cancer Chemother Pharmacol, 63*(3): 517-24.

Yau, W. P., Vathsala, A., Lou, H. X., Zhou, S., & Chan, E. (2009). Mechanism-based enterohepatic circulation model of mycophenolic acid and its glucuronide metabolite: assessment of impact of cyclosporine dose in Asian renal transplant patients. *J. Clin. Pharmacol.*, *49*(6): 684-699.

APPENDIX A

The following pages show some representative pharmacokinetic models, evaluated during the population PK analysis of total Ezetimibe concentrations. A summary of the main model categories is provided in Figure C.4.3 (p.149) of the manuscript.

EZE PK Model (No. 1)

Model Description:

1-compartment PK model, with first-order absorption and elimination processes

Schematic Representation:

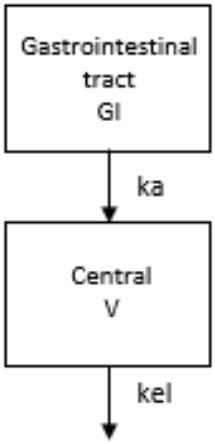

Numerical Criteria:

-2LL: 11604.84

AIC: 11622.84

BIC: 11641.98

Estimation of the population PK parameters:

	parameter	s.e. (lin)	r.s.e.(%)
ka_pop	6.64	1.7	25
V_pop	1.53e+005	1.5e+004	10
Cl_pop	1.07e+004	9.4e+002	9
omega_ka	1.01	0.27	27
omega_V	0.553	0.0035	1
omega_Cl	0.482	0.0028	1
gamma_ka	1.04	0.21	20
gamma_V	0	-	-
gamma_Cl	0	-	-
a	0.104	0.011	11
b	0.397	0.0079	2

***Goodness-of-fit plots*:**

Observed vs individual predicted concentrations plot

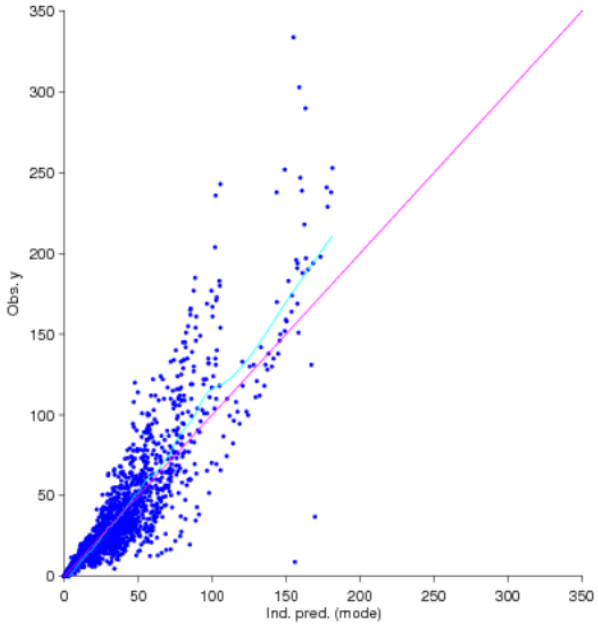

VPC plot

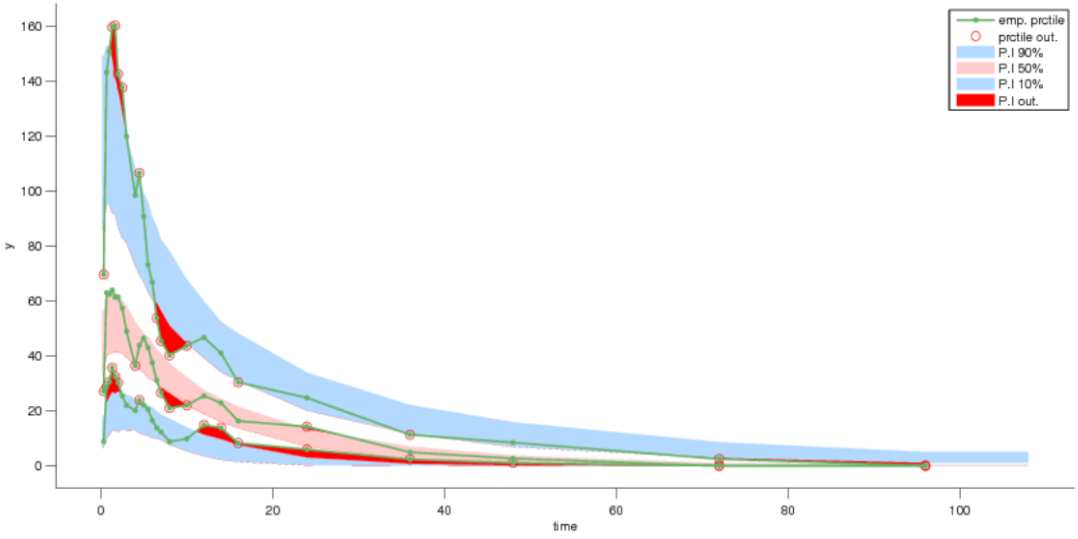

EZE PK Model (No. 2)

Model Description:

3-compartment PK model, with first-order absorption and elimination processes

Schematic Representation:

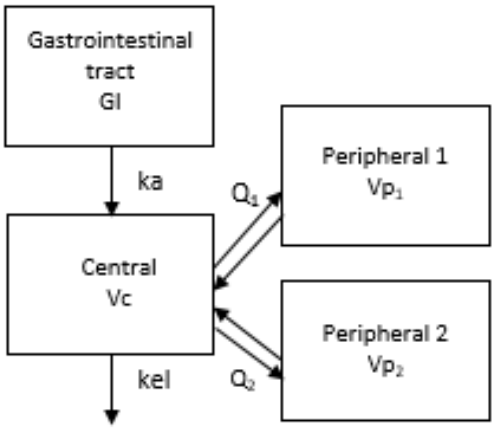

Numerical Criteria:

-2LL: 11024.08

AIC: 11058.08

BIC: 11094.24

Estimation of the population PK parameters:

	parameter	s.e. (lin)	r.s.e.(%)
ka_pop	0.86	0.13	15
cl_pop	1.11e+004	9.2e+002	8
v1_pop	4.65e+004	8.4e+003	18
Q2_pop	1.04e+005	1.1e+005	111
v2_pop	634	1.6e+003	245
Q3_pop	2.9e+004	5.8e+003	20
v3_pop	1.1e+005	1.3e+004	12
omega_ka	0.0539	0.9	1.67e+003
omega_cl	0.459	0.0028	1
omega_v1	0.604	0.011	2
omega_Q2	0.896	0.35	40
omega_v2	2.44	0.018	1
omega_Q3	1.04	0.023	2
omega_v3	0.583	0.0076	1
gamma_ka	0.532	0.078	15
gamma_cl	0	-	-
gamma_v1	0	-	-
gamma_Q2	0	-	-
gamma_v2	0	-	-
gamma_Q3	0	-	-
gamma_v3	0	-	-
a	0.249	0.024	10
b	0.295	0.0063	2

Goodness-of-fit plots:

Observed vs individual predicted concentrations plot
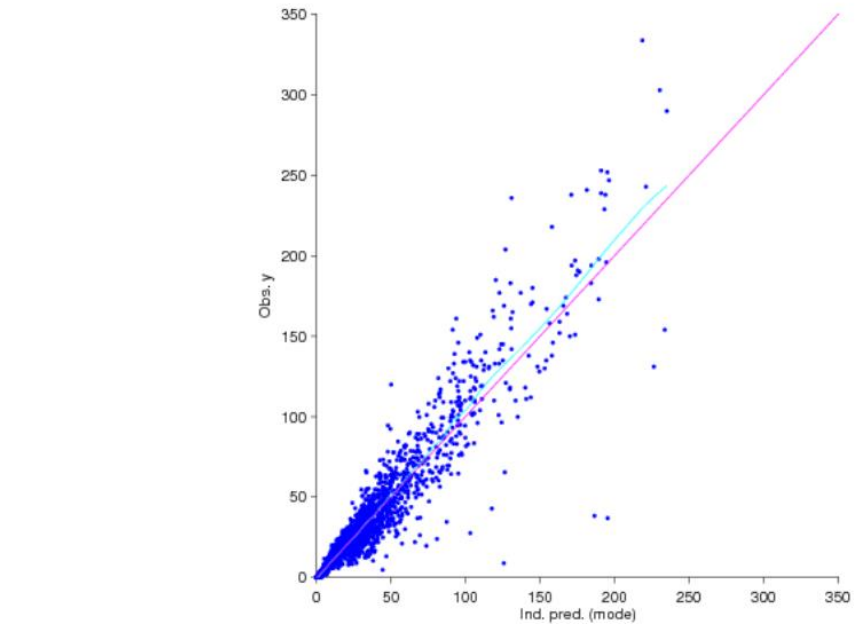
VPC plot
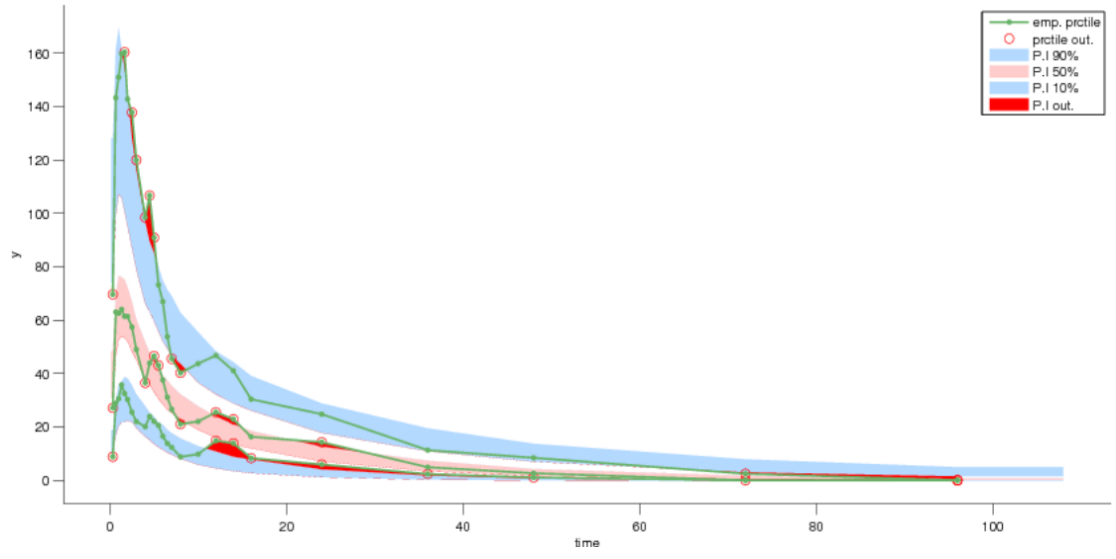

EZE PK Model (No. 3)

Model Description:

3-compartment PK model with first-order absorption and elimination processes, and EHC via direct drug transfer of the drug between the GI and Central compartments. Switch function release in specified time intervals (TGE) at mealtimes.

Schematic Representation:

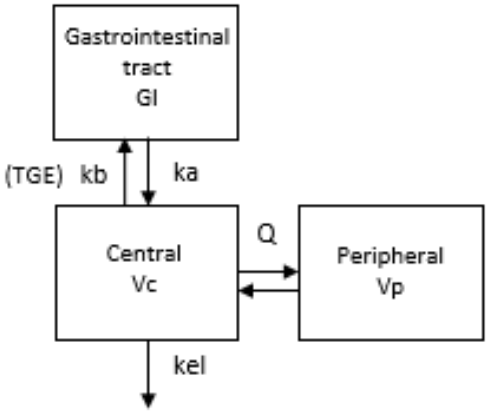

Numerical Criteria:

-2LL: 10952.28

AIC: 10986.28

BIC: 11022.44

Estimation of the population PK parameters:

	parameter	s.e. (lin)	r.s.e.(%)
ka_pop	0.601	0.047	8
Vc_pop	3.52e+004	3.4e+003	10
Vp_pop	7.95e+004	8.4e+003	11
Q_pop	2.29e+004	3.1e+003	14
kg_pop	0.00186	0.00093	50
k10_pop	0.0961	0.033	34
CL_pop	8.04e+003	6.2e+002	8
omega_ka	0.0931	0.31	336
omega_Vc	0.471	0.02	4
omega_Vp	0.519	0.01	2
omega_Q	0.673	0.029	4
omega_kg	0.744	0.54	72
omega_k10	1.68	0.013	1
omega_CL	0.376	0.0055	1
gamma_ka	0.519	0.071	14
gamma_Vc	0	-	-
gamma_Vp	0	-	-
gamma_Q	0	-	-
gamma_kg	0	-	-
gamma_k10	0	-	-
gamma_CL	0	-	-
a	0.248	0.026	11
b	0.289	0.0063	2

Goodness-of-fit plots:

Observed vs individual predicted concentrations plot
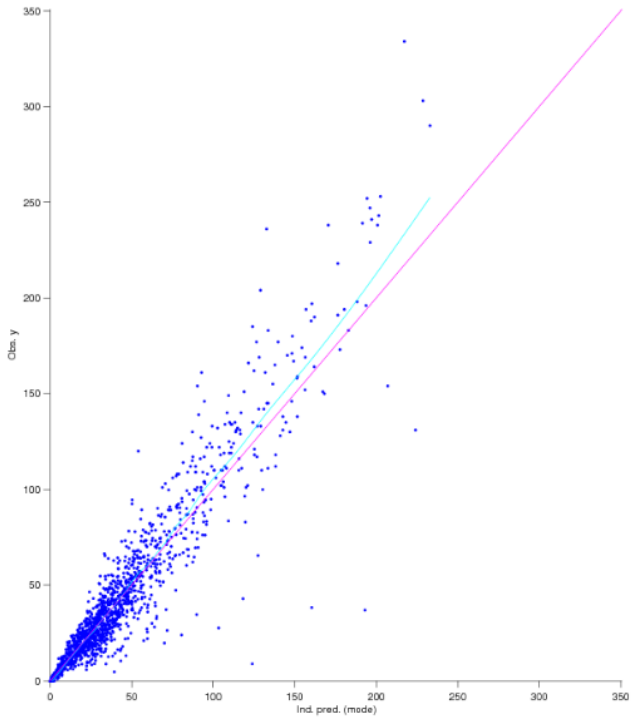
VPC plot
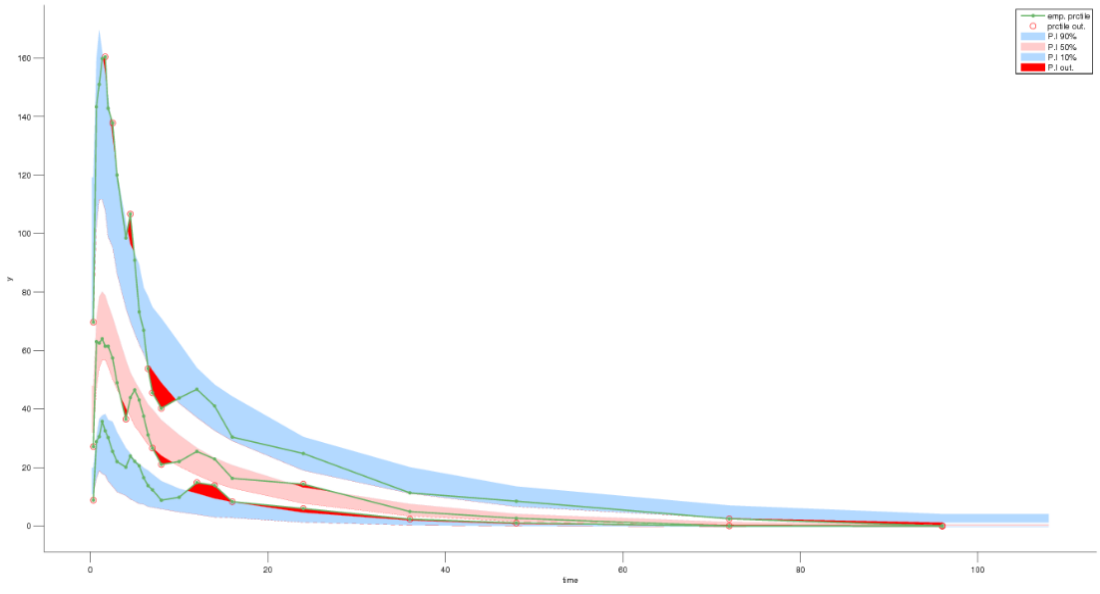

EZE PK Model (No. 4)

Model Description:

4-compartment PK model with first-order absorption and elimination processes, and EHC via first-order transfer of the drug between the GB and Central compartments. Switch function release in specified time intervals (TGE) at mealtimes and the fraction of dose undergoing EHC (Fb) as estimate.

Schematic Representation:

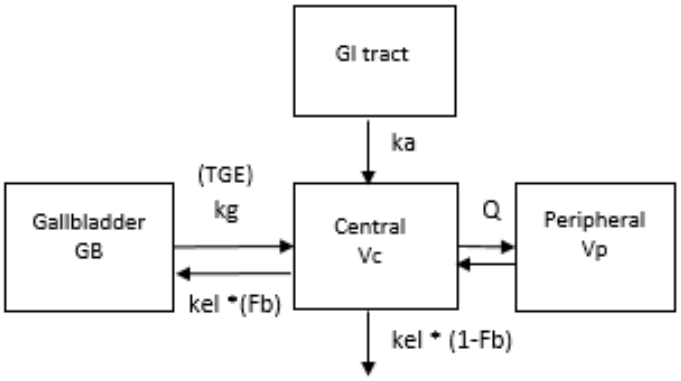

Numerical Criteria:

-2LL: 10010.42
AIC: 10048.42
BIC: 10086.90

Estimation of the population PK parameters:

	parameter	s.e. (lin)	r.s.e.(%)
ka_pop	0.914	0.074	8
Vc_pop	5.66e+004	5.1e+003	9
Vp_pop	1.21e+005	1.2e+004	10
Q_pop	2.9e+004	4e+003	14
k24_pop	0.282	0.015	5
k42_pop	0.393	0.035	9
Fb_pop	0.669	0.023	3
CL_pop	1.11e+004	9.7e+002	9
omega_ka	0.0843	0.41	486
omega_Vc	0.472	0.0046	1
omega_Vp	0.532	0.011	2
omega_Q	0.719	0.0048	1
omega_k24	0.259	0.00048	0
omega_k42	0.31	0.1	32
omega_Fb	0.375	0.082	22
omega_CL	0.332	0.046	14
gamma_ka	0.591	0.081	14
gamma_Vc	0	-	-
gamma_Vp	0	-	-
gamma_Q	0	-	-
gamma_k24	0	-	-
gamma_k42	0	-	-
gamma_Fb	0	-	-
gamma_CL	0	-	-
a	0.199	0.019	10
b	0.273	0.0063	2

***Goodness-of-fit plots*:**

Observed vs individual predicted concentrations plot
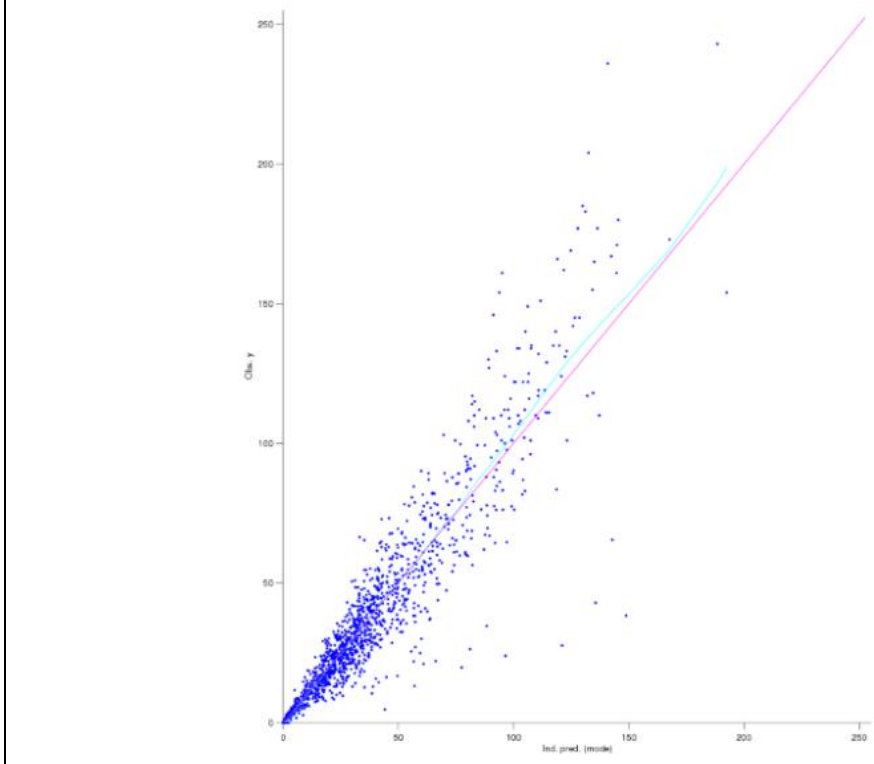
VPC plot
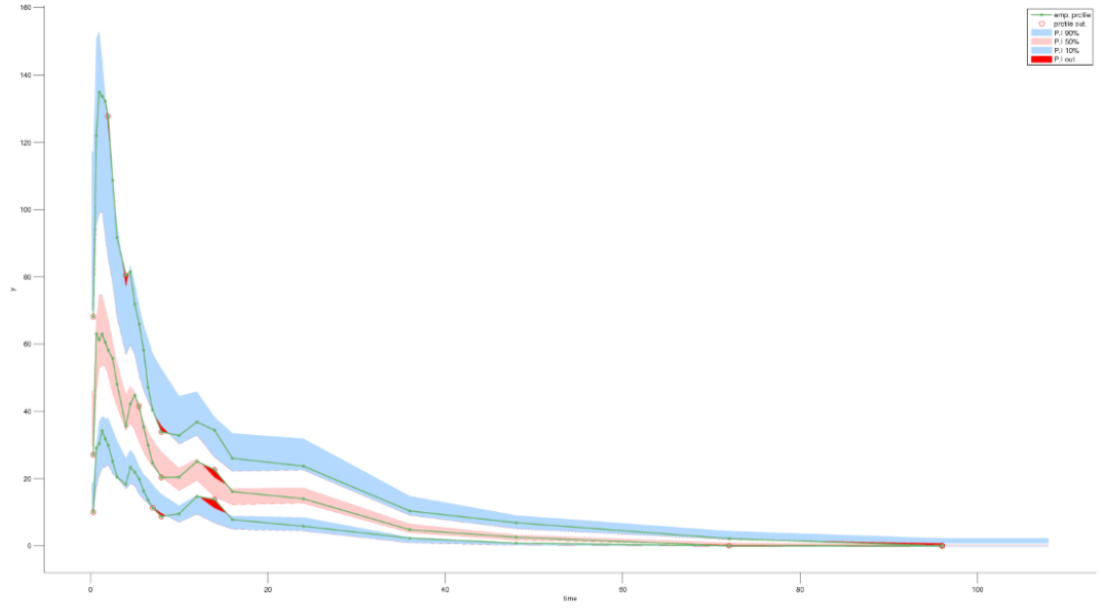

EZE PK Model (No. 5)

Model Description:

4-compartment PK model with first-order absorption and elimination processes, and EHC via bolus release of the drug between the GB and Central compartments. Switch function release in specified time intervals (TGE) at mealtimes and fecal elimination starting at 4 hours post-dose.

Schematic Representation:

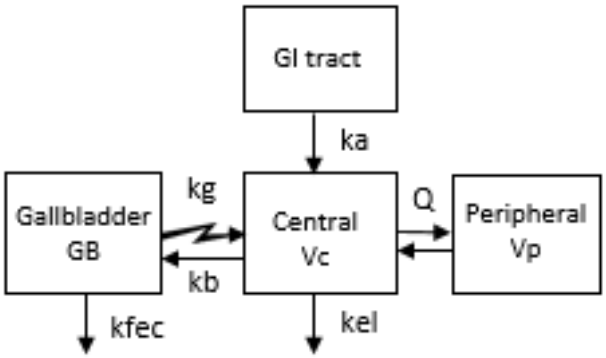

Numerical Criteria:

-2LL: 10115.89
AIC: 10149.89
BIC: 10184.32

Estimation of the population PK parameters:

	parameter	s.e. (lin)	r.s.e.(%)
ka_pop	0.924	0.07	8
Vc_pop	5.68e+004	5.7e+003	10
Vp_pop	1.32e+005	1.3e+004	10
Q_pop	2.98e+004	3.9e+003	13
k24_pop	0.0763	0.004	5
k40_pop	0.0154	0.0057	37
CL_pop	1e+004	7.2e+002	7
omega_ka	0.0652	0.47	715
omega_Vc	0.516	0.0084	2
omega_Vp	0.507	0.0069	1
omega_Q	0.674	0.0071	1
omega_k24	0.223	0.016	7
omega_k40	1.29	0.025	2
omega_CL	0.369	0.0061	2
gamma_ka	0.561	0.076	14
gamma_Vc	0	-	-
gamma_Vp	0	-	-
gamma_Q	0	-	-
gamma_k24	0	-	-
gamma_k40	0	-	-
gamma_CL	0	-	-
a	0.241	0.025	10
b	0.275	0.0064	2

Goodness-of-fit plots:

Observed vs individual predicted concentrations plot
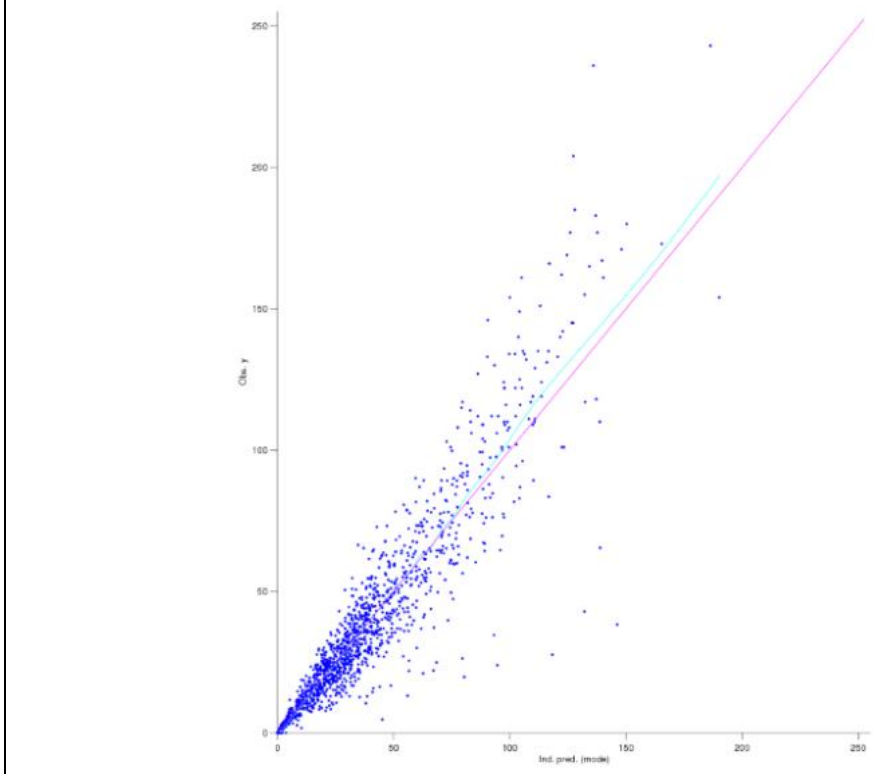
VPC plot
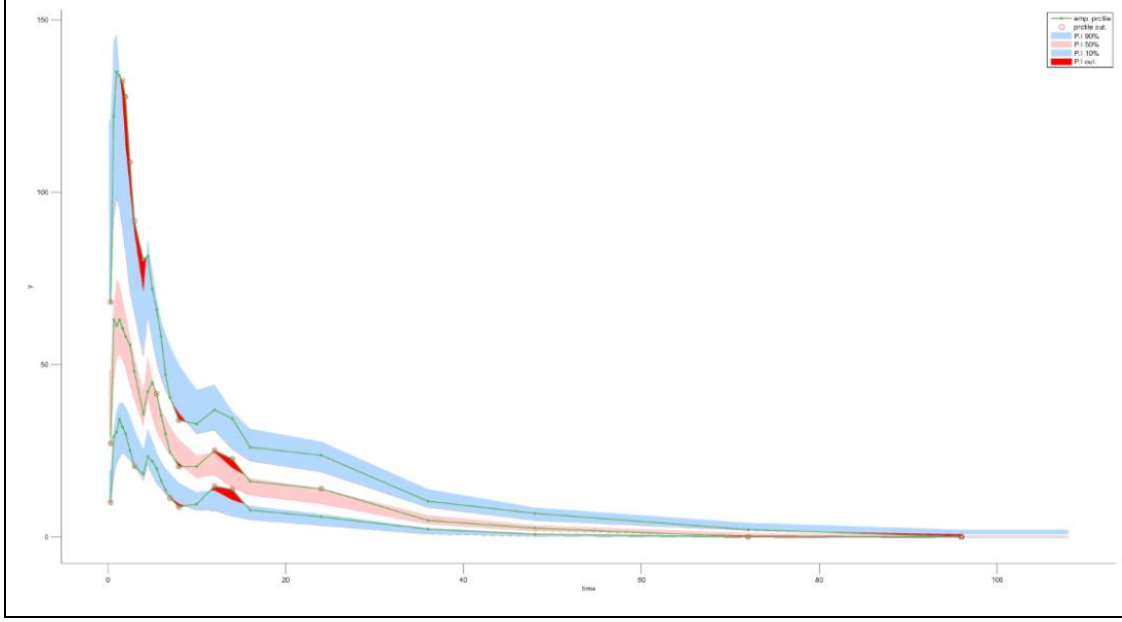

EZE PK Model (No. 6)

Model Description:

4-compartment PK model with first-order absorption and elimination processes, and EHC via zero-order release of the drug between the GB and Central compartments. Switch function release in specified time intervals (TGE) at mealtimes, first-pass effect and fecal elimination starting at 4 hours post-dose.

Schematic Representation:

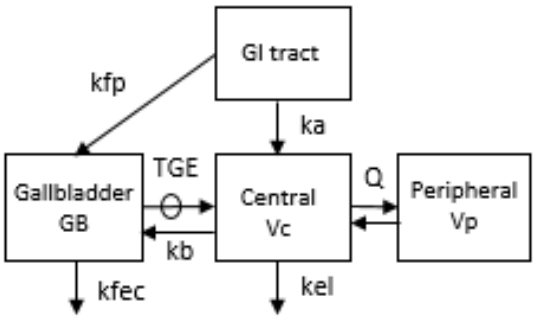

Numerical Criteria:

-2LL: 10119.55
AIC: 10161.55
BIC: 10204.08

Estimation of the population PK parameters:

	parameter	s.e. (lin)	r.s.e.(%)
ka_pop	0.998	0.074	7
F_pop	0.96	0.016	2
Vc_pop	5.41e+004	5.4e+003	10
Vp_pop	1.34e+005	1.3e+004	10
Q_pop	2.79e+004	3.6e+003	13
k24_pop	0.0814	0.0054	7
CL_pop	9.91e+003	7.1e+002	7
k14_pop	0.162	0.043	27
k40_pop	0.0185	0.0034	18
omega_ka	0.0567	NaN	NaN
omega_F	1.85	0.0046	0
omega_Vc	0.512	0.0093	2
omega_Vp	0.512	0.0098	2
omega_Q	0.674	0.011	2
omega_k24	0.289	0.0067	2
omega_CL	0.363	0.0074	2
omega_k14	0.953	0.0096	1
omega_k40	0.618	0.21	34
gamma_ka	0.541	NaN	NaN
gamma_F	0	-	-
gamma_Vc	0	-	-
gamma_Vp	0	-	-
gamma_Q	0	-	-
gamma_k24	0	-	-
gamma_CL	0	-	-
gamma_k14	0	-	-
gamma_k40	0	-	-
a	0.25	0.025	10
b	0.266	0.0063	2

***Goodness-of-fit plots*:**

Observed vs individual predicted concentrations plot
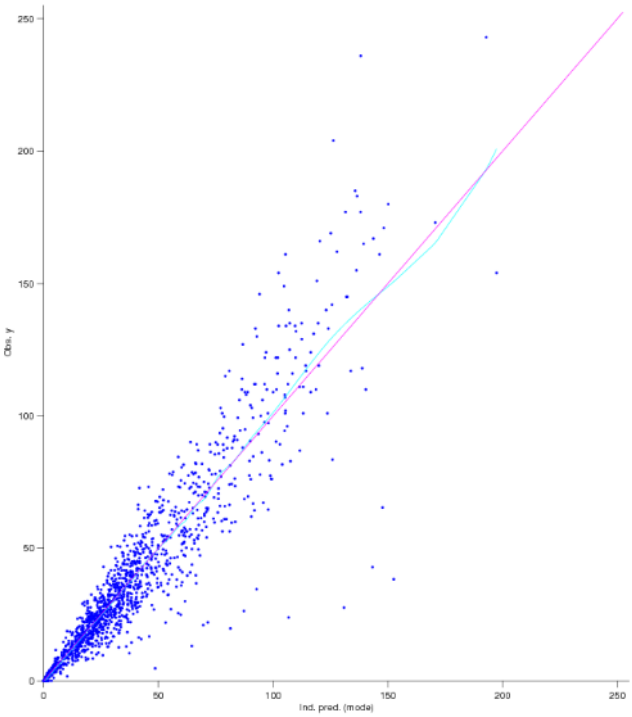
VPC plot
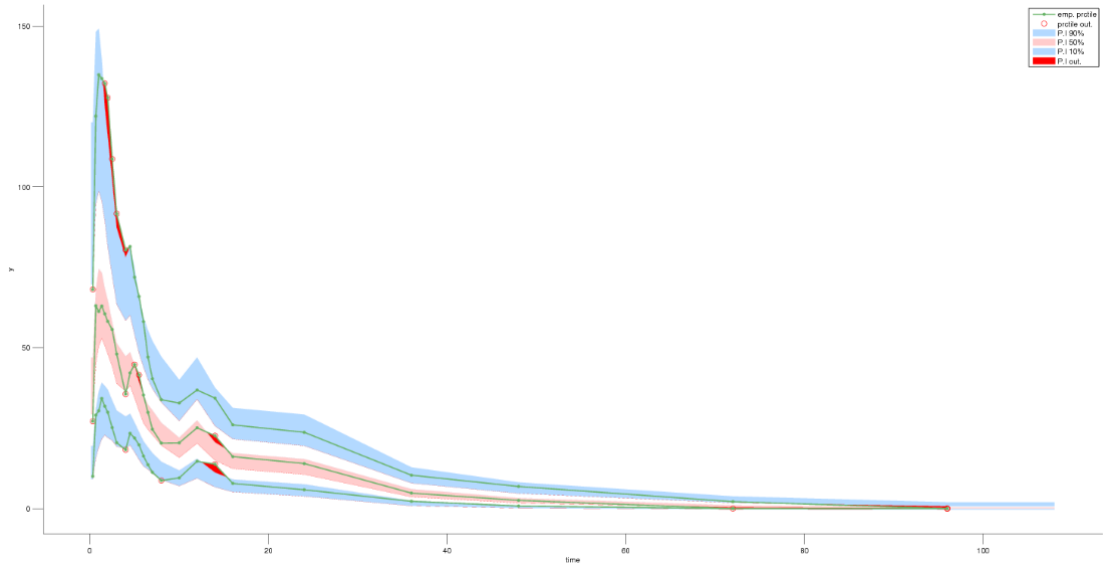

EZE PK Model (No. 7)

Model Description:

4-compartment PK model with first-order absorption and elimination processes, and EHC via transfer of the drug between the GB and Central compartments following a sine function. Sine function parameters fixed to certain values.

Schematic Representation:

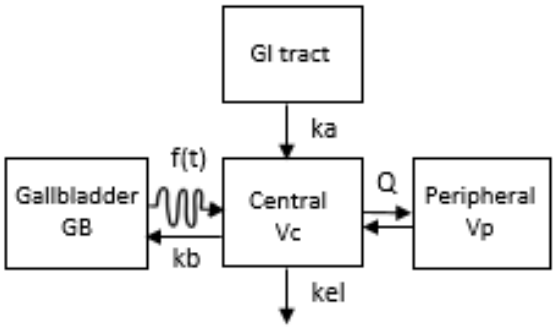

Numerical Criteria:

-2LL: 9856.65
AIC: 9890.65
BIC: 9925.08

Estimation of the population PK parameters:

	parameter	s.e. (lin)	r.s.e.(%)
ka_pop	1.26	0.11	9
Vc_pop	7.61e+004	8.1e+003	11
Vp_pop	8.02e+004	9.7e+003	12
Q_pop	2.26e+004	3.8e+003	17
k24_pop	0.0512	0.0041	8
k42_pop	0.855	0.017	2
CL_pop	1.16e+004	8.1e+002	7
omega_ka	0.0689	0.6	873
omega_Vc	0.546	0.0083	2
omega_Vp	0.597	0.017	3
omega_Q	0.799	0.035	4
omega_k24	0.281	0.09	32
omega_k42	0.0962	0.0045	5
omega_CL	0.36	0.006	2
gamma_ka	0.656	0.088	13
gamma_Vc	0	-	-
gamma_Vp	0	-	-
gamma_Q	0	-	-
gamma_k24	0	-	-
gamma_k42	0	-	-
gamma_CL	0	-	-
a	0.304	0.031	10
b	0.282	0.0066	2

Goodness-of-fit plots:

Observed vs individual predicted concentrations plot
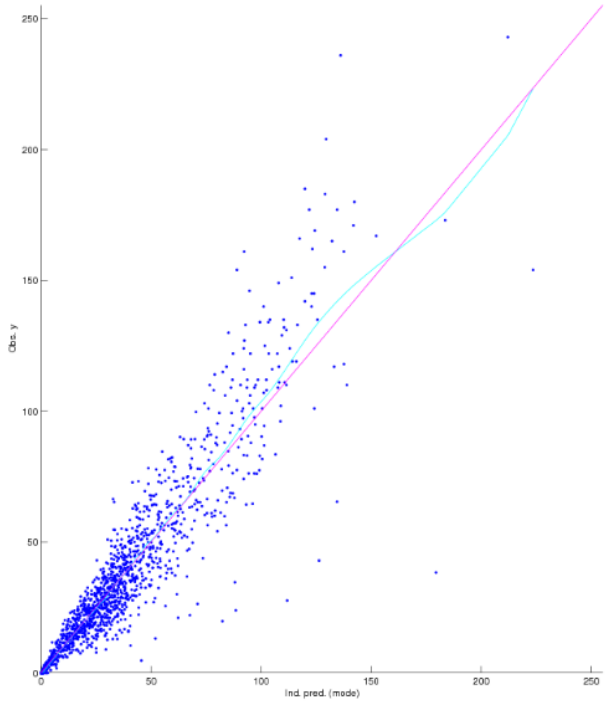
VPC plot
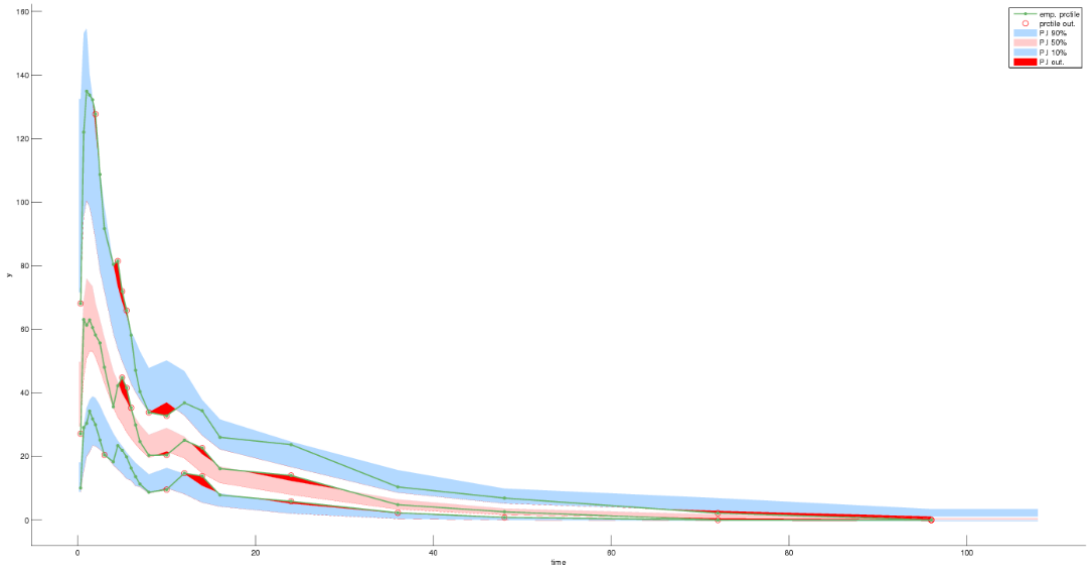

EZE PK Model (No. 8)

Model Description:

4-compartment PK model with first-order absorption and elimination processes, and EHC via first-order transfer of the drug from the GB to the GI compartment and subsequently to the Central compartment. Switch function release in specified time intervals (TGE) at mealtimes, and inclusion of a baseline bile release rate constant at inter-digestive periods.

Schematic Representation:

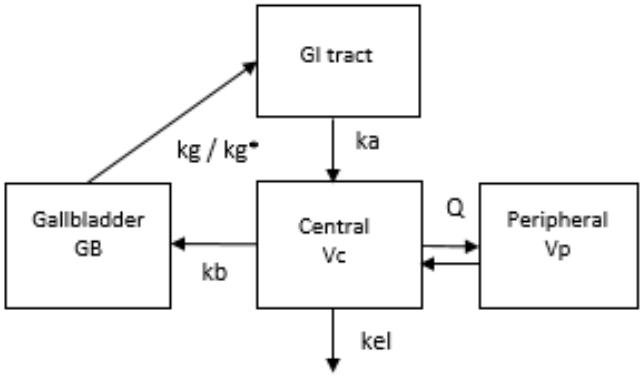

Numerical Criteria:

-2LL: 10113.83
AIC: 10149.83
BIC: 10186.29

Estimation of the population PK parameters:

	parameter	s.e. (lin)	r.s.e.(%)
ka_pop	0.816	0.056	7
Vc_pop	4.44e+004	4.3e+003	10
Vp_pop	6.99e+004	7.9e+003	11
Q_pop	2.26e+004	4.1e+003	18
k24_pop	0.258	0.056	22
k410_pop	0.281	0.021	8
k41_pop	1.12	0.36	32
CL_pop	1.2e+004	8.3e+002	7
omega_ka	0.254	0.055	21
omega_Vc	0.395	0.074	19
omega_Vp	0.41	0.097	24
omega_Q	0.793	0.14	18
omega_k24	0.979	0.16	16
omega_k410	0.301	0.062	20
omega_k41	1.55	NaN	NaN
omega_CL	0.355	0.05	14
a	0.243	0.026	11
b	0.313	0.007	2

***Goodness-of-fit plots*:**

Observed vs individual predicted concentrations plot
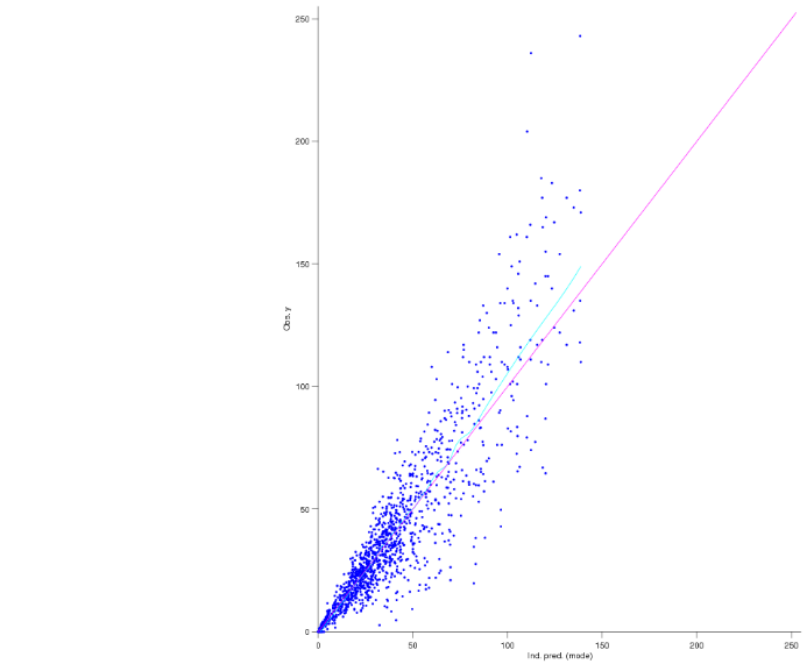
VPC plot
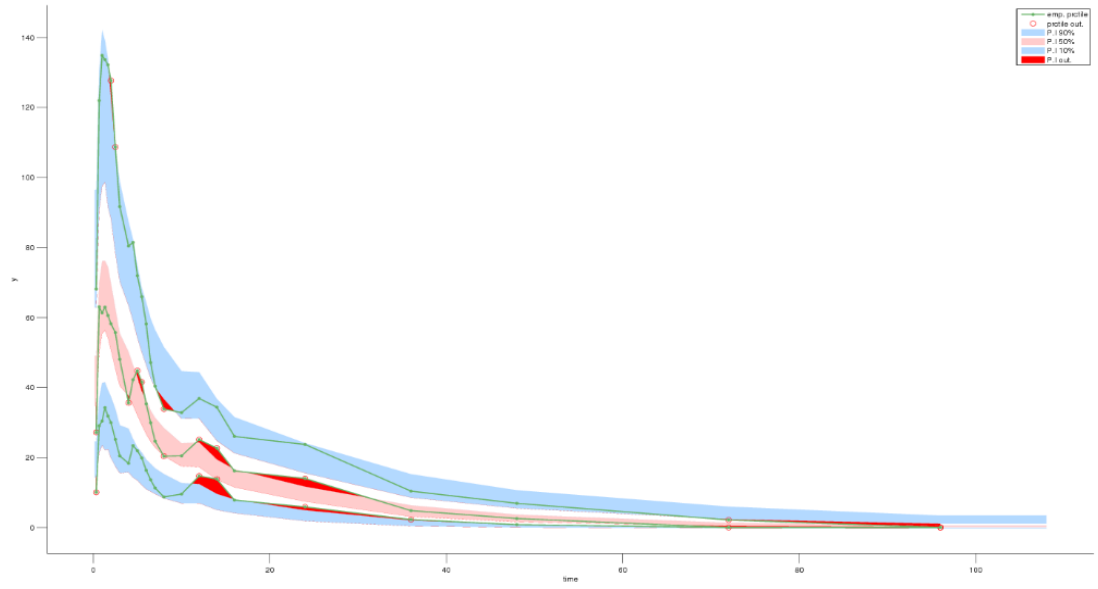

EZE PK Model (No. 9)

Model Description:

4-compartment PK model with first-order absorption and elimination processes, and EHC via zero-order transfer of the drug from the GB to the GI compartment and subsequently to the Central compartment. The time intervals (TGE) for bile release are estimated. Inclusion of first-pass effect.

Schematic Representation:

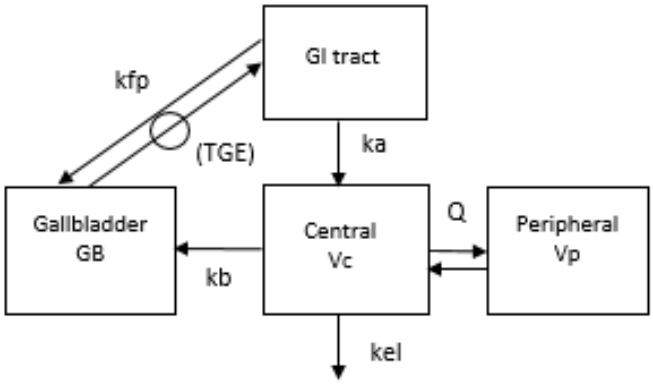

Numerical Criteria:

-2LL: 10371.72
AIC: 10413.72
BIC: 10456.25

Estimation of the population PK parameters:

	parameter	s.e. (lin)	r.s.e.(%)
ka_pop	1.69	0.16	9
k14_pop	0.015	0.0095	64
Fp_pop	0.338	0.021	6
Vc_pop	6.48e+004	6.5e+003	10
Vp_pop	1e+005	9.8e+003	10
Q_pop	2.21e+004	3.3e+003	15
k24_pop	0.0993	0.0077	8
T41_pop	0.362	0.094	26
CL_pop	7.27e+003	7.5e+002	10
omega_ka	0.0751	0.61	816
omega_k14	3.12	0.024	1
omega_Fp	0.47	0.0049	1
omega_Vc	0.516	0.0095	2
omega_Vp	0.489	0.016	3
omega_Q	0.74	0.023	3
omega_k24	0.301	0.017	6
omega_T41	1.3	0.00085	0
omega_CL	0.462	0.023	5
gamma_ka	0.683	0.088	13
gamma_k14	0	-	-
gamma_Fp	0	-	-
gamma_Vc	0	-	-
gamma_Vp	0	-	-
gamma_Q	0	-	-
gamma_k24	0	-	-
gamma_T41	0	-	-
gamma_CL	0	-	-
a	0.182	0.018	10
b	0.265	0.0062	2

Goodness-of-fit plots:

Observed vs individual predicted concentrations plot
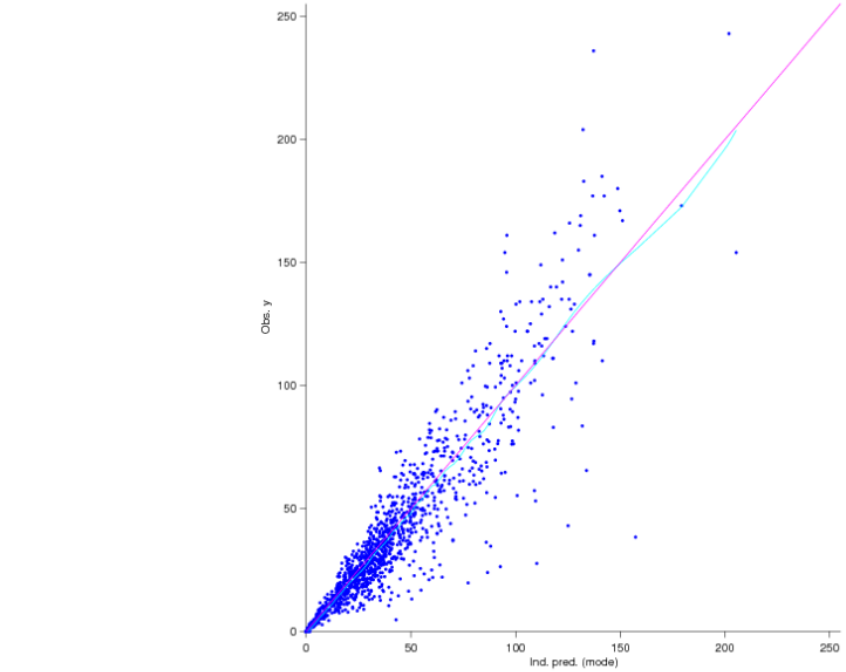
VPC plot
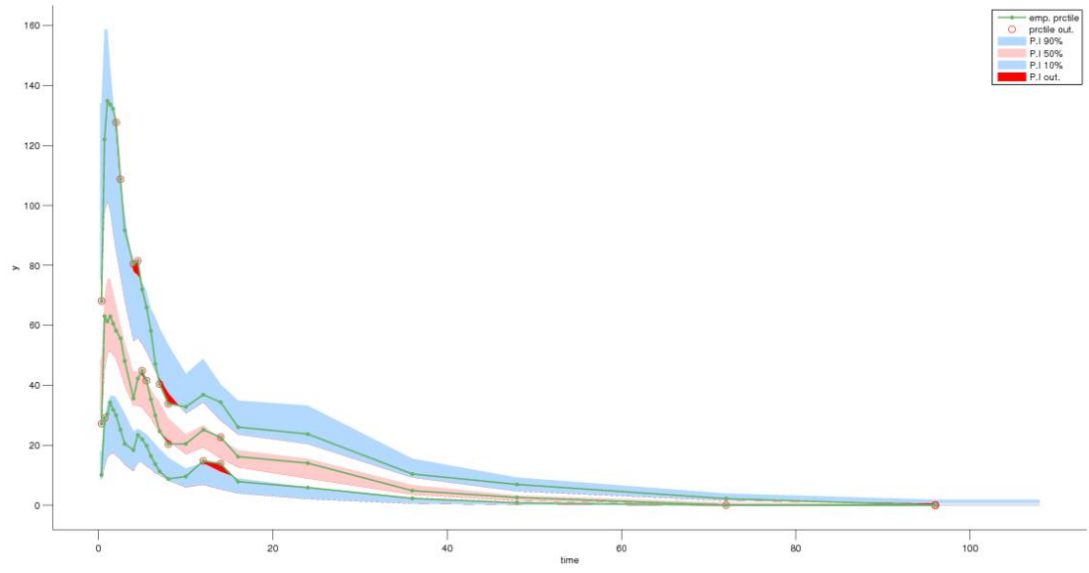

EZE PK Model (No. 10)

Model Description:

4-compartment PK model with first-order absorption and elimination processes, and EHC via bolus release of the drug from the GB to the GI compartment and subsequently to the Central compartment. Switch function release in specified time intervals (TGE) at mealtimes, and inclusion of a fraction of dose undergoing EHC (Fb) as estimate, and fecal elimination starting at 4 hours post-dose.

Schematic Representation:

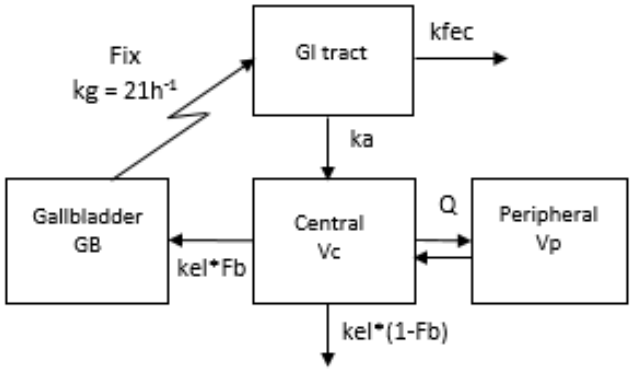

Numerical Criteria:

-2LL: 9745.13

AIC: 9777.13

BIC: 9809.53

Estimation of the population PK parameters:

	parameter	s.e. (lin)	r.s.e.(%)
ka_pop	0.884	0.061	7
Vc_pop	4.94e+004	3.1e+003	6
Vp_pop	1.42e+005	1.5e+004	10
Q_pop	3.33e+004	5.2e+003	16
Fb_pop	0.331	0.014	4
kel_pop	0.309	0.015	5
kfec_pop	0.0942	0.033	35
omega_ka	0.36	0.049	14
omega_Vc	0.29	0.047	16
omega_Vp	0.519	0.075	14
omega_Q	0.785	0.11	15
omega_Fb	0.187	0.063	34
omega_kel	0.196	0.041	21
omega_kfec	1.3	0.3	23
a	0.182	0.019	11
b	0.311	0.0068	2

Goodness-of-fit plots:

Observed vs individual predicted concentrations plot
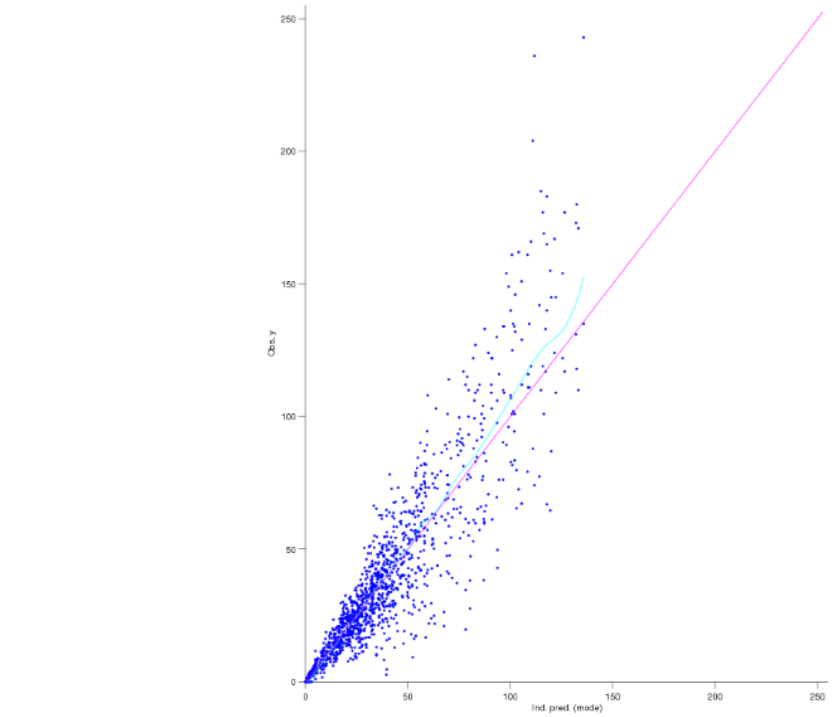
VPC plot
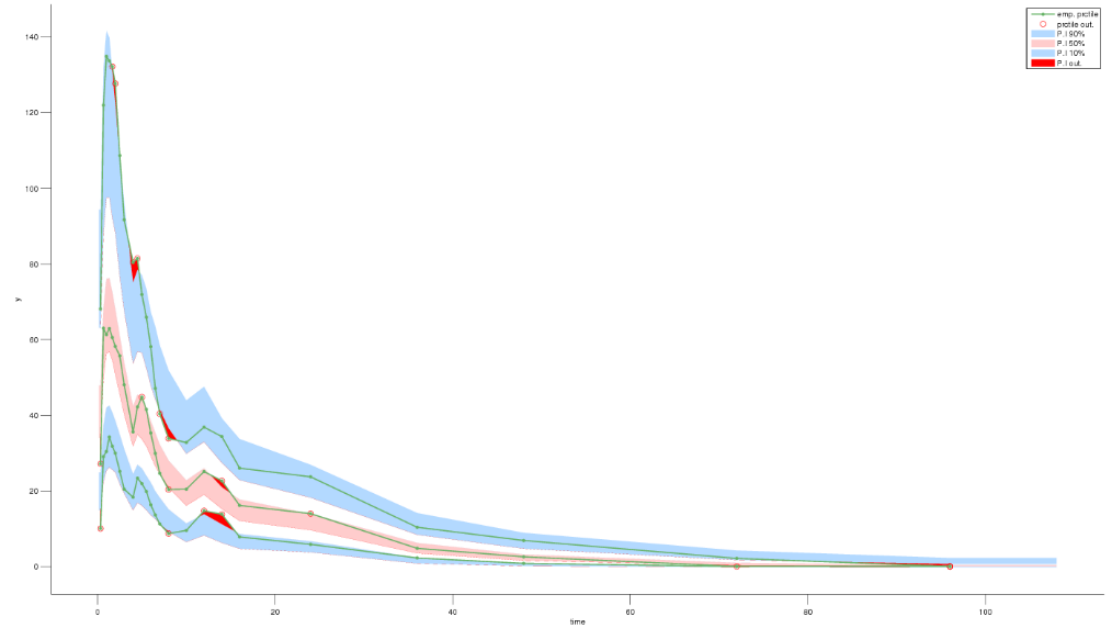

APPENDIX B

Published Papers:

Soulele, K., Macheras, P., Silvestro, L., Rizea Savu, S., Karalis, V. (2015). Population pharmacokinetics of fluticasone propionate/salmeterol using two different dry powder inhalers. *Eur. J. Pharm. Sci.*, 80: 33–42.

Soulele, K., Macheras, P., Karalis, V. (2017). Pharmacokinetic analysis of inhaled salmeterol in asthma patients: Evidence from two dry powder inhalers. *Biopharm Drug Dispos.*, 38(7):407-419.

Soulele, K., Macheras, P., Karalis, V. (2018). On the pharmacokinetics of two inhaled budesonide/formoterol combinations in asthma patients using modeling approaches. *Pulm Pharmacol Ther*, 48: 168–178.

Submitted Papers:

Soulele, K., Karalis, V. On the Population Pharmacokinetics and the Enterohepatic Recirculation of Total Ezetimibe. (*Biopharm Drug Dispos.*)

Soulele, K., Karalis, V. A Joint Population Pharmacokinetic Model for Ezetimibe and its Active Metabolite Ezetimibe. (*in preparation*)

Περίληψη

Η βαθύτερη κατανόηση της φαρμακοκινητικής συμπεριφοράς των φαρμάκων μπορεί να συμβάλλει στη βελτίωση της κλινικής τους αποτελεσματικότητας οδηγώντας τελικά στην επιτυχία της χορηγούμενης φαρμακευτικής αγωγής. Η πληθυσμιακή φαρμακοκινητική ανάλυση μπορεί να συμβάλλει ουσιαστικά σε αυτή την εξερεύνηση, αφού μπορεί να αποτελέσει ένα πολύτιμο εργαλείο για την περιγραφή και πρόβλεψη αυτής της συμπεριφοράς. Στόχος της παρούσας ανάλυσης είναι η εφαρμογή της πληθυσμιακής φαρμακοκινητικής μοντελοποίησης στη διερεύνηση της κινητικής συμπεριφοράς εισπνεόμενων φαρμάκων καθώς και φαρμάκων χορηγούμενων από το στόμα, τα οποία παρουσιάζουν ιδιαίτερα χαρακτηριστικά απορρόφησης και κατανομής. Στο πλαίσιο αυτό, το πρώτο μέρος της παρούσας εργασίας, αφορά την ανάλυση τεσσάρων διαφορετικών εισπνεόμενων φαρμάκων (fluticasone, salmeterol, budesonide, formoterol), χρησιμοποιώντας πληθυσμιακές και κλασσικές φαρμακοκινητικές μεθόδους. Απώτερος σκοπός είναι η εξερεύνηση ορισμένων πτυχών της πνευμονικής απορρόφησης καθώς και παραγόντων που σχετίζονται με την αποτελεσματικότητα της εισπνεόμενης φαρμακευτικής αγωγής. Στο δεύτερο μέρος της εργασίας, η φαρμακοκινητική ανάλυση εστιάζει κυρίως στην διερεύνηση των σύνθετων διεργασιών κατανομής φαρμάκων (συνολικό ezetimibe, ελεύθερο ezetimibe και του μεταβολίτη) που υφίστανται μεταβολισμό πρώτης διόδου και εντεροηπατική κυκλοφορία. Η ανάλυση αυτή πραγματοποιείται μέσω της εφαρμογής διαφορετικών στρατηγικών μοντελοποίησης. Συνολικά, σε αυτή τη διατριβή παρουσιάζονται επτά ξεχωριστές αναλύσεις, που έχουν ως στόχο να διευρύνουν την κατανόησή μας αναφορικά με την εφαρμογή της φαρμακοκινητικής μοντελοποίησης στη διερεύνηση της πορείας στο σώμα φαρμάκων με ιδιαίτερα φαρμακοκινητικά χαρακτηριστικά.